U.PORTO

DOUTORAMENTO EM CIÊNCIAS BIOMÉDICAS

Global biomechanics of cytokinesis: *unraveling the interplay between the contractile ring and the surrounding cortex*

Joana Leite

D

2022

Joana Leite.
Global biomechanics of cytokinesis: unravelling the interplay between *the contractile ring and the surrounding cortex*

D.ICBAS **2022**

Global biomechanics of cytokinesis: unravelling the interplay between the contractile ring and the surrounding cortex

Joana Leite

INSTITUTO DE CIÊNCIAS BIOMÉDICAS ABEL SALAZAR

U.PORTO

JOANA CATARINA SANTOS LEITE

GLOBAL BIOMECHANICS OF CYTOKINESIS: UNRAVELLING THE INTERPLAY BETWEEN THE CONTRACTILE RING AND THE SURROUNDING CORTEX

Tese de Candidatura ao grau de Doutor em Ciências Biomédicas;

Programa Doutoral da Universidade do Porto (Instituto de Ciências Biomédicas de Abel Salazar)

Orientador – Doutora Ana Xavier de Carvalho
Categoria – Investigador Principal
Afiliação – Instituto de Investigação e Inovação em Saúde (i3S)/Instituto de Biologia Molecular e Celular (IBMC), Universidade do Porto

Co-orientador – Doutor Hervé Turlier
Categoria – Investigador Principal
Afiliação – Collège de France

The experimental work present in this thesis was developed at:

i3S – Instituto de Investigação e Inovação em Saúde IBMC – Instituto de Biologia Molecular e Celular Universidade do Porto
Cytoskeletal Dynamics Group
Rua Alfredo Allen, 208
4200-135 Porto, Portugal

www.i3s.up.pt

DECLARAÇÃO DE HONRA

Declaro que a presente tese é de minha autoria e não foi utilizada previamente noutro curso ou unidade curricular, desta ou de outra instituição. As referências a outros autores (afirmações, ideias, pensamentos) respeitam escrupulosamente as regras da atribuição, e encontram-se devidamente indicadas no texto e nas referências bibliográficas, de acordo com as normas de referenciação. Tenho consciência de que a prática de plágio e auto-plágio constitui um ilícito académico.

Porto, Julho de 2024

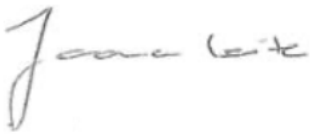

“An answer is invariably the parent of a great family of new questions. So we draw worlds and fit them like tracings against the world about us, and crumple them when they do not fit and draw new ones.”

John Steinbeck, The Log from the Sea of Cortez

ACKNOWLEDGEMENTS

Thank you to lovers,
Thank you to friends,
Thanks everyone who rings a bell.
Thanks to the ones who made it easy,
And to the ones who made it impossibly difficult,
For they all contributed to this day looking exactly like it does.
Thanks to the great mentors,
And to the not-so-great ones.
To those who passed me their purest knowledge,
To the ones who lacked any knowledge to give,
For they made me look for it elsewhere.
Thanks to my brain,
For making it miserably impossible to live inside my own head most of the times.

To my father, who, I'm afraid,
is the greatest explorer of the world I will ever know.

LIST OF PUBLICATIONS

Esta tese de Doutoramento é uma compilação de resultados originais, publicados ou em fase de preparação para publicação em revistas internacionais indexadas. A autora declara que teve participação activa na conceção, execução, análise, interpretação, discussão e redacção dos trabalhos aqui apresentados.

Faz parte integrante desta tese o seguinte artigo publicado:

This Doctoral thesis is a compilation of original data, published or in the process of preparation to submit for publication in international peer-reviewed journals. The author declares that she had an active role in the conception, execution, analysis, interpretation, discussion and writing of the work here presented.

The following published article is included in this thesis:

Article 1 (First-author):

Leite J., Chan F. Y., Osório D. S., Saramago J., **Sobral A. F.**, Silva A. M., Gassmann R., Carvalho A. X. (2020). Equatorial non-muscle myosin II and plastin cooperate to align and compact F-actin bundles in the cytokinetic ring. *Frontiers in Cell and Developmental Biology*, 25;8:573393. doi: 10.3389/fcell.2020.573393.

A autora teve também participação activa na concepção, pesquisa e redacção de um artigo de revisão publicado em revista internacional indexada.

The author had an active role in the conception, literature search and writing of a revision article published in an international journal:

Revision article 1 (co-first author*, parts of Chapter I):

Leite J.*, Osorio D. S.*, Sobral A. F.*, Silva A. M., Carvalho A. X. (2019). Network contractility during cytokinesis - from molecular to global Views. *Biomolecules*, 18;9(5):194. doi: 10.3390/biom9050194.

Adicionalmente, trabalho realizado durante a produção desta tese foi publicado nos artigos abaixo indicados que não constam como parte integrante desta tese:

Additionally, work developed during the production of this thesis was published in the following articles that are not an integrant part of this thesis:

Osório D. S.*, Chan F. Y.*, Saramago J.*, **Leite J.,** Silva A. M., **Sobral A. F.**, Gassmann R., Carvalho A. X. (2019). Crosslinking activity of non-muscle myosin II is not sufficient for embryonic cytokinesis in *C. elegans*. *Development*, 12;146(21):dev179150. doi: 10.1242/dev.179150.

SUMÁRIO

O citoesqueleto de actina é essencial para uma grande variedade de processos celulares que envolvem a geração de força e mudanças na forma da célula, incluindo a divisão celular, motilidade e invasão, e morfogénese. Foi no início do século XX que D'Arcy Thompson começou a explorar como a morfogénese e mudanças de forma de organismos vivos podiam ser explicados por leis fundamentais da física. Contudo, apenas recentemente entrámos numa nova era da mecanobiologia, focada na compreensão de como mecanismos celulares e forças físicas atuam de forma dinâmica em fenómenos biológicos. A citocinese é a última fase da divisão celular, que leva à partição da célula mãe em duas células filhas. É um processo dependente de actomiosina que envolve a formação e constrição de um anel contráctil. No entanto, este anel não é uma entidade isolada, estando integrado no restante córtex celular. Na verdade, muitos componentes do anel contráctil também se localizam no córtex circundante, sendo que a sua localização cortical pode por isso contribuir para os processos biomecânicos que regulam a citocinese de no tempo e espaço. A investigação recente na área tem-se focado primariamente na compreensão do funcionamento de um anel contráctil isolado. Na presente tese, tentei abordar como o córtex que envolve o anel da citocinese afeta a sua dinâmica. No Capítulo III, começo por mostrar que perturbando proteínas que interferem com a distribuição de miosina e os padrões de ativação ao longo do córtex durante a citocinese afetam, no tempo e espaço, a dinâmica e cinética do processo. No capítulo IV, foquei-me principalmente na fase de formação do anel, concluindo que os fluxos corticais provenientes de gradientes de tensão na camada cortical não são essenciais para a formação do anel, mas sim consequência da tensão diferencial entre o córtex polar e equatorial. Descobri igualmente que a miosina-II não muscular, a proteína motora do córtex, e a plastina, um crosslinker da actina, cooperam localmente no equador para alinhar cabos de actina paralelos ao plano de divisão para formar o anel, o que é essencial para o sucesso da citocinese. Finalmente, no capítulo V, empreguei metodologias experimentais e teóricas para descobrir que a citocinese é resistente a diminuições dos níveis de miosina e que esta robustez está relacionada com um papel adicional da miosina em providenciar estabilidade ao córtex circundante durante a citocinese através da contribuição para a viscosidade do mesmo, para além da sua já conhecida função como geradora de contractilidade. No seu conjunto, estas descobertas revelam que a citocinese é na verdade controlada por um balanço de forças dinâmico entre o anel contráctil e o córtex circundante, que em última análise determina o seu sucesso ou fracasso. Acredito que o trabalho aqui desenvolvido terá um impacto significativo em como percecionaremos a mecânica da citocinese no futuro.

SUMMARY

The actin cytoskeleton is essential for a wide range of cellular processes that involve force generation and cell shape changes, including cell $_{division}$, motility and invasion, and tissue morphogenesis. It was in the beginning of the 20th century that D'Arcy Thompson first explored how morphogenesis and shape changes of living organisms could be explained by fundamental physical laws. Nevertheless, only recently we have entered a new age in mechanobiology, focused on understanding how cell mechanics and physical forces act as dynamic players in biological phenomena. Cytokinesis is the last stage of cell division that ultimately leads to the partitioning of the mother cell into two daughter cells. It is an actomyosin–dependent process and requires the assembly and constriction of an actomyosin contractile ring. However, this ring is not an isolated entity, it is integrated in the remaining cell cortex. In fact, many contractile ring components also localize in the surrounding cortex and their cortical localization may thus contribute to the overall biomechanics that spatiotemporally regulates cytokinesis. Recent research in the field has primarily focused in understanding the behavior of an isolated contractile ring.

In this thesis, I aimed at addressing how the cortex surrounding the cytokinetic ring impacts its dynamics. In Chapter III, I start by showing that perturbing proteins that interfere with myosin distribution and activation patterns throughout the cell cortex during cytokinesis have a spatiotemporal impact in the dynamics and kinetics of the process. In Chapter IV, I focused primarily on the ring assembly phase, where I concluded that cortical flows arising from gradients of tension in the cortical layer are not essential for contractile ring assembly but seem to be rather a consequence of the tension differential between the equatorial and the polar cortices. I also found that non-muscle myosin II, the motor protein of the cell cortex, and and the actin crosslinker plastin cooperate locally at the cell equator to align actin bundles parallel to the division plane to form the ring, which is essential for cytokinesis to succeed. Finally, in Chapter V, I employed experimental and theoretical efforts to discovered that cytokinesis is robust to the decrease in myosin levels and that this robustness is related with an additional role of myosin in providing stability to the surrounding cortex during cytokinesis by having a contribution to cortex viscosity, apart from its well-known function in generating contractility.

Altogether, these findings reveal that cytokinesis is in fact controlled by a dynamic force balance between the contractile ring itself and the surrounding cortex, which ultimately determines its success or failure. I believe the work conducted here will have significant impact on how we perceive the mechanics of cytokinesis in the future.

TABLE OF CONTENTS

ACKNOWLEDGEMENTS ..... *viii*

LIST OF PUBLICATIONS ..... *ix*

SUMÁRIO ..... *xi*

SUMMARY ..... *xii*

TABLE OF CONTENTS ..... *xiii*

CHAPTER I *3*

General Introduction *6*

The cell cytoskeleton 6

The actomyosin cortex 8

Actin 9

Actin domain structure 10

Actin Dynamics: the role of actin regulatory proteins 10

Actin filament crosslinkers: actin networks' structure and organization 14

Myosin 19

Myosin domain structure 20

Mechanism of filament sliding and force generation 21

Regulation of myosin activity 22

Regulation of NMII by RLC phosphorylation 22

Regulation of NMII by heavy-chain phosphorylation 25

Cytokinesis – the last stage of cell division 30

Division plane specification and contractile ring assembly 31

Positive equatorial signalling 32

Central-spindle dependent stimulation 32

Central spindle-independent / astral microtubule-dependent stimulation 33

Inhibitory polar signalling 34

Cortical actomyosin flows 36

Contractile ring constriction 38

Actomyosin structure of the contractile ring 38

Ring constriction independently of myosin motor activity 41

The role of F-actin dynamics in ring constriction 42

The role of actin filament crosslinkers in contractile ring constriction 43

Modeling of actomyosin networks 46

Modelling cytokinesis 47

Models of contractile ring constriction 48

The influence of the surrounding cortex 51

C. elegans as a model organism to study cytokinesis 53

C. elegans 53

Figure 1.9. *C. elegans* life cycle and developmental stages. (A) *C. elegans* life cycle at 25ºC. (B) Micrographs of laid eggs, larval stages and adults. Images from (Fielenbach and Antebi, 2008) (Erkut, Cihan, 2014), used under permission. 54

RNA interference in *C. elegans* 54

Mos Single Copy Insertion in *C. elegans* 55

References....55
CHAPTER II.... 98
Overview and Objectives.... 100
CHAPTER III.... 102
Myosin levels, distribution and activity in the surrounding cortex impact contractile ring dynamics.... 104
Abstract....104
Introduction....104
Results....106
Myosin and other cortical proteins are cleared from the poles and accumulate at the cell equator, which triggers periods of cortical flow....106
Increasing active myosin levels at the polar cortex delays contractile ring assembly and constriction....109
Decreasing myosin levels earlier leads to faster contractile ring assembly....114
Coarse-grained simulations of myosin activity in the cortex suggest a role for the polar cortex in coordinating the ingressing furrow kinetics....116
Discussion....120
Conclusion....123
Measurement of cytokinesis, ring assembly and furrow initiation time intervals, and ring constriction rate....126
Fluorescence intensity measurements....127
Cortical flow quantification....127
Image analysis, quantifications, and statistics....127
CHAPTER IV.... 130
Equatorial Non-muscle Myosin II and Plastin Cooperate to Align and Compact F-actin Bundles in the Cytokinetic Ring.... 132
Abstract....132
Introduction....132
Results....134
Long-Range Cortical F-actin Flows Are Dispensable for Contractile Ring Formation and Furrow Ingression....134
Cortical Flows Are Dispensable for Accumulation of Myosin in the Ingressing Furrow....139
The F-actin Crosslinker Plastin Cooperates With Myosin to Align F-actin Bundles at the Division Plane....142
Discussion....145
Unidirectional Long-Range Cortical Flows Play a Minor Role During Cytokinesis....145
Myosin Accumulation at the Cell Equator Occurs Primarily by Recruitment From the Cytoplasm....146
Plastin-Mediated Bundling and Myosin Motor Activity Are Locally Required for F-actin Alignment at the Division Plane and Deformation of the Equator....147
Conclusion....149
Materials and Methods....149

C. elegans Strains....149
RNA Interference....150
Live Imaging....151
Fluorescence Intensity Measurements....151
Calculation of Myosin Dissociation Rate....152
Cortical Flows Quantification....152
Calculation of Cortical Compression Rates....153
Analysis of Bundle Alignment at the Equatorial Cortex....153

CHAPTER V 168

Myosin tunes both contractility and viscosity at the cell cortex to ensure robust cytokinesis kinetics 170

Abstract....170

Introduction....171

Results....173
Cytokinesis kinetics are robust to the decrease of total myosin levels at the ingressing furrow 173
Expressing an increasing amount of inactive myosin slows down the constriction rate progressively....187
Inhibition of the passive actin crosslinker plastin in inactive or motor-dead myosin mutant backgrounds accelerates ring constriction....193

Discussion....201
Cytokinesis kinetics depend on the relative amounts of active and inactive myosin in the cortex 203

Conclusion....216

Materials and Methods....216
C. elegans strains....216
RNA interference....218
Live imaging....220
Measurement of cytokinesis, ring assembly and furrow initiation time intervals, and ring constriction rate....221
Fluorescence intensity measurements....221
Cortical flow quantification....221
Measurement of NMY-2::GFP, GFP::AHPH (RhoA biosensor) profiles along the cortex contour 222
Fittings of NMY-2::GFP and GFP::AHPH profiles....222
Image processing, quantifications and statistical analysis....223

Supplementary Material....224

APPENDIX I: Additional findings and observations....226

References....228

CHAPTER VI 241

Concluding Remarks and Future Perspectives 242

LIST OF ABBREVIATIONS

ABD – actin-binding domain
ABP – actin-binding protein
ADF – actin depolymerizing protein
AFM – atomic force microscopy
ARP – actin-related protein
C. elegans – Caenorhabditis elegans
CDK1 – cyclin-dependent kinase
CH - calponin homology
CLIP170 - cytoplasmic linker protein 170
CPC - chromosome passenger complex
CR – contractile ring
DAD - diaphanous auto-regulatory domain
D. Discoideum - Dictyostelium discoideum
DID - diaphanous inhibitory domain
DRF – Diaphanous-related Formin
DNA – Deoxyribonucleic Acid
dsRNA – double-strand RNA
EM – electron microscopy
F-actin – filamentous actin
FH – formin homology (domain)
FRAP - Fluorescence Recovery after Photobleaching
G-actin – monomeric actin
GBD – GTPases binding domain
GDP - guanosine diphosphate
GFP - Green fluorescent protein
GTP - guanosine triphosphate
GAP - GTPase-activating proteins
GEF - guanine nucleotide exchange factor
HMM - heterodimeric smooth muscle heavy meromyosin
LHS - Left homology sequence
MLCK - myosin light chain kinase
MRCK - myotonic dystrophy kinase-related CDC42-binding kinase
MosSCI - Mos Single Copy Insertion
NGM - Nematode growth medium
NMHC– non-muscle myosin II heavy chain
NPF - nucleation promotion factor
NRK – normal rat kidney cells
MRLC/MLC-4 – myosin regulatory light chain
NMII / NMYII / NMY-2 / myosin – non-muscle myosin II
PCR - Polymerase chain reaction
PIV – particle image velocimetry
PKC – protein kinase C
Plk-1 – Polo-like Kinase 1
PP1 - protein phosphatase 1
RHS - Right homology sequence
RNA – Ribonucleic acid
RNAi – RNA interference
ROCK - Rho-associated, coiled coil-containing kinase
S. Cerevisiae - Saccharomyces cerevisiae
S. Pombe – Schizosaccharomyces pombe
TIRF - Total Internal Reflection Fluorescence
WASP - Wiskott-Aldrich syndrome family protein
ZIPK - leucine zipper interacting kinase

CHAPTER I

GENERAL INTRODUCTION

*This chapter includes parts from **Leite J.***, Osorio D. S.*, Sobral A. F.*, Silva A. M., Carvalho A. X. (2019). Network contractility during cytokinesis - from molecular to global Views. *Biomolecules*, 18;9(5):194. doi: 10.3390/biom9050194.

General Introduction

The cell cytoskeleton

In 1903, the biologist Nikolai Koltsov pioneered the idea that the shape of cells was defined by a network of tubular structures, shortly after named the cytoskeleton (Koltzoff, 1924). At first, the cytoskeleton was considered a gel-like structure that would simply maintain the organelles in place. The continuous study of this structure over the years revealed that it endows the cell with a certain shape and rigidity, much like the skeletal system of the human body. However, unlike bones, the components of the cytoskeleton are constantly changing in order to drive dynamic processes such as cellular movement and cellular division (Fletcher and Mullins, 2010).

The cytoskeleton is responsible for three essential functions: spatially organizing the cell contents, connecting the cell with its external environment and generating forces that allow the cell to move and change shape. It is composed of three major types of polymeric structures – microfilaments, microtubules and intermediate filaments – which are very briefly introduced below. All of them are organized into networks that resist deformation and reorganize in response to externally applied forces (Fletcher and Mullins, 2010).

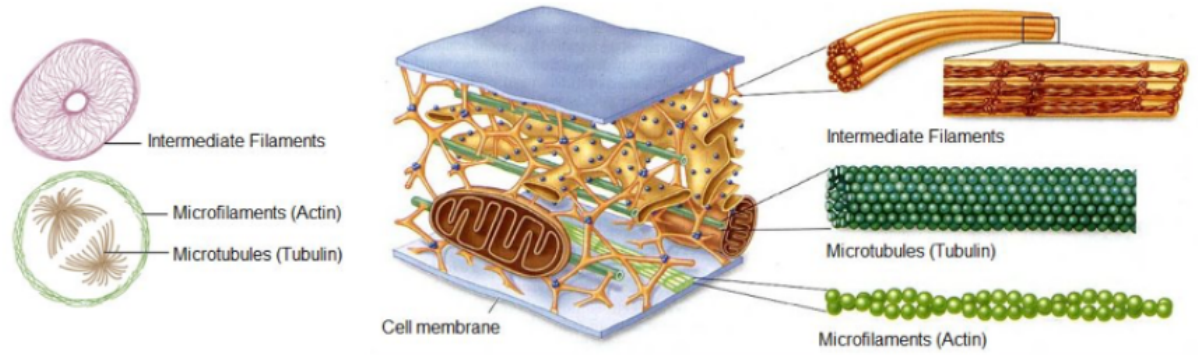

FIGURE 1.1. The cell cytoskeleton: microfilaments, microtubules and intermediate filaments. Microfilaments are composed of actin subunits which form two intertwined strands (Bottom).They thicken the cortex around the inner edge of the cell and are involved in resisting tension. Microtubules are made up of globular protein subunits called α-tubulin and β-tubulin and are found in the interior of the cell, where they maintain cell shape by resisting compressive forces (Middle). Intermediate filaments are made of several strands of fibrous proteins that are wound together and are essentially found throughout the cell to hold organelles in place (Top). Image from https://cnx.org/contents/YJx4WKaS@1/07-5-The-Cytoskeleton-MS, used under permission.

Microfilaments

Microfilaments are also known as actin filaments (Figure 1.1). Actin monomers hydrolyse ATP to ADP to polymerize into filaments, which have a diameter of ~7 nm. Actin filaments are polar structures, with a plus (or barbed) end, where monomers preferentially assemble, and a minus (or pointed) end, where monomers preferentially disassemble. These can form relatively stiff structures and organize into networks with different architectures and tuneable mechanical properties, ranging from isotropic to branched or even bundled networks. While bundles of aligned filaments are mostly involved in filopodial protrusions during chemotaxis, contractile ring formation during cytokinesis and cell–cell communication, branched filaments instead support the leading edge of motile cells, the cortex surrounding the contractile ring in cytokinesis and generate the forces involved in shape changes, such as those occurring in phagocytosis (reviewed in Blanchoin *et al.*, 2014).

Microtubules

Microtubules are cylindrical hollow structures with a diameter of ~25 nm that are built from 13 parallel protofilaments made of α-tubulin and β-tubulin heterodimeric subunits. As actin filaments, microtubules are also polar, with the plus end growing faster than the minus end. These structures can switch between two states through a process called dynamic instability or catastrophy. This means they can stably grow or rapidly shrink (Mitchison and Kirschner, 1984), which is essential for them to adapt to variations in their constituent subunits very quickly (Holy and Leibler, 1994). This can go up to 1000-fold faster than structures that depend on regulatory proteins like actin filaments. They are the stiffest of the three types of polymers in the cytoskeleton, with a persistent length of around 5 mm, even though they buckle under compression (Gittes *et al.*, 1993). They are highly dynamic and one of their essential functions is to allow the mitotic spindle to align the chromosomes correctly during division (reviewed in Wittmann, Hyman and Desai, 2001).

Intermediate filaments

Intermediate filaments are composed of tetrameric subunits formed by two antiparallel half-staggered dimers. The filament forms by lateral association of these tetramers that anneal longitudinally. These structures have a total diameter of ~11 nm and are the least stiff of all the filaments that compose the cytoskeleton (reviewed in Mostowy & Cossart, 2012). As such, they resist tensile forces much better than compressive forces. Unlike microtubules and actin filaments, intermediate filaments are not polar, thus there is no possible directional movement of molecular motors.

This manuscript focuses on the actin cytoskeleton, specifically on the mechanical properties of a thin layer of actin filaments lying underneath the plasma membrane of cells - the actomyosin cortex – during the last step of cell division. A detailed introduction on the main components of this cortical actin layer, their structures, main functions and regulation mechanisms is provided in Section “The actomyosin cortex” below. Brief references to microtubules are also to be expected throughout the manuscript.

The actomyosin cortex

The cell cortex, also known as the actomyosin cortex, is a thin layer (100-200 nm in thickness) (Clark, Dierkes and Paluch, 2013) of cytoplasmic proteins - actin filaments, myosin motors and other actin-binding proteins - that lies directly beneath the plasma membrane in most eukaryotic cells (Salbreux, Charras and Paluch, 2012; Clark *et al.*, 2014; Svitkina, 2020). It essentially enables cells to resist extracellular stresses, perform mechanical work, and change shape. Due to a combination of myosin II motor activity and actin network architecture and connectivity, a cortical tension is generated in the network, which is defined as the force per unit length exerted on a piece of cortex by the cortical network around it (Salbreux, Charras and Paluch, 2012).

In the sections below, the structure and function of the main cell cortex components are thoroughly discussed and possible effects these may have in regulating cortical mechanical properties and cortical tension are highlighted.

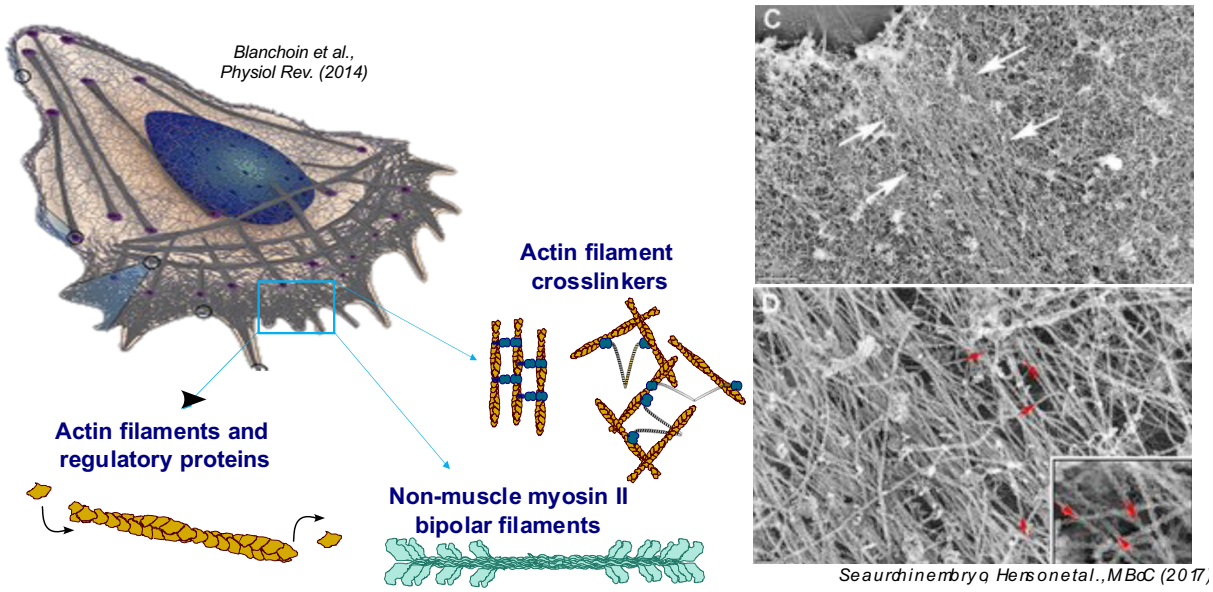

FIGURE 1.2. The actomyosin cortex. Left - The cortex is a very thin network (~100-200 nm) composed of actin filaments, myosin motors and actin binding proteins that lies directly beneath the plasma membrane in animal cells. **Right -** Electron microscopy images of the cell cortex in a Sea urchin embryo during cytokinesis, showing distinct network architectures. Images adapted from Blanchoin et al, 2014 and Henson et al, 2017, used under permission.

Actin

Actin is one of the most abundant proteins in the cell, in the human body and on the surface of planet Earth. It was discovered in the 1940s, along with the motor protein myosin, in Szent-Gyorgyi's lab, where these proteins were extracted and purified from skeletal muscle (Banga & Szent-Györgyi, 1942; A. Szent-Györgyi, 1942, 1945). The authors discovered that when actin and myosin were mixed together in the presence of ATP, they would build up fibers that could contract. In the 1950s, Huxley first documented the mechanism for muscle contraction, which would consist in actin filaments sliding past myosin filaments (HUXLEY, 1953; Huxley, 1963). However, until then, it was not known that actin and myosin existed outside muscles. It was in the mid-late 1960s that Hatano & Oosawa and Adelman & Taylor, two independent groups working on a slime mold called *Physarum*, first reported the existence of actin and myosin in a non-muscle cell (Adelman & Taylor, 1969; Hatano & Oosawa, 1966). This paved the way to the hypothesis, and later discovery, that actin and myosin were universal components of all eukaryotic cells.

The structure of the actin molecule was revealed by Kabsch & Holmes (Kabsch *et al.*, 1990). In the center, there is a molecule of ATP, which is clamped between the two sides of the actin molecule. A ribbon diagram from their work can be found in Figure 1.3 - Top Left. A space filling model of the actin monomer is shown in Figure 1.3 – Bottom.

Actin spontaneously polymerizes into filaments, under physiological concentrations of salt, a process that can be observed by electron microscopy (EM). A model of the actin filament is represented in Figure 1.3-Right. Two strands of actin subunits wrapped around each other can be observed. Also, the filament has two different ends, essentially because each of the subunits along the filament is oriented in the same direction. In 1975, Woodrum and colleagues showed that actin filaments grow at different rates at those two distinct ends (Woodrum, Rich and Pollard, 1975). They observed that by adding actin subunits to actin filaments already decorated with myosin, filaments formed arrowhead-shaped complexes (see EM micrograph in Figure 1.3-Middle) that grew rapidly at the end where the barbs on the arrowheads point to, whereas growing more slowly at the other end. That is the reason why today we call these the barbed (or plus) and the pointed (or minus) end, respectively.

Almost 10 years later, the rate constants for the addition of ATP-actin and ADP-actin to the ends of the filaments were measured for the first time by EM. After the actin monomer is incorporated into the filament, ATP is hydrolysed. The half time for this reaction is around 2 seconds, and then the subsequent dissociation of the phosphate group is much slower, taking about 6 minutes. Once the phosphate has dissociated, the properties of the filament change

and there are different rate constants for the dissociation and association of ADP-actin and ATP-actin. The rate of dissociation of ADP-actin is much higher than the rate of dissociation of ATP-actin from the filament barbed end (Pollard, 1986).

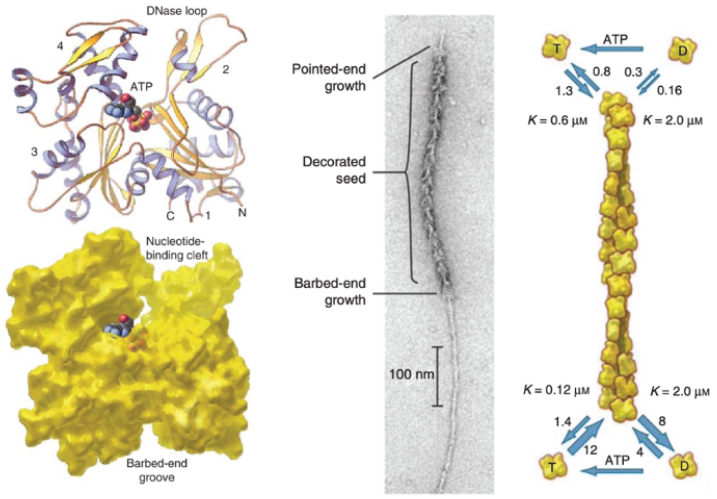

FIGURE 1.3. Structures of the actin monomer and of the actin filament. Left – a ribbon diagram of the actin molecule with an ATP core and below a space-filling model of the monomer showing the nucleotide-biding cleft with ATP *in situ* and the barbed-end groove. Right - Structure and dynamics of the actin filament, with polymerization and depolymerization kinetics at its barbed-end and pointed-ends, respectively. Actin treadmilling happens when an equilibrium is reached between the polymerization at its barbed-end and depolymerization at its pointed-end happens (steady-state). Images are from Pollard and Earnshaw, 2007 and Woodrum et al., 1975, used under permission.

Actin domain structure

Single actin molecules are globular proteins of 375 amino acids (~43 kDa). Each actin monomer - globular actin, hereafter, G-actin - has tight binding sites that mediate head-to-tail interactions with two other actin monomers (Straub and Feuer, 1950). This allows these monomers to polymerize into filaments, forming the so-called filamentous actin – hereafter, F-actin. Interestingly, each monomer is rotated by 166° in the filaments, which confers them the structure of a double-stranded helix. Because all the actin monomers are oriented in the same direction, actin filaments are polar structures, which means their plus end differs from their minus end. This polarity is important both in their assembly and in establishing a unique direction of myosin movement relative to actin (Pollard and Cooper, 2009; Chen and Pollard, 2013), as discussed later in this chapter.

Actin Dynamics: the role of actin regulatory proteins

Theoretically, if all actin could polymerize, and knowing it would polymerize spontaneously under favorable conditions, then the process could go on indefinitely as long as there were

monomers available. But that is not what happens in the cell. In the cell, things are tightly controlled, and this control is generally achieved by regulatory proteins.

Therefore, after the discovery of actin (and myosin), people in the field started looking for regulatory proteins, which are summarized in Figure 1.4.

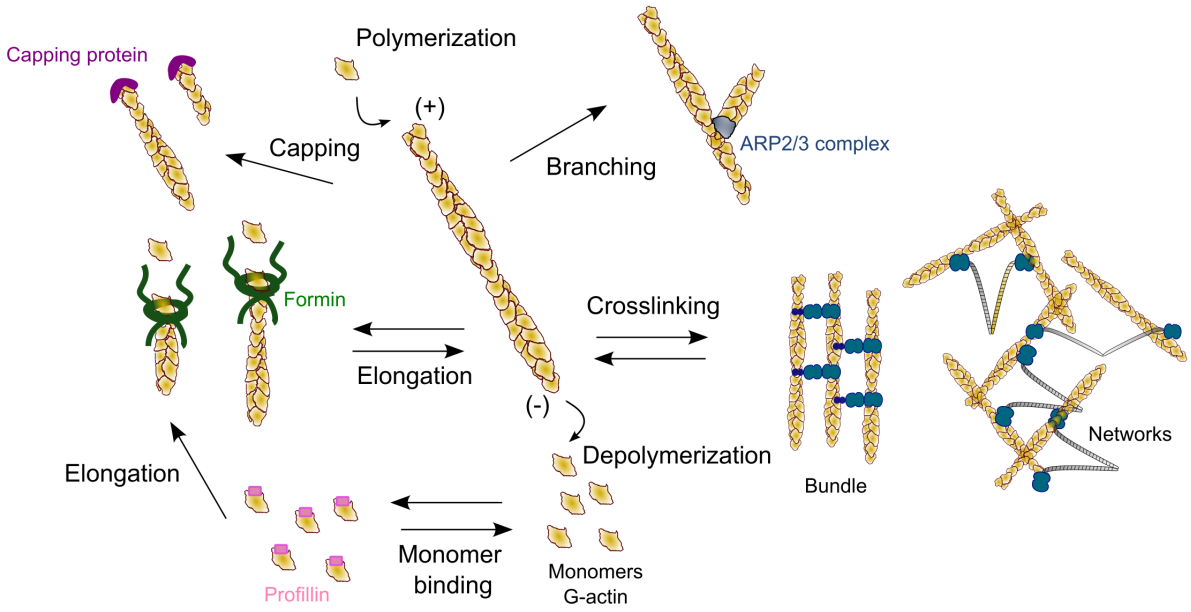

FIGURE 1.4. Actin Regulation: the role of actin regulatory proteins. G-actin monomers are polymerized and into elongated or branched F-actin through actin nucleators and elongators (e.g. formin, ARP2/3 complex). In actomyosin networks, actin filaments can be connected and organized by crosslinkers, severed and disassembled by severing proteins as well as capped by capping proteins to prevent F-actin elongation. Actin sequestering proteins bind to actin monomers to prevent/regulate actin polymerization.

One of the first to be discovered was profilin, by Tilney and Lindberg and colleagues (Carlsson *et al.*, 1977; Tilney *et al.*, 1983), followed by the capping protein in 1980, by Isenberg and Pollard (Isenberg, Aebi and Pollard, 1980). Both these proteins, together, allow the cell to maintain a large pool of unpolymerized actin. Profilin is a small protein with ~125 amino acids with residues that interact with the barbed end of the actin subunit. When it binds in this position, it affects actin assembly reactions. In a normal scenario, actin filament assembly starts with actin monomers forming dimers and then trimers and so on by continuously adding actin subunits to form longer filaments (Courtemanche and Pollard, 2013). When profilin binds an actin monomer, it has two effects: 1) blocks the formation of dimers and trimers, meaning it essentially inhibits spontaneous nucleation of new filaments, and 2) blocks the binding of more actin monomers to the pointed end of growing filaments. However, profilin does not interfere with the actin subunits binding to the barbed end of the filament, and thus, could not, alone, prevent polymerization there. The capping protein, though, binds to the barbed end with high affinity. As such, the combination of both proteins maintains the above mentioned

unpolymerized actin pool. Another important protein, actin depolymerizing factor ADF/cofilin was discovered by Bamburg (Bamburg, Harris and Weeds, 1980) and owes its name to the fact that, in his experiments, it seemed to depolymerize actin filaments. It is now known that cofilin specifically functions by severing actin filaments (de la Cruz, 2009; Galkin *et al.*, 2011; Chen and Pollard, 2013; McCall *et al.*, 2019).

In the 1990s, Machesky and colleagues discovered the ARP2/3 complex (Machesky *et al.*, 1994), a complex of seven proteins firstly purified from amoebas. Years later, this complex was associated with a family of proteins called Wiskott-Aldrich syndrome proteins (WASP) (Machesky *et al.*, 1997). At first, it was not known what this complex was doing, until it was found out that the top two subunits were actin-related proteins number 3 (Arp3) and 2 (Arp2). In the same decade, EM experiments by Mullins revealed that the ARP2/3 complex would make branches on the sides of pre-existing actin filaments (Mullins, Heuser and Pollard, 1998). More recently, this could be observed by time-lapse TIRF microscopy (Amann and Pollard, 2001; Mahaffy and Pollard, 2006). The discovery of the ARP2/3 complex was critical for establishing the first great hypothesis of how actin assembles and disassembles within the cell (Mullins, Heuser and Pollard, 1998).

In the 1990s, another actin filament nucleator and elongator - the formin - was also identified in several organisms (Mass *et al.*, 1990; Jackson-Grusby, Kuo and Leder, 1992; Castrillon and Wasserman, 1994; Kohno *et al.*, 1996). However, its nucleation activity was only reported later, in the 2000s.

Formins

Formins were first identified in *D. melanogaster*, mice and yeast, as mutations in these genes caused severe defects in cytokinesis, polarity, and cell and tissue morphogenesis (Mass *et al.*, 1990; Jackson-Grusby, Kuo and Leder, 1992; Castrillon and Wasserman, 1994; Kohno *et al.*, 1996). Later studies involving the budding yeast *S. cerevisiae* showed for the first time that formins directly nucleate actin filaments, an essential function for the assembly of actin cables in polarized cell growth (Evangelista *et al.*, 2002; Pruyne *et al.*, 2002; Sagot *et al.*, 2002; Sagot, Klee and Pellman, 2002). Several formin genes have been identified in multiple organisms, including fifteen in mammals, two in *S. cerevisiae*, three in *S. pombe*, six in *D. melanogaster* and seven in *C. elegans*, all of which do not seem to play redundant functions (Courtemanche, 2018). Formins have been associated with an increasing range of cytoskeleton-based structures, including cytokinetic contractile rings, filopodia, polarized actin cables, and stress fibers (Campellone & Welch, 2010; Jan Faix & Grosse, 2006; Goode & Eck, 2007). Recently,

variations in the fission yeast formin Cdc12 nucleation efficiency have been shown to impact the probability and timing of contractile ring assembly (Homa *et al.*, 2021).

Formins are relatively large, dimeric multidomain proteins with a modular structure. Relevant domains that are believed to be important for actin binding and protein-protein interactions. At the C-terminus, they exhibit the formin homology 1 and 2 domains - FH1 and FH2, respectively) - which are common to all formins. Most of them also have C-terminal tail regions that include the diaphanous auto-regulatory domain (DAD). The N-terminus of these proteins is more variable and generally has a role in directing their localization and function. An intramolecular interaction between the diaphanous inhibitory domain (DID) and the DAD domain prevents formin from nucleating new actin filaments. However, when the small GTPase RhoA binds to the GTPase binding domain (GBD or CRIB domain), there are conformational changes that allow the structure to "open up" and allow the FH2 domains to dimerize (Chesarone et al., 2010; Schönichen & Geyer, 2010). Crystal structures showed that FH2 domains form tethered dimers (Lu et al., 2007; Thompson et al., 2013; Wise & Thompson, 2010; Xu et al., 2004). Each FH2 monomer consists of an elongated, alpha-helical structure that self-associates in a head-to-tail manner to form a closed, ring-like dimer. Formins can both nucleate and elongate actin filaments. Their role in nucleation consists in energetically stabilizing unstable actin dimers and trimers by encircling them with their FH2 domains. Since profilin interacts with the formin's FH1 domain, the addition of profilin-bound actin monomers is favored (Chang, Drubin and Nurse, 1997; Watanabe *et al.*, 1997). They have been hypothesized to contribute to protrusive forces by remaining attached to the barbed end of actin filaments (reviewed in Higgs, 2005)), which is consistent with excessive formin having a role in promoting cell migration. During cytokinesis, formins localize, accumulate, and get specifically activated in the equatorial region of the cell, allowing for *de novo* assembly of linear actin filaments, which may be more suitable for force generation by the motor-protein myosin to form the contractile ring (Neidt, Skau and Kovar, 2008; Chan *et al.*, 2019; Homa *et al.*, 2021).

Arp2/3 complex

The Arp2/3 complex was discovered in the early 1990s, as mentioned above (Machesky *et al.*, 1994) and seems to be crucial for numerous functions that involve force generation in the actin cortex. For example, it can be found at the leading edge of motile cells (lamellipodia) and in motile patches in yeast, it is required for phagocytosis in mammals and *D. discoideum* (May *et al.*, 2000; Insall *et al.*, 2001), as well as crucial for polarity establishment and migration of fibroblasts (Magdalena *et al.*, 2003) and meiotic asymmetric division in mouse oocytes (Yi *et al.*, 2011). It is composed of seven subunits: Arp2, Arp3, ARPC1, ARPC2, ARPC3, ARPC4,

ARPC5 (Goley and Welch, 2006). The Arp2 and Arp3 subunits closely resemble the structure of actin monomers and therefore work as nucleation sites for new actin filaments. However, the crystal structure of the complex reveals that it is initially in an inactive conformation, where the other subunits hold the Arp2 and Arp3 physically apart and prevent nucleation activity (Robinson R.C. *et al.*, 2001) since that depends on these subunits getting together. EM studies assessing the structure of the branch junction in the complex showed that there are substantial conformational changes both in the ARP2/3 complex and the mother filament at the time they get together to make the branch. Specifically, Arp2 must move around 30 Å so it can be in close contact with Arp3 (Rouiller *et al.*, 2008).

The exact mechanism of filament nucleation by the Arp2/3 complex has been debated over the years. It is believed that all seven subunits coordinate to anchor the pointed end of the new filament at a precise 78° angle to the existing actin filament (Rouiller *et al.*, 2008). The question essentially revolves around where the complex binds the old filament and nucleates the new one. Two models have been proposed, but data from EM and biochemical experiments on the filament nucleation and capping mechanisms ended up favoring the side branching model, according to which the Arp2/3 complex binds to the side of a pre-existing actin filament at a point different from the initial nucleation site (Egile et al., 2005; Rouiller et al., 2008; Volkmann, Amann, et al., 2001). Nevertheless, the Arp2/3 complex is an inefficient nucleator of actin by itself and requires nucleation promoting factors (NPFs) to be activated which include members of the WASP family (WASP, N-WASP, WAVE, and WASH proteins). These proteins generally work by delivering actin subunits to the Arp2/3 complex at the barbed end.

Actin filament crosslinkers: actin networks' structure and organization

Actin-crosslinking proteins are actin binding proteins (ABPs) that link two or multiple actin filaments together and organize them into dynamic and complex subcellular structures, as shown in Figure 1.5. Crosslinking of actin filaments is a critical step in cell motility and is a fundamental process in filopodia protrusion (Mogilner and Rubinstein, 2005), lamellipodia formation (Lewis and Bridgman, 1992) and cytokinesis (Sobral *et al.*, 2021).

This protein family includes for example, α-actinin (Djinović-Carugo *et al.*, 1999), fimbrin/plastin (hereafter, plastin) (Klein *et al.*, 2004), filamin (Stossel *et al.*, 2001) and spectrin (reviewed in Coleman et al., 1989).

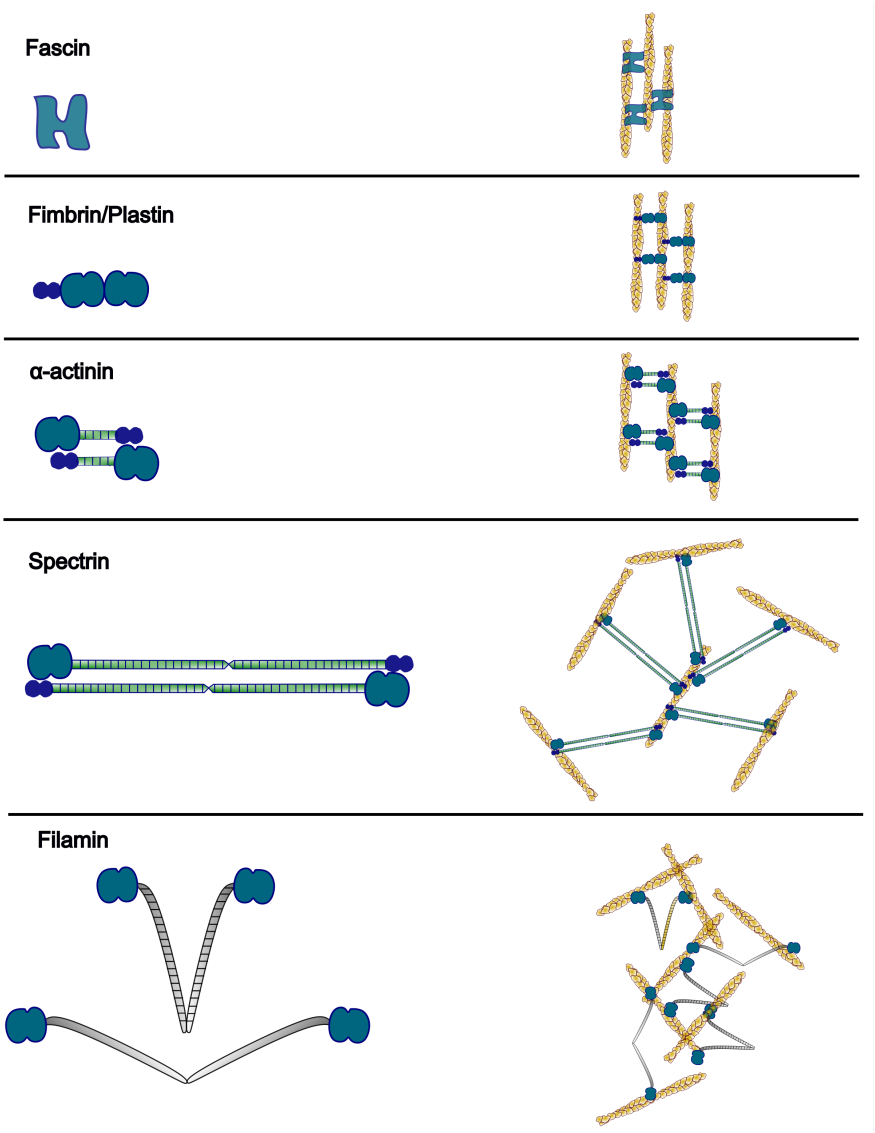

FIGURE 1.5. Actin filament crosslinkers: building structural and mechanical diversity in actin networks. Smaller cross-linking proteins that are more globular, like fascin, or have more than one actin binding site, such as fimbrin or α-actinin, primarily form actin bundles. Larger crosslinking proteins, including spectrin or filamin, create more space between actin filaments and generally form actin meshworks.

Different crosslinkers perform different functions in cells, but how and why they are sorted to those locations has not been fully worked out. In fact, several crosslinkers can localize simultaneously in the same subcellular structures, which may suggest redundant functions (Bartles, 2000; Wu, Bähler and Pringle, 2001; Elkhatib *et al.*, 2014; Foley and Young, 2014; Lamsoul, Dupré and Lutz, 2020). Yet, not all crosslinkers are necessarily present in the same cell or tissue (Esue et al., 2009; Tseng et al., 2002; Washington & Knecht, 2008), which can also indicate specificity.

It is rather intuitive that the molecular properties of the crosslinking proteins largely determine the microstructure, viscoelastic properties and dynamics of the resulting networks.

There are three properties of actin crosslinkers that have an influence in the mechanical properties of actomyosin network: 1) concentration and density; 2) the number and nature of the binding domains (ABDs); 3) spacer domains, which include both crosslinker length and crosslinker stiffness (Lieleg, Claessens and Bausch, 2010). Most of the information available of how crosslinkers affect these properties comes from *in vitro or in silico* experiments, essentially because the diversity of behaviours the network may produce is already complex enough using one type of crosslinker, that adding the *in vivo* complexity, where they probably coexist with other crosslinkers and other proteins, would significantly complicate the analysis. Additionally, most studies of actomyosin networks to date addressed mainly the crosslinker number or density (Coleman and Mooseker, 1985; Kim *et al.*, 2009; Murrell and Gardel, 2014; Ennomani *et al.*, 2016; Belmonte, Leptin and Nédélec, 2017; Descovich, 2017; Stam *et al.*, 2017; Weirich *et al.*, 2021). This is because it is a critical parameter for the transition of a network from the entangled (not crosslinked) to the crosslinked phase. It essentially dictates the average crosslinker distance - also known as the percolation threshold - at which the crosslinker density is high enough to allow for an overall network response (reviewed in Alvarado *et al.*, 2017). A recent study has proposed that plastin and βH-spectrin different sizes may underlie their synergy in cytokinesis in the *C. elegans* early embryo (Sobral *et al.*, 2021), however more studies will be needed to disclose whether that happens for all different-sized crosslinkers and work out the mechanical principles behind those network changes.

The crosslinker length is defined by the number of spacer domains. While small crosslinkers, such as α-actinin, plastin or fascin tend to form tightly packed F-actin bundles (Skau *et al.*, 2011; Winkelman *et al.*, 2016), long ones like filamin or spectrin generally form meshworks, which can be more or less flexible (Kasza et al., 2010; Machnicka et al., 2014), as depicted in Figure 1.5. However, it has been hypothesized that even long crosslinkers can also form bundles under certain conditions (Lieleg, Claessens and Bausch, 2010). In addition, crosslinkers of similar size have been shown to control filament spacing and limit the binding of crosslinkers of different sizes (Winkelman *et al.*, 2016), revealing spatial segregation effects, even though this may apply only from small towards large crosslinkers and not the other way around.

The number and nature of ABDs may also influence the behaviour of the network. The classical structure of an actin crosslinker, including α-actinin, plastin, filamin or spectrin, consists of two ABDs with two well-conserved calponin-homology (CH) domains. However, these proteins may act as monomers, or form higher order structures, such as dimers or

tetramers (Lieleg, Claessens and Bausch, 2010). This can interfere with how many filaments they can simultaneously bridge. Moreover, other scaffolding proteins that can also bundle actin filaments, such as anillin or septin, as well as myosin itself as an active crosslinker, may have varying affinities to actin and have extra functions and regulatory mechanisms.

Here, fimbrin/plastin structure and function are covered separately, as the role of this crosslinker will be addressed in several experiments throughout this thesis. Molecular and structural details of other crosslinkers are out of the scope of this specific work.

Fimbrin/Plastin

The largest family of actin crosslinkers, which includes the proteins fimbrin, α-actinin, and β-spectrin, is characterized by a conserved ABD, with a sequence of around 250 amino acids (Matsudaira, 1991), which is itself composed of two 125 residue CH domains, tandemly arranged.

Fimbrin, also known as plastin, is quite unique among this family, as it harbours two tandem repeats of the ABD within a single polypeptide chain. Because the ABDs are very close to each other, fimbrin is known to form F-actin tight bundles, which has been implicated in several biological processes, including cytokinesis in yeast (Wu, Bähler and Pringle, 2001) and *C. elegans* embryos (Ding, Ong, Hara, Wongsantichon, Toyama, Robert C Robinson, *et al.*, 2017; Leite *et al.*, 2020), as well as host cell invasion by enteropathic bacteria (Prévost *et al.*, 1992; Adam *et al.*, 1995; Galan and Zhou, 2000).

Fimbrin was discovered in 1980, by Bretscher and Weber, as an actin-associated protein present in the microvillus core of intestinal epithelial cells, as well as in membrane ruffles of tissue culture cells and structures containing highly ordered microfilament bundles (Bretscher and Weber, 1980). A year after its identification, it has been shown to bind actin *in vitro* (Bretscher, 1981) and to specifically form bundled structures (Glenney *et al.*, 1981). There are three conserved fimbrin/plastin human isoforms, I-, L- and T-plastin, each encoded by a different gene and with tissue-specific expression (Lin *et al.*, 1993).

Domain structure. Fimbrin/plastin is a monomeric protein comprising a N-terminal Ca^{2+}-binding regulatory domain with two EF-hand motifs, followed by two closely arranged ABDs – ABD1 and ABD2 – assembled in a core domain (N Volkmann *et al.*, 2001). This tight arrangement of the ABDs has been attributed to the formation of densely-packed bundles and allosteric regulation of both domains (Schwebach *et al.*, 2022). Although the structure of the core domain has been shown in yeast and plants, it has not been uncovered for animal plastins (Klein *et al.*, 2004). Each ABD contains two tandem CH domains that interact with subdomains 1 and 2 of adjacent actin subunits in the filament (N Volkmann *et al.*, 2001; Schwebach *et al.*,

2017, 2022). Even though the two CH domains, CH1-2 in ABD1 and CH3-4 in ABD2 are homologous, they show very different affinities for actin. For example, whilst ABD2 of human L-plastin binds F-actin very tightly with a low dissociation constant in the nanomolar range, ABD1 binding is weak, with dissociation constant in the micromolar range. Both ABDs interact with actin in a similar manner, but ABD2 seems to have higher affinity. The location of EF-hands relative to the ABD core has not been disclosed, but they are predicted to be docked at the loop-rich region between CH2 (ABD1) and CH3 (ABD2)**.**

Bundling mechanism. Fimbrin has been shown to crosslink actin filaments in both parallel and antiparallel arrangements (Skau *et al.*, 2011; Mei *et al.*, 2022). The dense parallel bundles have approximately 12 nm inter-filament distance (Matsudaira *et al.*, 1983; N Volkmann *et al.*, 2001), and it is spaced after every ~13.5 actin monomers along the filaments (N Volkmann *et al.*, 2001). This bundling mechanism is achieved by the separation of the ABD1 and ABD2 upon actin binding, which is facilitated by the flexibility of its interdomain linkers (Mei *et al.*, 2022; Schwebach *et al.*, 2022). However, the details are not completely understood. A cryo-EM structure analysis using machine learning suggested that ABD2 binds first to the actin filament forming a pre-bundling state that released the interdomain inhibition, thus reorienting ABD1 for a second filament binding, either in parallel or antiparallel orientation (Galkin *et al.*, 2008; Mei *et al.*, 2022). However, biochemical studies suggested otherwise that ABD1 is always accessible for actin binding and binds first, whilst ABD2 binding is further regulated by autoinhibition due to ABD1 and Ca^{2+} binding (Schwebach *et al.*, 2017, 2022).

Regulation by Ca^{2+}

Actin bundling, but not binding, activity of human plastin is known to be inhibited in the presence of Ca^{2+} (Namba *et al.*, 1992; Miyakawa *et al.*, 2012; Schwebach *et al.*, 2017). It has been proposed that, in the presence of Ca^{2+}, ABD2 is masked by the Ca^{2+}-binding regulatory domain and therefore, only ABD1 would be available for actin binding. This constraint is supposedly released when Ca^{2+} dissociates from the regulatory domain, thus ABD2 becomes available for filament binding (Schwebach *et al.*, 2020). The inhibitory allosteric interaction of ABD1 with ABD2 enables fine-tuning of the plastin's crosslinking strength as the release of this inhibition by a phospho-mimicking S406E mutation (reproducing a physiologically relevant modification) converts human L-plastin into a highly potent bundling protein, essentially resistant to Ca^{2+} (Schwebach *et al.*, 2017, 2022).

Myosin

Myosins constitute a superfamily of cytoskeletal motor proteins that play essential roles in several cellular processes that require both force generation and translocation. No cell on our planet can operate in the absence of these molecular machines. More than 140 myosins have been reported in eukaryotes (Vale, 2003) and the human genome is thought to contain 40 genes that encode myosin motor proteins. These proteins can have distinct head, neck and tail domains (described in detail in the sections below), and according to this, they are usually divided in categories and classes. Phylogenetic analysis of their conserved heads, domain structure, amino acid sequences and organism distributions have produced 35 different myosin classes (Richards and Cavalier-Smith, 2005; Foth, Goedecke and Soldati, 2006; Odronitz and Kollmar, 2007). Most myosins belong to class II and, together with actin, make up the major contractile proteins of cardiac, skeletal and smooth muscle. Here, we will focus on class II myosins, particularly the non-muscle version.

The discovery of non-muscle myosin II (NMII) is closely linked to the history of muscle contraction (reviewed in A. G. Szent-Györgyi, 2004). The skeletal muscle myosin, myosin II (MII), was the first cytoskeletal motor protein identified. Back in 1864, Köhler purified a viscous substance from muscle, to which he called myosin, that he thought to be somehow related with the muscle contractile properties (Szent-Györgyi, 2004; Hartman and Spudich, 2012). Only in 1939, myosin has been identified as an ATPase composed of two components, myosin and actin, which has put forward the concept of myosin and actin being two types of interacting filaments (Engelhardt and Liubimova, 1994). Proteolytic studies in the 1950s revealed the main myosin structural and functional constituents: a heavy meromyosin (HMM) that interacted with actin and contained the ATPase activity and a light meromyosin that enabled the formation of myosin filaments (Szent-Györgyi, 2004). Myosin light chains were also identified around this time. All these discoveries, together with crystallographic and functional evidence of the different bands that comprise the muscle sarcomere, culminated in Huxley proposing, in 1963, that muscle contraction was due to the sliding of actin and myosin filaments with respect to each other (Huxley, 1963).
Ever since, an incredible amount of research has focused on understanding myosin structure and functionality, and a vast catalog of information has been gathered. We now know that outside muscle, myosin-driven contraction may not follow the sarcomeric mechanism, as actin networks seem to be generally disordered and randomly oriented.

NMII has a fundamental role in processes that require cellular reshaping and movement, such as cell adhesion, cell migration and cell division (Hartman & Spudich, 2012a; Krendel & Mooseker, 2005; Vicente-Manzanares et al., 2009), in which its actin crosslinking and motor functions are regulated by phosphorylation and the irability of to form filaments.

Myosin domain structure

The myosins of class II, including muscle myosin II and non-muscle myosin II, are formed by two heavy chains and two copies of each of the two light chains, and can be subdivided into three major functional domains: the head, the neck and the tail. Similarly to MII, NMII consists of three pairs of chains: two heavy chains (NMHC) of 230 kDa, two 20 kDa regulatory light chains (RLCs) that regulate NMII activity and two 17 kDa essential light chains (ELCs) that stabilize the heavy chain structure (Vicente-Manzanares *et al.*, 2009).

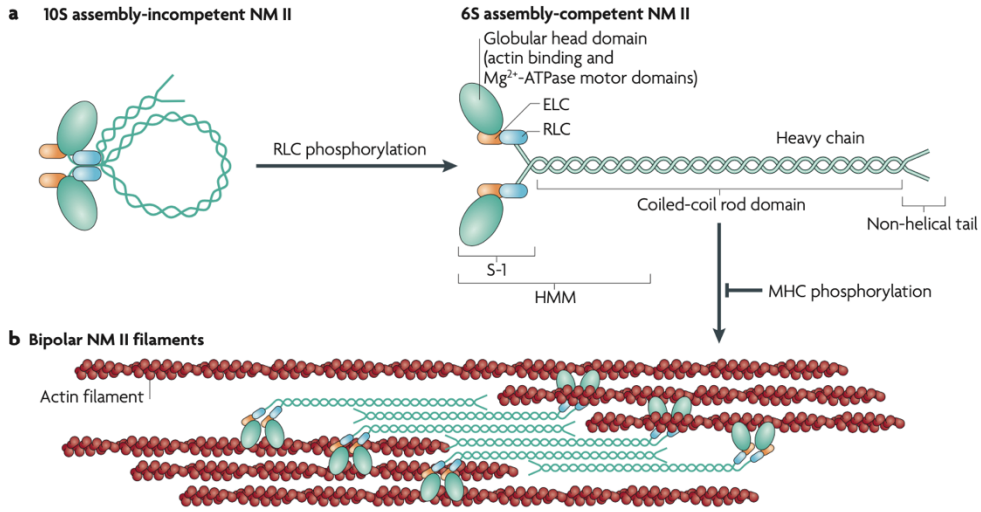

FIGURE 1.6. Myosin domain structure and bipolar filament assembly. Top left: the domain structure of NMII is shown. It forms dimer through interactions between the α-helical coiled-coil rod domains. The globular head domain contains the actin-binding regions and the Mg^{2+}-ATPase motor domains. The ELCs and and the RLCs bind to the heavy chains at the lever arms. In the absence of RLC phosphorylation, NM II forms a compact molecule through a head to tail interaction. This results in an assembly-incompetent form (10S) that is supposedly unable to associate with other NMIIs. Top right: upon RLC phosphorylation, the 10S structure unfolds and becomes an assembly-competent form (6S). The S-1 fragment of NM II contains the motor domain and neck, while Heavy meromyosin (HMM) is a fragment that contains the motor domain, neck and enough of the rod to effect dimerization. Bottom: NM II molecules assemble into bipolar filaments through interactions between their rod domains. These filaments bind to actin through their head domains and the ATPase activity of the head enables a conformational change that moves actin filaments in an anti-parallel manner. Bipolar myosin filaments link actin filaments together in thick bundles. Image from (Vicente-Manzanares et al., 2009), used under permission.

The two globular head domains at the N-terminus contain a binding site for both ATP and actin and are responsible for force generation. These are followed by the neck regions, which bind the two light chains, RLC and ELC. The neck domain acts as a lever arm to amplify head

rotation upon conversion of the chemical energy of ATP into mechanical force to move the myosin head. The neck domain is followed by a long α-helical coiled coil and ends in a short non-helical tail at the C-terminus. The coiled-coil tail bundles itself with the tails of other myosins. These tail-tail interactions result in the formation of large bipolar thick filaments that can have up to a hundred myosin heads oriented in opposite directions at the two ends of the myosin filament (Vicente-Manzanares *et al.*, 2009).

Myosin from either muscle or nonmuscle cells can form bipolar thick filaments by antiparallel association of the heavy chain tail domain (Clarke & Spudich, 1974; Huxley, 1963). It is thought that myosin must be in the form of bipolar thick filaments to carry out its role in cytokinesis.

Mechanism of filament sliding and force generation

As abovementioned, EM experiments of muscle tissue in the 1960s revealed myosin cross-bridges from myosin thick filaments connecting the actin filaments. This was coupled with findings by Lymn and Taylor in 1971 on the myosin enzymatic cycle, according to which the actomyosin complex was dissociated by ATP binding and that the power stroke was most likely associated with phosphate release after the hydrolytic step (Lymn and Taylor, 1971).

The contractile activity of NMII on actin filaments depends on the mechanochemical cycle of NMII molecules, through which they convert chemical energy into mechanical force. The NMII-based filament sliding, also called the ATPase cycle, can be described according to the *swing cross-bridge model* (Spudich, 2001) and is depicted in Figure 1.7. The process can be divided in four steps: 1) ATP-bound NMII is free, not associated with the actin filament; 2) when ATP is hydrolyzed by the Mg^{2+}-actin-dependent ATPase activity of the head domain, NMII binds to the actin filament; 3) the phosphate (P_i) resulting from this reaction is released, triggering a conformational movement that slides the actin filament with respect to the NMII bipolar filament – the power stroke - corresponding to a 10 nm/step, on average; 4) the exchange of ADP for ATP restarts the cycle. Mechanical work at a cellular level results from the concerted movement of many bundles of actin filaments propelled by multiple NMII bipolar filaments. A very important concept is the duty ratio, which can be defined as the fraction of time during which NMII remains bound strongly to actin in the ATPase cycle (Encyclopedia of signalling molecules, Nonmuscle myosin II, Manzanares, 2018 Edition).

Regulation of myosin activity

The regulation of Mg^{2+}-ATP hydrolysis and filament formation of NMII involves the reversible phosphorylation of specific amino acids present in the 20 kDa RLCs and the heavy chains. The function of the ELC pair is to stabilize the NMHC and there is no evidence that they undergo reversible phosphorylation.

Regulation of NMII by RLC phosphorylation

The regulation of NMII as well as that of smooth muscle myosin is dependent on the reversible phosphorylation of the RLC on Ser19. In mammalian cultured cells, there is phosphorylation of both Ser19 and Thr18 (reviewed in Vicente-Manzanares *et al.*, 2009). This phosphorylation increases the Mg^{2+}-ATPase activity of myosin in the presence of actin by regulating the conformation of the myosin heads (Wendt *et al.*, 2001; Somlyo and Somlyo, 2003). Still, it does not seem to have a significant effect on the affinity of myosin for actin (Sellers, Eisenberg and Adelstein, 1982). This may indicate that dephosphorylated myosin may have the same affinity for actin.

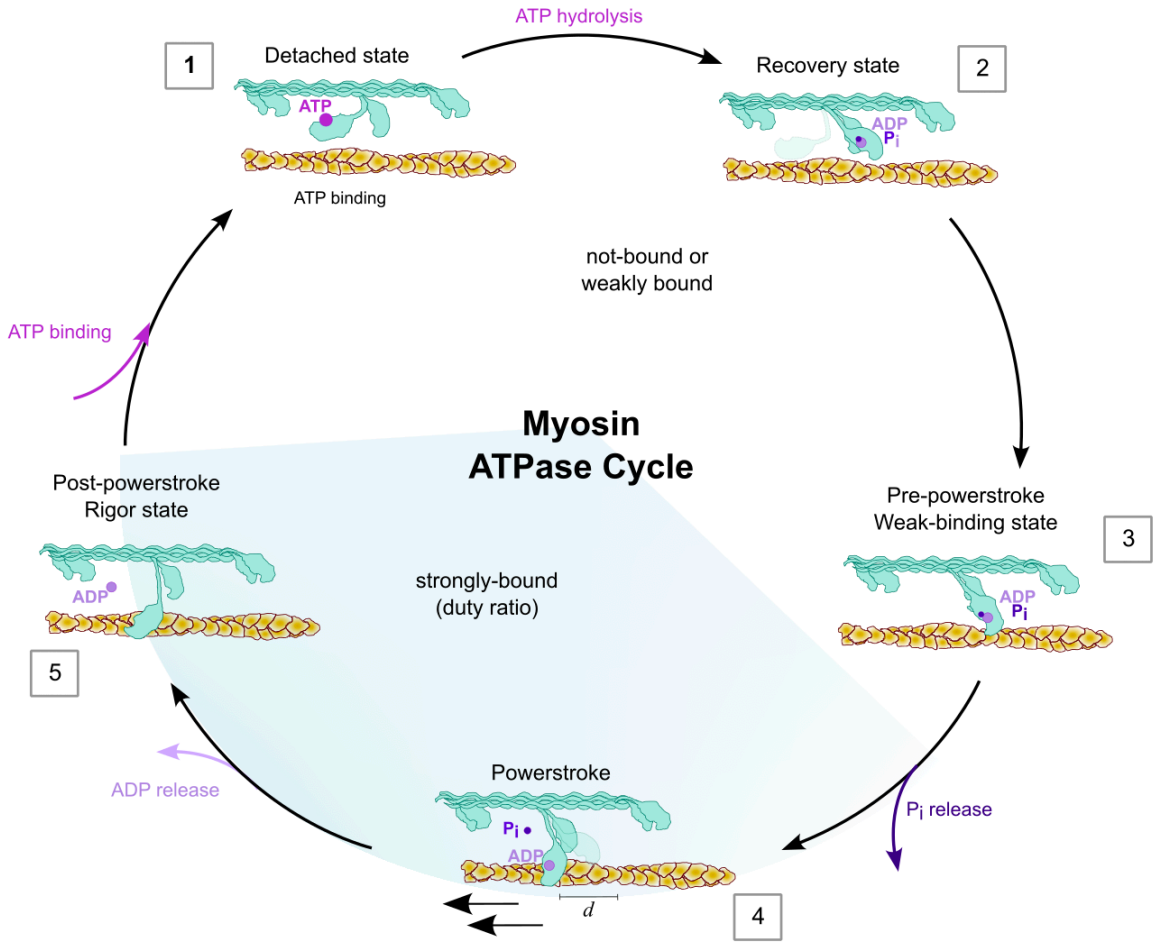

FIGURE 1.7. Myosin mechanochemical ATPase cycle. 1 - ATP binding dissociates NMII from actin - actin release. 2 – Myosin's motor head hydrolyzes ATP and transitions into a pre-power stroke/recovery state. 3 – The motor head re-attaches to actin in a weak-binding state. 4 - The release of the phosphate (Pi) triggers a conformational change that promotes movement and powers the contraction of actin filaments - the powerstroke. 5 - Finally, post-powertstroke, ADP is released, but the myosin head remains tightly bound at the new position before dissociating - rigor state. The binding of another ATP molecule restarts the cycle. The light blue colored region corresponds to the duty ratio - the portion of the cycle during which the NMII motor head is strongly bound to actin.

In vitro experiments revealed that phosphorylation of the RLC also regulates the assembly of NMII bipolar filaments (Scholey, Taylor and Kendrick-jones, 1980). Indeed, in the presence of ATP, dephosphorylated NMII folds into a compact conformation, in which one head blocks the second head of the same molecule through an asymmetrical interaction. This is called the assembly-incompetent form (Burgess et al., 2007; Thomas Wendt et al., 2001; Woodhead et al., 2005). Phosphorylation of the RLCs has been appointed as responsible for the transition from this "closed" compact faster sedimenting (10S) structure to an elongated slower sedimenting (6S) one, which forms bipolar filaments at physiological ionic strengths. A very important point to keep in mind is that these changes in conformation have been shown *in*

vitro, where conditions are tightly controlled, but lack the *in vivo* complexity. As such, there is currently no strong evidence that they also occur this way *in vivo*.

Several kinases have been shown to phosphorylate the RLC on Ser19 or both Thr18 and Ser19 to activate myosin. These include myosin light chain kinase (MLCK), Rho-associated, coiled coil-containing kinase (ROCK), citron kinase, leucine zipper interacting kinase (ZIPK) and myotonic dystrophy kinase-related CDC42-binding kinase (MRCK). However, the activation mechanisms for these kinases are different. For example, MLCK is activated through Ca^{2+}-calmodulin, which seems to be specific for the NMII RLCs, whilst ROCK and citron kinase are activated downstream of the small GTP-binding protein RhoA and, unlike MLCK, phosphorylate several substrates apart from the NMII RLCs (reviewed in Vicente-Manzanares *et al.*, 2009). In addition, even though ROCK can phosphorylate the RLC directly, there is evidence that it acts primarily to inhibit the most important myosin phosphatase, protein phosphatase 1 (PP1), which is responsible for NMII dephosphorylation (Matsumura and Hartshorne, 2008). Protein kinase C (PKC) acts differently than all these kinases, as it phosphorylates RLCs on Ser1, Ser2 and Thr9, which makes the RLC a worse substrate for MLCK, thus decreasing the activity of NMII (Nishikawa *et al.*, 1984).

NMII monomers assemble into bipolar filaments by antiparallel association of their elongated coiled-coil helical tails. The filaments of non-muscle myosin II are appreciably smaller than filaments of muscle myosins, with lengths of about 300 nm, consisting of ~30 monomers for filaments of NMIIA and NMIIB, and ~14 monomers for filaments of NMIIC (Billington *et al.*, 2013). As described originally for smooth muscle myosin (Suzuki *et al.*, 1982; Trybus, Huiatt and Lowey, 1982; Ikebe, Koretz and Hartshorne, 1988), filaments of unphosphorylated NMII in physiological buffer are thought to depolymerize extensively to monomers upon addition of ATP, and repolymerize upon phosphorylation of the RLC (Scholey, Taylor and Kendrick-jones, 1980; Scholey *et al.*, 1982) at Serine 19 or at both Serine 19 and Threonine 18 (Ikebe, Hartshorne and Elzinga, 1986). An explanation of this phenomenon has been that NMII filaments are in equilibrium with monomers, a mixed population of compact folded structures (10 S monomers) that are unable to form filaments, and of extended structures (6 S monomers) that can polymerize. Addition of ATP to non-RLC phosphorylated myosin favors the folded monomer, in which the motor domains of the two heavy chains associate (Wendt *et al.*, 1999, 2001) and the helical tail folds back and interacts with the RLC (Jung *et al.*, 2011). Phosphorylation of the RLC inhibits both the interaction of the two motor domains (Ni *et al.*, 2012; Taylor *et al.*, 2014), and the interaction between the motor domain and tail, thereby shifting the monomer equilibrium from folded to unfolded structures, and enhancing filament polymerization in the presence of ATP (Cross, 1988).

Whether the two heads of a myosin molecule act independently or cooperatively remains under debate, as there is evidence supporting both scenarios (Margossian and Lowey, 1973, 1978; Cooke and Franks, 1978; Harada *et al.*, 1987; Toyoshima *et al.*, 1987; Conibear and Geeves, 1998; Katayama, 1998; Ito *et al.*, 1999). Specifically, it was shown that, at the single-molecule level, the double-headed myosin produces twice the unitary displacement and force of single-headed myosin (Tyska *et al.*, 1999). A more recent study showed that the HMM heterodimer produces the same step size whether it is single- or double-headed, and twice the step size of a single-headed S1. This suggests that only one of the two heads displaces actin, and that the presence of a second head (presumably inactive) is necessary for the other active head to produce a maximal displacement. Here, the second head could act by weakly associating with actin, or by stabilizing the head–rod junction, thus minimizing unfavorable orientations of the active head (Kad *et al.*, 2003).

Regulation of NMII by heavy-chain phosphorylation

The regulation of myosin activity by NMHC phosphorylation is far less understood than that by the RLC. In *Dictyostelium*, myosin filament assembly is regulated by heavy-chain phosphorylation of three threonine residues in the tail at positions 1823, 1833, and 2029 (Vaillancourt, Lyons and Côté, 1988; Lück-Vielmetter *et al.*, 1990; T T Egelhoff, Lee and Spudich, 1993). The role of thick filament formation *in vivo* has been studied by making mutant myosins where each of the three threonines has been converted to either alanine (3XAla-myosin) or aspartic acid (3XAsp-myosin). When the three threonines are phosphorylated, filament formation i*n vitro* is inhibited (Kuczmarski and Spudich, 1980; Pasternak *et al.*, 1989; Ravid and Spudich, 1989; T T Egelhoff, Lee and Spudich, 1993) and *D. Discoideum* cells expressing 3XAsp-myosin that cannot form bipolar thick filaments fail to divide when grown in suspension (Thomas T. Egelhoff, Lee and Spudich, 1993). These observations suggest that myosin must be in bipolar thick filaments to be able to correctly localize in the cortex and carry out its motor function during cytokinesis. The role of the heavy-chain phosphorylation in other organisms, such as *C. elegans* or mammalians has not been defined and the equivalent region of the tail is not so well conserved among species. Indeed, several potential phosphorylation sites exist near the C-terminus in *C. elegans*, including both the coiled-coil domain and the non-helical tail. In each case phosphorylation of the heavy chain either dissociates myosin filaments or prevents their formation *in vitro*.

Whether the two regulatory mechanisms of NMII activation need to occur for myosin bipolar filaments to form remains to be clarified. According to the traditional view that is commonly illustrated in textbooks, myosins with dephosphorylated RLCs cannot form thick filaments (Vicente-Manzanares *et al.*, 2009) The schematic that is generally presented to illustrate

myosin regulation through RLC phosphorylation (see Figure 1.6) shows the myosin hexamer in a closed conformation, with the tail closed onto the neck, meaning it cannot interact with other tails from other myosins. Only when RLC is phosphorylated on Thr18 and Ser19, the molecule opens up and the tail becomes available to interact with other tails. This implies that only myosin hexamers that carry phosphorylated RLCs are included in bipolar filaments, as these form by tail-tail interactions and therefore, tails must be available to interact. So, according to this model, if heavy chain phosphorylation is also necessary for bipolar filament formation, then RLC phosphorylation must precede it.

Scaffolding proteins

Anillin

Anillin was first isolated from *D. melanogaster* embryos as an F-actin-binding protein in 1989 (Miller, Field and Alberts, 1989). It is a conserved 124 kDa protein with a unique multi-domain structure that implicates it in the connection of several structural and regulatory elements (Piekny and Glotzer, no date). It is mainly involved in cell cortex dynamics as a scaffold during cytokinesis (Piekny and Glotzer, no date; Piekny and Maddox, 2010), and cellularization, including in *Drosophila* cells (Christine M. Field and Alberts, 1995) or *C. elegans* embryos (Maddox *et al.*, 2007), where it establishes contractile ring asymmetry together with septins.

Numerous anillin-like protein homologues exist in different organisms and seem to play different, non-redundant functions(Maddox et al., 2005; Saha & Pollard, 2012; Tasto et al., 2003; Toya et al., 1999).

At the N-terminus of the protein, there are actin- and myosin-binding domains. At the C-terminus, there is a conserved PH domain essential for anillin functionality and an anillin homology domain (AHD) that directly interacts with RhoA (Piekny and Glotzer, no date). Even though this domain may not be conserved among species, it is thought to also interact with the RhoGEF Ect2, the RhoGAP and microtubules(Naydenov, Koblinski and Ivanov, 2021). It is not well-established whether these binding partners compete for binding during different cellular processes involving the actomyosin cortex.

Anillin was shown not only to bind, but also to bundle F-actin *in vitro*, therefore it can also act as an actin crosslinker. Still, the protein's structure differs from that of a traditional actin crosslinker, acting more as a scaffolding protein. Scaffolds are expected to act as tethers that bring multiple components of a signaling pathway together into a complex, thus favouring their interactions and providing spatiotemporal regulation (Langeberg and Scott, 2015). For this reason, the effect of anillin perturbations on the cortex mechanical properties is still not well-understood and may be context- and organism-dependent.

Septins

Septins were first discovered by Hartwell in 1971 in the budding yeast *S. cerevisiae* using mutagenesis screens to find genes that were essential for cell division (Hartwell, 1971). These proteins are highly conserved in eukaryotes and considered by some, the fourth component of the cytoskeleton (Mostowy and Cossart, 2012). Contrarily to actin or microtubules, Septin complexes are non-polar, less dynamic and more stable. The number of septin genes is variable among species and they also seem to play redundant functions. While humans are known to have thirteen, *S. cerevisiae* has seven and *C. elegans* only two (Russell and Hall, 2011).

They are small GTP-binding proteins of around 30-65 kDa that form hetero-oligomeric complexes. Interactions between these hetero-oligomers allows them to form rod-shaped complexes, which can then organize into supramolecular structures that include filaments, networks, and rings. Septin complexes are generally tetrameric in *C. elegans*, hexameric in humans and octameric in *S. cerevisiae*. Their functions range from localizing other proteins by working as scaffolds (Kinoshita, 2006) or forming a barrier to the diffusion of molecules in cell compartments and diffusion of membrane-bound proteins in the cell cortex (Bridges and Gladfelter, 2015).

The mechanisms of septin assembly are not very well understood, but they are likely to be context-dependent. A recent work in fission yeast suggested that the anillin-like protein Mid2 bundles septin filaments in an orientation parallel to the division plane during cytokinesis, favoring their compaction into two septin rings that delineate the furrow (Arbizzani *et al.*, 2022). Also, it has been suggested that membrane binding controls ordered self-assembly of animal septins (Szuba *et al.*, 2021). Computational simulations suggest that increased filament flexibility and reduced filament fragmentation promote assembly of septin rings, whereas reduced flexibility in crowded environments promotes local septin filament alignment (Woods and Gladfelter, 2021). Interestingly, they have been shown to promote the formation of actin rings by crosslinking F-actin into curved bundles (Mavrakis *et al.*, 2014).

Role of cortical proteins in regulating mechanical properties of the cell cortex

Most of the information available on how specific cortex constituents affect its mechanical properties relies on *in vitro* and *in silico* approaches, which are incredibly informative in terms of uncoupling different and isolated contributions. Nevertheless, at some point, these

approaches must be integrated with increasing degree of complexity, so they more closely reproduce *in vivo* scenarios, or be effectively tested *in vivo*.

It is now well-established that myosin motors are the primary force generators in the cell cortex (Clark et al., 2014; M. Murrell et al., 2015; Guillaume Salbreux et al., 2012).
However, the efficiency of that force generation, as well as its propagation across the network depends not only on the concentration of motors, but also on the actin density, network architecture and intrinsic mechanical properties of the constituents, which can impose both structural and spatial constraints as well as limitations due the intrinsic mechanical behavior of the cortical material. These strictly depend on the actin dynamics (assembly, disassembly) controlled by different regulatory proteins as well as the number and type of crosslinking proteins.

As already discussed, crosslinked actin filaments self-organize into a panoply of architectures, from disordered meshworks to ordered bundles. Several studies have already shown that crosslinked actin networks exhibit a bell-shape behavior, with an intermediate level of crosslinking favoring maximal contraction (Bendix *et al.*, 2008; Ennomani *et al.*, 2016; Belmonte, Leptin and Nédélec, 2017). Lower levels of crosslinking do not allow sufficient connectivity between filaments and this absence of percolation leads to only local contraction, whereas higher crosslinking levels essentially stall the network due to crowding effects Interestingly, a similar behavior is observed when regulators of actin cortex thickness, density and architecture are perturbed. Depleting both formin - lower cortex thickness - and cofilin or capping protein – higher cortex thickness – lead to a reduction in cortical tension (Chugh *et al.*, 2017).

Formin inhibition has been shown to result in the formation of large blebs and decrease in cortical stiffness, as measured by atomic force microscopy (AFM) (Bovellan *et al.*, 2014; Fritzsche *et al.*, 2016). Conversely, ARP2/3 inhibition results in smaller blebs and presumably, increased stiffness (Cao *et al.*, 2020). The addition of chemical compounds that inhibited myosin or actin polymerization consistently showed a reduction in cortical tension, while adding the ARP2/3 inhibitor CK666 led to a pronounced increase in cortical tension (Cartagena-Rivera *et al.*, 2016). Moreover, as the ARP2/3 complex is known to nucleate new actin filaments on the side of pre-existing ones, it can create crosslinking points in the network and therefore have an effect in the overall cortex viscosity, which has never been addressed or measured. Indeed, during cytokinesis in *C. elegans* embryos, the ARP2/3 is excluded from the equatorial furrowing region, that is exclusively populated by the formin nucleator (Chan *et al.*, 2019), which may indicate that cortical tension may be amplified by a linear array of actin filaments rather than a branched network, which would rather stabilize the surrounding cortex.

Importantly, this may happen because linear filaments are easiest to align by myosin motors than the branched ones, leading to a higher degree of nematic alignment that also amplifies tension.

In a recent study, ADF/cofilin has been suggested to generate torsional stress on crosslinked actin filaments while severing them, generating torques that increase filament fragmentation, which raises the possibility that crosslinker filaments may be more prone to severing than isolated filaments (Wioland, Jegou and Romet-Lemonne, 2019).

The contribution of scaffolding proteins such as anillin or the septins may be harder to establish in *in vivo* scenarios due to the several functions they play and the number of binding partners.

Additionally, not all types of network architecture favor contraction the same way, even if the actin and motor densities are the same. For example, it has been proposed that the presence of mixed polarity actin bundles formed by rigid crosslinkers (e.g. α-actinin) supports slow, bidirectional myosin II movement onto the filaments, with periods of stalled motion, whereas those same mixed-polarity bundles formed by compliant and large crosslinkers (e.g. filamin) support fast, bidirectional myosin movement with no traps. Numerical simulations predict that these sites of stalled myosin motion correspond to regions of high and persistent force where filament polarity is balanced (Weirich *et al.*, 2021).

Still, apart from differences in crosslinker size, which control inter-filament spacing, differences in crosslinker stiffness, which regulate mechanical compliance of the bundle, should also be accounted for, as decreasing the stiffness of the bundle on which motors build up force will likely decrease the total force generation. Importantly, these two parameters must not to be extrapolated from each other, as a bigger crosslinker may or may not be more compliant, meaning a direct relationship between the concepts does not apply. In fact, changing the inter-filament spacing likely impacts the number of accessible binding sites for myosin motors, whereas changes in the bundle compliance may have an impact in the force-dependent motor binding affinity (Albert, Erdmann and Schwarz, 2014; Stam *et al.*, 2015).

Turnover of cortex components is likely to influence cortex viscoelastic properties and contractility, as it allows the network to be renewed and essentially defines a typical timescale for tension propagation and mechanical deformation (Salbreux, Charras and Paluch, 2012; Turlier, Audoly, Prost and J.-F. Joanny, 2014; Hiraiwa and Salbreux, 2016). Actin is estimated to turn over within a few tens of seconds in the cortex (Mukhina, Wang and Murata-Hori, 2007; Fritzsche *et al.*, 2013). Myosin activity has been shown to increase the actin turnover rate at the CR (Guha, Zhou and Wang, 2005; Murthy and Wadsworth, 2005a), whereas the presence of actin crosslinkers may decrease it, as it happens when α-actinin is overexpressed (Mukhina, Wang and Murata-Hori, 2007). In *D. Discoideum*, turnover of cortical components is slower at the equator during cytokinesis, where tension must be higher, than at the poles (Srivastava

and Robinson, 2015). In HeLa cells, however, an actin population nucleated by the formins showed slower turnover than a population resulting from addition of monomers to free barbed ends (Fritzsche *et al.*, 2013). Surprisingly enough, the turnover of myosin RLC and α actinin have been suggested to be faster than that of actin.

Also, crosslinkers that have a fast turn over led to slower ring ingression, and others that turn over slower proved to be crucial to generate cortical tension (Reichl *et al.*, 2008). Overall, the exact influence of the turnover of cortex proteins on its mechanical behavior is not well understood, partially due to the lack of reliable probes and tools to measure actin turnover (as formins seem to exclude fluorescently tagged G-actin).

Cytokinesis – the last stage of cell division

Cytokinesis is the last stage of cell division in which the cytoplasmic contents of one cell are physically partitioned into two daughter cells. It takes place concomitantly with the later stages of nuclear division in both mitosis and meiosis. The microtubule-based mitotic spindle apparatus partitions and transports duplicated chromatids into the cytoplasm of the separating daughter cells, thereby ensuring that the genetic material is conserved from one generation to the next (Alberts *et al.*, 2002). When a cell undergoes cytokinesis, it is crucial that it occurs at the right time and place: for instance, it must not occur at metaphase, when the chromatids have not separated yet; also, it must occur at the right place so that two segregating sets of chromosomes separate properly, and each daughter cell receives a complete set (Rappaport, 1986; Alberts *et al.*, 2002). As such, this process requires an intricate crosstalk between the mitotic spindle and the cortical actomyosin network, so the sister chromatids are properly segregated during division (Ramkumar and Baum, 2016).

When the cell goes into anaphase, the isotropic metaphase actin cortex progressively polarizes as the anaphase spindle starts elongating. This means symmetry must be broken so inhomogeneities are introduced in the actomyosin cortical network and different regions of the cortex acquire different properties (Li and Bowerman, 2010; Sugioka, 2022). That is generally achieved by two spatially distinct, concomitant, and, believed by some, independent mechanisms, where actomyosin components are cleared from the cell poles and accumulate at the cell equator. Due to these changes in mechanical properties, a contractile ring composed of tightly packed F-actin bundles and myosin motors assembles at the cell equator (Figure 1.8). Cytokinesis can be divided in three subsequent stages: 1) division plane specification and contractile ring assembly 3) Ring constriction; 4) abscission. In this manuscript, we will only focus on the first two phases.

Division plane specification and contractile ring assembly

Precise positioning of the division plane between the two masses of segregated chromosomes is essential to guarantee equal distribution of the genetic material between the two daughter cells. Therefore, changes in the actomyosin cortex must be spatiotemporally coordinated with the spindle apparatus so the ring assembles and ingresses at the proper position.

There are currently three models of the molecular signals that induce the formation of a furrow during cytokinesis. These are depicted on Figure 1.9 and include 1) central spindle stimulation; 2) astral stimulation, and 3) polar relaxation. Noteworthy, these models are not necessarily mutually exclusive (e.g. spindle- and aster-dependent have been shown to coexist *C.elegans* using laser manipulation (Bringmann and Hyman, 2005)).

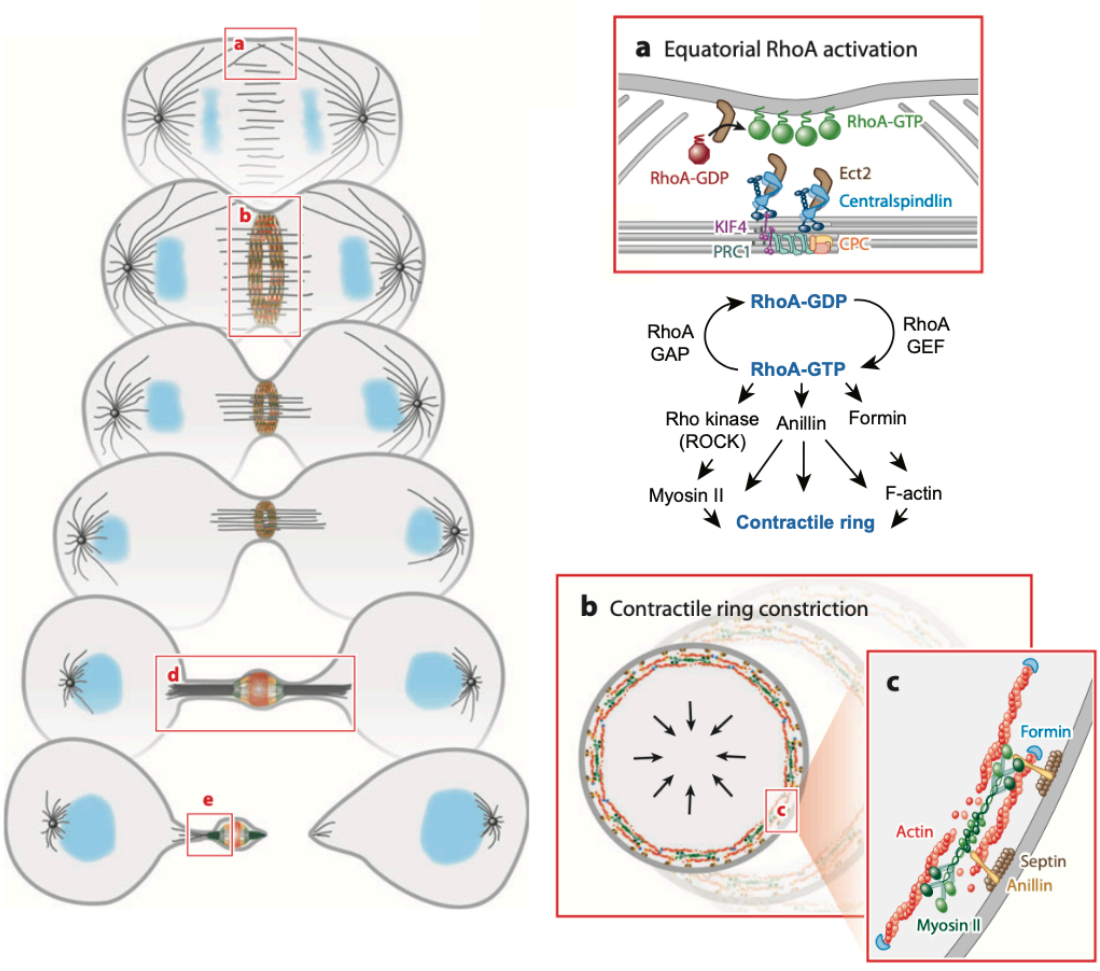

FIGURE 1.8. Cytokinesis phases and contractile ring structure and constituent proteins. Cytokinesis starts with signaling between the anaphase spindle and cortex to generate an equatorial zone of active RhoA. The central spindle forms in the midzone between the separating chromosomes. (a) The central spindle recruits the Rho-GEF, Ect2 to the cortical layer where it activates RhoA. Active RhoA assembly of the contractile ring though its downstream effectors shown on the signaling cascade, which constricts to change cell shape. (b) and (c) The contractile ring is a filamentous network composed of formin-nucleated actin filaments, myosin motors, actin

crosslinkers, membrane-associated septin filaments, and the scaffolding protein anillin. (d) After the ring constricts, the spindle midzone forms the midbody, which organizes the intercellular bridge during abscission. Images (except the Rho Signaling cascade) are from (Green, Rebeca; Paluch and Oegema, 2012), used under permission.

A pioneering experiment by Rappaport in echinoderm embryos - known as the "torus" experiment – was the first indication that the astral microtubules could themselves positively induce a furrow. In these experiments, embryos deformed into a torus shape using a microneedle at the site predicted by the position of the mitotic spindle, leading to a "horseshoe" shaped binucleated cell. In the second division, two spindles formed and a primary furrow was induced between the segregating chromosomes. However, a secondary furrow was occasionally observed where neither chromosomes or spindles were localized. These experiments demonstrated that a furrow can be formed independently of the spindle and chromosomes and that astral microtubules could induce furrowing at the zone where asters from both sides meet (Rappaport, 1961). The three mechanisms are further explained in the subsections below.

Positive equatorial signalling

Central-spindle dependent stimulation

The best understood mechanism for the positive equatorial signal that stimulates contractile ring formation is well-established and is known to depend on the spindle spatiotemporal regulation of the small GTPase RhoA at the cell equator (see Figure 1.9-Left).

The central spindle is formed by anti-parallel bundling of the microtubules between the two DNA masses derived from the metaphase spindle or polymerized *de novo* after anaphase onset (Uehara and Goshima, 2010). (Mastronarde *et al.*, 1993).

Upon anaphase entry, RhoA at the cell equator is converted to its active form, RhoA-GTP, which locally and directly activates formin-mediated F-actin assembly and indirectly promotes myosin II activation by recruiting ROCK (Matsumura, 2005; Otomo et al., 2005). This mechanism of RhoA activation is mediated by the central spindle, more specifically the centralspindlin protein complex, and depends on ECT2, a conserved guanine nucleotide exchange factor (GEF). The centralspindlin is an heterotetrameric complex composed of a dimer of the GTPase activating protein (GAP) RACGAP1 (MgcRacGAP in mammals; CYK-4 in *C. elegans*; RacGAP50C/Tumbleweed in Drosophila) and a dimer of the kinesin-6 motor protein MKLP1 (Sellitto and Kuriyama, 1988; Nislow *et al.*, 1990) (KIF23 in mammals; ZEN-4 in *C. elegans*; and Pavarotti in *Drosophila*). It is recruited to the array of central spindle microtubules, stabilizing the midzone (Pavicic-Kaltenbrunner, Mishima and Glotzer, 2007) and

recruiting ECT2 to activate RhoA and its downstream effectors (Basant & Glotzer, 2018; Mishima, 2016; E. A. White & Glotzer, 2012). This complex assembly initiates with the phosphorylation of RACGAP1 by Polo-like Kinase 1 (PLK-1) (Basant *et al.*, 2015)(Petronczki *et al.*, 2007; Burkard *et al.*, 2009)and subsequent binding of this phosphorylation site by the Ect2 N-terminus (Wolfe *et al.*, 2009). Ect2 is then recruited to the membrane through its PH domain and other regions in the C-terminus (Su, Takaki and Petronczki, 2011). Membrane recruitment of RACGAP1 involves both its C1 and GAP domains and its ability to bind to MKLP1 (Zhang and Glotzer, 2015). It has been hypothesized that, since the RACGAP1 GAP domain is involved in its membrane association, active RhoA can itself favor the recruitment of centralspindlin to the membrane and consequently promote Ect2 activation in a positive feedback mechanism (Zhang and Glotzer, 2015). The RACGAP1 GAP domain also appears to activate Ect2, which seems to require RhoA binding and could induce a second mechanism of positive feedback. These reactions also depend on centralspindlin oligomerization which requires that the chromosome passenger complex (CPC) antagonizes the action of 14-3-3 proteins (Basant *et al.*, 2015). The assembly of a structurally functional and mechanically robust spindle midzone also involves the highly conserved microtubule bundling protein PRC1 (PRC1 in mammals, Feo in *Drosophila* and SPD-1 in *C. elegans*), known to bundle microtubules in an anti-parallel manner (Subramanian *et al.*, 2010) and to act as a hub for protein interactions in the midzone (Jiang *et al.*, 1998; Mollinari *et al.*, 2002; Verbrugghe and White, 2004; Vernì *et al.*, 2004).

Further molecular details are out of the scope of this thesis and can be consulted on detailed literature reviews (Mishima, 2016; Basant and Glotzer, 2018). It should be noted that the protein interactions and regulatory pathways mentioned here may not necessarily be all strictly required for cytokinesis in distinct cells or organisms, as differences likely appear.

Astral microtubule-dependent stimulation

Even though Ect2 activation generally requires centralspindlin, evidence in *C. elegans* embryos demonstrated that centralspindlin is partially redundant with NOP-1, a non-essential protein specific of this organism that is known to activate Ect2 globally on the cell cortex during polarization and early embryo development (Y. C. Tse *et al.*, 2012). While disrupting centralspindlin alone allowed the furrow to form (although it ultimately regressed), double perturbation of NOP-1 and centralspindlin impairs RhoA accumulation on the membrane and prevents furrow formation (Yu Chung Tse *et al.*, 2012). Whether parallel activators of Ect2

during cytokinesis exist in other organisms is not known. Also, a recent study provided support for the astral-dependent furrowing mechanism proposed by Rappaport, as illustrated in Figure 1.9-Middle. In this work, central spindle–independent midbodies at the end of constriction appeared to form by bundling of astral microtubules at the furrow tip, suggesting that astral microtubules can support midbody assembly in the absence of a central spindle (Hirsch et al 2022).

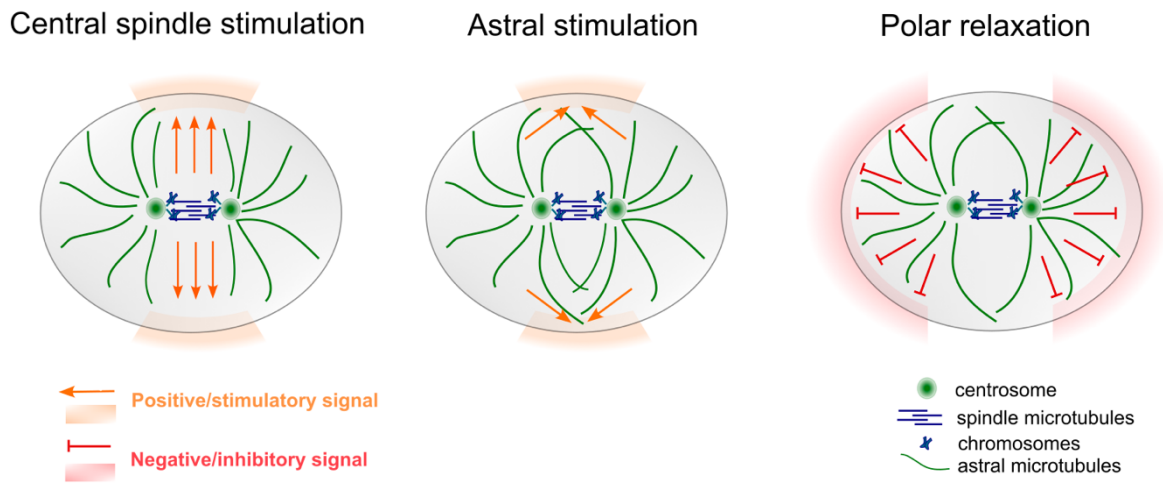

FIGURE 1.9. Conceptual models of division plane specification and furrow induction**. Left:** spindle-dependent stimulation. **Middle:** astral-dependent stimulation. **Right:** astral-dependent polar relaxation.

Inhibitory polar signalling

A theory for polar inhibition of contractility has been put forward as early as 1960 by Lewis Wolpert (Wolpert, 1961). This theory proposed that relaxation at the poles is a result of signalling cues from the astral microtubules, thus allowing the furrow region to contract more easily (see Figure 1.9-Right). Nevertheless, for many years, it remained elusive what the molecular players involved in this pathway were, consequently these inhibitory mechanisms are far less understood than those involved in the equatorial stimulation. In addition, they also seem to be less conserved or more variable among species. This topic has been redeemed in the past few years and some interesting efforts have been made to unveil the molecular basis of polar relaxation, but in general, questions remain. Particularly, in the *C. elegans* early embryo, clearance of anillin and actin from the anterior polar cortex have been proposed to be an active process requiring the activation of Aurora A kinase by TPXL-1 (Ozlü *et al.*, 2005; Mangal *et al.*, 2018), while the microtubule minus-end motor protein dynein has been shown to be involved in myosin removal from the poles (Chapa-Y-Lazo *et al.*, 2020). According to the former, TPXL-1 accumulation on astral microtubules coincides with polar clearance of anillin and actin following anaphase onset. According to the latter, mutants that position centrosomes

closer to the poles led to faster ring assembly, whereas suppression of dynein activity delayed furrowing. Still, despite presenting some convincing evidence that dynein inhibition leads to reduced myosin polar clearance and delays ring assembly by tracking myosin particles "falling-off" from the cortex through microtubules, no specific mechanism for this clearing event has been clearly established. For example, does dynein-mediated myosin removal happen by direct binding or interaction between both proteins, or is it an indirect effect of other defects such as the alteration of spindle geometry? Does myosin stay at the poles when dynein is perturbed? The authors show there are less myosin particles coming off the cortex, but it is not clear whether myosin fluorescence intensity increases significantly at the poles over time when dynein or its binding partners are perturbed. If polar clearance did not happen at all, then would it be expected that the myosin intensity would not decrease over time?

In HeLa cells, polar clearance of actin has been attributed to Aurora B, the principal member of the chromosome passenger complex (CPC). This protein localizes to the overlapping spindle microtubules at the central spindle during anaphase, and upon its depletion, actin is not cleared from the poles of the cell. Even though this did not affect ring assembly, there were delays in anaphase cell elongation (Ramkumar *et al.*, 2021). Also using HeLa cells, a detailed mechanism for polar actin assembly inhibition at the cell poles has been proposed, directly involving a population of formins DIAPH1 and CLIP170 (a microtubule associated linker protein that binds IQGAP1 on the same domain that interacts with DIAPH1). During anaphase, CLIP170 is delivered to the cortex by astral microtubules and displaces IQGAP1 (a DIAPH1 interactor involved in its recruitment to the cortex and nucleation activity) from DIAPH1, leading to its autoinhibition, a decrease in cortical stiffness and consequently, polar membrane blebbing (Chen *et al.*, 2021).

In summary, the exact relevance of polar clearance mechanisms for a successful cytokinesis is likely to be variable and cell type- or organism-dependent. In the *Drosophila* notum, cells that do not undergo polar clearance can successfully complete cytokinesis, despite showing some defects (Rodrigues *et al.*, 2015). Also, in HeLa cells, it has been previously demonstrated that inhibition of polar relaxation leads to cell shape oscillations and instabilities in the contractile ring that could sometimes result in cytokinesis failure (Sedzinski *et al.*, 2011). In fact, while human tissue-cultured cells have a rather large spindle that establishes a close physical contact with the polar cortex, in *C. elegans* early embryos the spindle poles are not so close to the polar cortex, which suggests that polar clearance mechanisms will most likely differ. In general, there seems to be some solid evidence, even across different species, that the Aurora kinase family (Aurora A in *C. elegans* and Aurora B in human cells) is indeed an essential part of this inhibitory polar signal. It remains unclear, though, whether other proteins

are involved, if the interaction between these and the cortex components is direct or indirect, and whether the latter are cleared through similar or different mechanism or just as a consequence of the clearance of one of them (e.g. myosin).

Cortical actomyosin flows

The symmetry breaking arising from the stimulatory equatorial signal *versus* the inhibitory polar signal, in which cortical proteins are cleared from the poles and accumulate at the equator, triggers a period of cortical flows in the actomyosin cortex eggs (Benink, Mandato and Bement, 2000; Munro, Nance and James R. Priess, 2004; Mayer *et al.*, 2010). In the *C. elegans* early embryo, there is also a period of intense cortical flow during the polarization of the embryo, before the first mitosis, when a pseudocleavage occurs (Munro, Nance and James R Priess, 2004; Reymann *et al.*, 2016).

These flows consist in the advection of cortical proteins along the membrane from regions of relaxation (poles) towards regions of contraction (division plane), due to the tension differential building up between the two regions (Bray and Whe, 1988). Flows accompanying cytokinesis have been documented in several organisms or cells, including *C. elegans* embryos (Mayer et al., 2010; Munro et al., 2004; Anne-Cecile Reymann et al., 2016), *Xenopus* eggs (Benink, Mandato and Bement, 2000), and *Drosophila* neuroblasts (Oon and Prehoda, 2021). Besides cell division, these have also been reported in several other biological phenomena, including neutrophil migration (Malawista and De Boisfleury Chevance, 1982), amoeboid and fibroblast locomotion (Grębecki, 1984). In the *C. elegans* early embryo, that divides asymmetrically, cortical flows are initially unidirectional, starting at the posterior and moving towards the anterior pole. This starts once the embryo enters anaphase and the DNA masses start separating and goes on during the very first stages of ring assembly (Reymann *et al.*, 2016). A bidirectional flow phase follows, in which cortical proteins move away from both poles towards the cell center (Khaliullin *et al.*, 2018a). Importantly, these flows are long-ranged in nature, which is a hallmark of the macroscopic viscous nature of the cortical layer.

The relevance of cortical flows for the success of cell division and organism development has been debated. While some believe that these flows are indeed essential and sufficient to align actin filaments by compression at the equatorial cortex to generate a furrow (Salbreux, Prost and Joanny, 2009; Reymann *et al.*, 2016; Khaliullin *et al.*, 2018a), others argue that, despite leading to some equatorial compression that may assist ring assembly, the main driver is the localized equatorial recruitment of actin and myosin from the cytoplasm (Leite et al., 2020; Younan Li & Munro, 2021; Spira et al., 2017). Essentially, the turnover of actin filaments or myosin motors is too fast compared to the rate of compression by flow (Leite *et al.*, 2020; Li and Munro, 2021). This means other mechanisms need to operate to make compression

by flow more effective, otherwise filaments could tend to relax more easily back to isotropy. Particularly, a new mechanism proposes thar existing filaments work as templates to orient the growth of new assembling filaments (Younan Li & Munro, 2021). In addition, the actin crosslinker plastin locally cooperates with myosin at the equatorial cortex to provide a template for myosin to efficiently align actin bundles, as double perturbation of these proteins results in highly unstable and misoriented equatorial actin bundles (Leite *et al.*, 2020). It is likely that both filament-guided new filament assembly and scaffolding by actin crosslinking proteins work together with myosin motor-activity to assemble a structurally robust contractile machine. Overall, one may ask whether the emergence of cortical flows is indeed the cause or the consequence of the cortical network rearrangements to assemble the ring. The ideal scenario would consist in uncoupling both contributions, localized recruitment from the cytoplasm and advection by cortical flow. However, every protein that tends to affect one of the events, also affects the other, which makes the uncoupling a hard task.

Even though the flow contribution along the anterior-posterior (A-P) axis is the most relevant for cytokinesis as it contributes to equatorial compression of actin filaments and CR assembly, there is also a rather dramatic flow component along the Dorsal-Ventral (D-V) direction, orthogonal to the A-P axis (Naganathan *et al.*, 2014; Singh *et al.*, 2019; Leite *et al.*, 2020). This D-V (hereafter, rotational) component has been shown to be dispensable for ring assembly and constriction events as embryos filmed without compression in which rotational flows are absent still assemble a ring with normal kinetics (Leite *et al.*, 2020). This implies that the dramatic rotational component may be an artifact of compression during filming, at least to some extent (Singh *et al.*, 2019). Despite this, several recent studies have tried to uncover the origin and mechanism of these rotational flows, especially when they exhibit a chiral counter-rotating behavior, which means they are rotating in opposite directions in the two halves of the embryo (Naganathan *et al.*, 2014, 2016). Chirality in the cell, especially during polarization or division, has been attributed to both the actomyosin cortex (Danilchik, Brown and Riegert, 2006; Hozumi *et al.*, 2006; Spéder, Adám and Noselli, 2006) and microtubules (Nonaka *et al.*, 1998; Ishida, Thitamadee and Hashimoto, 2007). For a long time, though, it remained elusive whether any particular component of the actin cortex was involved in triggering and amplifying the torques generated at the molecular level, and how these translated into a macroscopically coordinated behavior. Recently, the formins have been shown to drive the emergence of macroscopic torques in the actomyosin network (Middelkoop *et al.*, 2021; Zaatri, Perry and Maddox, 2021), due to their intrinsic property of rotating actin filaments while elongating them (Mizuno *et al.*, 2011). These would then be propagated or amplified throughout the cortical layer by myosin motors (Middelkoop *et al.*, 2021). Also interesting, these chiral flows were shown to be lineage-dependent and drive cell

rearrangements in the earliest *C. elegans* embryonic divisions (Pimpale *et al.*, 2020), and hypothesized to drive spindle skews. Nevertheless, a similar question as mentioned above for the longitudinal flows remains, on whether the chiral flows are the cause or, alternatively, a consequence of spindle skews. Further studies will likely bring new information to advance our knowledge on the role of chiral flows in cell division and development.

Contractile ring constriction

Actomyosin structure of the contractile ring

Earlier in this manuscript, we mentioned that skeletal muscle contracts through a sarcomeric mechanism. The muscle is organized in myofibrils composed of a series of sarcomeres. In short, each sarcomere is limited by two Z-discs, in which actin filaments are anchored by their barbed-ends, are parallel to each other and have their pointed-ends oriented towards the center of the sarcomere. These actin filaments are intercalated with myosin bipolar filaments that are anchored at the M-band in the middle of the sarcomere. Contraction is achieved as the myosin heads move towards the barbed-ends of the actin filaments, causing a displacement that moves the filaments towards the center. Of note, the sarcomeric contraction is limited by the maximum overlap between actin and myosin filaments. Earlier studies of contractile ring tried to investigate whether it constricted through a sarcomeric-like mechanism (Schroeder, 1972; Sanger and Sanger, 1980), however, a modular sarcomeric structure has never been observed by EM. In addition, ring constriction has been associated with actin disassembly as its perimeter decreases, which may be incompatible with the existence of sarcomeres. Therefore, the actomyosin network in the contractile ring seems to be significantly different from that of muscle.

The filamentous nature of the ring in sea urchin and jellyfish embryos and human HeLa cells was revealed for the first time by Schroeder's EM experiments in the 1970s (Schroeder, 1968, 1972, 1973). According to his data, the contractile ring was formed just below the plasma membrane at the furrowing region and exhibited a closely packed array of parallel actin filaments. Its width was 3–17 μm in sea urchin eggs, 6 μm in jelly fish eggs, and 10 μm in HeLa cells, whereas its thickness was about 0.1–0.2 μm.

The actin filaments were shown to bind HMM (Schroeder, 1973) and subsequent HMM-labelling revealed that actin filament exhibited opposite polarities in the ring (Sanger and Sanger, 1980). The presence of myosin filaments was first documented by fluorescence microscopy of cultured cells using myosin specific antibodies (Fujiwara and Pollard, 1976; Nunnally, D'Angelo and Craig, 1980), and later reported at the ultrastructural level where myosin-like filaments were visualized alternating with actin filaments (Sanger and Sanger,

1980; Maupin and Pollard, 1986). Additionally, the furrow membrane presented underlying round patches of electron dense material that appeared to be associated with the ends of actin filaments, thus constituting potential anchor sites for the contractile ring at the plasma membrane (Maupin and Pollard, 1986). A recent study using platinum replica EM of isolated cortices of dividing sea urchin embryos confirmed the overall organization reported in earlier studies (Henson *et al.*, 2017). This study showed that the ring is a specialized structure integrated within a continuous actomyosin cell cortex. Actin filaments within ring are primarily organized into compacted non-branched bundles, aligned parallel to the cleavage axis. The surrounding cortex, on the other hand, mainly consists of a crisscross F-actin meshwork(Davies *et al.*, 2014; Ding, Cui, Zhao, Zhang, Sun and Lijun Zheng, 2017; Henson *et al.*, 2017; Chan *et al.*, 2019). Unlike other organisms, *D. discoideum* contractile rings were shown to be a disorganized meshwork of actin filaments throughout cytokinesis (Descovich *et al.*, 2018). Whether the actin filaments that form the ring are recruited from adjacent regions of the cortex or assembled *de novo* at the cell equator during ring assembly in animal cells is still unclear. In support of the first, it has recently been proposed that actin filaments flow along the cell cortex towards the cell equator, and that compression due to persistent unidirectional flows towards the equator of the cell is the main driver for actin filament alignment at the equator and furrow formation in one-cell *C. elegans* embryos (Reymann *et al.*, 2016). In support of the second, cytokinetic formins responsible to nucleate and elongate the actin filaments in the ring are activated at the cell equator where Rho-GTP localizes (Kishi *et al.*, 1993; Otomo, Otomo, Diana R. Tomchick, *et al.*, 2005; Watanabe *et al.*, 2008; Loria, Longhini and Glotzer, 2012).

Ring constriction driven by myosin motor activity

It is well-established that contractile ring constriction depends on myosin-motor activity, as the conversion of chemical energy through ATP hydrolysis via myosin is necessary to produce mechanical force. How exactly this motor-dependent contractility happens, especially in terms of structural organization, is not so well understood. Structural data agree with a sliding mechanism of antiparallel actin filaments by myosin motors. However, this would still allow for filaments to be in a parallel arrangement in contraction units or in a continuous random orientation (reviewed in Mendes Pinto et al., 2013). As previously mentioned, a modular structure has been proposed, but never observed by EM. Particularly, in fission yeast, a nodal organization of the ring has been reported. Nodes' positions change throughout constriction, indicating lateral mobility on the plasma membrane (Laplante *et al.*, 2016; Wollrab *et al.*, 2016). Lateral mobility of myosin was also reported in *C. elegans*, in which rings have been proposed

to be organized in a series of equal-sized contractile units (Carvalho, Desai and Oegema, 2009). Still and rotating clusters of myosin and other actomyosin components were also observed in mammalian cells (Wollrab *et al.*, 2016). These results favor the idea that some structural or functional organization exists and persists as the ring constricts. Recent studies also support some degree of structural organization, yet they do not necessarily favor the existence of units (Spira *et al.*, 2017; Leite *et al.*, 2020; Li and Munro, 2021). These include cooperation of myosin motor activity with passive actin crosslinkers, in which the latter would provide some structure and templating for myosin to progressively align F-actin more efficiently (Leite *et al.*, 2020) and/or orientation of new formin-nucleated filaments using pre-existing filaments as templates (Li and Munro, 2021).

Importantly, all the above-mentioned mechanisms are dependent on myosin motor activity., but evidence for the exact requirements of this motor activity in animal cytokinesis is still limited. Several studies used Blebbistatin, knockdown or inactivation of myosin through temperature-sensitive mutants and non-phosphorylatable mutants of the RLC to test the extent of this requirement (Straight *et al.*, 2003; Davies *et al.*, 2014; Reymann *et al.*, 2016; Descovich *et al.*, 2018). However, all these approaches could, in principle, have problems in distinguishing the motor and crosslinking contributions of myosin. First, neither myosin depletion nor inactivation allow the distinction between these two functions. Blebbistatin inhibits the myosin ATPase activity and therefore the force generation, by binding halfway between the nucleotide binding pocket and the actin binding cleft, predominantly in an actin detached conformation (Kovács *et al.*, 2004; Allingham, Smith and Rayment, 2005). Finally, perturbing the RLC may affect myosin localization or structure (Vasquez, Tworoger and Martin, 2014; Heissler and Sellers, 2015; Liu *et al.*, 2016). To tackle this question, some studies tried to express different point mutations in the myosin head that would affect motor-activity. For example, in fission yeast, the expression of a myo2 mutant containing three point mutations (G345R, Q640H and F641I) that still binds tightly to actin and abolishes actin sliding *in vitro*, was sufficient for ring assembly but not constriction (Palani *et al.*, 2017). In *D. Discoideum*, myosin-null cells were able complete cytokinesis when adhered to a surface, but grew slowly in suspension (De Lozanne and Spudich, 1987; Shimada *et al.*, 1997). Also, the expression of motor impaired mutants supports this observation. For example, expression of a myosin mutant that bound tightly to actin but was motor-dead (Shimada *et al.*, 1997), led to slow growth in suspension and multinucleation in adherent cells. However, expression of slower myosins (Shimada *et al.*, 1997; Reichl *et al.*, 2008) or a motor-dead myosin that seemed to bind weakly to actin (Shimada *et al.*, 1997) strongly affected cell growth in suspension but allowed for successful cytokinesis in adherent cells. Adherent COS-7 cells (that lack myosin IIA and IIC) expressing a motor-dead myosin capable of binding actin, was able to complete cytokinesis after RNAi depletion of endogenous myosin IIB (Y. Ma *et al.*,

2012). In *C. elegans* embryos, expression of two motor-dead myosins that could still bind actin did not support cytokinesis (Osório *et al.*, 2019). In conclusion, the expression of motor-dead myosins seems to support cytokinesis in adhered cultured-cells, however it does not support division in *C. elegans* embryos or non-adherent *D. discoideum*, highlighting different mechanisms in these systems.

In the context of a continuous F-actin bundle lacking modularity, myosin motor activity can also lead to contraction by actin filament buckling or polarity sorting. The former stems from the intrinsic properties of actin filaments since they can support large tensile stresses but buckle readily when under compression (De La Cruz and Gardel, 2015). In a continuous structure of actin filaments with random orientations, these intrinsic properties lead to net contraction of the network. Actin filament buckling has been proposed to be caused by the action of myosin filaments with slightly different velocities (Lenz, Gardel and Dinner, 2012). Filament buckles have higher curvature and should therefore be more prone to severing (Murrell and Gardel, 2012; Vogel *et al.*, 2013). Whether a buckling mechanism is functionally relevant *in vivo*, where networks with short actin filaments and compact mesh sizes seem to exist, remains unclear. The alternative mechanism is based on myosin-driven polarity sorting, which requires the observed capacity of myosin to dwell at the end of several actin filaments after processively running along them (Dickinson, Caro and Purich, 2004; Oelz, Rubinstein and Mogilner, 2015; Wollrab *et al.*, 2018). This activity leads to the formation of actin asters that can act as contractile nodes, which drive contraction in crosslinked networks with dense mesh sizes.

Ring constriction independently of myosin motor activity

Besides myosin motor-activity driven constriction, it has also been envisioned that the contractile ring could constrict through a mechanism that would involve F-actin disassembly or the presence of end-tracking crosslinkers – crosslinkers that are able to remain bound to the depolymerizing filament ends – which could also produce stress in the network. However, no non-motor end-tracking crosslinkers have been identified to date and testing whether F-actin dynamics can drive ring constriction in the absence of myosin motors is not easy. The latter is because it is hard to uncouple the contribution of myosin motor-activity from that of F-actin disassembly, as myosin itself has been shown to disassemble actin filaments (Wilson *et al.*, 2010; Mendes Pinto *et al.*, 2012; Murrell and Gardel, 2012; Reymann *et al.*, 2012; Vogel *et al.*, 2013). One way of attempting to test the possibility that end-tracking crosslinkers could drive contractility in the absence of motors would be to express myosin mutants that do not translocate but still bind actin and, in case cytokinesis still occurs, inhibit on top other passive

crosslinkers. Yet, cytokinesis may fail due to a lack of connectivity in the network during ring assembly, thus precluding an evaluation during constriction. Overall, given the current experimental evidence, it is unlikely that any of these mechanisms, alone, could drive ring constriction in non-adherent animal cells. Although myosin motor function has been shown to be crucial for ring constriction in *C. elegans* embryos (Osório *et al.*, 2019) and the yeast *S. pombe* (Palani *et al.*, 2017), its requirement has been questioned in mammalian cells (Chew *et al.*, 2017), in *D. discoideum* dividing on a substrate and in *S. cerevisiae* (Lord, Laves and Pollard, 2005; Fang *et al.*, 2010; Mendes Pinto *et al.*, 2012). This may happen because adherent cells can crawl on the substrate, generating forces that may facilitate furrowing (Zhang and Robinson, 2005; Dix *et al.*, 2018). The most likely is that a combination of both mechanisms contributes to overall ring constriction, which has been already considered in several studies (Carvalho, Desai and Oegema, 2009; Mendes Pinto *et al.*, 2012; Stachowiak *et al.*, 2014; Turlier, Audoly, Prost and J.-F. Joanny, 2014).

The role of F-actin dynamics in ring constriction

Actin filament turnover in the cell happens through continuous F-actin assembly and disassembly regulated by ABPs. Acute drug treatments with actin-interfering drugs have been used and revealed actin turnover is essential for ring constriction. Addition of Latrunculin A - that binds actin monomers and prevents them from polymerizing (Braet *et al.*, 1996) - or Cytochalasin D - that binds to the barbed end of actin filaments blocking both their assembly and disassembly (Cooper, 1987) - to mammalian cells, sea urchin embryos or fission yeast during contractile ring constriction leads to cytokinesis failure (Schroeder, 1972; Murthy and Wadsworth, 2005a; Proctor *et al.*, 2012; Wollrab *et al.*, 2016; Chew *et al.*, 2017). In agreement, in *C. elegans* embryos, addition of Latrunculin A after furrow initiation slows down ring constriction (Carvalho, Desai and Oegema, 2009; Ana M Silva *et al.*, 2016).

Addition of Latrunculin or Cytochalasin close to the cytokinetic furrow in normal kidney epithelial cells (NRK) led to disassembly of the equatorial actin network and facilitated furrowing, while the addition at the polar cortex inhibited cytokinesis progression, suggesting that polar and equatorial actin networks are regulated differently and require distinct dynamics to drive CR constriction(O'Connell, Warner and Wang, 2001). Addition of Jasplakinolide – that stabilizes F-actin and antagonizes the action of Cytochalasin by stabilizing actin dimers and therefore enhancing ectopic nucleation (Pospich *et al.*, 2021) – or a mix of this drug and Latrunculin led to constriction slowdown in yeast (Chew et al., 2017; Mendes Pinto et al., 2012) and cytokinesis arrest in LLCK1 cells (Murthy and Wadsworth, 2005a). Overall, results are not consistent among different systems as F-actin dynamics likely differs, but they all support the idea that actin dynamics are always required for cytokinesis. Hopefully, in the future, more

refined methods including photo-caged drugs, that would allow for a tight spatiotemporal control over the experiments, will provide more insight into actin turnover mechanisms in the contractile ring.

Fluorescence Recovery after Photobleaching (FRAP), a technique for evaluation of protein diffusion and binding (reaction) in cells and tissues (Axelrod *et al.*, no date), may also provide valuable information on F-actin dynamics, especially at a quantitative level through the measurement of mathematical parameters such as association (k_{on}) and dissociation (k_{off}) constants, which are essential to build more reliable computational models of ring constriction. Even though this method been used to analyze dynamics of other contractile ring components, including myosin (Carvalho, Desai and Oegema, 2009; Khaliullin *et al.*, 2018a; Leite *et al.*, 2020; Thiyagarajan *et al.*, 2022), its application to measure actin dynamics is limited in several systems. This is partially due to the fact that a fluorescent probe for G-actin would be needed and even though this exists, measurements may not be reliable as the formins tend to exclude fluorescently tagged actin monomers from nucleation and elongation processes (Wu and Pollard, 2005; Carvalho, Desai and Oegema, 2009; Chen, Nag and Pollard, 2012), which may bias the measurements to nucleated by the ARP2/3 complex. Total Internal Reflection Fluorescence (TIRF) microscopy coupled to a single-molecule tracking approach has also been employed to measure actin dynamics in *C. elegans* embryos.

The role of actin filament crosslinkers in contractile ring constriction

The role of passive actin filament crosslinkers during cytokinesis is quite less explored. It is still not completely clear whether the simultaneous expression of several crosslinkers is due to functional redundancy or necessary diversification. Evidence for redundancy is limited, but very likely to exist. In fission yeast, single mutants of α-actinin and fimbrin are viable, and a double mutant is not, due to problems during cytokinesis (Wu, Bähler and Pringle, 2001). The fact that each crosslinker alone does not have an effect *per se* may be related with possible redundancies or robustness of the system. Recently, it has been shown that the mutual perturbation of plastin and beta-heavy-spectrin leads to cytokinesis failure during the contractile ring assembly phase in the *C. elegans* one-cell embryo, indicating that these two different crosslinkers with very different structures may synergize to provide the cortical network with diverse properties (Sobral *et al.*, 2021).

Inhibition of individual crosslinkers does not necessarily lead to cytokinesis failure. Alpha-actinin was shown to be dispensable for early embryonic cytokinesis in *C. elegans* (Ding, Cui, Zhao, Zhang, Sun and Lijun Zheng, 2017), whereas its depletion was found to accelerate furrow ingression in NRK mammalian cells (Mukhina, Wang and Murata-Hori, 2007). Depletion of cortexillins in *D. discoideum*, and anillin in *D. melanogaster* S2 and human HeLa cells were

described to lead to significant cytokinesis failure (Piekny and Glotzer, no date; Faix *et al.*, 1996; Robinson and Spudich, 2000; Maddox *et al.*, 2007; Jananji *et al.*, 2017). Nevertheless, cortexillins do not seem to be well conserved in higher organisms, and anillin has additional functions, meaning its requirements may not be due to its F-actin crosslinking activity. Overexpression of crosslinkers, though, seems to lead to multinucleation in a variety of systems (Robinson and Spudich, 2000; Wu, Bähler and Pringle, 2001; Mukhina, Wang and Murata-Hori, 2007; Reichl *et al.*, 2008; Laporte *et al.*, 2012). In *C. elegans* embryos, plastin loss of function led to reduced actin filament connectivity and impaired flows towards the cell equator but did not affect ring constriction rate (Ding, Cui, Zhao, Zhang, Sun and Lijun Zheng, 2017). A combination of *in vivo* experiments and computational modelling in fission yeast suggested that α-actinin and fimbrin cooperate with myosin during the initial self-organization of the contractile ring (Laporte *et al.*, 2012), and α-actinin turnover is necessary to better organize ring components and facilitate node coalescence (Y. Li *et al.*, 2016). The mobility/dynamics of the crosslinkers dynacortin, fimbrin, and primarily cortexillin was found to be decreased at the cleavage furrow when compared to the polar regions (Reichl, 2008) and interphase cortex of *D. discoideum* (Srivastava, 2015). This decrease could be due to increased mechanical tension at the furrow region. Cooperative accumulation of myosin and cortexillin I was observed during micropipette aspiration of polar regions during cytokinesis in *D. discoideum* (Effler *et al.*, 2006; Ren *et al.*, 2009). The cooperativity between myosin and cortexillin I was proposed to result from myosin inducing or stabilizing conformational changes of the actin filaments, which in turn potentiate enhanced binding of myosin itself and cortexillin I (Orlova *et al.*, 1997; Luo *et al.*, 2012). In agreement, in *C. elegans* early embryos, plastin was shown to cooperate with non-muscle myosin II to align F-actin bundles in the equatorial cortex and form a ring (Leite *et al.*, 2020). When plastin is perturbed simultaneously with mild depletion of NMII, which by itself does not lead to cytokinesis failure, F-actin equatorial alignment is severely compromised, with bundles adopting a quasi-horizontal orientation and failing to assemble a contractile ring.

Indeed, NMII together with non-motor crosslinkers have been shown to regulate the structure and dynamics of the actin cortex, intrinsically adjusting the mechanical properties of the network to different biological contexts. Computational models and *in vitro* studies revealed that actin crosslinkers are crucial for network interconnectivity (Ennomani *et al.*, 2016; Jia *et al.*, 2018). The general importance of connectivity for the mechanical behavior of actomyosin networks has been previously discussed in this manuscript. Here, we will focus on the effects of actin network architecture and connectivity in contractile ring dynamics. Research is mostly based on *in vitro* minimal systems consisting of micropatterned rings of purified components that contract in the presence of myosin (Reymann *et al.*, 2012; Ennomani *et al.*, 2016) and

reproduce the features of *in vivo* rings. Micropatterned rings composed of ordered anti-parallel filaments contracted faster than those consisting of branched filaments, but both slowed down in the presence of the crosslinker α-actinin. Yet, rings formed by parallel filaments of mixed polarity only contracted in the presence of α-actinin. These results showed that increasing or decreasing the amount of crosslinking could both favor or impair constriction, depending on the F-actin network architecture. This has been supported by several other *in vitro* and *in silico* studies (Y. Li *et al.*, 2016; Ding, Cui, Zhao, Zhang, Sun and Lijun Zheng, 2017; Descovich *et al.*, 2018). Of note, these studies used a double-headed HMM version of myosin VI, which is a minus-end directed motor, contrarily to non-muscle myosin II, and therefore, differences may apply. Altogether, the evidence shows that the contraction of an actomyosin filament network is determined by its global architecture and degree of interconnectivity. Then again, it is not known whether ordered anti-parallel filaments or alternatively, disordered filaments with mixed polarity mimic the cytokinetic ring organization. In addition, the organization of the contractile ring may change as constriction progresses as the process is highly dynamic, and these *in vitro* systems do not necessarily incorporate that *in vivo* complexity.

An *in vivo* study using *C. elegans* early embryos partially depleted of anillin or non-muscle myosin II indicated that control levels of these proteins in the contractile ring were not optimized for maximum speed, as partial depletions led to an increase and stronger depletions to a decrease in the constriction rate (Descovich *et al.*, 2018). However, this study analysed these results only in terms of an isolated ring. Yet, in *C. elegans*, the ring remains integrated in the surrounding cortex, which may also affect its constriction kinetics.

An interesting point in the future would be to check possible synergies/cooperation with other proteins, as the presence or absence of crosslinkers may facilitate constriction in cases where the actomyosin network in the ring is already compromised. The problem has to do with the localization of these proteins during cytokinesis. Some of them have been shown to localize in CRs, but they also localize in the surrounding cortex, including alpha-actinin (Fujiwara, Porter and Pollard, 1978), fimbrin/plastin (Watanabe *et al.*, 1998, 2000; Nakano *et al.*, 2001; Ding, Cui, Zhao, Zhang, Sun and Lijun Zheng, 2017), anillin (C M Field and Alberts, 1995), and septins (Maddox *et al.*, 2007), and therefore, it is difficult to uncouple both contributions, as F-actin network architecture in the ring and in the surrounding cortex are different.

Theoretical modelling of cytokinesis

The field of mechanobiology focuses on understanding how cell mechanics and physical forces act as dynamic players in biological phenomena and how they translate into biochemical responses through mechanotransduction. Physics began to percolate into the

cytokinesis research as an attempt to explain the dramatic deformation and shape changes occurring during the process. The contribution of mathematical modeling has been and will continue to be fundamental to increase our global understanding of this complex process.

Modelling of actomyosin networks

Theoretical modelling of biological systems consists of developing theory, algorithms, data structures, and other tools that can simulate components as well as interactions and interplays between them, predicting outcomes in different biological contexts. It has the power to predict the behaviour of complex biological systems by greatly simplifying the molecular details, keeping only the essential variables and reducing the number of parameters to be considered. Currently, two general types of computational models can be identified in the study of actomyosin networks: agent-based and coarse-grained continuum models, as depicted in Figure 1.10.

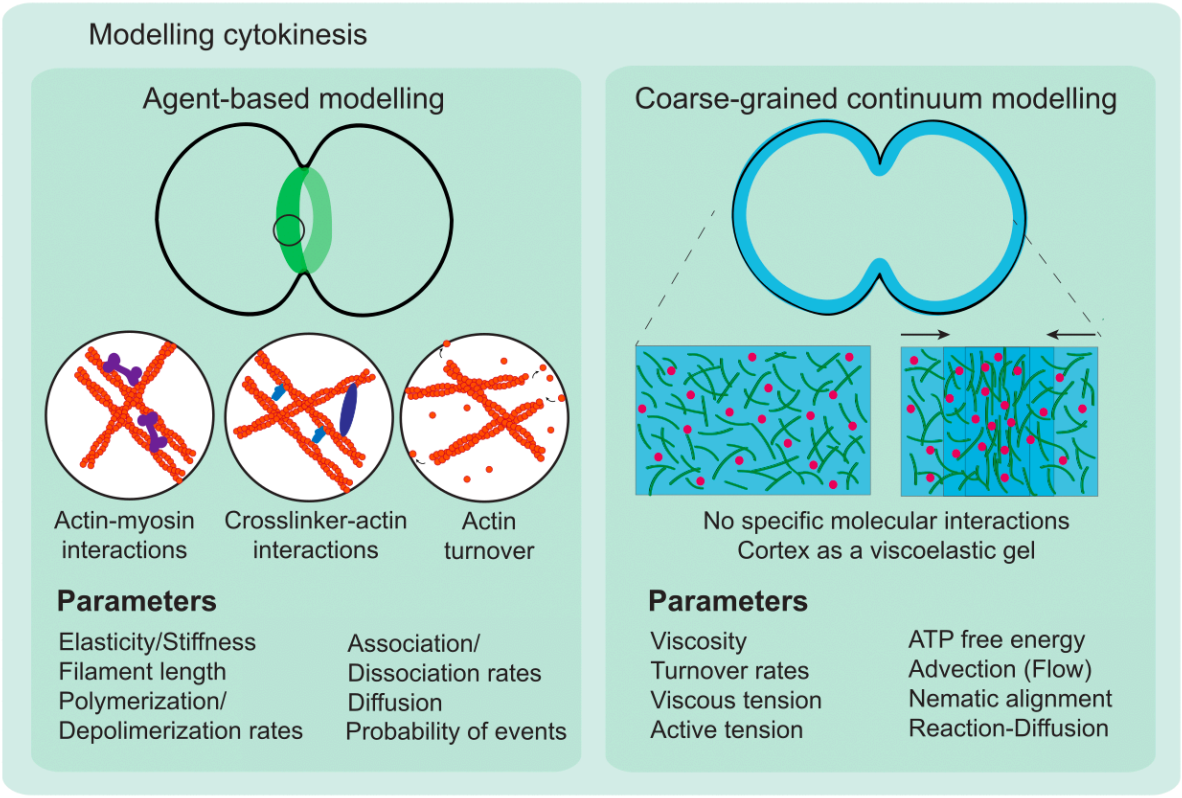

FIGURE 1.10. Modeling of cytokinesis is generally subdivided into two distinct approaches: agent-based simulations and coarse-grained continuum models. Agent-based models focus mostly on the CR alone and specific interactions and dynamics between cortex components are considered (myosin-actin and actin-crosslinkers interactions, as well as actin turnover dynamics). Coarse-grained models provide a description of the entire cell surface, where the cortex is seen as a viscoelastic gel able to contract in response to stress arising from physico-chemical gradients.

Agent-based modelling requires detailed information on the components and mechanisms at the molecular level, including number of molecules, filaments or molecular ensembles. By contrast, coarse-grained continuum models do not require detailed knowledge of the interactions between specific components, but rather describe the network as a continuous macroscopic material. Each type of model has its own advantages and limitations and, as such, the model chosen to address a given biological problem will always depend on the question itself and the level of detail required to answer it. While agent-based models are generally attractive as proteins' numbers and properties can be individually played with, their main limitation arises from the difficulty in knowing exactly how each component contributes to set the network mechanical properties. Moreover, numerical simulations may become computationally unworkable when modeling large-scale systems such as the entire cell cortex during cytokinesis. This may be simplified by simulating only a portion of the CR and a portion of the rest of the cortex. Still, coarse-grained approaches may be more adequate to describe the mechanics of the whole cortex, especially when it comes to relate mechanics at the equator with mechanics at the poles and may prove particularly suitable when the biological system is poorly characterized biochemically. Nevertheless, these types of models do not provide the mechanistic understanding of the mechanical properties arising from molecular processes that often biologists are looking for. Additionally, they still require the input of chemical constants and coefficients, which need to be measured experimentally or matched to experimental results. A great example of this approach is the active gel theory (Kruse *et al.*, 2005a)(Prost, Jülicher and Joanny, 2015)(Joanny *et al.*, 2007) that has been successful in predicting cell cortex behaviour in several biological processes such as cell migration (Kruse *et al.*, 2006) and cytokinesis (Turlier, Audoly, Prost and J.-F. Joanny, 2014)(Salbreux, Prost and Joanny, 2009). In short, the active gel theory aims to apply general hydrodynamic equations to biological systems composed of cytoskeletal filaments and motor proteins that present gel-like behavior. This description retains the minimal, yet essential, properties of the cytoskeleton: dynamic polar filaments and motors with network contracting ability(Kruse *et al.*, 2005a), whose equations are similar to the ones used for non-biological systems.

Modelling cytokinesis

How to mechanically explain the dramatic deformations occurring during cytokinesis has been a long-standing question. The first theoretical models of cytokinesis were inspired by pivotal experiments of cleavage in animal cells that showed that division occurs through a differential distribution of stresses and forces over the cell surface, with the tension at the equator being higher than the tension at the poles (Mitchison & Swann, 1955; Rappaport, 1967; Wolpert, 1966; Hiramoto, 1967; Hiramoto, 1968; Yoneda and Dan, 1972; Wolpert & Mercer, 1963;

Marsland and Landau, 1954). One of the first theories by Mitchison and Swann - the expanding membrane theory - proposed that cytokinetic furrow formation and ingression was a passive event resulting from active expansion at the poles (Mitchison & Swann, 1955; Swann & Mitchison, 1958; Mitchison, 1952). In opposition, Marsland postulated that the furrow region was itself contractile, independently of the poles (Marsland, 1950; Marsland, 1956). Wolpert put forward the astral relaxation theory, which posits that relaxation at the poles is a result of signalling cues from the astral microtubules, thus allowing the furrow region to contract (Wolpert, 1961). The first mathematical models proposed between the late 1970s and the 1990s were purely theoretical and consisted of continuous descriptions of the entire cell surface (Greenspan, 1977; Akkas, 1980; White and Borisy, 1983; Zinemanas & Nir, 1987; Zinemanas and Nir, 1990; He and Dembo, 1997). White and Borisy (White and Borisy, 1983) developed the first purely computational model of cytokinesis, capitalizing on the astral relaxation theory (Wolpert, 1961). They suggested that the development of cortical tension anisotropy drives furrow assembly and ingression. In their model, the cortex was considered a random network of linear elements evenly distributed, where elements between the poles and the equator moved towards the equator due to a laterally directed force arising from the gradient of cortical tension. This would drive the accumulation of contractile elements at the equator, leading to higher cortical tension in this region. More recent computational models of cytokinesis have mostly focused on understanding the behavior of the contractile ring during the constriction phase, generally disregarding the contribution of the surrounding cortex in setting constriction dynamics. These models are either coarse-grained (Zumdieck *et al.*, 2005; Salbreux, Prost and Joanny, 2009; Sain, Inamdar and Jullicher, 2015; Dorn *et al.*, 2016) or agent-based microscopic descriptions that mostly focus on interactions between actin filaments and myosin motors (Biron *et al.*, 2005; Zumdieck *et al.*, 2007; Mendes Pinto *et al.*, 2012; Stachowiak *et al.*, 2014; Descovich *et al.*, 2018) and will be discussed in more detail below.

Models of contractile ring constriction

Ring constriction has been a subject of extensive mathematical modelling. Actin filaments, as well as myosin motors and non-motor crosslinkers are common components to all mathematical models of ring constriction. As actin filament architecture in the ring is still not clear, most models assume that the ring is simply a region with higher degree of actin filament alignment and higher myosin concentration. Models are starting to include the ideas that motor- and non-motor mechanisms can generate contractility and network dynamics, as molecules are constantly turning over, which defines characteristic timescales for interactions and mechanical properties.

Carlsson et al. evaluated the force generated by myosin filaments in actin gels and estimated that network contraction by motors does not generate the necessary force for ring constriction. For that to happen, actin filaments must be crosslinked into long units, which would compensate for the small size of individual actin filaments (Carlsson, 2006). Zumdieck et al. suggested that, in addition to myosin motors, contractile stress can also be generated by actin depolymerization coupled to the action of end-tracking crosslinkers (Zumdieck *et al.*, 2007). In their microscopic model, myosin motors produce stress in the network by sliding actin filaments, which can polymerize and depolymerize. These molecular details were then coarse-grained into a continuum description, where polar actin filaments could change orientation due to diffusion, as well as polymerization and depolymerization, and the roles of myosin and end-tracking crosslinkers were represented by coefficients of tension contribution. Finally, these coefficients were interpreted in terms of a phenomenological model that considers the stress generated in filament bundles, and how this results in constriction. Following up on this study, another microscopic model was able to recapitulate part of ring constriction in budding yeast by including actin filaments, end-tracking crosslinkers and myosin motors to compute macroscopic parameters describing constriction dynamics. Actin filaments in the ring were allowed to overlap, change orientation and length, but effects of actin polymerization during constriction were not considered. Also, actin filament sliding by myosin and binding of crosslinkers were not allowed to occur simultaneously for the same filament. This model provided evidence for a major role of actin disassembly in driving ring constriction (Mendes Pinto *et al.*, 2012). Of note, none of these agent-based models considered the likely contribution of membrane-anchoring of the barbed-ends of actin filaments via formins and/or myosin to the generation of tension.

A recent study in the *C. elegans* embryo addressed the topic of network crosslinking and the idea that wild-type rings are not optimized for maximum constriction speed. The authors used an agent-based model to simulate isolated contractile rings consisting of actin filaments, myosin motor ensembles and actin crosslinkers, whose amounts were extrapolated from fission yeast and scaled to *C. elegans* rings. They proposed a mechanism in which intermediate concentrations of motor and non-motor crosslinkers prompt faster constriction, which is attenuated by higher or lower concentrations of these components (Descovich *et al.*, 2018). The first evidence that the CR generates tension dates to Rappaport experiments in sea-urchin embryos with glass microneedles. Rappaport showed that cleavage furrows of dividing embryos produce tensions in the range of 8–16 nN, based on their ability to bend the microneedles (Rappaport, 1967, 1977). However, how the ring organizes and belts up to generate this tension is still a subject of debate. In an attempt to uncover the mechanisms through which the ring produces tension, Stachowiak et al. proposed an agent-based model of the *S. pombe* contractile ring including experimentally measured amounts of actin filaments,

actin-elongating formins, myosin and the crosslinker α -actinin, as well as rates of actin filament elongation, turnover of myosin and formins, force generated by myosin motors and drag resulting from membrane-anchors and crosslinkers (Stachowiak *et al.*, 2014). This model, driven by myosin-dependent actin filament sliding and uniformly distributed anchors connecting the ring to the membrane, reliably reproduced the organization, dynamics and tension observed experimentally in rings from fission yeast protoplasts (Jochová, Rupes and Streiblová, 1991). Importantly, the authors show that effects of turnover, not only for actin filaments, but also for other ring proteins, are essential to renew ring organization and sustain force, thus avoiding the accumulation of myosin into clusters and consequent loss of tension. To reproduce ring closure time and asymmetric furrowing in *C. elegans* zygotes, a coarse-grained description of the contractile ring used energetic parameters associated with progressive membrane curvature-dependent F-actin alignment and force generation by myosin. In this model, the ring was considered a membrane-bound series of contractile units connected by spring-like connections mimicking actin crosslinkers. Unit constriction was achieved by myosin-dependent actin filament sliding, where actin filaments on each unit had a random orientation initially and progressively aligned as the ring constricted. Ring constriction was driven by a positive feedback mechanism where membrane curvature promoted actin filament alignment and consequently contractility, which in turn increased membrane curvature (Dorn *et al.*, 2016).

Recently, a 3D microscopic model based on electron cryotomography data ('Coarse-grained simulations of actomyosin rings point to a nodeless model involving both unipolar and bipolar myosins', 2018; Swulius *et al.*, 2018) suggested that constriction in fission yeast contractile rings is achieved by an interplay between two distinct myosin structures—bipolar and unipolar. Actin filaments, bipolar and unipolar myosins and actin crosslinkers were all modelled as beads connected by springs, while the membrane was modelled as a sheet of beads, initially presenting a cylindrical shape. The ATPase cycle of myosin, which dictates the binding state of myosin to actin, was also integrated, as an attempt to make actomyosin interactions more realistic. The authors tested all possible configurations of actin filaments and myosins (bipolar or unipolar), including attachment to the membrane, and concluded that their simulations support a model in which ring tension is primarily generated by sliding of actin filaments via bipolar myosins and transmitted to the membrane via unipolar myosins, which would be attached to the membrane individually('Coarse-grained simulations of actomyosin rings point to a nodeless model involving both unipolar and bipolar myosins', 2018). However, neither bipolar nor unipolar myosin filaments could be resolved in the cryotomography data (Swulius *et al.*, 2018), and therefore this hypothesis still lacks support from experimental data.

The influence of the surrounding cortex

Despite cytokinesis being inherently associated with the constriction of a contractile ring, one should not disregard the fact that this is only differentiated part of the cortex in animal cells. Even though recent models have mostly focused on the ring itself, disregarding the contribution of the surrounding cortex, there is both theoretical and, to lesser extent, experimental evidence indicating that the cortex surrounding the ring impacts its behavior. One of the first theoretical models of cytokinesis, by Yoneda and Dan, considered that the polar cortices, which were approximated to two portions of a sphere under tension, resisted ring constriction. Based on Hooke's law and considering a uniform surface tension at the cell poles, they were able to estimate the minimal equatorial force required for furrow contraction (Yoneda and Dan, 1972). This model was used later to test experimental observations in *D. discoideum* (Zhang and Robinson, 2005; Surcel *et al.*, 2010). Work from the Robinson lab revealed that the small GTPase RacE and the actin crosslinker dynacortin, both enriched in polar regions, act together to slow down cytokinesis. Their modelling approach revealed that after the furrow initial deformation, once the geometry of the daughter cells changes to establish an intercellular bridge, viscoelastic compressive stresses slow down bridge thinning, which is itself accomplished through myosin-dependent contractile stress. In the absence of dynacortin/RacE, compressive stresses decrease, and furrow thinning accelerates (Zhang and Robinson, 2005). This study proposed that resistive forces from the surrounding cortex counteract actively generated contractile tension at the cell equator. Moreover, Poirier et al. developed a computational model that pinpointed several stress-generating mechanisms contributing to furrow ingression in *D. discoideum*: myosin-mediated force generation, polar protrusive forces, viscoelasticity of the cytoskeleton, cortical tension and surface curvature. Their simulations indicated that polar protrusion forces or myosin-dependent contractile forces are sufficient to initiate furrow ingression, while passive forces from cortical tension and surface curvature contribute to complete ingression (Poirier *et al.*, 2012). Also, in support of cortical resisting forces counteracting ring constriction, laser microsurgery in constricting CRs of *C. elegans* embryos showed that the ring snaps open immediately after laser cutting, with severed ends pointing outwards and adopting a straight conformation, implying that the ring is countering cortical tension (Ana M Silva *et al.*, 2016).

Turlier et al. developed a theoretical model of the dividing sea-urchin embryo based on the active gel theory (Turlier, Audoly, Prost and J.-F. Joanny, 2014). Here, the cortex was considered a thin layer generating both viscous and active tensions and subjected to uniform cytoplasmic pressure. An overactivity at the equator reflecting RhoA activation necessary for furrow initiation was simulated with a gaussian distribution imposed along the cortex and centered at the equator, according to previous experimental observations (Bement, Benink and Von Dassow, 2005). This model used the same hydrodynamic theory already developed

by Salbreux et al. (Salbreux, Prost and Joanny, 2009), but actin filament turnover was considered, allowing the thickness of the cortical layer to vary during constriction. Actin filament turnover was found to be key for the rate and completion of ring constriction. A scaling model, in light of previous work from White and Borisy (White and Borisy, 1983) and Bray and White (Bray and White, 1988), successfully explained and reproduced the properties of furrow ingression and demonstrated that the contractility difference between the poles and the furrow region was the key parameter for both constriction dynamics and cytokinesis completion.

Interestingly, a recent study has hypothesized, inspired by earlier experiments (DAN, 1954; Dan et al., 1937; DAN & ONO, 1954; Swann, 1958), that cytokinesis is driven by positive feedback between contractile ring myosin and ring-directed cortical flow, with no significant resistance from cortical tension (Khaliullin *et al.*, 2018a). The authors showed that the per-unit-length amounts of ring myosin and anillin, ring-directed cortical flow and the constriction rate all increase with parallel exponential kinetics. In short, relaxation of the poles and membrane deposition at the polar regions would allow the cortex to be constantly pulled by myosin in the ring and ultimately loaded into the ring itself. Continuous loading of additional myosin would allow for more cortex to be pulled. This positive feedback would explain the increase in the constriction rate per unit length as the ring perimeter decreases, and consequently an overall constant constriction rate. This model implies that cortical flow and ring constriction velocity are exclusively dependent on the concentration of myosin in the ring, but no additional parameters, such as the concentration of F-actin or other crosslinkers, were evaluated.

Overall, the role of the surrounding cortex in setting cytokinesis dynamics is still a subject of debate. It is intuitive to think that the contractile ring must produce enough force to pinch the equator over a globally distributed actomyosin network, but experimental data of exactly when or how much the surrounding cortex resists constriction is missing outside *D. discoideum*. The contribution of cortical flows in promoting ring constriction, as proposed by Khaliulin et al. (Khaliullin *et al.*, 2018a), remains also to be further clarified. Cortical flows have been previously proposed to be essential for ring assembly and furrow formation (Reymann *et al.*, 2016); however, it is not totally clear whether they are a cause or a consequence of furrow ingression, or how much active material they actually load onto the constricting ring. This lack of experimental evidence is partly due to most actomyosin network components localizing both in the equatorial and surrounding cortex, therefore it becomes difficult to understand how the perturbation of a specific protein affects the mechanics of the ring or the cortex surrounding it. A challenge for the future includes the development of approaches to perturb involved proteins in a spatial and temporally controlled manner, such as rapid and reversible temperature shifts in fast-acting temperature-sensitive mutants (Davies *et al.*, 2014), acute and localized release or uncaging of chemical compounds (reviewed in Ellis-Davies, 2007), and localized

optogenetic control of protein function and localization (Wagner and Glotzer, 2016; Valon *et al.*, 2017).

C. elegans as a model organism to study cytokinesis

C. elegans

C. elegans is a microscopic roundworm of about 1 mm in length and 50 μm wide belonging to the Phylum Nematoda, barely visible to the naked eye. It owes its role as a model organism in scientific research to the cell biologist Sydney Brenner, who used it primarily to study neuronal development back in the 1960s. This worm is one of the simplest organisms that contains a nervous system and, as surprising as it may seem, that includes 302 neurons.
This nematode was the first organism to have its entire genome sequenced, which contains around 20470 protein-coding genes ("WS227 Release Letter". WormBase. 10 August 2011. Archived from the original on 28 November 2013. Retrieved 2013-11-19), 35% of which have human homologs. Interestingly, several human genes have been shown to replace their *C. elegans* homologs when introduced into *C. elegans*. Also, many *C. elegans* genes can function similarly to mammalian genes.
This animal can be found directly in temperate soil environments and usually feeds on bacteria. One of its most useful features is the transparency so one can observe all its cells and tissues. Other advantages include its simple anatomy, as explained above, cell lineage invariance and a short life cycle (as depicted in Figure 1.11) with large brood size, which allows experiments to be launched and completed relatively fast.

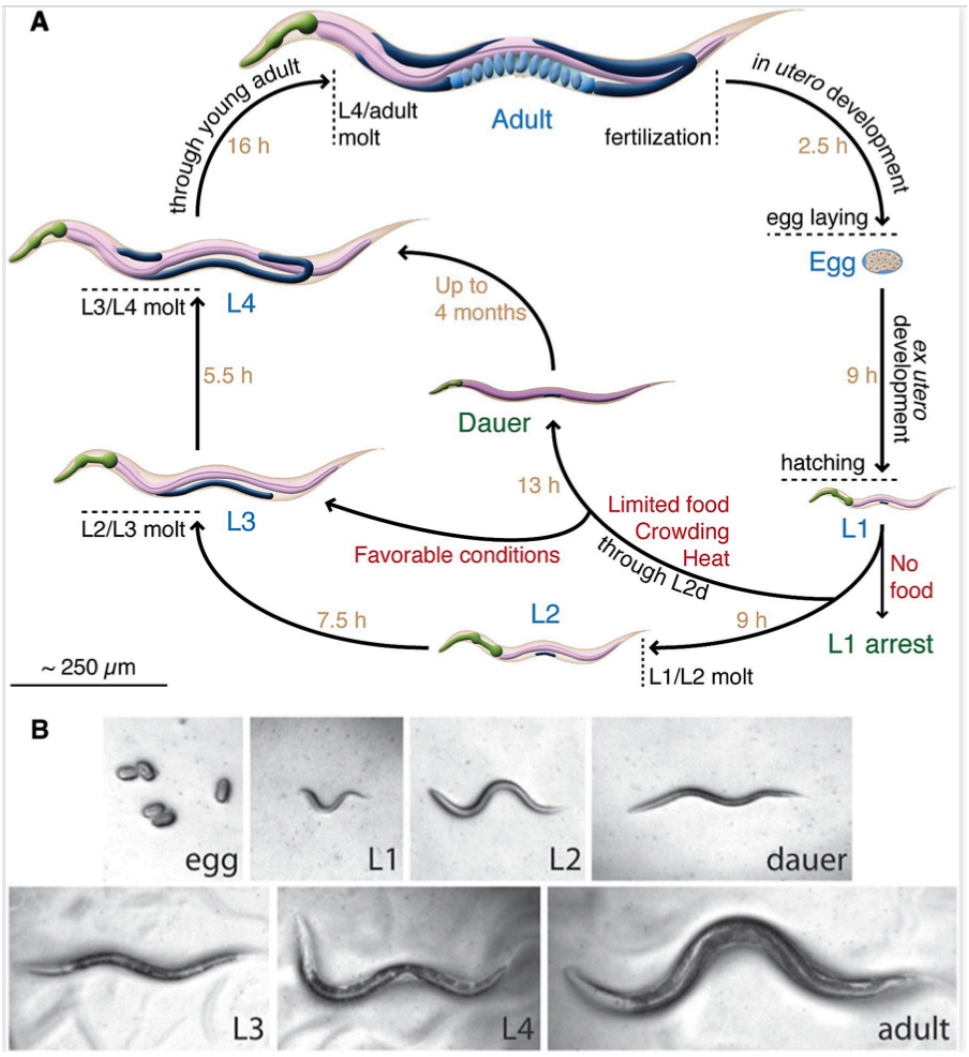

FIGURE 1.11. *C. elegans* life cycle and developmental stages. (A) *C. elegans* life cycle at 25ºC. (B) Micrographs of laid eggs, larval stages and adults. Images from (Fielenbach and Antebi, 2008 and Erkut, Cihan, 2014), used under permission.

RNA interference in *C. elegans*

RNA interference (RNAi), first discovered and characterized in *C. elegans* (Fire et al., 1998), is a regulatory mechanism in which cells use small double-stranded RNA (dsRNA) molecules to silence genes activity via an homology-dependent pathway. In brief, naturally occuring long dsRNA molecules are recognized and cut by Dicer, an RNase endonuclease, into small fragments (siRNA). These then bind to a complex, called RNA-induced silencing complex (RISC) that includes the protein Argonaute. The siRNA-RISC are directed to messenger RNAs (mRNAs) that share complementar homology with the siRNA fragment and they pair. Argonaute then cleaves the mRNA, which is degraded, blocking its transcription (Kim & Rossi, 2008; Neumeier & Meister, 2020). In *C. elegans*, dsRNA can be administered by injection, feeding or soaking of worms. Introduction of dsRNA triggers the degradation of the

corresponding mRNA in the gonad of Worm, while the target protein already existing in the gonad is continually packed into oocytes. As a result, protein levels in newly fertilized embryos gradually decrease between 12 and 48 hours after RNA injection. Importantly, the rate of protein depletion is largely independent of the protein's intrinsic turnover properties, because even proteins with long half-lives are gradually diluted out from the gonad by being packaged into oocytes. This means that embryos gradually more depleted of a specific protein can be readily obtained and gradually more severe phenotypes can be characterized.

Mos Single Copy Insertion in *C. elegans*

Mos Single Copy Insertion (MosSCI) is gene manipulation technique that allows the rapid generation of worm strains expressing tagged transgenes at physiological levels. MosSCI allows transgene insertions in a specific chromosomal site in single copy, under the control of the endogenous promoter and 3'-untranslated regions. The worms are injected with a mix of plasmids, one of them carrying the coding sequence of the tagged transgene of interest and another carrying the coding sequence for a transposase. The transposase excises a Mos1 transposon located in a known and defined locus, generating a double strand break. The break is repaired by transferring the DNA from the extrachromosomal template that includes the transgene of interest into the chromosomal site. Positive integration events can be easily screened and final strains will stably express the transgene at endogenous levels in the female and male germline (Frøkjær-jensen et al., 2009). This method is of particular interest when phenotypic analysis of *wild-type* versus mutant versions of a protein are the basis of a study.

References

Adam, T. *et al.* (1995) 'Cytoskeletal rearrangements and the functional role of T-plastin during entry of Shigella flexneri into HeLa cells.', *The Journal of cell biology*, 129(2), pp. 367–381. Available at: https://doi.org/10.1083/jcb.129.2.367.

Adelman, M.R. and Taylor, E.W. (1969) 'Isolation of an Actomyosin-Like Protein Complex from Slime Mold Plasmodium and the Separation of the Complex into Actin- and Myosin-like Fractions', *Biochemistry*, 8(12), pp. 4964–4975. Available at: https://doi.org/10.1021/bi00840a046.

ADELSTEIN, R.S. and ANNE CONTI, M. (1975) 'Phosphorylation of platelet myosin increases actin-activated myosin ATPase activity', *Nature*, 256(5518), pp. 597–598. Available at: https://doi.org/10.1038/256597a0.

Akkas, N. (1980) 'A model for cell division.', *Journal of biomechanics*, 13(5), pp. 459–461. Available at: https://doi.org/10.1016/0021-9290(80)90041-x.

Albert, P.J., Erdmann, T. and Schwarz, U.S. (2014) 'Stochastic dynamics and mechanosensitivity of myosin II minifilaments', *New Journal of Physics*, 16, pp. 1–27. Available at: https://doi.org/10.1088/1367-2630/16/9/093019.

Alberts, B. *et al.* (2002) *Molecular biology of the cell*. 4th Editio. New York: Garland Science; 2002. Available at: https://search.library.wisc.edu/catalog/999598982402121.

Allingham, J.S., Smith, R. and Rayment, I. (2005) 'The structural basis of blebbistatin inhibition and specificity for myosin II.', *Nature structural & molecular biology*, 12(4), pp. 378–379. Available at: https://doi.org/10.1038/nsmb908.

Alvarado, J. *et al.* (2017) 'Force percolation of contractile active gels', *Soft Matter*, 13(34), pp. 5624–5644. Available at: https://doi.org/10.1039/c7sm00834a.

Amann, K.J. and Pollard, T.D. (2001) 'Direct real-time observation of actin filament branching mediated by Arp2/3 complex using total internal reflection fluorescence microscopy.', *Proceedings of the National Academy of Sciences of the United States of America*, 98(26), pp. 15009–15013. Available at: https://doi.org/10.1073/pnas.211556398.

Amano, M. *et al.* (1996) 'Phosphorylation and activation of myosin by Rho-associated kinase (Rho-kinase).', *The Journal of biological chemistry*, 271(34), pp. 20246–20249. Available at: https://doi.org/10.1074/jbc.271.34.20246.

Aras, B.S. *et al.* (2018) 'The importance of mechanical constraints for proper polarization and psuedo-cleavage furrow generation in the early Caenorhabditis elegans embryo', *PLoS Computational Biology*, 14(7), pp. 1–19. Available at: https://doi.org/10.1371/journal.pcbi.1006294.

Arbizzani, F. *et al.* (2022) 'Septin filament compaction into rings requires the anillin Mid2 and contractile ring constriction', *Cell Reports*, 39(3), p. 110722. Available at: https://doi.org/10.1016/j.celrep.2022.110722.

Archibald Vivian Hill (1938) 'The heat of shortening and the dynamic constants of muscle', *Proceedings of the Royal Society of London. Series B - Biological Sciences*, 126(843), pp. 136–195. Available at: https://doi.org/10.1098/rspb.1938.0050.

Axelrod, D. *et al.* (no date) *MOBILITY MEASUREMENT BY ANALYSIS OF FLUORESCENCE PHOTOBLEACHING RECOVERY KINETICS*. Available at: https://www.ncbi.nlm.nih.gov/pmc/articles/PMC1334945/pdf/biophysj00300-0068.pdf (Accessed: 19 October 2018).

Bamburg, J.R., Harris, H.E. and Weeds, A.G. (1980) 'Partial purification and characterization of an actin depolymerizing factor from brain.', *FEBS letters*, 121(1), pp. 178–182. Available at: https://doi.org/10.1016/0014-5793(80)81292-0.

Banga, I. and Szent-Györgyi, A. (1942) 'Preparation and properties of myosin A and B', *Stud. Inst. Med. Chem. Univ. Szeged*, 1, pp. 5–15.

Bartles, J.R. (2000) 'Parallel actin bundles and their multiple actin-bundling proteins', *Current Opinion in Cell Biology*, 12(1), pp. 72–78. Available at: https://doi.org/10.1016/S0955-0674(99)00059-9.

Basant, A. *et al.* (2015) 'Aurora B Kinase Promotes Cytokinesis by Inducing Centralspindlin Oligomers that Associate with the Plasma Membrane', *Developmental Cell*, 33(2), pp. 204–215. Available at: https://doi.org/10.1016/j.devcel.2015.03.015.

Basant, A. and Glotzer, M. (2018a) 'Spatiotemporal Regulation of RhoA during Cytokinesis', *Current Biology*, 28(9), pp. R570–R580. Available at: https://doi.org/10.1016/j.cub.2018.03.045.

Basant, A. and Glotzer, M. (2018b) 'Spatiotemporal Regulation of RhoA during Cytokinesis', *Current Biology*, 28(9), pp. R570–R580. Available at: https://doi.org/10.1016/j.cub.2018.03.045.

Beach, J.R. *et al.* (2014) 'Nonmuscle myosin II isoforms coassemble in living cells', *Current Biology*, 24(10), pp. 1160–1166. Available at: https://doi.org/10.1016/j.cub.2014.03.071.

Belmonte, J.M., Leptin, M. and Nédélec, F. (2017) 'A theory that predicts behaviors of disordered cytoskeletal networks.', *Molecular systems biology*, 13(9), p. 941. Available at: https://doi.org/10.15252/msb.20177796.

Bement, W.M., Benink, H.A. and Von Dassow, G. (2005) 'A microtubule-dependent zone of active RhoA during cleavage plane specification', *Journal of Cell Biology*, 170(1), pp. 91–101. Available at: https://doi.org/10.1083/jcb.200501131.

Bement, W.M., Miller, A.L. and von Dassow, G. (2006) 'Rho GTPase activity zones and transient contractile arrays.', *BioEssays : news and reviews in molecular, cellular and developmental biology*, 28(10), pp. 983–993. Available at: https://doi.org/10.1002/bies.20477.

Bendix, P.M. *et al.* (2008) 'A quantitative analysis of contractility in active cytoskeletal protein networks.', *Biophysical journal*, 94(8), pp. 3126–3136. Available at: https://doi.org/10.1529/biophysj.107.117960.

Benink, H.A., Mandato, C.A. and Bement, W.M. (2000) 'Analysis of cortical flow models in vivo', *Molecular Biology of the Cell*, 11(8), pp. 2553–2563. Available at: https://doi.org/10.1091/mbc.11.8.2553.

Billington, N. *et al.* (2013) 'Characterization of three full-length human nonmuscle myosin II paralogs.', *The Journal of biological chemistry*, 288(46), pp. 33398–33410. Available at: https://doi.org/10.1074/jbc.M113.499848.

Biron, D. *et al.* (2005) 'Molecular model of the contractile ring', *Physical Review Letters*, 95(9), pp. 1–4. Available at: https://doi.org/10.1103/PhysRevLett.95.098102.

Blanchoin, L. *et al.* (2014) 'Actin dynamics, architecture, and mechanics in cell motility.', *Physiological reviews*, 94(1), pp. 235–63. Available at: https://doi.org/10.1152/physrev.00018.2013.

Borja da Rocha, H., Bleyer, J. and Turlier, H. (2022) 'A viscous active shell theory of the cell cortex', *Journal of the Mechanics and Physics of Solids*, 164, p. 104876. Available at: https://doi.org/https://doi.org/10.1016/j.jmps.2022.104876.

Bovellan, M. *et al.* (2014) 'Cellular control of cortical actin nucleation.', *Current biology : CB*, 24(14), pp. 1628–1635. Available at: https://doi.org/10.1016/j.cub.2014.05.069.

Braet, F. *et al.* (1996) 'Microfilament-disrupting agent latrunculin A induces an increased number of fenestrae in rat liver sinusoidal endothelial cells: Comparison with cytochalasin B', *Hepatology*, 24(3), pp. 627–635. Available at: https://doi.org/10.1053/jhep.1996.v24.pm0008781335.

Bray, D. and Whe, J.G. (1988) 'D. bray', 282(1987).

Bray, D. and White, J.G. (1988) 'Cortical flow in animal cells.', *Science (New York, N.Y.)*, 239(4842), pp. 883–888. Available at: https://doi.org/10.1126/science.3277283.

Bretscher, A. (1981) 'Fimbrin is a cytoskeletal protein that crosslinks F-actin in vitro', *Proceedings of the National Academy of Sciences of the United States of America*, 78(11 II), pp. 6849–6853. Available at: https://doi.org/10.1073/pnas.78.11.6849.

Bretscher, A. and Weber, K. (1980) 'Fimbrin, a new microfilament-associated protein present in microvilli and other cell surface structures', *Journal of Cell Biology*, 86(1), pp. 335–340. Available at: https://doi.org/10.1083/jcb.86.1.335.

Bridges, A.A. and Gladfelter, A.S. (2015) 'Septin form and function at the cell cortex', *Journal of Biological Chemistry*, 290(28), pp. 17173–17180. Available at: https://doi.org/10.1074/jbc.R114.634444.

Bringmann, H. and Hyman, A.A. (2005) 'A cytokinesis furrow is positioned by two consecutive signals.', *Nature*, 436(7051), pp. 731–734. Available at: https://doi.org/10.1038/nature03823.

Burgess, S.A. *et al.* (2007) 'Structures of Smooth Muscle Myosin and Heavy Meromyosin in the Folded, Shutdown State', *Journal of Molecular Biology*, 372(5), pp. 1165–1178. Available at: https://doi.org/10.1016/j.jmb.2007.07.014.

Burkard, M.E. *et al.* (2009) 'Plk1 Self-Organization and Priming Phosphorylation of HsCYK-4 at the Spindle Midzone Regulate the Onset of Division in Human Cells', *PLOS Biology*, 7(5), p. e1000111. Available at: https://doi.org/10.1371/journal.pbio.1000111.

Cai, Y. *et al.* (2003) 'Apical complex genes control mitotic spindle geometry and relative size of daughter cells in Drosophila neuroblast and pI asymmetric divisions', *Cell*, 112(1), pp. 51–62. Available at:

https://doi.org/10.1016/S0092-8674(02)01170-4.

Campbell, G.R. and Chamley, J.H. (1975) 'Thick filaments in vertebrate smooth muscle', *Cell and Tissue Research*, 156(2), pp. 201–216. Available at: https://doi.org/10.1007/BF00221803.

Campellone, K.G. and Welch, M.D. (2010) 'A nucleator arms race: Cellular control of actin assembly', *Nature Reviews Molecular Cell Biology*, 11(4), pp. 237–251. Available at: https://doi.org/10.1038/nrm2867.

Cao, L. *et al.* (2020) 'SPIN90 associates with mDia1 and the Arp2/3 complex to regulate cortical actin organization.', *Nature cell biology*, 22(7), pp. 803–814. Available at: https://doi.org/10.1038/s41556-020-0531-y.

Carlsson, A.E. (2006) 'Contractile stress generation by actomyosin gels.', *Physical review. E, Statistical, nonlinear, and soft matter physics*, 74(5 Pt 1), p. 51912. Available at: https://doi.org/10.1103/PhysRevE.74.051912.

Carlsson, L. *et al.* (1977) 'Actin polymerizability is influenced by profilin, a low molecular weight protein in non-muscle cells.', *Journal of molecular biology*, 115(3), pp. 465–483. Available at: https://doi.org/10.1016/0022-2836(77)90166-8.

Cartagena-Rivera, A.X. *et al.* (2016) 'Actomyosin Cortical Mechanical Properties in Nonadherent Cells Determined by Atomic Force Microscopy', *Biophysical Journal*, 110(11), pp. 2528–2539. Available at: https://doi.org/10.1016/j.bpj.2016.04.034.

Carvalho, A., Desai, A. and Oegema, K. (2009) 'Structural Memory in the Contractile Ring Makes the Duration of Cytokinesis Independent of Cell Size', *Cell*, 137(5), pp. 926–937. Available at: https://doi.org/10.1016/j.cell.2009.03.021.

Castrillon, D.H. and Wasserman, S.A. (1994) 'Diaphanous is required for cytokinesis in Drosophila and shares domains of similarity with the products of the limb deformity gene.', *Development (Cambridge, England)*, 120(12), pp. 3367–3377. Available at: https://doi.org/10.1242/dev.120.12.3367.

Chan, F.-Y. *et al.* (2019) 'The ARP2/3 complex prevents excessive formin activity during cytokinesis.', *Molecular biology of the cell*, 30(1), pp. 96–107. Available at: https://doi.org/10.1091/mbc.E18-07-0471.

Chang, F., Drubin, D. and Nurse, P. (1997) 'cdc12p, a protein required for cytokinesis in fission yeast, is a component of the cell division ring and interacts with profilin.', *The Journal of cell biology*, 137(1), pp. 169–182. Available at: https://doi.org/10.1083/jcb.137.1.169.

Chapa-Y-Lazo, B. *et al.* (2020) 'Polar relaxation by dynein-mediated removal of cortical myosin II.', *The Journal of cell biology*, 219(8). Available at: https://doi.org/10.1083/jcb.201903080.

Charras, G.T. *et al.* (2006) 'Reassembly of contractile actin cortex in cell blebs.', *The Journal of cell*

biology, 175(3), pp. 477–490. Available at: https://doi.org/10.1083/jcb.200602085.

Chen, A. *et al.* (2021) 'Inhibition of polar actin assembly by astral microtubules is required for cytokinesis.', *Nature communications*, 12(1), p. 2409. Available at: https://doi.org/10.1038/s41467-021-22677-0.

Chen, Q., Nag, S. and Pollard, T.D. (2012) 'Formins filter modified actin subunits during processive elongation.', *Journal of structural biology*, 177(1), pp. 32–39. Available at: https://doi.org/10.1016/j.jsb.2011.10.005.

Chen, Q. and Pollard, T.D. (2013) 'Actin filament severing by cofilin dismantles actin patches and produces mother filaments for new patches', *Current Biology*, 23(13), pp. 1154–1162. Available at: https://doi.org/10.1016/j.cub.2013.05.005.

Chesarone, M.A., Dupage, A.G. and Goode, B.L. (2010) 'Unleashing formins to remodel the actin and microtubule cytoskeletons', *Nature Reviews Molecular Cell Biology*, 11(1), pp. 62–74. Available at: https://doi.org/10.1038/nrm2816.

Chew, T.G. *et al.* (2017) 'Actin turnover maintains actin filament homeostasis during cytokinetic ring contraction', *Journal of Cell Biology*, 216(9), pp. 2657–2667. Available at: https://doi.org/10.1083/jcb.201701104.

Chikireddy, J. *et al.* (2024) 'Fascin-induced bundling protects actin filaments from disassembly by cofilin', *The Journal of cell biology*, 223(6). Available at: https://doi.org/10.1083/jcb.202312106.

Chugh, P. *et al.* (2017) 'Actin cortex architecture regulates cell surface tension', *Nature Cell Biology*, 19(6), pp. 689–697. Available at: https://doi.org/10.1038/ncb3525.

Clark, A.G. *et al.* (2014) 'Stresses at the cell surface during animal cell morphogenesis', *Current Biology*, 24(10), pp. R484–R494. Available at: https://doi.org/10.1016/j.cub.2014.03.059.

Clark, A.G., Dierkes, K. and Paluch, E.K. (2013) 'Monitoring actin cortex thickness in live cells.', *Biophysical journal*, 105(3), pp. 570–580. Available at: https://doi.org/10.1016/j.bpj.2013.05.057.

Clarke, M. and Spudich, J.A. (1974) 'Biochemical and structural studies of actomyosin-like proteins from non-muscle cells. Isolation and characterization of myosin from amoebae of Dictyostelium discoideum', *Journal of Molecular Biology*, 86(2). Available at: https://doi.org/10.1016/0022-2836(74)90013-8.

'Coarse-grained simulations of actomyosin rings point to a nodeless model involving both unipolar and bipolar myosins' (2018). Available at: https://doi.org/10.1091/mbc.E17-12-0736.

Coleman, T.R. *et al.* (1989) 'Functional diversity among spectrin isoforms.', *Cell motility and the cytoskeleton*, 12(4), pp. 225–247. Available at: https://doi.org/10.1002/cm.970120405.

Coleman, T.R. and Mooseker, M.S. (1985) 'Effects of actin filament cross-linking and filament length on actin-myosin interaction', *Journal of Cell Biology*, 101(5), pp. 1850–1857. Available at: https://doi.org/10.1083/jcb.101.5.1850.

Conibear, P.B. and Geeves, M.A. (1998) 'Cooperativity between the two heads of rabbit skeletal muscle heavy meromyosin in binding to actin.', *Biophysical journal*, 75(2), pp. 926–937. Available at: https://doi.org/10.1016/S0006-3495(98)77581-2.

Cooke, R. and Franks, K.E. (1978) 'Generation of force by single-headed myosin', *Journal of Molecular Biology*, 120(3), pp. 361–373. Available at: https://doi.org/10.1016/0022-2836(78)90424-2.

Cooper, J.A. (1987) 'Effects of cytochalasin and phalloidin on actin.', *The Journal of cell biology*, 105(4), pp. 1473–1478. Available at: https://doi.org/10.1083/jcb.105.4.1473.

Courtemanche, N. (2018) 'Mechanisms of formin-mediated actin assembly and dynamics'.

Courtemanche, N. and Pollard, T.D. (2013) 'Interaction of profilin with the barbed end of actin filaments.', *Biochemistry*, 52(37), pp. 6456–6466. Available at: https://doi.org/10.1021/bi400682n.

Cross, R.A. (1988) 'What is 10S myosin for?', *Journal of Muscle Research & Cell Motility*, 9(1), pp. 108–110. Available at: https://doi.org/10.1007/BF01682153.

Cuda, G. *et al.* (1997) 'In vitro actin filament sliding velocities produced by mixtures of different types of myosin', *Biophysical Journal*, 72(4), pp. 1767–1779. Available at: https://doi.org/10.1016/S0006-3495(97)78823-4.

D'Avino, P.P. (2009) 'How to scaffold the contractile ring for a safe cytokinesis - lessons from Anillin-related proteins.', *Journal of cell science*, 122(Pt 8), pp. 1071–1079. Available at: https://doi.org/10.1242/jcs.034785.

Daeden, A. *et al.* (2023) 'Polarized branched Actin modulates cortical mechanics to produce unequal-size daughters during asymmetric division', *Nature Cell Biology*, 25(2), pp. 235–245. Available at: https://doi.org/10.1038/s41556-022-01058-9.

DAN, K. (1954) 'THE CORTICAL MOVEMENT IN ARBACIA PUNCTULATA EGGS THROUGH CLEAVAGE CYCLES*', *Embryologia*, 2(12), pp. 115–122. Available at: https://doi.org/https://doi.org/10.1111/j.1440-169X.1954.tb00045.x.

Dan, K., Dan, J.C. and Yanagita, T. (no date) *Behaviour of the Cell Surface During Cleavage. II*. Available at: https://www.jstage.jst.go.jp/article/cytologia1929/8/3-4/8_3-4_521/_pdf (Accessed: 25 November 2018).

DAN, K. and ONO, T. (1954) 'A METHOD OF COMPUTATION OF THE SURFACE AREA OF THE CELL*', *Embryologia*, 2(10), pp. 87–99. Available at: https://doi.org/https://doi.org/10.1111/j.1440-

169X.1954.tb00043.x.

Dan, K., Yanagita, T. and Sugiyama, M. (1937) 'Behavior of the cell surface during cleavage. I', *Protoplasma*, 28(1), pp. 66–81. Available at: https://doi.org/10.1007/BF01624958.

Danilchik, M. V, Brown, E.E. and Riegert, K. (2006) 'Intrinsic chiral properties of the Xenopus egg cortex: an early indicator of left-right asymmetry?', *Development (Cambridge, England)*, 133(22), pp. 4517–4526. Available at: https://doi.org/10.1242/dev.02642.

Davies, T. *et al.* (2014) 'Article High-Resolution Temporal Analysis Reveals a Functional Timeline for the Molecular Regulation of Cytokinesis', *Developmental Cell*, 30, pp. 209–223. Available at: https://doi.org/10.1016/j.devcel.2014.05.009.

Dean, S.O. and Spudich, J.A. (2006) 'Rho kinase's role in myosin recruitment to the equatorial cortex of mitotic Drosophila S2 cells is for myosin regulatory light chain phosphorylation.', *PloS one*, 1(1), p. e131. Available at: https://doi.org/10.1371/journal.pone.0000131.

DeBiasio, R.L. *et al.* (1996) 'Myosin II transport, organization, and phosphorylation: evidence for cortical flow/solation-contraction coupling during cytokinesis and cell locomotion.', *Molecular biology of the cell*, 7(8), pp. 1259–1282. Available at: https://doi.org/10.1091/mbc.7.8.1259.

Descovich, C.P. *et al.* (2018) 'Cross-linkers both drive and brake cytoskeletal remodeling and furrowing in cytokinesis.', *Molecular biology of the cell*, 29(5), pp. 622–631. Available at: https://doi.org/10.1091/mbc.E17-06-0392.

Descovich, C.P. et al. (2017) 'Crosslinkers both drive and brake cytoskeletal remodeling and furrowing in cytokinesis', *Molecular Biology of the Cell*, 2, pp. 3–4.

Devine, C.E. and Somlyo, A.P. (1971) 'Thick filaments in vascular smooth muscle.', *The Journal of cell biology*, 49(3), pp. 636–649. Available at: https://doi.org/10.1083/jcb.49.3.636.

Dickinson, R.B., Caro, L. and Purich, D.L. (2004) 'Force generation by cytoskeletal filament end-tracking proteins.', *Biophysical journal*, 87(4), pp. 2838–2854. Available at: https://doi.org/10.1529/biophysj.104.045211.

Ding, W.Y., Ong, H.T., Hara, Y., Wongsantichon, J., Toyama, Y., Robinson, Robert C, *et al.* (2017) 'Plastin increases cortical connectivity to facilitate robust polarization and timely cytokinesis.', *The Journal of cell biology*, 216(5), pp. 1371–1386. Available at: https://doi.org/10.1083/jcb.201603070.

Ding, W.Y., Ong, H.T., Hara, Y., Wongsantichon, J., Toyama, Y., Robinson, Robert C., *et al.* (2017) 'Plastin increases cortical connectivity to facilitate robust polarization and timely cytokinesis', *Journal of Cell Biology*, 216(5), pp. 1371–1386. Available at: https://doi.org/10.1083/jcb.201603070.

Ding, Y., Cui, L., Zhao, Q., Zhang, W., Sun, H. and Zheng, Lijun (2017) 'Platelet-Rich Fibrin Accelerates

Skin Wound Healing in Diabetic Mice.', *Annals of plastic surgery*, 79(3), pp. e15–e19. Available at: https://doi.org/10.1097/SAP.0000000000001091.

Dix, C.L. *et al.* (2018) 'The Role of Mitotic Cell-Substrate Adhesion Re-modeling in Animal Cell Division.', *Developmental cell*, 45(1), pp. 132-145.e3. Available at: https://doi.org/10.1016/j.devcel.2018.03.009.

Djinović-Carugo, K. *et al.* (1999) 'Structure of the alpha-actinin rod: molecular basis for cross-linking of actin filaments.', *Cell*, 98(4), pp. 537–546. Available at: https://doi.org/10.1016/s0092-8674(00)81981-9.

Dorn, J.F. *et al.* (2016) 'A theoretical model of cytokinesis implicates feedback between membrane curvature and cytoskeletal organization in asymmetric cytokinetic furrowing.', *Molecular biology of the cell*, 27(8), pp. 1286–1299. Available at: https://doi.org/10.1091/mbc.E15-06-0374.

Dulyaninova, N.G. *et al.* (2005) 'Regulation of myosin-IIA assembly and Mts1 binding by heavy chain phosphorylation.', *Biochemistry*, 44(18), pp. 6867–6876. Available at: https://doi.org/10.1021/bi0500776.

Effler, J.C. *et al.* (2006) 'Mitosis-specific mechanosensing and contractile-protein redistribution control cell shape.', *Current biology : CB*, 16(19), pp. 1962–1967. Available at: https://doi.org/10.1016/j.cub.2006.08.027.

Egelhoff, T T, Lee, R.J. and Spudich, J.A. (1993) 'Dictyostelium myosin heavy chain phosphorylation sites regulate myosin filament assembly and localization in vivo.', *Cell*, 75(2), pp. 363–371. Available at: https://doi.org/10.1016/0092-8674(93)80077-r.

Egelhoff, Thomas T., Lee, R.J. and Spudich, J.A. (1993) 'Dictyostelium myosin heavy chain phosphorylation sites regulate myosin filament assembly and localization in vivo', *Cell*, 75(2), pp. 363–371. Available at: https://doi.org/10.1016/0092-8674(93)80077-R.

Egile, C. *et al.* (2005) 'Mechanism of filament nucleation and branch stability revealed by the structure of the Arp2/3 complex at actin branch junctions', *PLoS Biology*, 3(11), pp. 1902–1909. Available at: https://doi.org/10.1371/journal.pbio.0030383.

Eisenberg, E., Hill, T.L. and Chen, Y. (1980) 'Cross-bridge model of muscle contraction. Quantitative analysis.', *Biophysical journal*, 29(2), pp. 195–227. Available at: https://doi.org/10.1016/S0006-3495(80)85126-5.

Elkhatib, N. *et al.* (2014) 'Fascin plays a role in stress fiber organization and focal adhesion disassembly', *Current Biology*, 24(13), pp. 1492–1499. Available at: https://doi.org/10.1016/j.cub.2014.05.023.

Ellis-Davies, G.C.R. (2007) 'Caged compounds: photorelease technology for control of cellular

chemistry and physiology.', *Nature methods*, 4(8), pp. 619–628. Available at: https://doi.org/10.1038/nmeth1072.

Engelhardt, W.A. and Liubimova, M.N. (1994) '[Myosin and adenosine triphosphatase (Nature, 144, 688, Oct. 14, 1939)].', *Molekuliarnaia biologiia*, 28(6), pp. 1229–1230.

Ennomani, H. *et al.* (2016) 'Architecture and Connectivity Govern Actin Network Contractility.', *Current biology : CB*, 26(5), pp. 616–626. Available at: https://doi.org/10.1016/j.cub.2015.12.069.

Esue, O., Tseng, Y. and Wirtz, D. (2009) 'A-Actinin and Filamin Cooperatively Enhance the Stiffness of Actin Filament Networks', *PLoS ONE*, 4(2), pp. 1–6. Available at: https://doi.org/10.1371/journal.pone.0004411.

Evangelista, M. *et al.* (2002) 'Formins direct Arp2/3-independent actin filament assembly to polarize cell growth in yeast.', *Nature cell biology*, 4(1), pp. 32–41. Available at: https://doi.org/10.1038/ncb718.

Faix, J. *et al.* (1996) 'Cortexillins, major determinants of cell shape and size, are actin-bundling proteins with a parallel coiled-coil tail.', *Cell*, 86(4), pp. 631–642. Available at: https://doi.org/10.1016/s0092-8674(00)80136-1.

Faix, J. and Grosse, R. (2006) 'Staying in Shape with Formins', *Developmental Cell*, 10(6), pp. 693–706. Available at: https://doi.org/10.1016/j.devcel.2006.05.001.

Fang, X. *et al.* (2010) 'Biphasic targeting and cleavage furrow ingression directed by the tail of a myosin II.', *The Journal of cell biology*, 191(7), pp. 1333–1350. Available at: https://doi.org/10.1083/jcb.201005134.

Fenn, W.O. (1923) 'A quantitative comparison between the energy liberated and the work performed by the isolated sartorius muscle of the frog.', *The Journal of physiology*, 58(2–3), pp. 175–203. Available at: https://doi.org/10.1113/jphysiol.1923.sp002115.

Field, C M and Alberts, B.M. (1995) 'Anillin, a contractile ring protein that cycles from the nucleus to the cell cortex.', *The Journal of cell biology*, 131(1), pp. 165–178. Available at: https://doi.org/10.1083/jcb.131.1.165.

Field, Christine M. and Alberts, B.M. (1995) 'Anillin, a contractile ring protein that cycles from the nucleus to the cell cortex', *Journal of Cell Biology*, 131(1), pp. 165–178. Available at: https://doi.org/10.1083/jcb.131.1.165.

Fletcher, D.A. and Mullins, R.D. (2010) 'Cell mechanics and the cytoskeleton', *Nature*, 463(7280), pp. 485–492. Available at: https://doi.org/10.1038/nature08908.

Foley, K.S. and Young, P.W. (2014) 'The non-muscle functions of actinins: An update', *Biochemical Journal*, 459(1), pp. 1–13. Available at: https://doi.org/10.1042/BJ20131511.

Foth, B.J., Goedecke, M.C. and Soldati, D. (2006) 'New insights into myosin evolution and classification', *Proceedings of the National Academy of Sciences of the United States of America*, 103(10), pp. 3681–3686. Available at: https://doi.org/10.1073/pnas.0506307103.

Fritzsche, M. *et al.* (2013) 'Analysis of turnover dynamics of the submembranous actin cortex', *Molecular Biology of the Cell*, 24(6), pp. 757–767. Available at: https://doi.org/10.1091/mbc.E12-06-0485.

Fritzsche, M. *et al.* (2016) 'Actin kinetics shapes cortical network structure and mechanics.', *Science advances*, 2(4), p. e1501337. Available at: https://doi.org/10.1126/sciadv.1501337.

Fujiwara, K. and Pollard, T.D. (1976) 'Fluorescent antibody localization of myosin in the cytoplasm, cleavage furrow, and mitotic spindle of human cells.', *Journal of Cell Biology*, 71(3), pp. 848–875. Available at: https://doi.org/10.1083/jcb.71.3.848.

Fujiwara, K., Porter, M.E. and Pollard, T.D. (1978) 'Alpha-actinin localization in the cleavage furrow during cytokinesis.', *The Journal of cell biology*, 79(1), pp. 268–275. Available at: https://doi.org/10.1083/jcb.79.1.268.

Galan, J.E. and Zhou, D. (2000) 'Striking a balance: modulation of the actin cytoskeleton by Salmonella.', *Proceedings of the National Academy of Sciences of the United States of America*, 97(16), pp. 8754–8761. Available at: https://doi.org/10.1073/pnas.97.16.8754.

Galkin, V.E. *et al.* (2008) 'High-resolution cryo-EM structure of the F-actin-fimbrin/plastin ABD2 complex.', *Proceedings of the National Academy of Sciences of the United States of America*, 105(5), pp. 1494–1498. Available at: https://doi.org/10.1073/pnas.0708667105.

Galkin, V.E. *et al.* (2011) 'Remodeling of actin filaments by ADF/cofilin proteins', *Proceedings of the National Academy of Sciences of the United States of America*, 108(51), pp. 20568–20572. Available at: https://doi.org/10.1073/pnas.1110109108.

Ge, J. *et al.* (2016) 'Macromolecular Crowding Modulates Actomyosin Kinetics', *Biophysical Journal*, 111(1), pp. 178–184. Available at: https://doi.org/10.1016/j.bpj.2016.05.035.

Gittes, F. *et al.* (1993) 'Flexural rigidity of microtubules and actin filaments measured from thermal fluctuations in shape.', *The Journal of cell biology*, 120(4), pp. 923–934. Available at: https://doi.org/10.1083/jcb.120.4.923.

Glenney, J.R. *et al.* (1981) 'F-actin binding and bundling properties of fimbrin, a major cytoskeletal protein of microvillus core filaments', *Journal of Biological Chemistry*, 256(17), pp. 9283–9288. Available at: https://doi.org/10.1016/s0021-9258(19)52543-1.

Gokhin, D.S. and Fowler, V.M. (2013) 'A two-segment model for thin filament architecture in skeletal muscle', *Nature Reviews Molecular Cell Biology*, 14(2), pp. 113–119. Available at:

https://doi.org/10.1038/nrm3510.

Goley, E.D. and Welch, M.D. (2006) 'The ARP2/3 complex: An actin nucleator comes of age', *Nature Reviews Molecular Cell Biology*, 7(10), pp. 713–726. Available at: https://doi.org/10.1038/nrm2026.

Goode, B.L. and Eck, M.J. (2007) 'Mechanism and function of formins in the control of actin assembly', *Annual Review of Biochemistry*, 76, pp. 593–627. Available at: https://doi.org/10.1146/annurev.biochem.75.103004.142647.

Grębecki, A. (1984) 'Relative motion inAmoeba proteus in respect to the adhesion sites. I. Behavior of monotactic forms and the mechanism of fountain phenomenon', *Protoplasma*, 123(2), pp. 116–134. Available at: https://doi.org/10.1007/BF01283582.

Green, Rebeca; Paluch, E. and Oegema, K. (2012) 'Cytokinesis in Animal Cells', *Annual Review of Cell and Developmental Biology*, 28, pp. 29–58. Available at: https://doi.org/10.1146/annurev-cellbio-101011-155718.

Greenberg, M.J. *et al.* (2016) 'A Perspective on the Role of Myosins as Mechanosensors', *Biophysical Journal*, 110(12), pp. 2568–2576. Available at: https://doi.org/10.1016/j.bpj.2016.05.021.

Greenspan, H.P. (1977) 'On the dynamics of cell cleavage', *Journal of Theoretical Biology*, 65(1), pp. 79–99. Available at: https://doi.org/10.1016/0022-5193(77)90078-9.

Grill, S.W. *et al.* (2001) 'Polarity controls forces governing asymmetric spindle positioning in the Caenorhabditis elegans embryo.', *Nature*, 409(6820), pp. 630–633. Available at: https://doi.org/10.1038/35054572.

Guha, M., Zhou, M. and Wang, Y.-L. (2005) 'Cortical actin turnover during cytokinesis requires myosin II.', *Current biology : CB*, 15(8), pp. 732–736. Available at: https://doi.org/10.1016/j.cub.2005.03.042.

Guo, S. and Kemphues, K.J. (1996) 'Molecular genetics of asymmetric cleavage in the early Caenorhabditis elegans embryo.', *Current opinion in genetics & development*, 6(4), pp. 408–415. Available at: https://doi.org/10.1016/s0959-437x(96)80061-x.

Halavatyi, A.A. *et al.* (2010) 'A mathematical model of actin filament turnover for fitting FRAP data', *European Biophysics Journal*, 39(4), pp. 669–677. Available at: https://doi.org/10.1007/s00249-009-0558-2.

Harada, Y. *et al.* (1987) 'Sliding movement of single actin filaments on one-headed myosin filaments', *Nature*, pp. 805–808. Available at: https://doi.org/10.1038/326805a0.

Hartman, M.A. and Spudich, J.A. (2012) 'The myosin superfamily at a glance', *Journal of Cell Science*, 125(7), pp. 1627–1632. Available at: https://doi.org/10.1242/jcs.094300.

Hartwell, L.H. (1971) ‘Genetic control of the cell division cycle in yeast. IV. Genes controlling bud emergence and cytokinesis.’, *Experimental cell research*, 69(2), pp. 265–276. Available at: https://doi.org/10.1016/0014-4827(71)90223-0.

Hatano, S. and Oosawa, F. (1966) ‘Extraction of an actin-like protein from the plasmodium of a myxomycete and its interaction with myosin a from rabbit striated muscle’, *Journal of Cellular Physiology*, 68(2), pp. 197–202. Available at: https://doi.org/10.1002/jcp.1040680214.

Haviv, L. *et al.* (2008) ‘A cytoskeletal demolition worker: myosin II acts as an actin depolymerization agent.’, *Journal of molecular biology*, 375(2), pp. 325–330. Available at: https://doi.org/10.1016/j.jmb.2007.09.066.

He, X. and Dembo, M. (1997) ‘On the mechanics of the first cleavage division of the sea urchin egg.’, *Experimental cell research*, 233(2), pp. 252–273. Available at: https://doi.org/10.1006/excr.1997.3585.

Heissler, S.M. and Sellers, J.R. (2015) ‘Four things to know about myosin light chains as reporters for non-muscle myosin-2 dynamics in live cells’, *Cytoskeleton*, 72(2), pp. 65–70. Available at: https://doi.org/https://doi.org/10.1002/cm.21212.

Henson, J.H. *et al.* (2017) ‘The Ultrastructural Organization of Actin and Myosin II Filaments in the Contractile Ring: New Support for an Old Model of Cytokinesis’, *Molecular Biology of the Cell*, 28(5), pp. 613–623.

Higgs, H.N. (2005) ‘Formin proteins: A domain-based approach’, *Trends in Biochemical Sciences*, 30(6), pp. 342–353. Available at: https://doi.org/10.1016/j.tibs.2005.04.014.

Higuchi, H. and Goldman, Y.E. (1991) ‘Sliding distance between actin and myosin filaments per ATP molecule hydrolysed in skinned muscle fibres’, *Nature*, 352(6333), pp. 352–354. Available at: https://doi.org/10.1038/352352a0.

Hiraiwa, T. and Salbreux, G. (2016) ‘Role of Turnover in Active Stress Generation in a Filament Network.’, *Physical review letters*, 116(18), p. 188101. Available at: https://doi.org/10.1103/PhysRevLett.116.188101.

Hiramoto, Y. (1967) ‘Observations and measurements of sea urchin eggs with a centrifuge microscope’, *Journal of Cellular Physiology*, 69(2), pp. 219–230. Available at: https://doi.org/https://doi.org/10.1002/jcp.1040690212.

Hiramoto, Y. (1968) ‘The mechanics and mechanism of cleavage in the sea-urchin egg.’, *Symposia of the Society for Experimental Biology*, 22, pp. 311–327.

Holy, T.E. and Leibler, S. (1994) ‘Dynamic instability of microtubules as an efficient way to search in space’, *Proceedings of the National Academy of Sciences of the United States of America*, 91(12), pp. 5682–5685. Available at: https://doi.org/10.1073/pnas.91.12.5682.

Homa, K.E. *et al.* (2021) 'Formin Cdc12's specific actin assembly properties are tailored for cytokinesis in fission yeast', *Biophysical Journal*, 120(15), pp. 2984–2997. Available at: https://doi.org/10.1016/j.bpj.2021.06.023.

Homsher, E., Wang, F. and Sellers, J.R. (1992) 'Factors affecting movement of F-actin filaments propelled by skeletal muscle heavy meromyosin.', *The American journal of physiology*, 262(3 Pt 1), pp. C714-23. Available at: https://doi.org/10.1152/ajpcell.1992.262.3.C714.

Hozumi, S. *et al.* (2006) 'An unconventional myosin in Drosophila reverses the default handedness in visceral organs.', *Nature*, 440(7085), pp. 798–802. Available at: https://doi.org/10.1038/nature04625.

Huxley, H.E. (1963) 'Electron microscope studies on the structure of natural and synthetic protein filaments from striated muscle', *Journal of Molecular Biology*, 7(3), pp. 281–308. Available at: https://doi.org/10.1016/S0022-2836(63)80008-X.

HUXLEY, H.E. (1953) 'X-ray analysis and the problem of muscle.', *Proceedings of the Royal Society of London. Series B, Biological sciences*, 141(902), pp. 59–62. Available at: https://doi.org/10.1098/rspb.1953.0017.

HUXLEY, H.E. (1963) 'ELECTRON MICROSCOPE STUDIES ON THE STRUCTURE OF NATURAL AND SYNTHETIC PROTEIN FILAMENTS FROM STRIATED MUSCLE.', *Journal of molecular biology*, 7, pp. 281–308. Available at: https://doi.org/10.1016/s0022-2836(63)80008-x.

Ikebe, M., Hartshorne, D.J. and Elzinga, M. (1986) 'Identification, phosphorylation, and dephosphorylation of a second site for myosin light chain kinase on the 20,000-dalton light chain of smooth muscle myosin.', *The Journal of biological chemistry*, 261(1), pp. 36–39.

Ikebe, M., Koretz, J. and Hartshorne, D.J. (1988) 'Effects of phosphorylation of light chain residues threonine 18 and serine 19 on the properties and conformation of smooth muscle myosin.', *The Journal of biological chemistry*, 263(13), pp. 6432–6437.

Insall, R. *et al.* (2001) 'Dynamics of the Dictyostelium Arp2/3 complex in endocytosis, cytokinesis, and chemotaxis.', *Cell motility and the cytoskeleton*, 50(3), pp. 115–128. Available at: https://doi.org/10.1002/cm.10005.

Isenberg, G., Aebi, U. and Pollard, T.D. (1980) 'An actin-binding protein from acanthamoeba regulates actin filament polymerization and interactions', *Nature*, 288(5790), pp. 455–459. Available at: https://doi.org/10.1038/288455a0.

Ishida, T., Thitamadee, S. and Hashimoto, T. (2007) 'Twisted growth and organization of cortical microtubules.', *Journal of plant research*, 120(1), pp. 61–70. Available at: https://doi.org/10.1007/s10265-006-0039-y.

Ito, K. *et al.* (1999) 'Cooperativity between two heads of Dictyostelium myosin II in in vitro motility and

ATP hydrolysis', *Biophysical Journal*, 76(2), pp. 985–992. Available at: https://doi.org/10.1016/S0006-3495(99)77262-0.

Jackson-Grusby, L., Kuo, A. and Leder, P. (1992) 'A variant limb deformity transcript expressed in the embryonic mouse limb defines a novel formin.', *Genes & development*, 6(1), pp. 29–37. Available at: https://doi.org/10.1101/gad.6.1.29.

Jananji, S. *et al.* (2017) 'Multimodal and Polymorphic Interactions between Anillin and Actin: Their Implications for Cytokinesis.', *Journal of molecular biology*, 429(5), pp. 715–731. Available at: https://doi.org/10.1016/j.jmb.2017.01.020.

Janson, L.W., Kolega, J. and Taylor, D.L. (1991) 'Modulation of contraction by gelation/solation in a reconstituted motile model.', *The Journal of cell biology*, 114(5), pp. 1005–1015. Available at: https://doi.org/10.1083/jcb.114.5.1005.

Jia, H. *et al.* (2018) 'Predicting the pathological response to neoadjuvant chemoradiation using untargeted metabolomics in locally advanced rectal cancer', *Radiotherapy and Oncology*, 128(3), pp. 548–556. Available at: https://doi.org/10.1016/j.radonc.2018.06.022.

Jiang, W. *et al.* (1998) 'PRC1: a human mitotic spindle-associated CDK substrate protein required for cytokinesis.', *Molecular cell*, 2(6), pp. 877–885. Available at: https://doi.org/10.1016/s1097-2765(00)80302-0.

Joanny, J.F. *et al.* (2007) 'Hydrodynamic theory for multi-component active polar gels', *New Journal of Physics*, 9(11), p. 422. Available at: https://doi.org/10.1088/1367-2630/9/11/422.

Jochová, J., Rupes, I. and Streiblová, E. (1991) 'F-actin contractile rings in protoplasts of the yeast Schizosaccharomyces.', *Cell biology international reports*, 15(7), pp. 607–610. Available at: https://doi.org/10.1016/0309-1651(91)90007-6.

Jordan, S.N. and Canman, J.C. (2012) 'Rho GTPases in animal cell cytokinesis: an occupation by the one percent.', *Cytoskeleton (Hoboken, N.J.)*, 69(11), pp. 919–930. Available at: https://doi.org/10.1002/cm.21071.

Jung, H.S. *et al.* (2011) 'Role of the tail in the regulated state of myosin 2.', *Journal of molecular biology*, 408(5), pp. 863–878. Available at: https://doi.org/10.1016/j.jmb.2011.03.019.

Kabsch, W. *et al.* (1990) 'Atomic structure of the actin: DNase I complex ', *Nature*, 347(6288), pp. 37–44. Available at: https://doi.org/10.1038/347037a0.

Kad, N.M. *et al.* (2003) 'A mutant heterodimeric myosin with one inactive head generates maximal displacement.', *The Journal of cell biology*, 162(3), pp. 481–488. Available at: https://doi.org/10.1083/jcb.200304023.

Karess, R.E. *et al.* (1991) 'The regulatory light chain of nonmuscle myosin is encoded by spaghetti-squash, a gene required for cytokinesis in Drosophila', *Cell*, 65(7), pp. 1177–1189. Available at: https://doi.org/https://doi.org/10.1016/0092-8674(91)90013-O.

Kasza, K.E. *et al.* (2010) 'Actin filament length tunes elasticity of flexibly cross-linked actin networks', *Biophysical Journal*, 99(4), pp. 1091–1100. Available at: https://doi.org/10.1016/j.bpj.2010.06.025.

Kasza, K.E., Farrell, D.L. and Zallen, J.A. (2014) 'Spatiotemporal control of epithelial remodeling by regulated myosin phosphorylation.', *Proceedings of the National Academy of Sciences of the United States of America*, 111(32), pp. 11732–11737. Available at: https://doi.org/10.1073/pnas.1400520111.

Kasza, K.E., Supriyatno, S. and Zallen, J.A. (2019) 'Cellular defects resulting from disease-related myosin II mutations in Drosophila', *Proceedings of the National Academy of Sciences*, 116(44), pp. 22205–22211. Available at: https://doi.org/10.1073/pnas.1909227116.

Katayama, E. (1998) 'Quick-freeze deep-etch electron microscopy of the actin-heavy meromyosin complex during the in vitro motility assay.', *Journal of molecular biology*, 278(2), pp. 349–367. Available at: https://doi.org/10.1006/jmbi.1998.1715.

Kelly, R.E. and Rice, R. V (1969) 'Ultrastructural studies on the contractile mechanism of smooth muscle.', *The Journal of cell biology*, 42(3), pp. 683–694. Available at: https://doi.org/10.1083/jcb.42.3.683.

Khaliullin, R.N. *et al.* (2018a) 'A positive-feedback-based mechanism for constriction rate acceleration during cytokinesis in Caenorhabditis elegans', *eLife*, 7. Available at: https://doi.org/10.7554/eLife.36073.

Khaliullin, R.N. *et al.* (2018b) 'A positive-feedback-based mechanism for constriction rate acceleration during cytokinesis in Caenorhabditis elegans', *eLife*, 7. Available at: https://doi.org/10.7554/eLife.36073.

Khaliullin, R.N. *et al.* (2018c) 'A positive feedback-based mechanism for constriction rate acceleration during cytokinesis in C. elegans', *eLife*, 7, p. e36073. Available at: https://doi.org/10.7554/eLife.36073.

Kim, K.-Y. *et al.* (2005) 'Disease-associated mutations and alternative splicing alter the enzymatic and motile activity of nonmuscle myosins II-B and II-C.', *The Journal of biological chemistry*, 280(24), pp. 22769–22775. Available at: https://doi.org/10.1074/jbc.M503488200.

Kim, T. *et al.* (2009) 'Computational Analysis of Viscoelastic Properties of Crosslinked Actin Networks', *PLOS Computational Biology*, 5(7), p. e1000439. Available at: https://doi.org/10.1371/journal.pcbi.1000439.

Kinoshita, M. (2006) 'Diversity of septin scaffolds', *Current Opinion in Cell Biology*, 18(1), pp. 54–60. Available at: https://doi.org/10.1016/j.ceb.2005.12.005.

Kishi, K. *et al.* (1993) 'Regulation of cytoplasmic division of Xenopus embryo by rho p21 and its inhibitory GDP/GTP exchange protein (rho GDI).', *The Journal of cell biology*, 120(5), pp. 1187–1195. Available at: https://doi.org/10.1083/jcb.120.5.1187.

Kiyomitsu, T. (2015) 'Mechanisms of daughter cell-size control during cell division.', *Trends in cell biology*, 25(5), pp. 286–295. Available at: https://doi.org/10.1016/j.tcb.2014.12.003.

Klein, M.G. *et al.* (2004) 'Structure of the actin crosslinking core of fimbrin', *Structure*, 12(6), pp. 999–1013. Available at: https://doi.org/10.1016/j.str.2004.04.010.

Kohno, H. *et al.* (1996) 'Bni1p implicated in cytoskeletal control is a putative target of Rho1p small GTP binding protein in Saccharomyces cerevisiae.', *The EMBO journal*, 15(22), pp. 6060–6068.

Koltzoff, N. (1924) 'Experimental Biology and the Work of the Moscow Institute', *Science*, 59(1536), pp. 497–502. Available at: https://doi.org/10.1126/science.59.1536.497.

Kosako, H. *et al.* (2000) 'Rho-kinase/ROCK is involved in cytokinesis through the phosphorylation of myosin light chain and not ezrin/radixin/moesin proteins at the cleavage furrow.', *Oncogene*, 19(52), pp. 6059–6064. Available at: https://doi.org/10.1038/sj.onc.1203987.

Kovács, M. *et al.* (2004) 'Mechanism of blebbistatin inhibition of myosin II', *Journal of Biological Chemistry*, 279(34), pp. 35557–35563. Available at: https://doi.org/10.1074/jbc.M405319200.

Koyama, H. *et al.* (2012) 'A High-Resolution Shape Fitting and Simulation Demonstrated Equatorial Cell Surface Softening during Cytokinesis and Its Promotive Role in Cytokinesis'. Available at: https://doi.org/10.1371/journal.pone.0031607.

Krendel, M. and Mooseker, M.S. (2005) 'Myosins: tails (and heads) of functional diversity.', *Physiology (Bethesda, Md.)*, 20, pp. 239–251. Available at: https://doi.org/10.1152/physiol.00014.2005.

Kruse, K. *et al.* (2005a) 'Generic theory of active polar gels: a paradigm for cytoskeletal dynamics', *The European Physical Journal E*, 16(1), pp. 5–16. Available at: https://doi.org/10.1140/epje/e2005-00002-5.

Kruse, K. *et al.* (2005b) 'Generic theory of active polar gels: A paradigm for cytoskeletal dynamics', *European Physical Journal E*, 16(1), pp. 5–16. Available at: https://doi.org/10.1140/epje/e2005-00002-5.

Kruse, K. *et al.* (2006) 'Contractility and retrograde flow in lamellipodium motion.', *Physical biology*, 3(2), pp. 130–137. Available at: https://doi.org/10.1088/1478-3975/3/2/005.

Kuczmarski, E.R. and Spudich, J.A. (1980) 'Regulation of myosin self-assembly: phosphorylation of Dictyostelium heavy chain inhibits formation of thick filaments.', *Proceedings of the National Academy of Sciences of the United States of America*, 77(12), pp. 7292–7296. Available at:

https://doi.org/10.1073/pnas.77.12.7292.

de la Cruz, E.M. (2009) 'How cofilin severs an actin filament', *Biophysical Reviews*, 1(2), pp. 51–59. Available at: https://doi.org/10.1007/s12551-009-0008-5.

De La Cruz, E.M. and Gardel, M.L. (2015) 'Actin Mechanics and Fragmentation.', *The Journal of biological chemistry*, 290(28), pp. 17137–17144. Available at: https://doi.org/10.1074/jbc.R115.636472.

Lamsoul, I., Dupré, L. and Lutz, P.G. (2020) 'Molecular Tuning of Filamin A Activities in the Context of Adhesion and Migration', *Frontiers in Cell and Developmental Biology*, 8(November), pp. 1–10. Available at: https://doi.org/10.3389/fcell.2020.591323.

Langeberg, L.K. and Scott, J.D. (2015) 'Signalling scaffolds and local organization of cellular behaviour.', *Nature reviews. Molecular cell biology*, 16(4), pp. 232–244. Available at: https://doi.org/10.1038/nrm3966.

Laplante, C. *et al.* (2016) 'Molecular organization of cytokinesis nodes and contractile rings by super-resolution fluorescence microscopy of live fission yeast.', *Proceedings of the National Academy of Sciences of the United States of America*, 113(40), pp. E5876–E5885. Available at: https://doi.org/10.1073/pnas.1608252113.

Laporte, D. *et al.* (2012) 'α-Actinin and fimbrin cooperate with myosin II to organize actomyosin bundles during contractile-ring assembly.', *Molecular biology of the cell*, 23(16), pp. 3094–3110. Available at: https://doi.org/10.1091/mbc.E12-02-0123.

Leite, J. *et al.* (2019) 'Network Contractility During Cytokinesis-from Molecular to Global Views.', *Biomolecules*, 9(5). Available at: https://doi.org/10.3390/biom9050194.

Leite, J. *et al.* (2020) 'Equatorial Non-muscle Myosin II and Plastin Cooperate to Align and Compact F-actin Bundles in the Cytokinetic Ring.', *Frontiers in cell and developmental biology*, 8, p. 573393. Available at: https://doi.org/10.3389/fcell.2020.573393.

Lenz, M., Gardel, M.L. and Dinner, A.R. (2012) 'Requirements for contractility in disordered cytoskeletal bundles.', *New journal of physics*, 14. Available at: https://doi.org/10.1088/1367-2630/14/3/033037.

Lewis, A.K. and Bridgman, P.C. (1992) 'Nerve growth cone lamellipodia contain two populations of actin filaments that differ in organization and polarity.', *The Journal of cell biology*, 119(5), pp. 1219–1243. Available at: https://doi.org/10.1083/jcb.119.5.1219.

Li, J. *et al.* (2017) 'Buckling-induced F-actin fragmentation modulates the contraction of active cytoskeletal networks', *Soft Matter*, 13(17), pp. 3213–3220. Available at: https://doi.org/10.1039/c6sm02703b.

Li, R. and Bowerman, B. (2010) 'Symmetry breaking in biology.', *Cold Spring Harbor perspectives in*

biology, 2(3), p. a003475. Available at: https://doi.org/10.1101/cshperspect.a003475.

Li, T. *et al.* (2016) 'The E3 ligase Ubr3 regulates Usher syndrome and MYH9 disorder proteins in the auditory organs of Drosophila and mammals.', *eLife*, 5. Available at: https://doi.org/10.7554/eLife.15258.

Li, Y. *et al.* (2016) 'The F-actin bundler α-actinin Ain1 is tailored for ring assembly and constriction during cytokinesis in fission yeast.', *Molecular biology of the cell*, 27(11), pp. 1821–1833. Available at: https://doi.org/10.1091/mbc.E16-01-0010.

Li, Y. and Munro, E. (2021) 'Filament-guided filament assembly provides structural memory of filament alignment during cytokinesis', *Developmental Cell*, 56(17), pp. 2486-2500.e6. Available at: https://doi.org/10.1016/j.devcel.2021.08.009.

Lieleg, O., Claessens, M.M.A.E. and Bausch, A.R. (2010) 'Structure and dynamics of cross-linked actin networks', *Soft Matter*, 6(2), pp. 218–225. Available at: https://doi.org/10.1039/b912163n.

Lin, C.S. *et al.* (1993) 'Human plastin genes. Comparative gene structure, chromosome location, and differential expression in normal and neoplastic cells.', *The Journal of biological chemistry*, 268(4), pp. 2781–2792.

Liu, X. *et al.* (2016) 'Mammalian Nonmuscle Myosin II Binds to Anionic Phospholipids with Concomitant Dissociation of the Regulatory Light Chain *', *Journal of Biological Chemistry*, 291(48), pp. 24828–24837. Available at: https://doi.org/10.1074/jbc.M116.739185.

Liu, X. *et al.* (2017) 'Effect of ATP and regulatory light-chain phosphorylation on the polymerization of mammalian nonmuscle myosin II', *Proceedings of the National Academy of Sciences of the United States of America*, 114(32), pp. E6516–E6525. Available at: https://doi.org/10.1073/pnas.1702375114.

Lord, M., Laves, E. and Pollard, T.D. (2005) 'Cytokinesis depends on the motor domains of myosin-II in fission yeast but not in budding yeast.', *Molecular biology of the cell*, 16(11), pp. 5346–5355. Available at: https://doi.org/10.1091/mbc.e05-07-0601.

Loria, A., Longhini, K.M. and Glotzer, M. (2012) 'The RhoGAP domain of CYK-4 has an essential role in RhoA activation.', *Current biology : CB*, 22(3), pp. 213–219. Available at: https://doi.org/10.1016/j.cub.2011.12.019.

De Lozanne, A. and Spudich, J.A. (1987) 'Disruption of the Dictyostelium myosin heavy chain gene by homologous recombination.', *Science (New York, N.Y.)*, 236(4805), pp. 1086–91. Available at: http://www.ncbi.nlm.nih.gov/pubmed/3576222 (Accessed: 30 September 2018).

Lu, J. *et al.* (2007) 'Structure of the FH2 Domain of Daam1: Implications for Formin Regulation of Actin Assembly', *Journal of Molecular Biology*, 369(5), pp. 1258–1269. Available at: https://doi.org/10.1016/j.jmb.2007.04.002.

Lück-Vielmetter, D. *et al.* (1990) 'Replacement of threonine residues by serine and alanine in a phosphorylatable heavy chain fragment of Dictyostelium myosin II.', *FEBS letters*, 269(1), pp. 239–243. Available at: https://doi.org/10.1016/0014-5793(90)81163-i.

Luo, T. *et al.* (2012) 'Understanding the cooperative interaction between myosin II and actin cross-linkers mediated by actin filaments during mechanosensation', *Biophysical Journal*, 102(2), pp. 238–247. Available at: https://doi.org/10.1016/j.bpj.2011.12.020.

Lymn, R.W. and Taylor, E.W. (1971) 'Mechanism of Adenosine Triphosphate Hydrolysis by Actomyosin', *Biochemistry*, 10(25), pp. 4617–4624. Available at: https://doi.org/10.1021/bi00801a004.

Ma, X. *et al.* (2012) 'Nonmuscle myosin II exerts tension but does not translocate actin in vertebrate cytokinesis.', *Proceedings of the National Academy of Sciences of the United States of America*, 109(12), pp. 4509–4514. Available at: https://doi.org/10.1073/pnas.1116268109.

Ma, Y. *et al.* (2012) 'An integrated proteomics and metabolomics approach for defining oncofetal biomarkers in the colorectal cancer', *Annals of Surgery*, 255(4), pp. 720–730. Available at: https://doi.org/10.1097/SLA.0b013e31824a9a8b.

Mabuchi, I. and Okuno, M. (1977) 'The effect of myosin antibody on the division of starfish blastomeres.', *The Journal of cell biology*, 74(1), pp. 251–63. Available at: https://doi.org/10.1083/JCB.74.1.251.

Machesky, L.M. *et al.* (1994) 'Purification of a cortical complex containing two unconventional actins from Acanthamoeba by affinity chromatography on profilin-agarose.', *The Journal of cell biology*, 127(1), pp. 107–115. Available at: https://doi.org/10.1083/jcb.127.1.107.

Machesky, L.M. *et al.* (1997) 'Mammalian actin-related protein 2/3 complex localizes to regions of lamellipodial protrusion and is composed of evolutionarily conserved proteins.', *The Biochemical journal*, 328 (Pt 1(Pt 1), pp. 105–112. Available at: https://doi.org/10.1042/bj3280105.

Machnicka, B. *et al.* (2014) 'Spectrins: A structural platform for stabilization and activation of membrane channels, receptors and transporters', *Biochimica et Biophysica Acta - Biomembranes*, 1838(2), pp. 620–634. Available at: https://doi.org/10.1016/j.bbamem.2013.05.002.

Maddox, A.S. *et al.* (2005) 'Distinct roles for two C. elegans anillins in the gonad and early embryo.', *Development (Cambridge, England)*, 132(12), pp. 2837–2848. Available at: https://doi.org/10.1242/dev.01828.

Maddox, A.S. *et al.* (2007) 'Anillin and the septins promote asymmetric ingression of the cytokinetic furrow.', *Developmental cell*, 12(5), pp. 827–835. Available at: https://doi.org/10.1016/j.devcel.2007.02.018.

Magdalena, J. *et al.* (2003) 'Involvement of the Arp2/3 complex and Scar2 in Golgi polarity in scratch

wound models.', *Molecular biology of the cell*, 14(2), pp. 670–684. Available at: https://doi.org/10.1091/mbc.e02-06-0345.

Mahaffy, R.E. and Pollard, T.D. (2006) 'Kinetics of the formation and dissociation of actin filament branches mediated by Arp2/3 complex.', *Biophysical journal*, 91(9), pp. 3519–3528. Available at: https://doi.org/10.1529/biophysj.106.080937.

Maître, J.L. *et al.* (2016) 'Asymmetric division of contractile domains couples cell positioning and fate specification', *Nature*, 536(7616), pp. 344–348. Available at: https://doi.org/10.1038/nature18958.

Malawista, S.E. and De Boisfleury Chevance, A. (1982) 'The cytokineplast: purified, stable, and functional motile machinery from human blood polymorphonuclear leukocytes.', *The Journal of cell biology*, 95(3), pp. 960–973. Available at: https://doi.org/10.1083/jcb.95.3.960.

Mangal, S. *et al.* (2018) 'TPXL-1 activates Aurora A to clear contractile ring components from the polar cortex during cytokinesis', *Journal of Cell Biology*, 217(3), pp. 837–848. Available at: https://doi.org/10.1083/jcb.201706021.

Margossian, S.S. and Lowey, S. (1973) 'Substructure of the myosin molecule', *Journal of Molecular Biology*, 74(3), pp. 313–330. Available at: https://doi.org/10.1016/0022-2836(73)90376-8.

Margossian, S.S. and Lowey, S. (1978) 'Interaction of Myosin Subfragments with F-Actin', *Biochemistry*, 17(25), pp. 5431–5439. Available at: https://doi.org/10.1021/bi00618a017.

Marsland, D. (1956) 'Protoplasmic Contractility in Relation to Gel Structure: Temperature – Pressure Experiments on Cytokinesis and Amoeboid Movement', in G.H. Bourne and J.F.B.T.-I.R. of C. Danielli (eds). Academic Press, pp. 199–227. Available at: https://doi.org/https://doi.org/10.1016/S0074-7696(08)62571-1.

MARSLAND, D. (1950) 'The mechanisms of cell division; temperature-pressure experiments on the cleaving eggs of Arbacia punctulata.', *Journal of cellular and comparative physiology*, 36(2), pp. 205–227. Available at: https://doi.org/10.1002/jcp.1030360207.

Marsland, D. and Landau, J. V. (1954) 'The mechanisms of cytokinesis: Temperature-pressure studies on the cortical gel system in various marine eggs', *Journal of Experimental Zoology*, 125(3), pp. 507–539. Available at: https://doi.org/10.1002/jez.1401250307.

Mass, R.L. *et al.* (1990) 'Disruption of formin-encoding transcripts in two mutant limb deformity alleles.', *Nature*, 346(6287), pp. 853–855. Available at: https://doi.org/10.1038/346853a0.

Mastronarde, D.N. *et al.* (1993) 'Interpolar spindle microtubules in PTK cells.', *Journal of Cell Biology*, 123(6), pp. 1475–1489. Available at: https://doi.org/10.1083/jcb.123.6.1475.

Matsuda, K. *et al.* (2024) 'Myosin-induced F-actin fragmentation facilitates contraction of actin

networks', *Cytoskeleton*, (January), pp. 1–17. Available at: https://doi.org/10.1002/cm.21848.

Matsudaira, P. *et al.* (1983) 'Role of fimbrin and villin in determining the interfilament distances of actin bundles', *Nature*, 301(5897), pp. 209–214. Available at: https://doi.org/10.1038/301209a0.

Matsudaira, P. (1991) 'Modular organization of actin crosslinking proteins.', *Trends in biochemical sciences*, 16(3), pp. 87–92. Available at: https://doi.org/10.1016/0968-0004(91)90039-x.

Matsumura, F. *et al.* (1998) 'Specific localization of serine 19 phosphorylated myosin II during cell locomotion and mitosis of cultured cells', *Journal of Cell Biology*, 140(1), pp. 119–129. Available at: https://doi.org/10.1083/jcb.140.1.119.

Matsumura, F. (2005) 'Regulation of myosin II during cytokinesis in higher eukaryotes.', *Trends in cell biology*, 15(7), pp. 371–377. Available at: https://doi.org/10.1016/j.tcb.2005.05.004.

Matsumura, F. and Hartshorne, D.J. (2008) 'Myosin phosphatase target subunit: Many roles in cell function', *Biochemical and Biophysical Research Communications*, 369(1), pp. 149–156. Available at: https://doi.org/10.1016/j.bbrc.2007.12.090.

Maupin, P. and Pollard, T.D. (1986) 'Arrangement of actin filaments and myosin-like filaments in the contractile ring and of actin-like filaments in the mitotic spindle of dividing HeLa cells.', *Journal of ultrastructure and molecular structure research*, 94(1), pp. 92–103. Available at: https://doi.org/10.1016/0889-1605(86)90055-8.

Mavrakis, M. *et al.* (2014) 'Septins promote F-actin ring formation by crosslinking actin filaments into curved bundles', *Nature Cell Biology*, 16(4), pp. 322–334. Available at: https://doi.org/10.1038/ncb2921.

May, R.C. *et al.* (2000) 'Involvement of the Arp2/3 complex in phagocytosis mediated by FcgammaR or CR3.', *Nature cell biology*, 2(4), pp. 246–248. Available at: https://doi.org/10.1038/35008673.

Mayer, M. *et al.* (2010) 'Anisotropies in cortical tension reveal the physical basis of polarizing cortical flows', *Nature*, 467(7315), pp. 617–621. Available at: https://doi.org/10.1038/nature09376.

McCall, P.M. *et al.* (2019) 'Cofilin drives rapid turnover and fluidization of entangled F-actin', *Proceedings of the National Academy of Sciences of the United States of America*, 116(26), pp. 12629–12637. Available at: https://doi.org/10.1073/pnas.1818808116.

McCarthy, E.K. and Goldstein, B. (2006) 'Asymmetric spindle positioning.', *Current opinion in cell biology*, 18(1), pp. 79–85. Available at: https://doi.org/10.1016/j.ceb.2005.12.006.

McFadden, W.M. *et al.* (2017) 'Filament turnover tunes both force generation and dissipation to control long-range flows in a model actomyosin cortex', *PLOS Computational Biology*, 13(12), p. e1005811. Available at: https://doi.org/10.1371/journal.pcbi.1005811.

Mei, L. *et al.* (2022) 'Structural mechanism for bidirectional actin cross-linking by T-plastin.', *Proceedings of the National Academy of Sciences of the United States of America*, 119(37), p. e2205370119. Available at: https://doi.org/10.1073/pnas.2205370119.

Mendes Pinto, I. *et al.* (2012) 'Article Actin Depolymerization Drives Actomyosin Ring Contraction during Budding Yeast Cytokinesis'. Available at: https://doi.org/10.1016/j.devcel.2012.04.015.

Mendes Pinto, I., Rubinstein, B. and Li, R. (2013) 'Force to divide: structural and mechanical requirements for actomyosin ring contraction.', *Biophysical journal*, 105(3), pp. 547–554. Available at: https://doi.org/10.1016/j.bpj.2013.06.033.

Michaux, J.B. *et al.* (2018) 'Excitable RhoA dynamics drive pulsed contractions in the early C. elegans embryo', *Journal of Cell Biology*, 217(12), pp. 4230–4252. Available at: https://doi.org/10.1083/jcb.201806161.

Middelkoop, T.C. *et al.* (2021) 'CYK-1/Formin activation in cortical RhoA signaling centers promotes organismal left-right symmetry breaking.', *Proceedings of the National Academy of Sciences of the United States of America*, 118(20). Available at: https://doi.org/10.1073/pnas.2021814118.

Millar, N.C. and Homsher, E. (1992) 'Kinetics of force generation and phosphate release in skinned rabbit soleus muscle fibers.', *The American journal of physiology*, 262(5 Pt 1), pp. C1239-45. Available at: https://doi.org/10.1152/ajpcell.1992.262.5.C1239.

Miller, K.G., Field, C.M. and Alberts, B.M. (1989) 'Actin-binding proteins from Drosophila embryos: A complex network of interacting proteins detected by F-actin affinity chromatography', *Journal of Cell Biology*, 109(6 I), pp. 2963–2975. Available at: https://doi.org/10.1083/jcb.109.6.2963.

Mishima, M. (2016) 'Centralspindlin in Rappaport's cleavage signaling', *Seminars in Cell and Developmental Biology*, 53, pp. 45–56. Available at: https://doi.org/10.1016/j.semcdb.2016.03.006.

Mitchison, J.M. (1952) 'Cell membranes and cell division', in *Symp. Soc. Exp. Biol*, pp. 105–127.

MITCHISON, J.M. and SWANN, M.M. (1955) 'The Mechanical Properties of the Cell Surface : III. The Sea-Urchin Egg from Fertilization to Cleavage', *Journal of Experimental Biology*, 32(4), pp. 734–750. Available at: https://doi.org/10.1242/jeb.32.4.734.

Mitchison, T. and Kirschner, M. (1984) 'Dynamic instability of microtubule growth', *Nature*, 312(5991), pp. 237–242. Available at: https://doi.org/10.1038/312237a0.

Mitsuhashi, M. *et al.* (2011) 'Dynamic assembly properties of nonmuscle myosin II isoforms revealed by combination of fluorescence correlation spectroscopy and fluorescence cross-correlation spectroscopy.', *Journal of biochemistry*, 149(3), pp. 253–263. Available at: https://doi.org/10.1093/jb/mvq134.

Miyakawa, T. *et al.* (2012) 'Different Ca2+-sensitivities between the EF-hands of T- and L-plastins', *Biochemical and Biophysical Research Communications*, 429(3), pp. 137–141. Available at: https://doi.org/https://doi.org/10.1016/j.bbrc.2012.10.126.

Mizuno, D. *et al.* (2007) 'Nonequilibrium mechanics of active cytoskeletal networks.', *Science (New York, N.Y.)*, 315(5810), pp. 370–373. Available at: https://doi.org/10.1126/science.1134404.

Mizuno, H. *et al.* (2011) 'Rotational movement of the formin mDia1 along the double helical strand of an actin filament.', *Science (New York, N.Y.)*, 331(6013), pp. 80–83. Available at: https://doi.org/10.1126/science.1197692.

Mogilner, A. and Rubinstein, B. (2005) 'The physics of filopodial protrusion.', *Biophysical journal*, 89(2), pp. 782–795. Available at: https://doi.org/10.1529/biophysj.104.056515.

Mollinari, C. *et al.* (2002) 'PRC1 is a microtubule binding and bundling protein essential to maintain the mitotic spindle midzone.', *The Journal of cell biology*, 157(7), pp. 1175–1186. Available at: https://doi.org/10.1083/jcb.200111052.

Morton, D.G. *et al.* (2002) 'The Caenorhabditis elegans par-5 gene encodes a 14-3-3 protein required for cellular asymmetry in the early embryo.', *Developmental biology*, 241(1), pp. 47–58. Available at: https://doi.org/10.1006/dbio.2001.0489.

Mostowy, S. and Cossart, P. (2012) 'Septins: The fourth component of the cytoskeleton', *Nature Reviews Molecular Cell Biology*, 13(3), pp. 183–194. Available at: https://doi.org/10.1038/nrm3284.

Mukhina, S., Wang, Y.-L. and Murata-Hori, M. (2007) 'Alpha-actinin is required for tightly regulated remodeling of the actin cortical network during cytokinesis.', *Developmental cell*, 13(4), pp. 554–565. Available at: https://doi.org/10.1016/j.devcel.2007.08.003.

Mullins, R.D. *et al.* (1998) 'Arp2/3 complex from Acanthamoeba binds profilin and cross-links actin filaments', *Molecular Biology of the Cell*, 9(4), pp. 841–852. Available at: https://doi.org/10.1091/mbc.9.4.841.

Mullins, R.D., Heuser, J.A. and Pollard, T.D. (1998) 'The interaction of Arp2/3 complex with actin: Nucleation, high affinity pointed end capping, and formation of branching networks of filaments', *Proceedings of the National Academy of Sciences of the United States of America*, 95(11), pp. 6181–6186. Available at: https://doi.org/10.1073/pnas.95.11.6181.

Munro, E., Nance, J. and Priess, James R. (2004) 'Cortical flows powered by asymmetrical contraction transport PAR proteins to establish and maintain anterior-posterior polarity in the early C. elegans embryo', *Developmental Cell*, 7(3), pp. 413–424. Available at: https://doi.org/10.1016/j.devcel.2004.08.001.

Munro, E., Nance, J. and Priess, James R (2004) *Cortical Flows Powered by Asymmetrical Contraction*

Transport PAR Proteins to Establish and Maintain Anterior-Posterior Polarity in the Early C. elegans Embryo the anterior cortex and are thus called the anterior PAR complex (Boyd et al The initial cue tha, *Developmental Cell*. Guo and Kemphues. Available at: http://www.developmentalcell.com/cgi/content/ (Accessed: 10 October 2018).

Murrell, M. *et al.* (2015) 'Forcing cells into shape: The mechanics of actomyosin contractility', *Nature Reviews Molecular Cell Biology*, 16(8), pp. 486–498. Available at: https://doi.org/10.1038/nrm4012.

Murrell, M. and Gardel, M.L. (2014) 'Actomyosin sliding is attenuated in contractile biomimetic cortices', *Molecular Biology of the Cell*, 25(12), pp. 1845–1853. Available at: https://doi.org/10.1091/mbc.e13-08-0450.

Murrell, M.P. and Gardel, M.L. (2012) 'F-actin buckling coordinates contractility and severing in a biomimetic actomyosin cortex.', *Proceedings of the National Academy of Sciences of the United States of America*, 109(51), pp. 20820–20825. Available at: https://doi.org/10.1073/pnas.1214753109.

Murthy, K. and Wadsworth, P. (2005a) 'Myosin-II-dependent localization and dynamics of F-actin during cytokinesis.', *Current biology : CB*, 15(8), pp. 724–731. Available at: https://doi.org/10.1016/j.cub.2005.02.055.

Murthy, K. and Wadsworth, P. (2005b) 'Myosin-II-Dependent Localization and Dynamics of F-Actin during Cytokinesis', *Current Biology*, 15, pp. 724–731. Available at: https://doi.org/10.1016/j.cub.2005.02.055.

Naganathan, S.R. *et al.* (2014) 'Active torque generation by the actomyosin cell cortex drives left-right symmetry breaking.', *eLife*, 3, p. e04165. Available at: https://doi.org/10.7554/eLife.04165.

Naganathan, S.R. *et al.* (2016) 'Actomyosin-driven left-right asymmetry: from molecular torques to chiral self organization.', *Current opinion in cell biology*, 38, pp. 24–30. Available at: https://doi.org/10.1016/j.ceb.2016.01.004.

Najafabadi, F.R., Leaver, M. and Grill, S.W. (2022) 'Orchestrating nonmuscle myosin II filament assembly at the onset of cytokinesis.', *Molecular biology of the cell*, 33(8), p. ar74. Available at: https://doi.org/10.1091/mbc.E21-12-0599.

Nakano, K. *et al.* (2001) 'Interactions among a fimbrin, a capping protein, and an actin-depolymerizing factor in organization of the fission yeast actin cytoskeleton.', *Molecular biology of the cell*, 12(11), pp. 3515–3526. Available at: https://doi.org/10.1091/mbc.12.11.3515.

Namba, Y. *et al.* (1992) 'Human T Cell L-Plastin Bundles Actin Filaments in a Calcium Dependent Manner1', *The Journal of Biochemistry*, 112(4), pp. 503–507. Available at: https://doi.org/10.1093/oxfordjournals.jbchem.a123929.

Nayak, A. *et al.* (2020) 'Single-molecule analysis reveals that regulatory light chains fine-tune skeletal

myosin II function', *Journal of Biological Chemistry*, 295(20), pp. 7046–7059. Available at: https://doi.org/10.1074/jbc.RA120.012774.

Naydenov, N.G., Koblinski, J.E. and Ivanov, A.I. (2021) 'Anillin is an emerging regulator of tumorigenesis, acting as a cortical cytoskeletal scaffold and a nuclear modulator of cancer cell differentiation.', *Cellular and molecular life sciences : CMLS*, 78(2), pp. 621–633. Available at: https://doi.org/10.1007/s00018-020-03605-9.

Neidt, E.M., Skau, C.T. and Kovar, D.R. (2008) 'The cytokinesis formins from the nematode worm and fission yeast differentially mediate actin filament assembly.', *The Journal of biological chemistry*, 283(35), pp. 23872–23883. Available at: https://doi.org/10.1074/jbc.M803734200.

Ni, S. *et al.* (2012) 'Modification of interface between regulatory and essential light chains hampers phosphorylation-dependent activation of smooth muscle myosin.', *The Journal of biological chemistry*, 287(26), pp. 22068–22079. Available at: https://doi.org/10.1074/jbc.M112.343491.

Nishikawa, M. *et al.* (1984) 'Protein kinase C modulates in vitro phosphorylation of the smooth muscle heavy meromyosin by myosin light chain kinase', *Journal of Biological Chemistry*, 259(14), pp. 8808–8814. Available at: https://doi.org/10.1016/s0021-9258(17)47225-5.

Nislow, C. *et al.* (1990) 'A monoclonal antibody to a mitotic microtubule-associated protein blocks mitotic progression', *Journal of Cell Biology*, 111(2), pp. 511–522. Available at: https://doi.org/10.1083/jcb.111.2.511.

Nonaka, S. *et al.* (1998) 'Randomization of left-right asymmetry due to loss of nodal cilia generating leftward flow of extraembryonic fluid in mice lacking KIF3B motor protein.', *Cell*, 95(6), pp. 829–837. Available at: https://doi.org/10.1016/s0092-8674(00)81705-5.

Norstrom, M. and Gardel, M.L. (2011) 'Shear thickening of F-actin networks crosslinked with non-muscle myosin IIB.', *Soft matter*, 2011(7), pp. 3228–3233. Available at: https://doi.org/10.1039/C0SM01157F.

Nunnally, M.H., D'Angelo, J.M. and Craig, S.W. (1980) 'Filamin concentration in cleavage furrow and midbody region: frequency of occurrence compared with that of alpha-actinin and myosin.', *Journal of Cell Biology*, 87(1), pp. 219–226. Available at: https://doi.org/10.1083/jcb.87.1.219.

O'Connell, C.B., Warner, A.K. and Wang, Y. (2001) 'Distinct roles of the equatorial and polar cortices in the cleavage of adherent cells.', *Current biology : CB*, 11(9), pp. 702–707. Available at: https://doi.org/10.1016/s0960-9822(01)00181-6.

Odronitz, F. and Kollmar, M. (2007) 'Drawing the tree of eukaryotic life based on the analysis of 2,269 manually annotated myosins from 328 species', *Genome Biology*, 8(9), pp. 1–23. Available at: https://doi.org/10.1186/gb-2007-8-9-r196.

Oelz, D.B., Rubinstein, B.Y. and Mogilner, A. (2015) 'A Combination of Actin Treadmilling and Cross-Linking Drives Contraction of Random Actomyosin Arrays.', *Biophysical journal*, 109(9), pp. 1818–1829. Available at: https://doi.org/10.1016/j.bpj.2015.09.013.

Oon, C.H. and Prehoda, K.E. (2021) 'Phases of cortical actomyosin dynamics coupled to the neuroblast polarity cycle', *eLife*, 10, pp. 1–11. Available at: https://doi.org/10.7554/eLife.66574.

Orlova, A. *et al.* (1997) 'Modulation of yeast F-actin structure by a mutation in the nucleotide-binding cleft.', *Journal of molecular biology*, 271(2), pp. 235–243. Available at: https://doi.org/10.1006/jmbi.1997.1163.

Osório, D.S. *et al.* (2019) 'Crosslinking activity of non-muscle myosin II is not sufficient for embryonic cytokinesis in C. elegans.', *Development (Cambridge, England)*, 146(21). Available at: https://doi.org/10.1242/dev.179150.

Otomo, T., Otomo, C., Tomchick, Diana R, *et al.* (2005) 'Structural basis of Rho GTPase-mediated activation of the formin mDia1.', *Molecular cell*, 18(3), pp. 273–281. Available at: https://doi.org/10.1016/j.molcel.2005.04.002.

Otomo, T., Otomo, C., Tomchick, Diana R., *et al.* (2005) 'Structural basis of Rho GTPase-mediated activation of the formin mDia1', *Molecular Cell*, 18(3), pp. 273–281. Available at: https://doi.org/10.1016/j.molcel.2005.04.002.

Ozlü, N. *et al.* (2005) 'An essential function of the C. elegans ortholog of TPX2 is to localize activated aurora A kinase to mitotic spindles.', *Developmental cell*, 9(2), pp. 237–248. Available at: https://doi.org/10.1016/j.devcel.2005.07.002.

Ozugergin, I. *et al.* (2022) 'Diverse mechanisms regulate contractile ring assembly for cytokinesis in the two-cell Caenorhabditis elegans embryo', *Journal of Cell Science*, 135(3), p. jcs258921. Available at: https://doi.org/10.1242/jcs.258921.

Palani, S. *et al.* (2017) 'Motor Activity Dependent and Independent Functions of Myosin II Contribute to Actomyosin Ring Assembly and Contraction in Schizosaccharomyces pombe.', *Current biology : CB*, 27(5), pp. 751–757. Available at: https://doi.org/10.1016/j.cub.2017.01.028.

Pasternak, C. *et al.* (1989) 'Intermolecular versus intramolecular interactions of Dictyostelium myosin: possible regulation by heavy chain phosphorylation.', *The Journal of cell biology*, 109(1), pp. 203–210. Available at: https://doi.org/10.1083/jcb.109.1.203.

Pate, E. and Cooke, R. (1989) 'A model of crossbridge action: the effects of ATP, ADP and Pi.', *Journal of muscle research and cell motility*, 10(3), pp. 181–196. Available at: https://doi.org/10.1007/BF01739809.

Pavicic-Kaltenbrunner, V., Mishima, M. and Glotzer, M. (2007) 'Cooperative assembly of CYK-

4/MgcRacGAP and ZEN-4/MKLP1 to form the centralspindlin complex.', *Molecular biology of the cell*, 18(12), pp. 4992–5003. Available at: https://doi.org/10.1091/mbc.e07-05-0468.

Petronczki, M. *et al.* (2007) 'Polo-like Kinase 1 Triggers the Initiation of Cytokinesis in Human Cells by Promoting Recruitment of the RhoGEF Ect2 to the Central Spindle', *Developmental Cell*, 12(5), pp. 713–725. Available at: https://doi.org/10.1016/j.devcel.2007.03.013.

Piekny, A., Werner, M. and Glotzer, M. (2005) 'Cytokinesis: welcome to the Rho zone', *Trends in Cell Biology*, 15(12), pp. 651–658. Available at: https://doi.org/https://doi.org/10.1016/j.tcb.2005.10.006.

Piekny, A.J. and Glotzer, M. (no date) 'Report Anillin Is a Scaffold Protein That Links RhoA, Actin, and Myosin during Cytokinesis', *Current Biology*, 18, pp. 30–36. Available at: https://doi.org/10.1016/j.cub.2007.11.068.

Piekny, A.J. and Maddox, A.S. (2010) 'The myriad roles of Anillin during cytokinesis.', *Seminars in cell & developmental biology*, 21(9), pp. 881–891. Available at: https://doi.org/10.1016/j.semcdb.2010.08.002.

Piekny, A.J. and Mains, P.E. (2002) 'Rho-binding kinase (LET-502) and myosin phosphatase (MEL-11) regulate cytokinesis in the early Caenorhabditis elegans embryo.', *Journal of cell science*, 115(Pt 11), pp. 2271–2282. Available at: https://doi.org/10.1242/jcs.115.11.2271.

Pimpale, L.G. *et al.* (2020) 'Cell lineage-dependent chiral actomyosin flows drive cellular rearrangements in early caenorhabditis elegans development', *eLife*, 9, pp. 1–35. Available at: https://doi.org/10.7554/eLife.54930.

Poirier, C.C. *et al.* (2012) 'Deconvolution of the cellular force-generating subsystems that govern cytokinesis furrow ingression', *PLoS Computational Biology*, 8(4). Available at: https://doi.org/10.1371/journal.pcbi.1002467.

Pollard, T.D. (1986) 'Rate constants for the reactions of ATP- and ADP-actin with the ends of actin filaments.', *The Journal of cell biology*, 103(6 Pt 2), pp. 2747–2754. Available at: https://doi.org/10.1083/jcb.103.6.2747.

Pollard, T.D. (2017) 'Nine unanswered questions about cytokinesis', *Journal of Cell Biology*, 216(10), pp. 3007–3016. Available at: https://doi.org/10.1083/jcb.201612068.

Pollard, T.D. and Cooper, J.A. (2009) 'Actin, a central player in cell shape and movement', *Science*, 326(5957), pp. 1208–1212. Available at: https://doi.org/10.1126/science.1175862.

Pospich, S. *et al.* (2021) 'High-resolution structures of the actomyosin-V complex in three nucleotide states provide insights into the force generation mechanism', *eLife*. Edited by S.L. Reck-Peterson, J.D. Faraldo-Gómez, and E.M. Ostap, 10, p. e73724. Available at: https://doi.org/10.7554/eLife.73724.

Prévost, M.C. *et al.* (1992) 'Unipolar reorganization of F-actin layer at bacterial division and bundling of actin filaments by plastin correlate with movement of Shigella flexneri within HeLa cells.', *Infection and immunity*, 60(10), pp. 4088–4099. Available at: https://doi.org/10.1128/iai.60.10.4088-4099.1992.

Proctor, S.A. *et al.* (2012) 'Contributions of turgor pressure, the contractile ring, and septum assembly to forces in cytokinesis in fission yeast.', *Current biology : CB*, 22(17), pp. 1601–1608. Available at: https://doi.org/10.1016/j.cub.2012.06.042.

Prost, J., Jülicher, F. and Joanny, J.-F. (2015) 'Active gel physics', *Nature Physics*, 11(2), pp. 111–117. Available at: https://doi.org/10.1038/nphys3224.

Pruyne, D. *et al.* (2002) 'Role of formins in actin assembly: Nucleation and barbed-end association', *Science*, 297(5581), pp. 612–615. Available at: https://doi.org/10.1126/science.1072309.

Ramkumar, N. *et al.* (2021) 'Aurora B-dependent polarization of the cortical actomyosin network during mitotic exit', *EMBO reports*, 22(10), pp. 1–13. Available at: https://doi.org/10.15252/embr.202152387.

Ramkumar, N. and Baum, B. (2016) 'Coupling changes in cell shape to chromosome segregation.', *Nature reviews. Molecular cell biology*, 17(8), pp. 511–521. Available at: https://doi.org/10.1038/nrm.2016.75.

Rappaport, R. (1961) 'Experiments concerning the cleavage stimulus in sand dollar eggs', *Journal of Experimental Zoology*, 148(1), pp. 81–89. Available at: https://doi.org/https://doi.org/10.1002/jez.1401480107.

Rappaport, R. (1967) 'Cell division: direct measurement of maximum tension exerted by furrow of echinoderm eggs.', *Science (New York, N.Y.)*, 156(3779), pp. 1241–1243. Available at: https://doi.org/10.1126/science.156.3779.1241.

Rappaport, R. (1977) 'Tensiometric studies of cytokinesis in cleaving sand dollar eggs.', *The Journal of experimental zoology*, 201(3), pp. 375–378. Available at: https://doi.org/10.1002/jez.1402010304.

Rappaport, R. (1986) 'Establishment of the Mechanism of Cytokinesis in Animal Cells', in G.H. Bourne, K.W. Jeon, and M.B.T.-I.R. of C. Friedlander (eds). Academic Press, pp. 245–281. Available at: https://doi.org/https://doi.org/10.1016/S0074-7696(08)61065-7.

Ravid, S. and Spudich, J.A. (1989) 'Myosin heavy chain kinase from developed Dictyostelium cells. Purification and characterization.', *The Journal of biological chemistry*, 264(25), pp. 15144–15150.

Reichl, E.M. *et al.* (2008) 'Interactions between Myosin and Actin Crosslinkers Control Cytokinesis Contractility Dynamics and Mechanics', *Current Biology*, 18(7), pp. 471–480. Available at: https://doi.org/10.1016/j.cub.2008.02.056.

Ren, Y. *et al.* (2009) 'Mechanosensing through cooperative interactions between myosin II and the actin

crosslinker cortexillin I.', *Current biology : CB*, 19(17), pp. 1421–1428. Available at: https://doi.org/10.1016/j.cub.2009.07.018.

Reymann, A.-C. *et al.* (2016) 'Cortical flow aligns actin filaments to form a furrow', *eLife*, 5. Available at: https://doi.org/10.7554/eLife.17807.

Reymann, A.C. *et al.* (2012) 'Actin network architecture can determine myosin motor activity', *Science*, 336(6086), pp. 1310–1314. Available at: https://doi.org/10.1126/science.1221708.

Richards, T.A. and Cavalier-Smith, T. (2005) 'Myosin domain evolution and the primary divergence of eukaryotes', *Nature*, 436(7054), pp. 1113–1118. Available at: https://doi.org/10.1038/nature03949.

Robinson, D.N. *et al.* (2002) 'Quantitation of the distribution and flux of myosin-II during cytokinesis', *BMC Cell Biology*, 3, pp. 1–13. Available at: https://doi.org/10.1186/1471-2121-3-4.

Robinson, D.N. and Spudich, J.A. (2000) 'Dynacortin, a genetic link between equatorial contractility and global shape control discovered by library complementation of a Dictyostelium discoideum cytokinesis mutant.', *The Journal of cell biology*, 150(4), pp. 823–838. Available at: https://doi.org/10.1083/jcb.150.4.823.

Robinson R.C. *et al.* (2001) 'Crystal Structure of Arp2 / 3 Complex', *Science*, 294(November), pp. 1679–1685.

Rodrigues, N.T.L. *et al.* (2015) 'Kinetochore-localized PP1-Sds22 couples chromosome segregation to polar relaxation.', *Nature*, 524(7566), pp. 489–492. Available at: https://doi.org/10.1038/nature14496.

Rosenfeld, S.S. *et al.* (2003) 'Myosin IIB is unconventionally conventional', *Journal of Biological Chemistry*, 278(30), pp. 27449–27455. Available at: https://doi.org/10.1074/jbc.M302555200.

Rouiller, I. *et al.* (2008) 'The structural basis of actin filament branching by the Arp2/3 complex.', *The Journal of cell biology*, 180(5), pp. 887–895. Available at: https://doi.org/10.1083/jcb.200709092.

Russell, S.E.H. and Hall, P.A. (2011) 'Septin genomics: a road less travelled.', *Biological chemistry*, 392(8–9), pp. 763–767. Available at: https://doi.org/10.1515/BC.2011.079.

Sabry, J.H. *et al.* (1997) 'Myosin heavy chain phosphorylation sites regulate myosin localization during cytokinesis in live cells', *Molecular Biology of the Cell*, 8(12), pp. 2605–2615. Available at: https://doi.org/10.1091/mbc.8.12.2605.

Sagot, I. *et al.* (2002) 'An actin nucleation mechanism mediated by Bni1 and profilin', *Nature Cell Biology*, 4(8), pp. 626–631. Available at: https://doi.org/10.1038/ncb834.

Sagot, I., Klee, S.K. and Pellman, D. (2002) 'Yeast formins regulate cell polarity by controlling the assembly of actin cables.', *Nature cell biology*, 4(1), pp. 42–50. Available at:

https://doi.org/10.1038/ncb719.

Saha, S. and Pollard, T.D. (2012) 'Characterization of structural and functional domains of the anillin-related protein Mid1p that contribute to cytokinesis in fission yeast', *Molecular Biology of the Cell*, 23(20), pp. 3993–4007. Available at: https://doi.org/10.1091/mbc.E12-07-0536.

Sain, A., Inamdar, M.M. and J??licher, F. (2015) 'Dynamic force balances and cell shape changes during cytokinesis', *Physical Review Letters*, 114(4), pp. 1–5. Available at: https://doi.org/10.1103/PhysRevLett.114.048102.

Salbreux, G., Charras, G. and Paluch, E. (2012) 'Actin cortex mechanics and cellular morphogenesis', *Trends in Cell Biology*, 22(10), pp. 536–545. Available at: https://doi.org/10.1016/j.tcb.2012.07.001.

Salbreux, G., Prost, J. and Joanny, J.F. (2009) 'Hydrodynamics of cellular cortical flows and the formation of contractile rings.', *Physical review letters*, 103(5), p. 58102. Available at: https://doi.org/10.1103/PhysRevLett.103.058102.

Sampayo, R.G. *et al.* (2023) 'Mechanosensitive stem cell fate choice is instructed by dynamic fluctuations in activation of Rho GTPases', *Proceedings of the National Academy of Sciences*, 120(22), p. e2219854120. Available at: https://doi.org/10.1073/pnas.2219854120.

Sanger, J.M. and Sanger, J.W. (1980) 'Banding and polarity of actin filaments in interphase and cleaving cells.', *The Journal of cell biology*, 86(2), pp. 568–575. Available at: https://doi.org/10.1083/jcb.86.2.568.

Schmoller, K.M., Semmrich, C. and Bausch, A.R. (2011) 'Slow down of actin depolymerization by cross-linking molecules', *Journal of Structural Biology*, 173(2), pp. 350–357. Available at: https://doi.org/10.1016/j.jsb.2010.09.003.

Schmutz, C., Stevens, J. and Spang, A. (2007) 'Functions of the novel RhoGAP proteins RGA-3 and RGA-4 in the germ line and in the early embryo of C. elegans.', *Development (Cambridge, England)*, 134(19), pp. 3495–3505. Available at: https://doi.org/10.1242/dev.000802.

Scholey, J.M. *et al.* (1982) 'Thymus myosin. Isolation and characterization of myosin from calf thymus and thymic lymphocytes, and studies on the effect of phosphorylation of its Mr = 20,000 light chain.', *The Journal of biological chemistry*, 257(13), pp. 7737–7745.

Scholey, J.M., Taylor, K.A. and Kendrick-jones, J. (1980) 'Regulation of non-muscle myosin assembly by calmodulin-dependent light chain kinase', *Nature*, pp. 233–235. Available at: https://doi.org/10.1038/287233a0.

Schönichen, A. and Geyer, M. (2010) 'Fifteen formins for an actin filament: A molecular view on the regulation of human formins', *Biochimica et Biophysica Acta - Molecular Cell Research*, 1803(2), pp. 152–163. Available at: https://doi.org/10.1016/j.bbamcr.2010.01.014.

Schroeder, T.E. (1968) 'Cytokinesis: Filaments in the cleavage furrow', *Experimental Cell Research*, 53(1), pp. 272–276. Available at: https://doi.org/https://doi.org/10.1016/0014-4827(68)90373-X.

Schroeder, T.E. (1972) 'The contractile ring. II. Determining its brief existence, volumetric changes, and vital role in cleaving Arbacia eggs.', *The Journal of cell biology*, 53(2), pp. 419–434. Available at: https://doi.org/10.1083/jcb.53.2.419.

Schroeder, T.E. (1973) 'Actin in Dividing Cells: Contractile Ring Filaments Bind Heavy Meromyosin', *Proceedings of the National Academy of Sciences*, 70(6), pp. 1688–1692. Available at: https://doi.org/10.1073/pnas.70.6.1688.

Schwebach, C.L. *et al.* (2017) 'The Roles of Actin-Binding Domains 1 and 2 in the Calcium-Dependent Regulation of Actin Filament Bundling by Human Plastins.', *Journal of molecular biology*, 429(16), pp. 2490–2508. Available at: https://doi.org/10.1016/j.jmb.2017.06.021.

Schwebach, C.L. *et al.* (2020) 'Osteogenesis imperfecta mutations in plastin 3 lead to impaired calcium regulation of actin bundling.', *Bone research*, 8, p. 21. Available at: https://doi.org/10.1038/s41413-020-0095-2.

Schwebach, C.L. *et al.* (2022) 'Allosteric regulation controls actin-bundling properties of human plastins', *Nature Structural & Molecular Biology*, 29(6), pp. 519–528. Available at: https://doi.org/10.1038/s41594-022-00771-1.

Sedzinski, J. *et al.* (2011) 'Polar actomyosin contractility destabilizes the position of the cytokinetic furrow', *Nature*, 476(7361), pp. 462–466. Available at: https://doi.org/10.1038/nature10286.

Sellers, J.R. (1985) 'Mechanism of the phosphorylation-dependent regulation of smooth muscle heavy meromyosin.', *Journal of Biological Chemistry*, 260(29), pp. 15815–15819. Available at: https://doi.org/https://doi.org/10.1016/S0021-9258(17)36331-7.

Sellers, J.R., Eisenberg, E. and Adelstein, R.S. (1982) 'The binding of smooth muscle heavy meromyosin to actin in the presence of ATP. Effect of phosphorylation.', *The Journal of biological chemistry*, 257(23), pp. 13880–13883.

Sellers, J.R., Spudich, J.A. and Sheetz, M.P. (1985) 'Light chain phosphorylation regulates the movement of smooth muscle myosin on actin filaments.', *The Journal of cell biology*, 101(5 Pt 1), pp. 1897–1902. Available at: https://doi.org/10.1083/jcb.101.5.1897.

Sellitto, C. and Kuriyama, R. (1988) 'Distribution of a matrix component of the midbody during the cell cycle in Chinese hamster ovary cells', *Journal of Cell Biology*, 106(2), pp. 431–439. Available at: https://doi.org/10.1083/jcb.106.2.431.

Shelton, C.A. *et al.* (1999) 'The nonmuscle myosin regulatory light chain gene mlc-4 is required for cytokinesis, anterior-posterior polarity, and body morphology during Caenorhabditis elegans

embryogenesis', *The Journal of cell biology*, 146(2), pp. 439–451.

Shimada, T. *et al.* (1997) 'Alanine scanning mutagenesis of the switch I region in the ATPase site of Dictyostelium discoideum myosin II.', *Biochemistry*, 36(46), pp. 14037–14043. Available at: https://doi.org/10.1021/bi971837i.

Shoenberg, C.F. (1969) 'An electron microscope study of the influence of divalent ions on myosin filament formation in chicken gizzard extracts and homogenates.', *Tissue & cell*, 1(1), pp. 83–96. Available at: https://doi.org/10.1016/s0040-8166(69)80007-8.

Shutova, M.S. *et al.* (2014) 'Endogenous species of mammalian nonmuscle myosin IIA and IIB include activated monomers and heteropolymers.', *Current biology : CB*, 24(17), pp. 1958–1968. Available at: https://doi.org/10.1016/j.cub.2014.07.070.

Siemankowski, R.F., Wiseman, M.O. and White, H.D. (1985) 'ADP dissociation from actomyosin subfragment 1 is sufficiently slow to limit the unloaded shortening velocity in vertebrate muscle.', *Proceedings of the National Academy of Sciences of the United States of America*, 82(3), pp. 658–662. Available at: https://doi.org/10.1073/pnas.82.3.658.

Silva, Ana M *et al.* (2016) 'Robust gap repair in the contractile ring ensures timely completion of cytokinesis.', *The Journal of cell biology*, 215(6), pp. 789–799. Available at: https://doi.org/10.1083/jcb.201605080.

Silva, A M *et al.* (2016) 'Robust Gap Repair in the Contractile Ring Ensures Timely Completion of Cytokinesis', 215(6), pp. 789–799. Available at: https://doi.org/10.1083/jcb.201605080.

Singh, D. *et al.* (2019) 'Mechanical stress induces a scalable switch in cortical flow polarization during cytokinesis', *Journal of Cell Science*, 132(19). Available at: https://doi.org/10.1242/jcs.231357.

Skau, C.T. *et al.* (2011) 'Actin filament bundling by fimbrin is important for endocytosis, cytokinesis, and polarization in fission yeast', *Journal of Biological Chemistry*, 286(30), pp. 26964–26977. Available at: https://doi.org/10.1074/jbc.M111.239004.

Small, J.V. and Sobieszek, A. (1980) 'The Contractile Apparatus of Smooth Muscle', in G.H. Bourne, J.F. Danielli, and K.W.B.T.-I.R. of C. Jeon (eds). Academic Press, pp. 241–306. Available at: https://doi.org/https://doi.org/10.1016/S0074-7696(08)60239-9.

Soares e Silva, M. *et al.* (2011) 'Active multistage coarsening of actin networks driven by myosin motors', *Proceedings of the National Academy of Sciences*, 108(23), pp. 9408–9413. Available at: https://doi.org/10.1073/pnas.1016616108.

Sobral, A.F. *et al.* (2021) 'Plastin and spectrin cooperate to stabilize the actomyosin cortex during cytokinesis.', *Current biology : CB*, 31(24), pp. 5415-5428.e10. Available at: https://doi.org/10.1016/j.cub.2021.09.055.

Somlyo, A. V. *et al.* (1981) 'Myosin filaments have non-phosphorylated light chains in relaxed smooth muscle', *Nature*, 294(5841), pp. 567–569. Available at: https://doi.org/10.1038/294567a0.

Somlyo, A. V *et al.* (1988) 'Cross-bridge kinetics, cooperativity, and negatively strained cross-bridges in vertebrate smooth muscle. A laser-flash photolysis study.', *Journal of General Physiology*, 91(2), pp. 165–192. Available at: https://doi.org/10.1085/jgp.91.2.165.

Somlyo, A.P. and Somlyo, A. V. (2003) 'Ca2+ sensitivity of smooth muscle and nonmuscle myosin II: Modulated by G proteins, kinases, and myosin phosphatase', *Physiological Reviews*, 83(4), pp. 1325–1358. Available at: https://doi.org/10.1152/physrev.00023.2003.

Spéder, P., Adám, G. and Noselli, S. (2006) 'Type ID unconventional myosin controls left-right asymmetry in Drosophila.', *Nature*, 440(7085), pp. 803–807. Available at: https://doi.org/10.1038/nature04623.

Spira, F. *et al.* (2017) 'Cytokinesis in vertebrate cells initiates by contraction of an equatorial actomyosin network composed of randomly oriented filaments', *eLife*, 6, pp. 1–24. Available at: https://doi.org/10.7554/eLife.30867.

Spudich, J.A. (2001) 'The myosin swinging cross-bridge model.', *Nature reviews. Molecular cell biology*, 2(5), pp. 387–392. Available at: https://doi.org/10.1038/35073086.

Srivastava, V. and Robinson, D.N. (2015) 'Mechanical stress and network structure drive protein dynamics during cytokinesis', *Current Biology*, 25(5), pp. 663–670. Available at: https://doi.org/10.1016/j.cub.2015.01.025.

Stachowiak, M.R. *et al.* (2014) 'Article Mechanism of Cytokinetic Contractile Ring Constriction in Fission Yeast'. Available at: https://doi.org/10.1016/j.devcel.2014.04.021.

Stam, S. *et al.* (2015) 'Isoforms confer characteristic force generation and mechanosensation by myosin II filaments', *Biophysical Journal*, 108(8), pp. 1997–2006. Available at: https://doi.org/10.1016/j.bpj.2015.03.030.

Stam, S. *et al.* (2017) 'Filament rigidity and connectivity tune the deformation modes of active biopolymer networks', *Proceedings of the National Academy of Sciences of the United States of America*, 114(47), pp. E10037–E10045. Available at: https://doi.org/10.1073/pnas.1708625114.

Stiernagle, T. (2006) 'Maintenance of C. elegans.', *WormBook : the online review of C. elegans biology*, pp. 1–11. Available at: https://doi.org/10.1895/wormbook.1.101.1.

Stossel, T.P. *et al.* (2001) 'Filamins as integrators of cell mechanics and signalling.', *Nature reviews. Molecular cell biology*, 2(2), pp. 138–145. Available at: https://doi.org/10.1038/35052082.

Straight, A.F. *et al.* (2003) 'Dissecting temporal and spatial control of cytokinesis with a myosin II

Inhibitor.', *Science (New York, N.Y.)*, 299(5613), pp. 1743–1747. Available at: https://doi.org/10.1126/science.1081412.

Straub, F.B. and Feuer, G. (1950) 'Adenosinetriphosphate the functional group of actin', *BBA - Biochimica et Biophysica Acta*, 4(C), pp. 455–470. Available at: https://doi.org/10.1016/0006-3002(50)90052-7.

Su, K.C., Takaki, T. and Petronczki, M. (2011) 'Targeting of the RhoGEF Ect2 to the Equatorial Membrane Controls Cleavage Furrow Formation during Cytokinesis', *Developmental Cell*, 21(6), pp. 1104–1115. Available at: https://doi.org/10.1016/j.devcel.2011.11.003.

Subramanian, R. *et al.* (2010) 'Insights into antiparallel microtubule crosslinking by PRC1, a conserved nonmotor microtubule binding protein', *Cell*, 142(3), pp. 433–443. Available at: https://doi.org/10.1016/j.cell.2010.07.012.

Sugioka, K. (2022) 'Symmetry-breaking of animal cytokinesis', *Seminars in Cell & Developmental Biology*, 127, pp. 100–109. Available at: https://doi.org/https://doi.org/10.1016/j.semcdb.2021.12.008.

Surcel, A. *et al.* (2010) 'Cytokinesis through biochemical-mechanical feedback loops.', *Seminars in cell & developmental biology*, 21(9), pp. 866–873. Available at: https://doi.org/10.1016/j.semcdb.2010.08.003.

Suzuki, H. *et al.* (1982) 'Adenosine triphosphate-induced reversible change in the conformation of chicken gizzard myosin and heavy meromyosin.', *Journal of biochemistry*, 91(5), pp. 1699–1705. Available at: https://doi.org/10.1093/oxfordjournals.jbchem.a133861.

Svitkina, T.M. (2020) 'Actin Cell Cortex: Structure and Molecular Organization.', *Trends in cell biology*, 30(7), pp. 556–565. Available at: https://doi.org/10.1016/j.tcb.2020.03.005.

SWANN, M.M. (1958) 'The control of cell division: a review. II. Special mechanisms.', *Cancer research*, 18(10), pp. 1118–1160.

SWANN, M.M. and MITCHISON, J.M. (1958) 'the Mechanism of Cleavage in Animal Cells', *Biological Reviews*, 33(1), pp. 103–135. Available at: https://doi.org/10.1111/j.1469-185X.1958.tb01409.x.

Swulius, M.T. *et al.* (2018) 'Structure of the fission yeast actomyosin ring during constriction.', *Proceedings of the National Academy of Sciences of the United States of America*, 115(7), pp. E1455–E1464. Available at: https://doi.org/10.1073/pnas.1711218115.

Szent-Györgyi, A. (1942) 'Discussion', *Studies from the Institute of Medical Chemistry University Szeged*.

Szent-Györgyi, A. (1945) 'Studies on muscle', *Acta Physiol. Scand. Suppl*, 25(9), pp. 1–116.

Szent-Györgyi, A.G. (2004) ‘Milestone in physiology: The early history of the biochemistry of muscle contraction’, *Journal of General Physiology*, 123(6), pp. 631–641. Available at: https://doi.org/10.1085/jgp.200409091.

Szuba, A. *et al.* (2021) ‘Membrane binding controls ordered self-assembly of animal septins’, *eLife*, 10, pp. 1–35. Available at: https://doi.org/10.7554/ELIFE.63349.

Taneja, N. *et al.* (2020) ‘Precise Tuning of Cortical Contractility Regulates Cell Shape during Cytokinesis.’, *Cell reports*, 31(1), p. 107477. Available at: https://doi.org/10.1016/j.celrep.2020.03.041.

Tasto, J.J., Morrell, J.L. and Gould, K.L. (2003) ‘An anillin homologue, Mid2p, acts during fission yeast cytokinesis to organize the septin ring and promote cell separation’, *Journal of Cell Biology*, 160(7), pp. 1093–1103. Available at: https://doi.org/10.1083/jcb.200211126.

Taylor, D.L. and Condeelis, J.S. (1979) ‘Cytoplasmic structure and contractility in amoeboid cells.’, *International review of cytology*, 56, pp. 57–144. Available at: https://doi.org/10.1016/s0074-7696(08)61821-5.

Taylor, K.A. *et al.* (2014) ‘Role of the essential light chain in the activation of smooth muscle myosin by regulatory light chain phosphorylation.’, *Journal of structural biology*, 185(3), pp. 375–382. Available at: https://doi.org/10.1016/j.jsb.2013.12.008.

Thielicke, W. and Stamhuis, E.J. (2014) ‘PIVlab – Towards User-friendly, Affordable and Accurate Digital Particle Image Velocimetry in MATLAB’, *Journal of Open Research Software*, 2. Available at: https://doi.org/10.5334/jors.bl.

Thiyagarajan, S. *et al.* (2022) ‘Myosin turnover controls actomyosin contractile instability.’, *Proceedings of the National Academy of Sciences of the United States of America*, 119(43), p. e2211431119. Available at: https://doi.org/10.1073/pnas.2211431119.

Thompson, M.E. *et al.* (2013) ‘FMNL3 FH2-actin structure gives insight into formin-mediated actin nucleation and elongation’, *Nature Structural and Molecular Biology*, 20(1), pp. 111–118. Available at: https://doi.org/10.1038/nsmb.2462.

Tilney, L.G. *et al.* (1983) ‘Actin from Thyone sperm assembles on only one end of an actin filament: a behavior regulated by profilin.’, *The Journal of cell biology*, 97(1), pp. 112–124. Available at: https://doi.org/10.1083/jcb.97.1.112.

Tinevez, Jean-Yves *et al.* (2009) ‘Role of cortical tension in bleb growth.’, *Proceedings of the National Academy of Sciences of the United States of America*, 106(44), pp. 18581–18586. Available at: https://doi.org/10.1073/pnas.0903353106.

Tinevez, J.-Y. *et al.* (2009) ‘Role of cortical tension in bleb growth’, *Proceedings of the National Academy of Sciences*, 106(44), pp. 18581–18586. Available at:

https://doi.org/10.1073/pnas.0903353106.

Toya, M., Iino, Y. and Yamamoto, M. (1999) 'Fission yeast Pob1p, which is homologous to budding yeast Boi proteins and exhibits subcellular localization close to actin patches, is essential for cell elongation and separation.', *Molecular biology of the cell*, 10(8), pp. 2745–2757. Available at: https://doi.org/10.1091/mbc.10.8.2745.

Toyoshima, Y.Y. *et al.* (1987) 'Myosin subfragment-1 is sufficient to move actin filaments in vitro.', *Nature*, 328(6130), pp. 536–539. Available at: https://doi.org/10.1038/328536a0.

Truong Quang, B.A. *et al.* (2021) 'Extent of myosin penetration within the actin cortex regulates cell surface mechanics', *Nature Communications*, 12(1), pp. 1–12. Available at: https://doi.org/10.1038/s41467-021-26611-2.

Trybus, K.M., Huiatt, T.W. and Lowey, S. (1982) 'A bent monomeric conformation of myosin from smooth muscle.', *Proceedings of the National Academy of Sciences of the United States of America*, 79(20), pp. 6151–6155. Available at: https://doi.org/10.1073/pnas.79.20.6151.

Trybus, K.M. and Lowey, S. (1984) 'Conformational states of smooth muscle myosin. Effects of light chain phosphorylation and ionic strength.', *The Journal of biological chemistry*, 259(13), pp. 8564–8571.

Tse, Y. C. *et al.* (2012) 'RhoA activation during polarization and cytokinesis of the early Caenorhabditis elegans embryo is differentially dependent on NOP-1 and CYK-4', *Molecular Biology of the Cell*, 23(20), pp. 4020–4031. Available at: https://doi.org/10.1091/mbc.E12-04-0268.

Tse, Yu Chung *et al.* (2012) 'RhoA activation during polarization and cytokinesis of the early Caenorhabditis elegans embryo is differentially dependent on NOP-1 and CYK-4', *Molecular Biology of the Cell*, 23(20), pp. 4020–4031. Available at: https://doi.org/10.1091/mbc.E12-04-0268.

Tseng, Y. *et al.* (2002) 'Functional synergy of actin filament cross-linking proteins', *Journal of Biological Chemistry*, 277(28), pp. 25609–25616. Available at: https://doi.org/10.1074/jbc.M202609200.

Turlier, H., Audoly, B., Prost, J. and Joanny, J.-F. (2014) 'Furrow constriction in animal cell cytokinesis.', *Biophysical journal*, 106(1), pp. 114–23. Available at: https://doi.org/10.1016/j.bpj.2013.11.014.

Turlier, H., Audoly, B., Prost, J. and Joanny, J.F. (2014) 'Furrow constriction in animal cell cytokinesis', *Biophysical Journal*, 106(1), pp. 114–123. Available at: https://doi.org/10.1016/j.bpj.2013.11.014.

Tyska, M.J. *et al.* (1999) 'Two heads of myosin are better than one for generating force and motion', *Proceedings of the National Academy of Sciences of the United States of America*, 96(8), pp. 4402–4407. Available at: https://doi.org/10.1073/pnas.96.8.4402.

Uehara, R. *et al.* (2010) 'Determinants of myosin II cortical localization during cytokinesis.', *Current*

biology : CB, 20(12), pp. 1080–1085. Available at: https://doi.org/10.1016/j.cub.2010.04.058.

Uehara, R. and Goshima, G. (2010) 'Functional central spindle assembly requires de novo microtubule generation in the interchromosomal region during anaphase.', *The Journal of cell biology*, 191(2), pp. 259–267. Available at: https://doi.org/10.1083/jcb.201004150.

Umemoto, S. and Sellers, J.R. (1990) 'Characterization of in vitro motility assays using smooth muscle and cytoplasmic myosins.', *The Journal of biological chemistry*, 265(25), pp. 14864–14869.

Uyeda, T.Q., Kron, S.J. and Spudich, J.A. (1990) 'Myosin step size. Estimation from slow sliding movement of actin over low densities of heavy meromyosin.', *Journal of molecular biology*, 214(3), pp. 699–710. Available at: https://doi.org/10.1016/0022-2836(90)90287-V.

Vaillancourt, J.P., Lyons, C. and Côté, G.P. (1988) 'Identification of two phosphorylated threonines in the tail region of Dictyostelium myosin II.', *The Journal of biological chemistry*, 263(21), pp. 10082–10087.

Vale, R.D. (2003) 'Myosin V motor proteins: marching stepwise towards a mechanism.', *The Journal of cell biology*, 163(3), pp. 445–450. Available at: https://doi.org/10.1083/jcb.200308093.

Vale, R.D., Spudich, J.A. and Griffis, E.R. (2009) 'Dynamics of myosin, microtubules, and Kinesin-6 at the cortex during cytokinesis in Drosophila S2 cells.', *The Journal of cell biology*, 186(5), pp. 727–738. Available at: https://doi.org/10.1083/jcb.200902083.

Valon, L. *et al.* (2017) 'Optogenetic control of cellular forces and mechanotransduction', *Nature Communications*, 8. Available at: https://doi.org/10.1038/ncomms14396.

Vasquez, C.G., Tworoger, M. and Martin, A.C. (2014) 'Dynamic myosin phosphorylation regulates contractile pulses and tissue integrity during epithelial morphogenesis.', *The Journal of cell biology*, 206(3), pp. 435–450. Available at: https://doi.org/10.1083/jcb.201402004.

Verbrugghe, K.J.C. and White, J.G. (2004) 'SPD-1 is required for the formation of the spindle midzone but is not essential for the completion of cytokinesis in C. elegans embryos.', *Current biology : CB*, 14(19), pp. 1755–1760. Available at: https://doi.org/10.1016/j.cub.2004.09.055.

Vernì, F. *et al.* (2004) 'Feo, the Drosophila homolog of PRC1, is required for central-spindle formation and cytokinesis.', *Current biology : CB*, 14(17), pp. 1569–1575. Available at: https://doi.org/10.1016/j.cub.2004.08.054.

Vicente-Manzanares, M. *et al.* (2009) 'Non-muscle myosin II takes centre stage in cell adhesion and migration.', *Nature reviews. Molecular cell biology*, 10(11), pp. 778–790. Available at: https://doi.org/10.1038/nrm2786.

Vogel, S.K. *et al.* (2013) 'Myosin motors fragment and compact membrane-bound actin filaments.',

eLife, 2, p. e00116. Available at: https://doi.org/10.7554/eLife.00116.

Volkmann, N *et al.* (2001) 'An atomic model of actin filaments cross-linked by fimbrin and its implications for bundle assembly and function.', *The Journal of cell biology*, 153(5), pp. 947–956. Available at: https://doi.org/10.1083/jcb.153.5.947.

Volkmann, N. *et al.* (2001) 'Structure of arp2/3 complex in its activated state and in actin filament branch junctions', *Science*, 293(5539), pp. 2456–2459. Available at: https://doi.org/10.1126/science.1063025.

Wagner, E. and Glotzer, M. (2016) 'Local RhoA activation induces cytokinetic furrows independent of spindle position and cell cycle stage', *Journal of Cell Biology*, 213(6), pp. 641–649. Available at: https://doi.org/10.1083/jcb.201603025.

Wakatsuki, T. *et al.* (2001) 'Effects of cytochalasin D and latrunculin B on mechanical properties of cells', *Journal of Cell Science*, 114(5), pp. 1025–1036. Available at: https://doi.org/10.1242/jcs.114.5.1025.

Warshaw, D.M. *et al.* (1990) 'Smooth muscle myosin cross-bridge interactions modulate actin filament sliding velocity in vitro', *Journal of Cell Biology*, 111(2), pp. 453–463. Available at: https://doi.org/10.1083/jcb.111.2.453.

Washington, R.W. and Knecht, D.A. (2008) 'Actin binding domains direct actin-binding proteins to different cytoskeletal locations', *BMC Cell Biology*, 9, pp. 1–16. Available at: https://doi.org/10.1186/1471-2121-9-10.

Watanabe, A. *et al.* (1998) 'A new Tetrahymena actin-binding protein is localized in the division furrow.', *Journal of biochemistry*, 123(4), pp. 607–613. Available at: https://doi.org/10.1093/oxfordjournals.jbchem.a021980.

Watanabe, A. *et al.* (2000) 'Cloning and sequencing of the gene for a Tetrahymena fimbrin-like protein.', *Journal of biochemistry*, 127(1), pp. 85–94. Available at: https://doi.org/10.1093/oxfordjournals.jbchem.a022587.

Watanabe, N. *et al.* (1997) 'p140mDia, a mammalian homolog of Drosophila diaphanous, is a target protein for Rho small GTPase and is a ligand for profilin', *EMBO Journal*, 16(11), pp. 3044–3056. Available at: https://doi.org/10.1093/emboj/16.11.3044.

Watanabe, S. *et al.* (2008) 'mDia2 induces the actin scaffold for the contractile ring and stabilizes its position during cytokinesis in NIH 3T3 cells.', *Molecular biology of the cell*, 19(5), pp. 2328–2338. Available at: https://doi.org/10.1091/mbc.e07-10-1086.

Weirich, K.L. *et al.* (2021) 'Actin bundle architecture and mechanics regulate myosin II force generation', *Biophysical Journal*, 120(10), pp. 1957–1970. Available at: https://doi.org/10.1016/j.bpj.2021.03.026.

Weißenbruch, K. *et al.* (2021) 'Distinct roles of nonmuscle myosin ii isoforms for establishing tension and elasticity during cell morphodynamics', *eLife*, 10, pp. 1–35. Available at: https://doi.org/10.7554/ELIFE.71888.

Wendt, T. *et al.* (1999) 'Visualization of head-head interactions in the inhibited state of smooth muscle myosin.', *The Journal of cell biology*, 147(7), pp. 1385–1390. Available at: https://doi.org/10.1083/jcb.147.7.1385.

Wendt, T. *et al.* (2001) 'Three-dimensional image reconstruction of dephosphorylated smooth muscle heavy meromyosin reveals asymmetry in the interaction between myosin heads and placement of subfragment 2', *Proceedings of the National Academy of Sciences of the United States of America*, 98(8), pp. 4361–4366. Available at: https://doi.org/10.1073/pnas.071051098.

West-Foyle, H. *et al.* (2018) '14-3-3 proteins tune non-muscle myosin II assembly', *Journal of Biological Chemistry*, 293(18), pp. 6751–6761. Available at: https://doi.org/10.1074/jbc.M117.819391.

White, E.A. and Glotzer, M. (2012) 'Centralspindlin: At the heart of cytokinesis', *Cytoskeleton*, 69(11), pp. 882–892. Available at: https://doi.org/10.1002/cm.21065.

White, J.G. and Borisy, G.G. (1983) 'On the mechanisms of cytokinesis in animal cells', *Journal of Theoretical Biology*, 101(2), pp. 289–316. Available at: https://doi.org/10.1016/0022-5193(83)90342-9.

Wilson, C.A. *et al.* (2010) 'Myosin II contributes to cell-scale actin network treadmilling through network disassembly.', *Nature*, 465(7296), pp. 373–377. Available at: https://doi.org/10.1038/nature08994.

Winkelman, J.D. *et al.* (2016) 'Fascin- and α-Actinin-Bundled Networks Contain Intrinsic Structural Features that Drive Protein Sorting', *Current Biology*, 26(20), pp. 2697–2706. Available at: https://doi.org/10.1016/j.cub.2016.07.080.

Wioland, H., Jegou, A. and Romet-Lemonne, G. (2019) 'Torsional stress generated by ADF/cofilin on cross-linked actin filaments boosts their severing.', *Proceedings of the National Academy of Sciences of the United States of America*, 116(7), pp. 2595–2602. Available at: https://doi.org/10.1073/pnas.1812053116.

Wise, D.R. and Thompson, C.B. (2010) 'Glutamine addiction : a new therapeutic target in cancer', *Trends in Biochemical Sciences*, 35(8), pp. 427–433. Available at: https://doi.org/10.1016/j.tibs.2010.05.003.

Wittmann, T., Hyman, A. and Desai, A. (2001) 'The spindle: a dynamic assembly of microtubules and motors', *Nature Cell Biology*, 3(1), pp. E28–E34. Available at: https://doi.org/10.1038/35050669.

Wolfe, B.A. *et al.* (2009) 'Polo-like kinase 1 directs assembly of the HsCyk-4 RhoGAP/Ect2 RhoGEF complex to initiate cleavage furrow formation', *PLoS Biology*, 7(5). Available at: https://doi.org/10.1371/journal.pbio.1000110.

Wollrab, V. *et al.* (2016) 'Still and rotating myosin clusters determine cytokinetic ring constriction.', *Nature communications*, 7, p. 11860. Available at: https://doi.org/10.1038/ncomms11860.

Wollrab, V. *et al.* (2018) 'Polarity sorting drives remodeling of actin-myosin networks.', *Journal of cell science*, 132(4). Available at: https://doi.org/10.1242/jcs.219717.

Wolpert, L. (1966) 'The mechanical properties of the membrane of the sea urchin egg during cleavage', *Experimental Cell Research*, 41(2), pp. 385–396. Available at: https://doi.org/https://doi.org/10.1016/S0014-4827(66)80146-5.

WOLPERT, L. (1961) 'The mechanics and mechanism of cleavage', *Int. Rev. Cytol*, 10, pp. 163–216.

WOLPERT, L. and MERCER, E.H. (1963) 'An electron microscope study of the development of the blastula of the sea urchin embryo and its radial polarity.', *Experimental cell research*, 30, pp. 280–300. Available at: https://doi.org/10.1016/0014-4827(63)90300-8.

Woodhead, J.L. *et al.* (2005) 'Atomic model of a myosin filament in the relaxed state', *Nature*, 436(7054), pp. 1195–1199. Available at: https://doi.org/10.1038/nature03920.

Woodrum, D.T., Rich, S.A. and Pollard, T.D. (1975) 'NOTES', 67, pp. 231–237.

Woods, B.L. and Gladfelter, A.S. (2021) 'The state of the septin cytoskeleton from assembly to function', *Current Opinion in Cell Biology*, 68, pp. 105–112. Available at: https://doi.org/10.1016/j.ceb.2020.10.007.

Wu, J.-Q. and Pollard, T.D. (2005) 'Counting cytokinesis proteins globally and locally in fission yeast.', *Science (New York, N.Y.)*, 310(5746), pp. 310–314. Available at: https://doi.org/10.1126/science.1113230.

Wu, J.Q., Bähler, J. and Pringle, J.R. (2001) 'Roles of a fimbrin and an α-actinin-like protein in fission yeast cell polarization and cytokinesis', *Molecular Biology of the Cell*, 12(4), pp. 1061–1077. Available at: https://doi.org/10.1091/mbc.12.4.1061.

Xu, Y. *et al.* (2004) 'Crystal structures of a formin homology-2 domain reveal a tethered dimer architecture', *Cell*, 116(5), pp. 711–723. Available at: https://doi.org/10.1016/S0092-8674(04)00210-7.

Yamakita, Y., Yamashiro, S. and Matsumura, F. (1994) 'In vivo phosphorylation of regulatory light chain of myosin II during mitosis of cultured cells.', *The Journal of cell biology*, 124(1–2), pp. 129–137. Available at: https://doi.org/10.1083/jcb.124.1.129.

Yamashiro, S., Noguchi, T. and Mabuchi, I. (2003) 'Localization of two IQGAPs in cultured cells and early embryos of Xenopus laevis', *Cell Motility*, 55(1), pp. 36–50. Available at: https://doi.org/https://doi.org/10.1002/cm.10109.

Yi, K. *et al.* (2011) 'Dynamic maintenance of asymmetric meiotic spindle position through Arp2/3-complex-driven cytoplasmic streaming in mouse oocytes', *Nature Cell Biology*, 13(10), pp. 1252–1258. Available at: https://doi.org/10.1038/ncb2320.

Yoneda, M. and Dan, K. (1972) 'Tension at the surface of the dividing sea-urchin egg.', *The Journal of experimental biology*, 57(3), pp. 575–587. Available at: https://doi.org/10.1242/jeb.57.3.575.

Yumura, S. (2001) 'Myosin II dynamics and cortical flow during contractile ring formation in Dictyostelium cells.', *The Journal of cell biology*, 154(1), pp. 137–146. Available at: https://doi.org/10.1083/jcb.200011013.

Zaatri, A., Perry, J.A. and Maddox, A.S. (2021) 'Septins and a formin have distinct functions in anaphase chiral cortical rotation in the Caenorhabditis elegans zygote.', *Molecular biology of the cell*, 32(14), pp. 1283–1292. Available at: https://doi.org/10.1091/mbc.E20-09-0576.

Zhang, D. and Glotzer, M. (2015) 'The RhoGAP activity of CYK-4/MgcRacGAP functions non-canonically by promoting RhoA activation during cytokinesis.', *eLife*, 4. Available at: https://doi.org/10.7554/eLife.08898.

Zhang, W. and Robinson, D.N. (2005) *Balance of actively generated contractile and resistive forces controls cytokinesis dynamics*. Available at: www.pnas.orgcgidoi10.1073pnas.0502545102 (Accessed: 25 November 2018).

Zhou, M. and Wang, Y.-L. (2008) 'Distinct pathways for the early recruitment of myosin II and actin to the cytokinetic furrow.', *Molecular biology of the cell*, 19(1), pp. 318–326. Available at: https://doi.org/10.1091/mbc.e07-08-0783.

Zhou, Q. *et al.* (2010) '14-3-3 coordinates microtubules, rac, and myosin II to control cell mechanics and cytokinesis', *Current Biology*, 20(21), pp. 1881–1889. Available at: https://doi.org/10.1016/j.cub.2010.09.048.

Zigmond, S.H., Furukawa, R. and Fechheimer, M. (1992) 'Inhibition of actin filament depolymerization by the Dictyostelium 30,000-D actin-bundling protein.', *The Journal of cell biology*, 119(3), pp. 559–567. Available at: https://doi.org/10.1083/jcb.119.3.559.

Zinemanas, D. and Nir, A. (1987) 'Fluid Mechanical Simulations of Cell Furrowing Due to Anisotropic Surface Forces BT - Biomechanics of Cell Division', in N. Akkas (ed.). Boston, MA: Springer US, pp. 281–305. Available at: https://doi.org/10.1007/978-1-4684-1271-0_14.

Zinemanas, D. and Nir, A. (1990) 'Surface viscoelastic effects in cell cleavage.', *Journal of biomechanics*, 23(5), pp. 417–424. Available at: https://doi.org/10.1016/0021-9290(90)90296-f.

Zumdieck, A. *et al.* (2005) 'Continuum description of the cytoskeleton: Ring formation in the cell cortex', *Physical Review Letters*, 95(25), pp. 1–4. Available at: https://doi.org/10.1103/PhysRevLett.95.258103.

Zumdieck, A. *et al.* (2007) ‘Stress generation and filament turnover during actin ring constriction.’, *PloS one*, 2(8), p. e696. Available at: https://doi.org/10.1371/journal.pone.0000696.

CHAPTER II

OVERVIEW AND OBJECTIVES

Overview and Objectives

Earlier theoretical models of cytokinesis considered the actomyosin cortex as a continuum where the deformation at the cell equator was largely influenced by the polar cortex. These models lacked however molecular details on how those forces in the cortical layer arise. More recent studies have addressed the roles of several proteins in cytokinesis dynamics but focused primarily on an isolated contractile ring. As the ring is integrated in the cell cortex, differences in protein levels, distribution and interplays in the whole layer are likely to affect its assembly and constriction. Even though mechanisms of ring assembly have been proposed, these have been debated and the molecular players have not been fully disclosed. Ring constriction is known to depend on myosin's motor-activity, however the extent of this dependence or which mechanical properties may be involved besides contractility is not known.

In this project, I proposed to experimentally probe the molecular basis of the forces generated in the ring and surrounding cortex during early embryonic divisions of *C. elegans* embryos and how they collectively affect ring assembly and constriction.

1. Investigate how the distribution of myosin throughout the cortex impacts cytokinesis kinetics.

Live imaging of the cell cortex and contractile ring were performed in embryos expressing fluorescently tagged myosin depleted of proteins speculated to have an effect in myosin's distribution throughout the cortex. This included determining relative myosin fluorescent intensities in the ring and cortex contour and correlate them with contractile ring kinetics, as well as computing cortical myosin flows with high temporal resolution. This not only allowed us to conclude that myosin distribution in the whole cortex indeed impacts contractile ring dynamics, but also to identify specific proteins (14-5-5^{PAR-5} and the microtubule bundler PRC1^{spd-1}) as modulators of myosin's distribution in the actomyosin cortex and potential players in polar clearance mechanisms.

2. Dissect contractile ring assembly mechanisms.

Single or double depletions (penetrant or partial) of myosin and the actin crosslinker plastin by RNAi were conducted in *wildtype* or motor-dead myosin mutant embryos expressing fluorescently tagged actin and myosin to determine how those collectively impact the cortex and ring mechanics. This included computing actin filament alignment and cortical actin and myosin flows with high temporal resolution, as well as determining contractile ring kinetic parameters and myosin turnover using fluorescence recovery after photobleaching. This allowed us to conclude that the contractile ring assembles primarily via localized recruitment

of myosin from the cytoplasm and that it cooperates locally with plastin to align actin filaments at the equator.

3. Probe the dependence of cytokinesis kinetics on myosin levels.

Live imaging of embryos depleted of myosin or with increasing inactive myosin levels expressing fluorescently tagged myosin or myosin light chain was performed to relate their levels with cytokinesis kinetic parameters. This involved measuring line profiles along the cortex contour and running computational simulations fed with these profiles, for which we established a collaboration with Dr. Hervé Turlier lab. We found that cytokinesis kinetics are robust to decreasing myosin levels, as myosin tunes both contractility and viscosity of the cortex.

In addition, I have also proposed to develop a novel experimental approach to probe the cortex mechanical properties in the *C. elegans* early embryo using magnetic beads. However, the optimization of this technique encountered many difficulties that precluded its implementation during the timeframe of these doctoral studies. This assay would have been useful in every part of this work as it would have provided direct measurements of changes in cortex mechanical properties.

CHAPTER III

MYOSIN LEVELS, DISTRIBUTION AND ACTIVITY IN THE SURROUNDING CORTEX IMPACT CONTRACTILE RING DYNAMICS

Myosin levels, distribution and activity in the surrounding cortex impact contractile ring dynamics

Abstract

Cytokinesis is accompanied by two concomitant mechanisms that break symmetry in the actomyosin cortex and allow shape changes to occur: a positive signal at the equatorial cortex coming from the central spindle and a negative signal at the polar cortex presumably dependent on astral microtubules. Here, perturbations of proteins known or hypothesized to interfere with myosin levels distribution and activation pattern were employed to evaluate the corresponding cytokinesis phenotypes and kinetic parameters. We found that increasing myosin activity at the polar cortex delays all phases of cytokinesis, and accelerating initial myosin polar clearance triggers earlier ring assembly and furrow initiation. Altogether, these results reveal that myosin concentration, activation and distribution pattern between the equatorial and the polar cortices dictate constriction kinetics. Importantly, this regulation is fine-tuned spatiotemporally, with changes in myosin distribution having direct consequences in the particular phase of cytokinesis during which they occur, not necessarily affecting the subsequent phases.

Introduction

Many studies have tried to identify proteins, protein-protein interactions and signaling cascades that regulate specific essential functions for cytokinesis. Other studies have addressed changes in mechanical properties, often creating shape oscillations or mechanical perturbations. However, what is mostly missing in the field is the integration of these two strategies in an attempt to uncover the molecular regulators of the cellular mechanical properties that actually drive the cell shape change during cytokinesis.

Here, I started by directly probing how the myosin distribution and/or activity in the surrounding cortex impacts cortical dynamics and contractile ring assembly and constriction. As previously discussed in this manuscript (Chapter I, section “Division plane specification and contractile ring assembly) cytokinesis is accompanied by two concomitant mechanisms that break symmetry in the actomyosin cortex and allow shape changes to occur: a positive signal at the equatorial cortex prevenient the central spindle and a negative signal at the polar cortex presumably originating on the astral microtubules. While the former allows RhoA-GTP downstream effectors - formins and ROCK – to increase the nucleation of new linear actin filaments and to recruit and activate myosin to promote contractility, the latter is involved in clearing contractile proteins from the poles. The tension differential arising between the equator and the poles triggers a period of cortical flows. We looked into two proteins that were

known to, or that I hypothesized to have a role in myosin levels at the polar cortex, the 14-3-3^{PAR-5} and PRC-1^{SPD-1}, and investigated how they impacted myosin distribution and cytokinesis dynamics. A brief introduction on what is known in the literature about these proteins is provided below.

14-3-3 proteins

14-3-3 proteins have been shown to be altered in a variety of human tumours (acting both as tumour suppressors or promotors depending on certain conditions) and were recently demonstrated to integrate key cytoskeletal components - microtubules, Rac and myosin II - to control cell mechanics and cytokinesis in the amoeba *D. discoideum* (Zhou *et al.*, 2010).

14-3-3 proteins are small acidic proteins of approximately 30 kDa which dimerize to form a protein-binding cleft. These proteins have been shown to be involved in many critical cellular functions, including cell cycle control, DNA damage repair and many other signalling pathways. Their mechanism of action, more generally but not always, consists in changing the conformation or sequestering their binding partners, interactions that are regulated by phosphorylation of the target proteins. 14-3-3 proteins seem to be highly conserved across eukaryotes. In *D. Discoideum*, there is only one 14-3-3 isoform and this protein has been shown to modulate cortical tension, cell shape and cytokinesis. This is mainly due to its role in regulating three key cytoskeletal components – microtubules, Rac and myosin II (Zhou et al., 2010). Specifically, 14-3-3 has been shown to bind directly to the tail of myosin II, inhibiting its assembly into bipolar thick filaments and promoting its turnover (West-Foyle *et al.*, 2018).

In *C. elegans*, the 14-3-3^{PAR-5} is known to inhibit the cortical localization of centralspindlin oligomers globally during cytokinesis, with the CPC antagonizing its activity at the cell equator where the contractile ring is expected to be formed upon RhoA activation (Basant et al 2015). Contrarily to *D. discoideum*, where 14-3-3 suppression results in a phenotype that largely resembles that of myosin null cells with a reduction in cortical tension, in the *C. elegans* early embryo 14-3-3^{par-5} knockdown by RNAi results in increased RhoA-GTP levels throughout the cortical layer and therefore, an expected increase in global cortical tension both during pseudocleavage and cytokinesis (Basant *et al.*, 2015, Morton *et al.*, 2002). Furthermote, the 14-3-3^{PAR-5} in *C. elegans* is a well-known regulator of embryo polarity, despite its centralspindlin oligomerization phenotype has been shown to be independent of the polarity defects also induced.

The microtubule bundling protein PRC-1^{SPD-1}

PRC-1^{SPD-1} is a microtubule bundling protein that localizes to the midzone and to microtubule bundles in the cytoplasm. Loss of function of PRC-1^{SPD-1} causes midzone disruptions, but is

not indispensable for cytokinesis, which generally completes (Verbrugghe and White, 2004). As microtubules become unbundled, the spindle elongates (Grill *et al.*, 2001) more in *spd-1*-depleted than in control embryos, a condition already observed for other midzone proteins (Verbrugghe and White, 2004).

Results

Myosin and other cortical proteins are cleared from the poles and accumulate at the cell equator, which triggers periods of cortical flow

Before investigating how different proteins affect cortex mechanical properties and dynamics during cytokinesis, it is crucial to inspect how each of them localizes, accumulates and patterns the cortical layer. In Figure 3.1, stills of the central and cortical plane of embryos expressing four major proteins of the actomyosin cortex - LifeAct::GFP, a probe for F-actin; Myosin^{NMY-2}::mKate2, a probe for the motor protein myosin; Plastin^{PLST-1}::GFP, a probe for the actin filament crosslinker plastin; and Anillin^{ANI-1}::GFP, a probe for the scaffolding protein anillin - throughout different phases of cytokinesis are displayed. LifeAct::GFP localizes in puncta and filamentous form, with puncta predominating in an anterior “cap”. At the time the equator starts deforming - shallow deformation - an enrichment of filamentous structures is observed at the equatorial cortex, whereas punctate structures remain at the polar cortices (these are known to be ARP2/3 dependent (Davies et al, 2014)(Chan et al, 2018). The filamentous structures get progressively more aligned as ingression proceeds - back-to-back membranes. In central plane images, LifeAct::GFP seems to increase at the furrow tip at 50% percent ingression, and only slightly cleared from the poles. Myosin follows a similar distribution pattern throughout cytokinesis, with a characteristic localization in cortical patches that become progressively enriched at the equatorial cortex, favoring contractile ring assembly and constriction. Conversely to F-actin, the enrichment of myosin at the furrow tip looks much more pronounced, as well as its polar clearance.

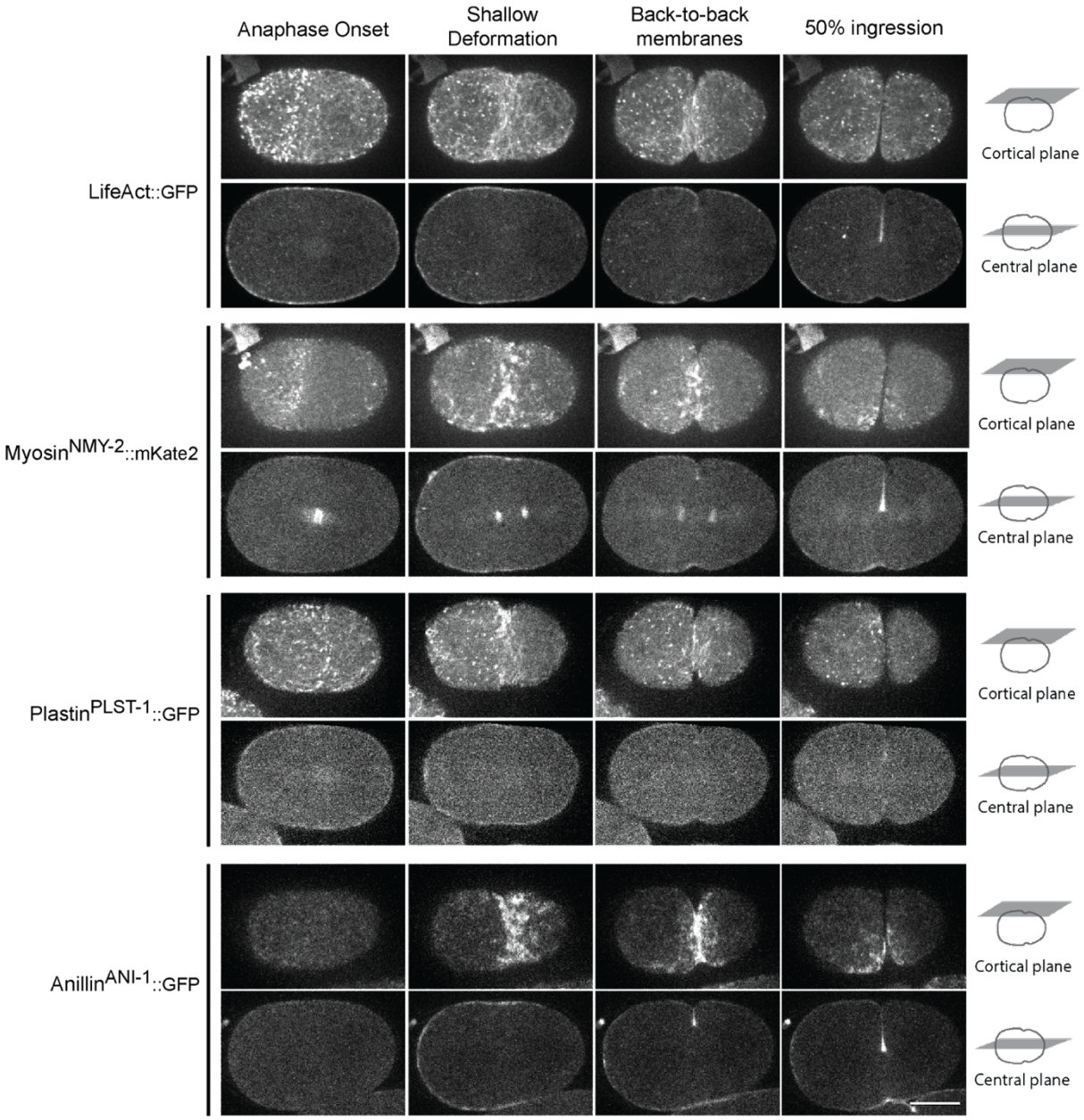

FIGURE 3.1. Cortical proteins' distribution throughout cytokinesis. Central and cortical plane images of fluorescently tagged cortical proteins, as indicated on the left, during different phases of cytokinesis: anaphase onset, shallow deformation, back-to-back membranes and at half ingression (from initial diameter). Scale bar: 10 μm.

Plastin, consistent with its role as an actin filament crosslinker, follows a very similar distribution as LifeAct::GFP. Even though its enrichment at the furrow tip in central plane images is not so clear, probably due to the probe being dimmer, the punctate and filamentous structures clearly follow the same pattern as F-actin throughout cytokinesis.

Anillin acts as a scaffolding protein. As such, it binds several proteins on the cortex, including actin and myosin. Interestingly, it shows a very similar localization pattern to myosin, including

cortical patches and very pronounced enrichment at the equatorial cortex and furrow tip, compared to the poles, which also show some extent of clearance.

Next, we inspected how F-actin and myosin flow in the cortical layer throughout cytokinesis. To quantitatively analyze cortical flows, we performed particle image velocimetry (PIV) analysis (Figure 3.2A). Flow velocity was calculated by averaging the X- or Y-components (anterior-posterior and dorsal-ventral, respectively) of the velocity vectors in two regions positioned over the anterior and posterior halves of the embryo, for each time point between anaphase onset and the end of constriction (Figure 3.2C). Negative velocity values indicate posterior-anterior oriented flows and positive velocity values indicate anterior-posterior oriented flows (Figure 3.2A). The analysis was performed in embryos expressing LifeAct::GFP and NMY-2::GFP, separately.

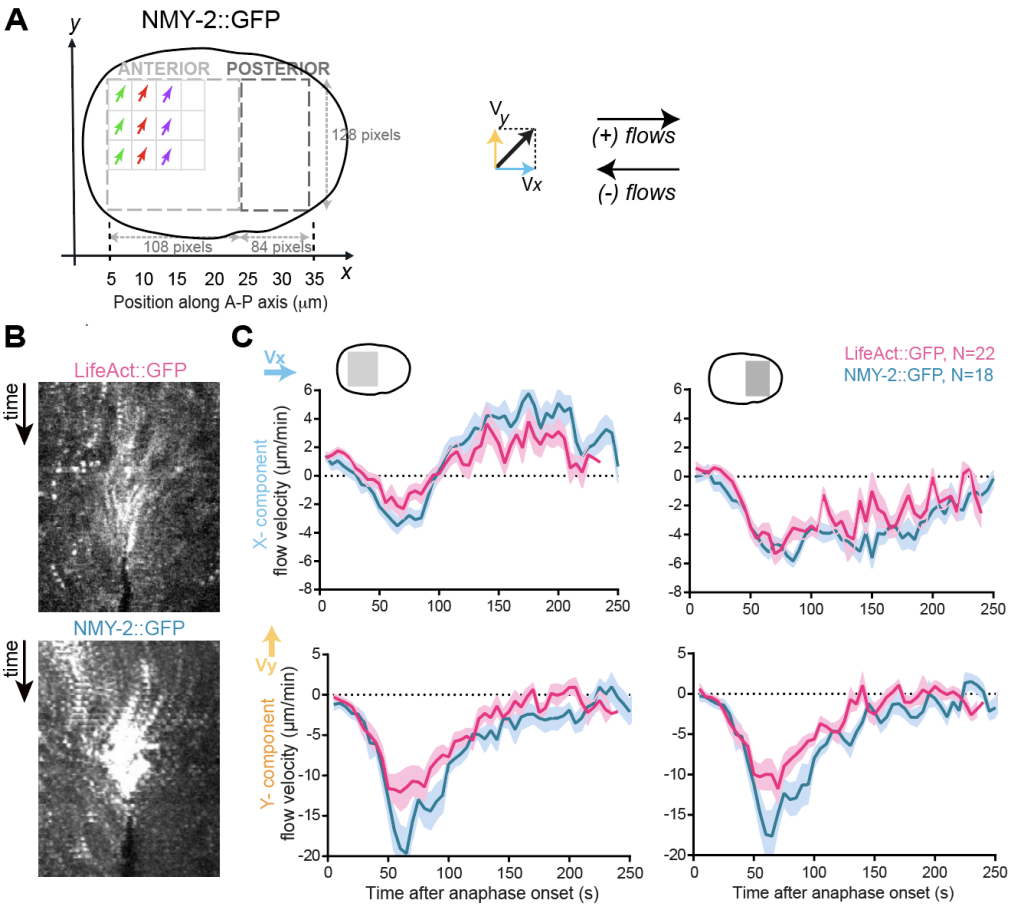

FIGURE 3.2. F-actin and myosin follow the same redistribution pattern, including polar clearance, equatorial accumulation and cortical flow velocities during cytokinesis. (A) Schematic illustrating how cortical NMY-2::GFP flows were analyzed by particle image velocimetry (PIV; see more details in "Materials and Methods" section). **(B)** Kymographs depicting Lifeact::GFP (top) and NMY-2::GFP (bottom) longitudinal cortical flows from anaphase onset until complete ingression. **(C)** Longitudinal (X-component) and rotational (Y-component) flow

velocities(mean ± SEM) for LifeAct::GFP and NMY-2::GFP in the anterior or posterior half of embryos, plotted over time starting at anaphase onset. The depicted interval covers both the period of unidirectional and the period of bidirectional flows.N is the number of embryos analyzed. Panels B and C were reproduced from (Leite *et al.*, 2020).

Control embryos presented anterior-directed actomyosin cortical flows that started just prior to equatorial shallow deformation, peaked shortly thereafter, and remained high for approximately 50 seconds (Figure 3.2C). These were accompanied by a very strong rotational flow component. This was then followed by a period of bidirectional flows in which flows come from both poles towards the cell equator. While the bidirectional longitudinal flows remained high during the constriction phase, the rotational flows become attenuated during this phase. In agreement, these rotational flows have been shown to be dispensable for ring assembly and could be an artifact of embryo compression during filming (Singh et al., 2019; Leite et al., 2020). Interestingly, I found that F-actin and myosin do not only follow a similar flow pattern, but also very similar flow velocities, which is very likely to happen with other cortical proteins known to localize both in the ring and the surrounding cortex (Figure 3.1).

Increasing active myosin levels at the polar cortex delays contractile ring assembly and constriction

To investigate the direct influence of the polar cortex in contractile ring dynamics, we sought to recreate situations where there was more myosin or less myosin at the poles, both during the assembly and the constriction phases. In *C. elegans* embryos, most proteins known to affect myosin force generation localize both in the contractile ring and in the surrounding cortex, which would affect how results are interpreted in terms of the phenotypes being derived from the polar resisting forces to contractile ring constriction. Molecular players whose depletion is known to increase RhoA levels in the polar cortices include the RhoA GAP RGA-3/4, the 14-3-3 PAR-5 (Basant *et al.*, 2015; Schmutz, Stevens and Spang, 2007). If the surrounding cortex is indeed resisting ring constriction, then cortical RhoA activation should increase contractility globally and is therefore expected to delay every phase of cytokinesis. For this, I fully depleted PAR-5 in embryos expressing NMY-2::GFP, a probe for myosin, and quantified NMY-2 fluorescence intensity both at the equatorial and polar regions (Figure 3.3B), for different reference points including ring assembly, furrow initiation and ring constriction (see schematic Figure 3.3C). The ring assembly corresponds to the time between anaphase onset and the formation of a shallow equatorial deformation, when contractile ring components are being recruited to the cell equator. The furrow initiation corresponds to the time between shallow deformation and the folding of the plasma membrane into a back-to-back configuration. The ring constriction is the time between a back-to-back configuration until full furrow ingression.

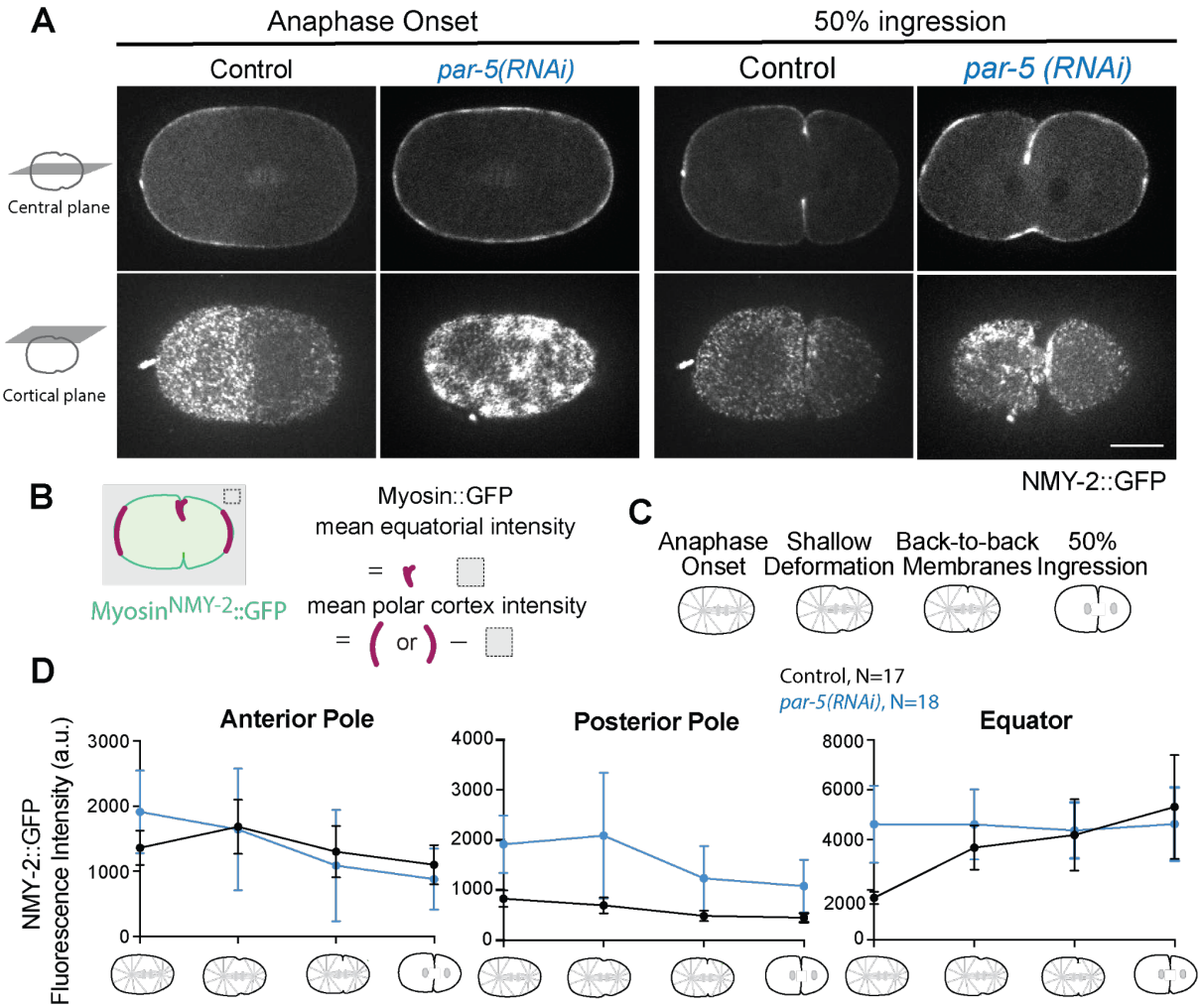

FIGURE 3.3. 14-3-3^{PAR-5} knockdown increases cortical myosin levels in the embryo, especially at the posterior pole, during cytokinesis. (A) Representative images of NMY-2::GFP levels in cortical and central plane of control and PAR-5 depleted embryos, at anaphase onset and 50% furrow ingression. **(B)** Schematic showing the regions used for NMY-2::GFP fluorescence intensity measurements. **(C)** Reference points used for measurements of ring assembly and furrow initiation intervals, as well as nmy-2 intensity. Ring assembly: between anaphase onset and the formation of a shallow equatorial deformation, when contractile ring components are being recruited to the cell equator. Furrow initiation: between shallow deformation and the folding of the plasma membrane into a back-to-back configuration. Ring constriction: between a back-to-back configuration until full furrow ingression. **(D)** Measurements of NMY-2::GFP intensity on the anterior pole, posterior pole and equator at anaphase onset, shallow deformation, back-to-back membranes and 50% ingression for controls and par-5 depleted embryos. N is the number of embryos analyzed. Scale Bars,10 µm.

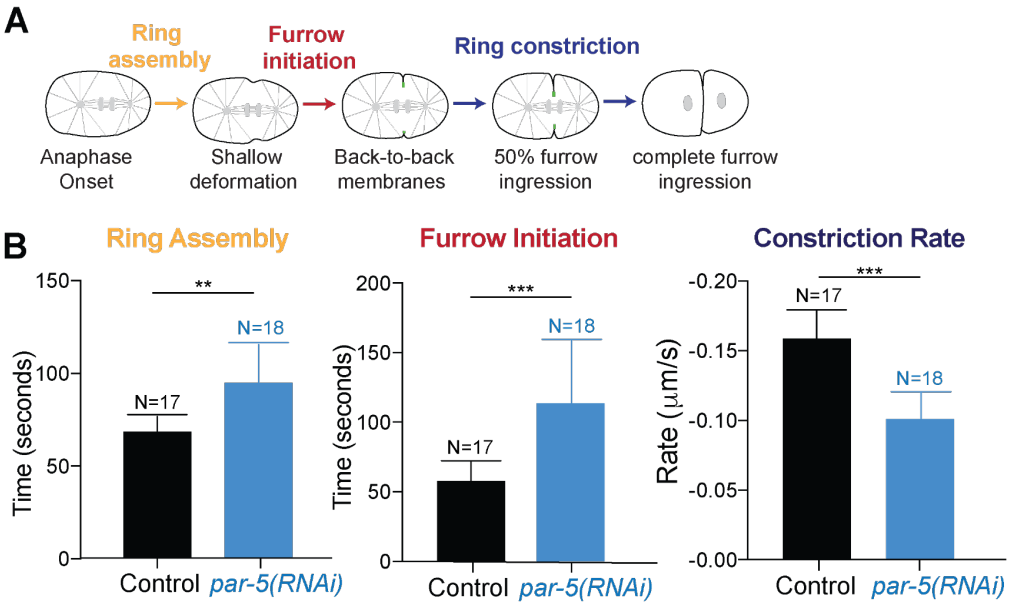

FIGURE 3.4. Increasing active myosin levels at the polar cortex through 14-3-3^{PAR-5} depletion leads to cortical instability, destabilizes the cleavage furrow and delays all phases of cytokinesis. (A) Reference points used for measurements of ring assembly and furrow initiation intervals, as well as nmy-2 intensity. Ring assembly: between anaphase onset and the formation of a shallow equatorial deformation, when contractile ring components are being recruited to the cell equator. Furrow initiation: between shallow deformation and the folding of the plasma membrane into a back-to-back configuration. Ring constriction: between a back-to-back configuration until full furrow ingression. **(B)** Time of ring assembly and furrow initiation, and constriction rate for controls and PAR-5 depleted embryos. The curves show mean± standard deviation for each timepoint. N is the number of analyzed embryos. Statistical significance was determined using unpaired t-test: * P<0.01, ** P<0.001,*** P<0.0001, **** P<0.00001.

In control embryos, NMY-2::GFP levels slightly decreased at the posterior and increased at the anterior pole from anaphase onset until shallow deformation, while increasing by almost 2-fold at the equatorial cortex (Figure 3.3A,D). This is concomitant with a period of anterior-directed unidirectional cortical flows (Figure 3.5A). After shallow deformation, NMY-2::GFP levels show a pronounced decrease from both poles, approximately by 2-fold at the anterior and 1.5-fold at the posterior, and keep accumulating at the equator, until a back-to-back membrane configuration is observed (Figure 3.3A,D). These changes are accompanied by a period of bidirectional cortical flows, which initiate from both poles towards the equator (Figure 3.5A). At 50% ingression (measured from the initial equatorial diameter), NMY-2::GFP levels at the equator have increased by almost 3-fold compared to anaphase onset and reach their lowest at both poles. Importantly, these changes are a result of the mechanisms of equatorial stimulation and polar clearance reviewed in Chapter I, section “Division plane specification and contractile ring assembly”.

When PAR-5 is depleted, NMY-2::GFP levels are significantly increased compared to control levels, at both poles and at the equatorial cortex, around 1.5-fold at the anterior and 2-fold at

the posterior cortex and equator (Figure 3.3A,D). Unlike control embryos, at shallow deformation myosin had not been cleared from the posterior pole and was slightly increased compared to anaphase onset levels. Also, myosin did not accumulate at the anterior side compared to anaphase levels and actually decreased. The increased myosin levels at the posterior pole during this phase, led to significant delays in ring assembly times (64 ± 5 seconds for controls *vs.* 102 ± 16 seconds for *par-5(RNAi)*). When the furrow reached a back-to-back membrane configuration, NMY-2::GFP levels had already started to decrease at the posterior pole, but remained high when compared to controls at the same timepoint. This was also enough to cause delays in furrow initiation times (51 ± 5 seconds for controls *vs.* 115 ± 48 seconds for *par-5(RNAi)*). During the constriction phase, NMY-2::GFP levels also remained higher than controls and, as a consequence, the constriction rate (measured between 70-30% of initial equatorial diameter) was also significantly slower (0.16 ± 5 seconds in controls *vs.* 0.10 ± 4 seconds in *par-5(RNAi))*. Surprisingly, NMY-2::GFP levels at the equator started higher than control levels, but remained approximately constant since anaphase onset and throughout constriction, and there was no equatorial myosin enrichment.

Interestingly, in the PAR-5 depleted embryos, the furrow was symmetric between the anterior and the posterior poles, which can be related with its suggested role in acting as a barrier between anterior and posterior PAR proteins (Morton *et al.*, 2002). A careful inspection of the plots of NMY-2::GFP intensity at different phases of cytokinesis (Figure 3.3D) seems to indicate a possible *"reversed polarity"* phenotype. This is suggested by the curves themselves, in which the curve of the posterior pole in PAR-5 depleted embryo seems very similar to the controls curve for the anterior pole, and vice-versa. Of note, despite all the defects observed upon PAR-5 depletion, this protein is not essential for cytokinesis in the early zygote, as cytokinesis still completes.

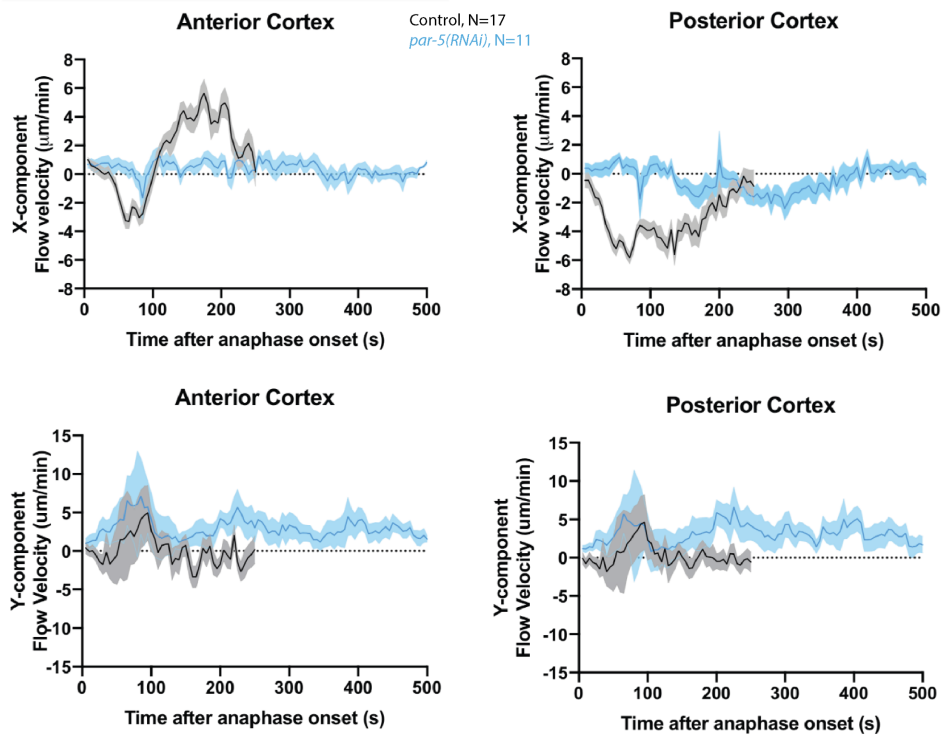

FIGURE 3.5. Par-5 depleted embryos display significantly attenuated longitudinal flow velocities and undergo rounds of strong intermittent rotational flows. NMY-2::GFP cortical flows measured by PIV (see "Materials and Methods" section) from anaphase onset until complete furrow ingression. **(A)** Longitudinal (X-component) flow velocities in the anterior (left) and posterior (right) cortices. **(B)** Rotational (Y-component) flow velocities in the anterior (left) and posterior (right) cortices. The curves show mean flow velocities ± SEM. N is the number of embryos analyzed.

To investigate how these changes in myosin distribution impacted cortical flow profiles, we used PIV to quantify both longitudinal (X-component) and rotational (Y-component) flows. The flow profiles are plotted in Figure 3.5A and B for the anterior and posterior cortices. In control embryos, as described above, there is a period for anterior directed unidirectional flows, followed by a period of ring directed bidirectional flows. Longitudinal flows, which are the ones believed to mostly contribute to compress F-actin bundles in the ring along the A-P axis, were significantly attenuated in PAR-5 depleted embryos. There was no detectable peak or consistent period of stronger flows that would precede ring formation. Instead, longitudinal flow velocities were significantly decreased compared to controls. Conversely, the rotational flows displayed an interesting profile. While in controls these flows have been shown to be dispensable for ring assembly and constriction as they could be an artifact of embryo compression during filming, PAR-5 depleted embryos underwent successive rounds of increased rotational flows, followed by periods of decreased flow velocities, with y-component

flow velocities peaking above 10 μm/min for the first round and around 5 μm/min for the subsequent rounds of rotational flow.
Interestingly, furrows in PAR-5 depleted embryos start ingressing from one side, as in controls, but they frequently stop ingressing from that side and start ingressing from the opposite site throughout constriction, which could be related with the alterations observed in rotational flows.

Decreasing myosin levels earlier leads to faster contractile ring assembly

Next, we tried to investigate how cytokinesis could be affected by a supposedly more pronounced polar clearance. If the polar inhibitory signal comes from the centrosomes and/or astral microtubules, we reasoned that perturbations that would affect the DNA-DNA distance (such as the microtubule bundler SPD-1) would have an increased impact in polar clearance. We started by checking that full SPD-1 depletions indeed result in increased DNA-DNA distances, with centrosomes coming closer to the embryo poles (data not shown, Verbrugghe and White, 2004). SPD-1 depletion resulted in earlier myosin clearance from the poles, which was particularly pronounced in the anterior pole (Figure 3.4A,D). In a control situation, myosin at the posterior pole is generally cleared earlier than at the anterior, which results in unidirectional actomyosin flows towards the anterior pole. It can be speculated that this happens because the spindle is shifted towards the posterior side, thus the centrosome is much closer to the posterior pole. In *spd-1(RNAi)* embryos, rings assembled significantly earlier than controls (57 ± 4 seconds for controls *vs.* 39 ± 3 seconds for *spd-1(RNAi)*), and also initiated furrowing prematurely (58 ± 5 seconds for controls *vs.* 42 ± 4 seconds for *spd-1(RNAi))*(Figure 3.5B). Even though there was a tendency for an increased constriction rate in SPD-1 depleted embryos, this was not statistically different than controls, which is consistent with myosin levels not being so different by the time the rings are effectively contracting. Analysis of myosin cortical flows in embryos expressing NMY-2::GFP revealed that, consistent with premature clearance of myosin from the anterior pole, bidirectional longitudinal cortical flows also started immediately after anaphase onset, conversely to controls, where flows are initially anterior-directed. Flow velocities at the anterior pole in SPD-1 depleted embryos were also higher than those in control embryos, reaching a maximum of around 8 μm/min for the former *vs.* -4 μm/min for the latter.

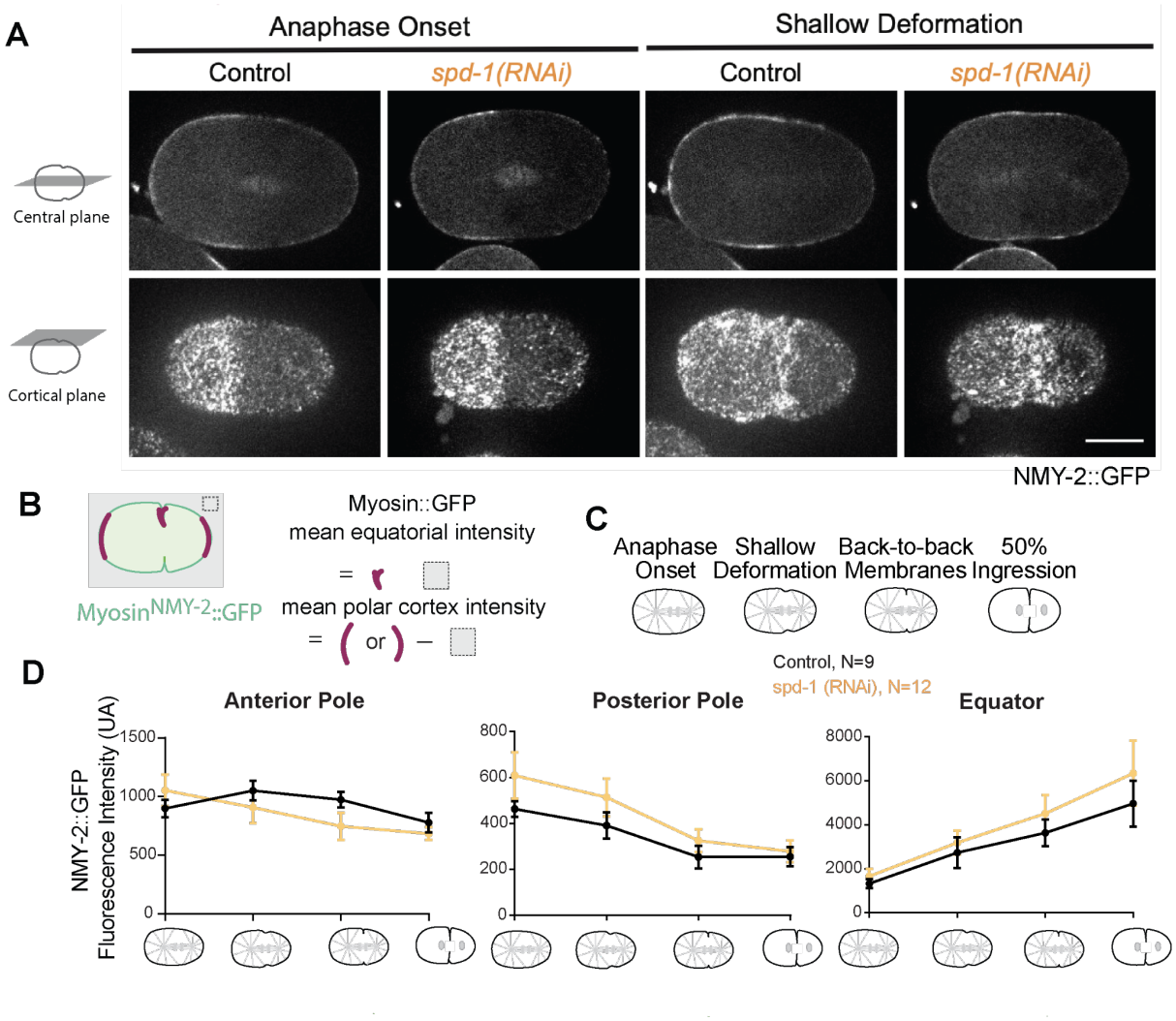

FIGURE 3.6. SPD-1 depletion triggers earlier myosin clearance from the poles. (A) Representative images of NMY-2::GFP levels in cortical and central plane of control and SPD-1 depleted embryos, at anaphase onset and shallow deformation. **(B)** Schematic showing the regions used for NMY-2::GFP fluorescence intensity measurements. **(C)** Reference points used for measurements of ring assembly and furrow initiation intervals, as well as nmy-2 intensity. Ring assembly: between anaphase onset and the formation of a shallow equatorial deformation, when contractile ring components are being recruited to the cell equator. Furrow initiation: between shallow deformation and the folding of the plasma mem- brane into a back-to-back configuration. Ring constriction: between a back-to-back configuration until full furrow ingression. **(D)** Measurements of NMY-2 fluorescence intensity on the anterior pole, posterior pole and equator at anaphase onset, shallow deformation, back-to-back membranes and 50% ingression for controls and SPD-1 depleted embryos. N is the number of embryos analyzed. Scale Bars,10 µm.

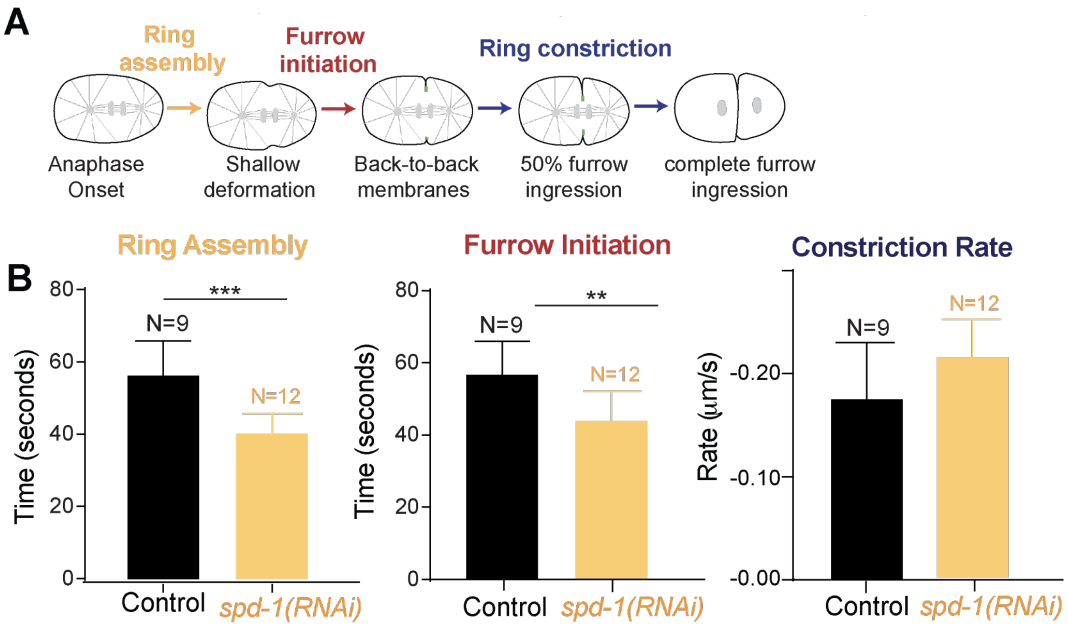

FIGURE 3.7. Accelerating the polar inhibitory signal by SPD-1 depletion triggers earlier myosin clearance from the poles and earlier ring assembly and furrow initiation. (A) Reference points used for measurements of ring assembly and furrow initiation intervals, as well as nmy-2 intensity. Ring assembly: between anaphase onset and the formation of a shallow equatorial deformation, when contractile ring components are being recruited to the cell equator. Furrow initiation: between shallow deformation and the folding of the plasma membrane into a back-to-back configuration. Ring constriction: between a back-to-back configuration until full furrow ingression. **(B)** Time of ring assembly and furrow initiation, and constriction rate for controls and SPD-1 depleted embryos. The curves show mean±−standard deviation for each timepoint. N is the number of analyzed embryos. Statistical significance was determined using unpaired t-test: * P<0.01, ** P<0.001,*** P<0.0001, **** P<0.00001.

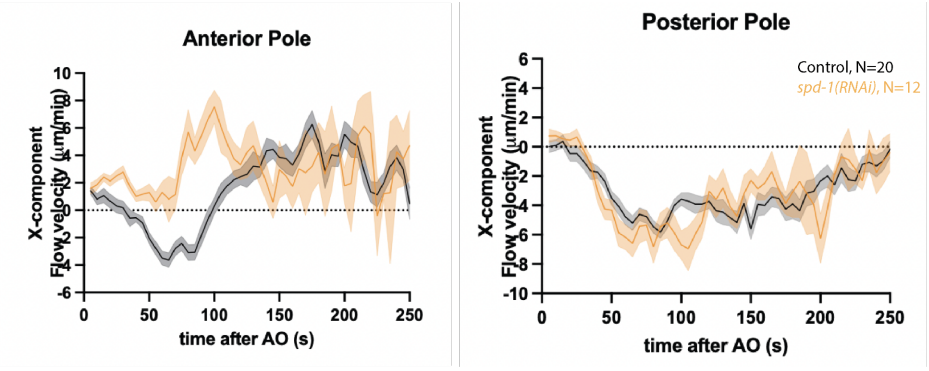

FIGURE 3.8. Spd-1 depleted embryos display premature bidirectional longitudinal flows. NMY-2::GFP cortical flows measured by PIV (see “Materials and Methods” section) from anaphase onset until complete furrow ingression in the anterior (left) and posterior (right) halves of the embryo.

Coarse-grained simulations of myosin activity in the cortex suggest a role for the polar cortex in coordinating the ingressing furrow kinetics

Because our main hypothesis was to unravel the effect of the surrounding cortex in cytokinesis dynamics, we wondered whether increasing or decreasing the contractility at the poles, maintaining the same activity at the equator, would be enough to impact ring constriction velocity (Figures 3.9 and 3.10). If the contractility at the poles is resisting ring constriction, then a decrease in the constriction rate when the activity at the poles is increased would be expected, or conversely, an increase in the constriction rate when the activity at the poles is decreased. Since it is not possible to have negative tensions, the decrease in activity at the poles was expressed as a function of the basal activity of the cortex, which was considered to be 1. To simulate polar hypercontractility, we altered the signal to contain a half gaussian at each pole with an amplitude 5-fold lower than the main equatorial gaussian (20 *vs.* 100, respectively). After some optimisation, we ended up simulating the decrease in contractility at the poles with two sigmoidal curves (Figure 3.10). The extent of contractility drop can be manipulated by changing the scale factor of the sigmoids. The overactivity at the equator was simulated with a gaussian distribution, as in controls (Figures 3.9 and 3.10). Plotting the radius *vs.* time of simulation curves (Figures 3.9 and 3.10) revealed that increasing polar contractility delayed ring constriction (Figure 3.9). In the case of further decreasing polar contractility, despite the curve for simulation in Figure 3.10B being steeper, indicating a faster decrease in ring radius with time than the control (Figure 3.10A), the difference between the two curves was not significant.

There are two possible hypotheses this: 1) The ratio between equator overactivity/poles underactivity was not enough to observe a significant effect. 2) The decrease in contractility at the poles is not enough to facilitate constriction at the equator. It is possible that viscous tension must also be decreased. We are implementing new functions in the model to test these possibilities, which are detailed in the discussion and future perspectives section.

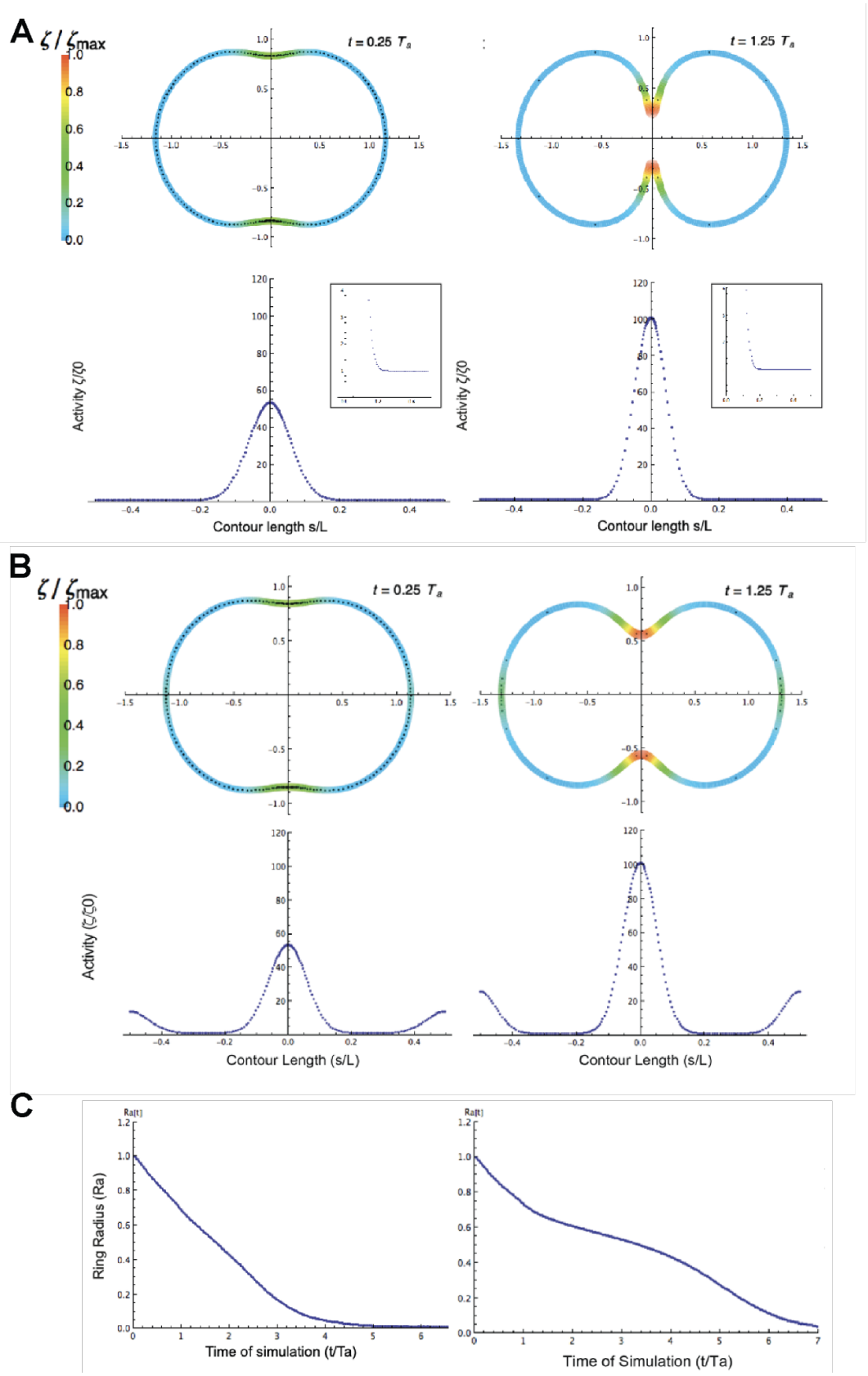

FIGURE 3.9. Effect of increasing contractility at the poles in the ring constriction velocity. (A) Simulation of an embryo with a gaussian overactivity signal at the equator of amplitude 100 and width 0.2 for the indicated timepoints. **(B)** Simulation of an embryo with an overactivity signal at the equator of amplitude 100 and width 0.2

and two sigmoidal signals at the poles. **(C)** Ring radius vs time of simulation for simulations (A) and (B), respectively.

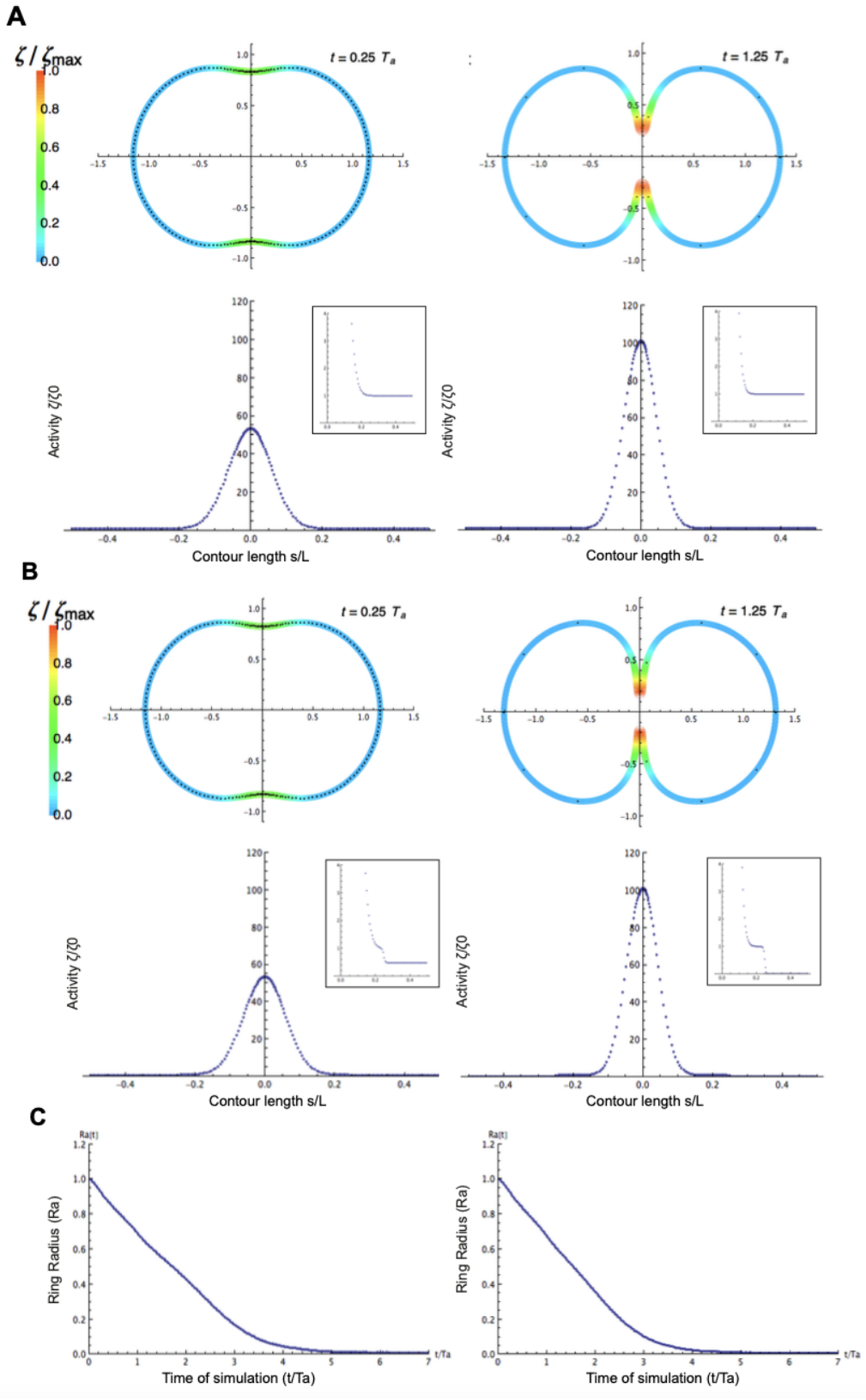

FIGURE 3.10. Effect of decreasing contractility at the poles in the ring constriction velocity. (A) Simulation of an embryo with a gaussian overactivity signal at the equator of amplitude 100 and width 0.2 for the indicated timepoints. **(B)** Simulation of an embryo with an overactivity signal at the equator of amplitude 100 and width 0.2 and two sigmoidal signals at the poles. **(C)** Ring radius vs time of simulation for simulations (A) and (B), respectively.

Discussion

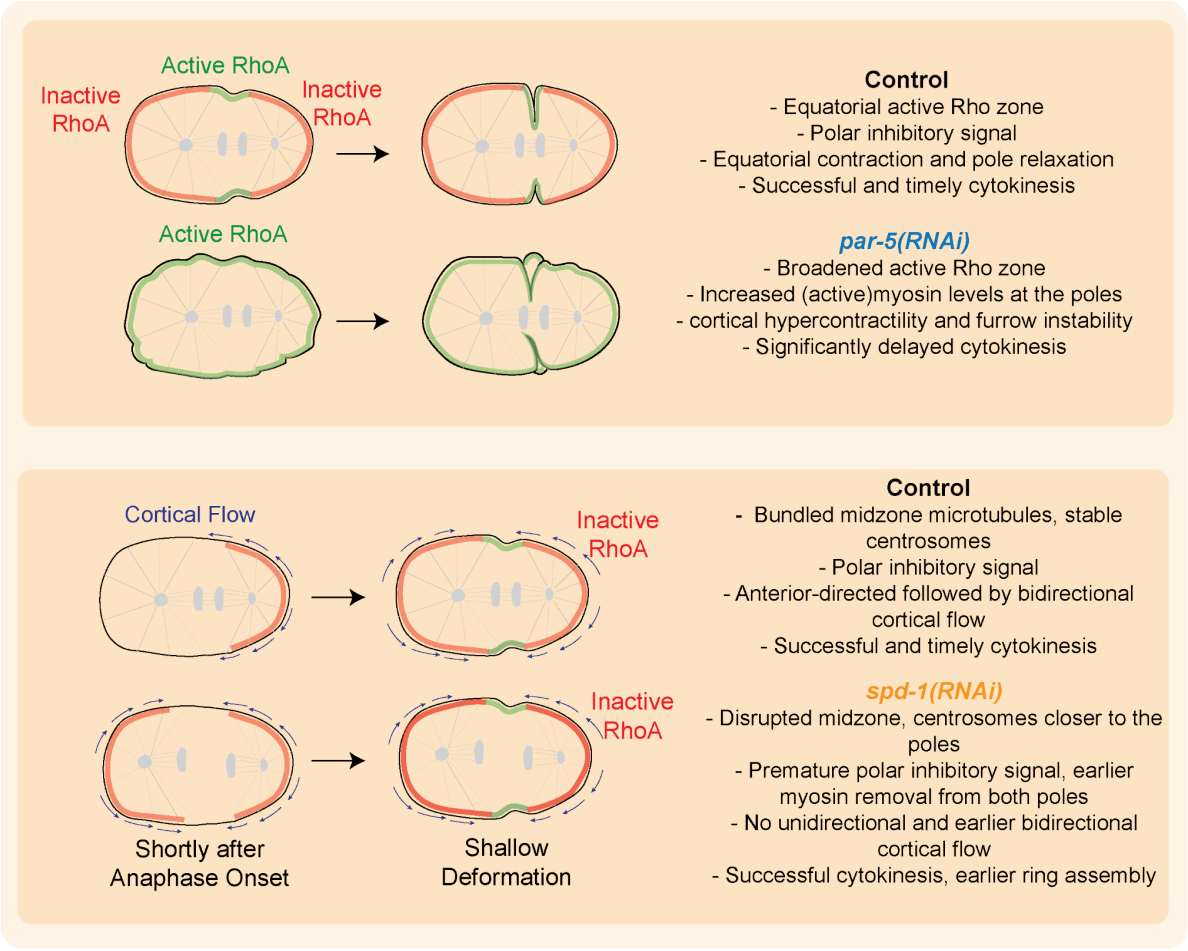

FIGURE 3.11. Summary of myosin activity and distribution pattern on the cortex during cytokinesis and observed phenotypes. Top: Effects of PAR-5 depletion on myosin distribution and activation pattern. **Bottom:** Effects of SPD-1 depletion on myosin distribution and cytokinesis.

Many questions remain unanswered in this chapter, some of them related with mechanical aspects which is the focus of this thesis, but also regarding possible new protein interactions. It is already known that in the *C. elegans* zygote, PAR-5 inhibits the cortical localization of centralspindlin oligomers, therefore inhibiting the RhoA-GEF Ect2 from converting RhoA-GDP into RhoA-GTP thus suppressing excessive contractility (Basant and Glotzer, 2018b). Therefore, its depletion presumably leads to an increased oligomerization of centralspindlin at the cortex and consequently, to increased RhoA-GTP levels. This implies nevertheless that the effect in increased active myosin levels is indirect, via a signalling cascade. It is currently

not known whether PAR-5 can interact directly with myosin, as in *D. Discoideum*. The mechanisms governed by the 14-3-3 ortholog are clearly different between the two organisms, as *D. discoideum* cells lacking 14-3-3 behave as myosin *nulls*, while in *C. elegans* myosin levels and contractility are clearly increased. Indeed, by visually inspecting the cortical images of *C. elegans* zygotes (Figure 3.3B), one can observe not only an increase in myosin levels, but also an increase in myosin patches all over the cortex. The interpatch cortical space seems to be more prone to the emergence of deformations that look like blebs, bulges that form on the cell surface due to the decoupling of the cell cortex from the plasma membrane (Charras *et al.*, 2006; Jean-Yves Tinevez *et al.*, 2009). A question that immediately arises is whether myosin turnover and mobility could be altered upon PAR-5 depletion. In *D. discoideum*, 14-3-3 inhibits bipolar filament assembly and promotes myosin turnover, so its depletion should lead to increased filament assembly and slower turnover. Even though the ultimate phenotype between the two organisms is exactly the opposite, it is possible that myosin turnover is also slower in *C. elegans*, due to the presence of more myosin patches that seem less dynamic than in control embryos. A careful quantification of myosin turnover using FRAP in PAR-5 depleted zygotes could more precisely confirm this hypothesis. Another interesting experiment would be to express a phosphomimetic myosin, which in principle could result in higher rates of bipolar filament assembly and inspect whether the cortical myosin pattern and dynamics is any similar to PAR-5 depleted embryos.

Another interesting question is whether the phenotypes observed are exclusive of PAR-5 depletion or if some, or all of these, are common to the depletion of any protein known to lead to increased RhoA-dependent contractility.

The rotational flows in PAR-5 depleted embryos are a quite curious observation. Whereas in control embryos there is a period of pronounced rotational cortical flow, starting shortly after anaphase onset concomitantly with the unidirectional longitudinal flows along the A-P axis and ceasing shortly after, when PAR-5 is depleted, the longitudinal flow velocities are significantly decreased, but the same does not happen to the rotational flows. These remained strong and underwent consecutive rounds of strong *vs.* weak flows during constriction. While rotational flows have been shown to be a possible artifact of embryo compression during filming and dispensable for cytokinesis (Singh *et al.*, 2019; Leite *et al.*, 2020), there is increasing evidence that some proteins might be involved in these rotational flows by inducing torques within the actomyosin networks (Naganathan *et al.*, 2014; Pimpale *et al.*, 2020; Middelkoop *et al.*, 2021; Zaatri, Perry and Maddox, 2021). Even though the velocities of rotational flow can be amplified by embryo compression, there must be a trigger for them to initiate and for those consecutive rounds of strong flow intercalated by periods of no flow. It can be hypothesized that these rotational flows are related with the closure asymmetry in the *C. elegans* zygote. Indeed, in control embryos there is an asymmetry of closure (apart from the left-right asymmetry) in which

the furrow always ingresses preferentially from one of the sides, whereas in PAR-5 depleted embryos the furrow starts ingressing preferentially from one of the sides but then it slows down and switches ingressing from the opposite side. It would be interesting to check whether there is a correlation between these switches in furrow closure and the rounds of strong *vs.* weak rotational flow. One could question whether those flows are themselves dictating the preferential side of furrow ingression or, alternatively, if there are molecular mechanisms that dictate that ingression profile and this in turn has an impact in flow velocity and directionality. Indeed, the formin ortholog in *C. elegans*, CYK-1, has been shown to constitute a trigger for active torque generation in the cortex and the emergence of chiral counter-rotating flows (Middelkoop *et al.*, 2021). If PAR-5 depletion indeed results in increased RhoA-GTP levels throughout the cortex, it is possible that besides increasing active myosin levels, it also increases CYK-1 levels outside the equatorial region, which would not only change cortex architecture and contractility patterns, but could also be a potential cause of the several rounds of rotational flow. This is something to confirm in future work. However, the literature indicates that CYK-1 is responsible for the emergence of chirality in the cortex, essentially meaning both halves of the embryo would rotate in opposite directions, while in PAR-5 depletions, both halves rotate in the same direction. This suggests other mechanisms may be involved.

The experiments with SPD-1 were not very conclusive on whether further decreasing myosin levels at the polar cortex during ring constriction leads to an acceleration in the closure rate, partially because the myosin levels at the poles during constriction are not statistically different than controls, thus the rate remains essentially the same. Surprisingly, the main effect was observed in earlier phases, more specifically during the assembly of the ring and the initiation of furrowing. Conversely to controls, in which the posterior pole is cleared first and the anterior is cleared only after the equator has slightly deformed, myosin clearance from the anterior pole began right after anaphase onset and simultaneously with clearance from the posterior pole in SPD-1 depleted embryos. We suspect the effect on the anterior pole is more drastic than on the posterior due to the distance of the respective centrosomes to each of the poles. In *C. elegans* embryos, the spindle is shifted towards the posterior half of the embryo and therefore, this may be sufficient to induce polar clearance right after anaphase onset. It is likely that the SPD-1 depletion, by unbundling the central spindle microtubules and increasing the DNA-DNA distance/spindle elongation (Verbrugghe and White, 2004), causes the centrosome on the anterior side to become close enough to the pole to also induce earlier clearance.
Interestingly, the premature clearance of the anterior pole was consistent with an earlier triggering of bidirectional longitudinal cortical flows, that also began immediately after anaphase onset, conversely to controls. As a possible consequence, or not, rings assembled and initiated furrowing earlier. It is unclear whether earlier ring assembly and furrow initiation

are a consequence of the earlier polar clearance and the bidirectional flows that cause earlier and increased compression at the equatorial cortex or, whether there is also a concomitant equatorial mechanism that facilitates early furrow ingression *per se* upon SPD-1 knockdown, via the kinesin ZEN-4 or RhoGAP CYK-4, a MgcRacGAP ortholog (Verbrugghe and White, 2004). In the latter scenario, the tension differential arising from increased equatorial stimulation and earlier clearance of the anterior pole would consequently trigger the bidirectional flows.

Simple computational simulations of the whole cell surface using a pre-existing model confirmed the findings of both PAR-5 and SPD-1 knockdown experiments. In this model, the trigger for furrow initiation is a gaussian signal with a certain width and amplitude that artificially simulates RhoA-GTP activity, which peaks at the equatorial region of the embryo and drops towards the poles (the ratio of equatorial overactivity *vs.* basal cortical activity was considered 100:1). To recapitulate the abovementioned experimental conditions, we slightly changed this signal to include 1) two half gaussians with lower amplitude than the central one at each pole to simulate increased myosin activity, which would correspond to the *par-5(RNAi)*; 2) two inverted sigmoid functions at each pole to simulate increased polar clearance, corresponding to the *spd-1(RNAi)*. As observed experimentally in PAR-5 depleted embryos, an increase in myosin activity at the poles led to delayed furrow constriction. Further decreasing myosin activity at the poles slightly increased the constriction rate, albeit not significantly. This agrees with SPD-1 depletions not significantly increasing the ring constriction rate.

Further decreasing polar myosin activity did not have a significant impact in the constriction rate, which may be explained by the fact that the ratio equatorial overactivity:basal polar activity is already very abrupt and dropping the basal activity from 1 to close to 0 was not enough to produce a significant effect. These first simulations display some limitations, essentially because they use an artificial profile to simulate contractility, which reaches the maximum amplitude very fast. This abrogated the possibility of testing any effect of these depletions in phases prior to effective ring constriction, such as assembly and furrow initiation.

Conclusion

In this chapter, perturbations of proteins known to interfere with myosin levels distribution and activation pattern were employed to evaluate the corresponding cytokinesis phenotypes and kinetic parameters. Increasing myosin activity at the polar cortex delays all phases of cytokinesis, and accelerating initial myosin polar clearance triggers earlier ring assembly and furrow initiation. Altogether, these results reveal that myosin concentration, activation and distribution pattern between the equatorial and the polar cortices dictate constriction kinetics. Importantly, this regulation is fine-tuned spatiotemporally, with changes in myosin distribution

having direct consequences in the phase of cytokinesis at which they occur, not necessarily affecting the subsequent phases.

Materials and Methods

C. elegans strains

Strains used in this study and their genotypes are listed in Table 3.1. and were maintained on nematode growth medium (NGM) plates seeded with OP50 *E. coli* at 20°C using standard techniques (Stiernagle, 2006).

Table 3.1. List of *C. elegans* strains used in this study.

Name	**Genotype**	**Source/ reference**
N2	Ancestral	*Caenorhabditis* Genetics Center
GCP22	ltIs157 [pAC16;pie-1/LifeAct::GFP; unc-119 (+)]; unc-119(ed3) III (?); prtSi2[pAC71;Pnmy-2:nmy-2reencoded::mCherrry::StrepTagII::3'UTR-nmy-2; cb-unc-119(+)]II	Our lab (Osório et al., 2019)
GCP113/ GCP812	nmy-2(cp13[nmy-2::GFP+LoxP]) I; unc-119(ed3) III (?); ltIs37 [pAA64; pie-1/mCherry::his-58; unc-119 (+)]	Our lab (Silva et al., 2016)
GCP179	nmy-2(cp13[nmy-2::gfp + LoxP]) I; ltIs44 [pAA173; pie-1/mCherry::PH(PLC1delta1); unc-119 (+)]	Our lab (Silva et al., 2016)
GCP380	nmy-2(cp13[nmy-2::gfp + LoxP]) I; unc-119(ed3) III; ltIs37 [pAA64; pie-1/mCHERRY::his-58; unc-119 (+)] IV; ltIs44 [pAA173; pie-1/mCherry::PH(PLC1delta1); unc-119 (+)]	This thesis
GCP752	nmy-2(cp52[nmy-2::mKate2 + LoxP unc-119(+) LoxP]) I; ltIs157 [pAC16;pie-1/LifeAct::GFP; unc-119 (+)]; ltIs37	This thesis

	[pAA64; pie-1/mCherry::his-58; unc-119 (+)] IV; unc-119(ed3) III	
GCP832	[plst-1(msn190[plst-1::GFP])] IV; ltIs37 [pAA64; pie-1::mCherry::his-58 +unc-119(+)] IV; unc-119(ed3) III (?)	Our lab (Sobral *et al.*, 2021)
GCP925	unc-119(ed3)III; prtSi2[pAC71; Pnmy-2:nmy-2reencoded::mCherry::StrepTagII::3'UTRnmy-2; cb-unc-119(+)]II; [pani-1:GFP::ANI-1; cb-unc-119(+)]IV	This thesis

RNA interference

RNAi was performed by feeding hermaphrodite worms with bacteria that expressed the dsRNA of interest. DNA fragments of interest were amplified using the primers in Table 3.2. from N2 cDNA or gDNA (the absence of primers means the feeding was obtained from the Ahringer library ((Kamath et al., 2003); RNAi feeding library distributed by Source BioScience, United Kingdom) . These fragments were cloned using the EcoRV restriction site in L4440 vector, which was transformed into HT115 *E. coli*. Expression of dsRNAs in transformed HT115 was induced with 1 mM IPTG and the bacteria were fed to hermaphrodites as described below.

For penetrant depletions of both *par-5* and *spd-1*, worms were feeded at 20ºC for 48h.

For RNAi feeding, bacteria expressing the dsRNA were grown overnight at 37 °C in LB with 100 µg/ml ampicillin and tetracycline (5 mg/mL) and Isopropyl β-d-1-thiogalactopyranoside IPTG (1mM). The overnight culture was grown until an OD600 of 1.6 was reached. The bacterial culture (~100 µl/plate) was spread onto 6 cm NGM agar plates. Plates were dried at room temperature for three days to induce RNA expression. After IPTG induction, animals were transferred to these plates.

Table 3.2. List of dsRNAs used in this study.

Name	Gene target	Forward Primer	Reverse Primer	RNAi type
par-5_RNA#1	*par-5* (M117.2)	AATTAACCCTCACTAAAGGtggacatctgacgttggagctga	TAATACGACTCACTATAGGgaatgacaatagtgacggagtga	Injection
par-5_RNA#2	*par-5*	——————	——————	Feeding (Ahringer library)

spd-1	*spd-1*	—----------	—----------	Feeding

Live-imaging

Gravid hermaphrodites were dissected and one-cell embryos were mounted in a drop of M9 (86 mM NaCl, 42 mM Na2HPO4, 22 mM KH2PO4, and 1 mM MgSO4) on 2% agarose pads overlaid with a coverslip. Live imaging of cytokinesis was performed at 20°C. Images were acquired on a spinning disk confocal system (Andor Revolution XD Confocal System; Andor Technology) with a confocal scanner unit (CSU-X1; Yokogawa Electric Corporation) mounted on an inverted microscope (Ti-E, Nikon) equipped with a 60x NA 1.4 oil-immersion Plan-Apochromat objective, and solid-state lasers of 405 nm (60 mW), 488 nm (50 mW), and 561 nm (50 mW). For image acquisition, an electron multiplication back-thinned charge-coupled device camera (iXon; Andor Technology) was used. Acquisition parameters, shutters and focus were controlled using Andor iQ3 software. For central plane imaging in one-cell embryos, 6 × 1 µm z-stacks were collected in the 488 nm and 561 nm channels every 5 seconds for strains GCP812, GCP179 and GCP380 in Figure 3.4B and 3.7B. For cortical dual-color imaging in one-cell embryos in Figures 3.1, 3.2B,C, 3.3A, 3.5, 3.6A and 3.8, 7 × 0.5 µm z-stacks were collected every 5 seconds for strains GCP812, GCP179, GCP380, GCP752, GCP832 and GCP925 and 2 x 1 µm stacks in the central plane were collected in the 488 nm or 561 nm channels every 5 seconds, respectively.

Measurement of cytokinesis, ring assembly and furrow initiation time intervals, and ring constriction rate

Measurement of cytokinesis, ring assembly and furrow initiation time intervals, as well as ring constriction rate were performed in one-cell embryos of the following strains: GCP812, GCP179 and GCP380. This analysis only included embryos that completed ring constriction. Ring assembly corresponded to the time interval between anaphase onset and the establishment of a shallow deformation in the equatorial region (time point when the equator shows first sign of deformation). Furrow initiation time corresponded to the time interval between the establishment of the shallow deformation and the time when the plasma membranes of the nascent daughter cells became juxtaposed to one another (back-to-back membrane configuration). During ring constriction, the distance between the two sides of the ring was measured in the z-plane where this distance was widest at each time point and plotted against time. Ring constriction rate was the slope of the linear region between ~70% and 30% ingression, or 80-20%, as indicated in the respective figures. All intervals and ring constriction rate were determined based on imaging of the embryo central plane.

Fluorescence intensity measurements

To quantify the levels of NMY-2::GFP at the equatorial and polar cortices, a segmented line was traced over the cortex contour: on top of the tip of the cytokinetic furrow for back-to-back membranes and at 50% ingression and on both polar contour until the region of maximum curvature. The mean intensity was calculated, to take into account the different lengths of the lines traced. A box of 20 x 20 pixels was used on the camera background, which was subtracted to each measurement, for every time point considered. All movies were corrected for photobleaching prior to intensity measurements.

Cortical flow quantification

Cortical flow dynamics were analyzed in one-cell embryos of strains GCP752 between anaphase onset until the end of constriction. Magnitude and direction of cortical flows were quantified using an Iterative Particle Image Velocimetry (PIV) plugin for ImageJ, Myosin cortical flows were determined in maximum projections of cortical planes in embryos expressing NMY–2::GFP. Flows were analyzed between anaphase onset and the end of cytokinetic furrow ingression. Magnitude and direction of cortical flows were quantified using a Particle Image Velocimetry (PIV) MATLAB script (Thielicke and Stamhuis, 2014). A 216 x 128 pixel (38.5 x 22.8 mm) region was applied to all embryos to exclude cortical curved peripheries. Two iterations were performed to calculate maximum particle displacement: a larger interrogation window of 64 x 64 pixels was used in the first iteration and a smaller interrogation window of 32 x 32 pixels was used in the second iteration. Consecutive interrogation windows overlapped by 50%. After flow field generation, the 216 x 128 pixel region was divided in two adjacent anterior and posterior regions: anterior cortex (1st-148th pixel; 0.0–26.3 mm) and posterior cortex (149th-216th pixel; 26.3–38.4 mm). Each velocity vector was resolved into a Vx component along the anterior-posterior axis and a Vy component along the dorsal-ventral axis. The mean Vx and Vy in the anterior and posterior cortex were estimated for each time point and plotted as a function of time to trace the cortical flow profiles.

Image analysis, quantifications, and statistics

All microscopy image processing and measurements were done using Fiji (ImageJ; National Institutes of Health) and MATLAB (MathWorks). Z-stacks taken on the cell cortex were projected using the maximum intensity projection tool. Flow kymographs shown in Fig. 3.2B were created by selecting a rectangular region of 80x10 pixels in the posterior region of the cortical plane of the embryo and stacking these region over time using the Make Montage tool. Graph plotting, linear regressions and statistical analyses were performed with Prism 6 or 7 (GraphPad Software). All error bars represent the 95% CI of the mean or SEM and statistical

significance tests were performed using one-way ANOVA or two-way ANOVA for repeated measures with Bonferroni correction as indicated in figure legends.

Coarse-grained simulations of the cell cortex

To simulate the effects of polar overactivity and polar clearance, changes were made to a preexisting C++ code (Turlier et al.,2014). MATHEMATICA software (Wolfram Alpha, https://www.wolfram.com/mathematica/) was used to analyze and plot numerical data. In the simulations shown on Figures 3.9 and 3.10, the numerical values used for each model parameter are listed on Table 3.3.

Table 3.3. Numerical values used in the computational simulations.

Notation	Quantity	Numerical value
R_0	Initial radius	1
e_0	Initial cortical thickness	0.02
w	RhoA-GTP equatorial signal width	0.2
p	Polar clearance width	70
T_a	Typical timescale	7
$1/2z_0D\mu$	Basal cortical active stress	1
η	Cortex viscosity	1
V_p	Polymerization rate	0.8
K_d	Depolymerization rate	40

References

Basant, A. *et al.* (2015) 'Aurora B Kinase Promotes Cytokinesis by Inducing Centralspindlin Oligomers that Associate with the Plasma Membrane', *Developmental Cell*, 33(2), pp. 204–215. Available at: https://doi.org/10.1016/j.devcel.2015.03.015.

Basant, A. and Glotzer, M. (2018) 'Spatiotemporal Regulation of RhoA during Cytokinesis', *Current Biology*, 28(9), pp. R570–R580. Available at: https://doi.org/10.1016/j.cub.2018.03.045.

Charras, G.T. *et al.* (2006) 'Reassembly of contractile actin cortex in cell blebs.', *The Journal of cell biology*, 175(3), pp. 477–490. Available at: https://doi.org/10.1083/jcb.200602085.

Grill, S.W. *et al.* (2001) 'Polarity controls forces governing asymmetric spindle positioning in the Caenorhabditis elegans embryo.', *Nature*, 409(6820), pp. 630–633. Available at:

https://doi.org/10.1038/35054572.

Leite, J. *et al.* (2020) 'Equatorial Non-muscle Myosin II and Plastin Cooperate to Align and Compact F-actin Bundles in the Cytokinetic Ring.', *Frontiers in cell and developmental biology*, 8, p. 573393. Available at: https://doi.org/10.3389/fcell.2020.573393.

Middelkoop, T.C. *et al.* (2021) 'CYK-1/Formin activation in cortical RhoA signaling centers promotes organismal left-right symmetry breaking.', *Proceedings of the National Academy of Sciences of the United States of America*, 118(20). Available at: https://doi.org/10.1073/pnas.2021814118.

Morton, D.G. *et al.* (2002) 'The Caenorhabditis elegans par-5 gene encodes a 14-3-3 protein required for cellular asymmetry in the early embryo.', *Developmental biology*, 241(1), pp. 47–58. Available at: https://doi.org/10.1006/dbio.2001.0489.

Naganathan, S.R. *et al.* (2014) 'Active torque generation by the actomyosin cell cortex drives left-right symmetry breaking.', *eLife*, 3, p. e04165. Available at: https://doi.org/10.7554/eLife.04165.

Pimpale, L.G. *et al.* (2020) 'Cell lineage-dependent chiral actomyosin flows drive cellular rearrangements in early caenorhabditis elegans development', *eLife*, 9, pp. 1–35. Available at: https://doi.org/10.7554/eLife.54930.

Schmutz, C., Stevens, J. and Spang, A. (2007) 'Functions of the novel RhoGAP proteins RGA-3 and RGA-4 in the germ line and in the early embryo of C. elegans.', *Development (Cambridge, England)*, 134(19), pp. 3495–3505. Available at: https://doi.org/10.1242/dev.000802.

Singh, D. *et al.* (2019) 'Mechanical stress induces a scalable switch in cortical flow polarization during cytokinesis', *Journal of Cell Science*, 132(19). Available at: https://doi.org/10.1242/jcs.231357.

Sobral, A.F. *et al.* (2021) 'Plastin and spectrin cooperate to stabilize the actomyosin cortex during cytokinesis.', *Current biology : CB*, 31(24), pp. 5415-5428.e10. Available at: https://doi.org/10.1016/j.cub.2021.09.055.

Stiernagle, T. (2006) 'Maintenance of C. elegans.', *WormBook : the online review of C. elegans biology*, pp. 1–11. Available at: https://doi.org/10.1895/wormbook.1.101.1.

Thielicke, W. and Stamhuis, E.J. (2014) 'PIVlab – Towards User-friendly, Affordable and Accurate Digital Particle Image Velocimetry in MATLAB', *Journal of Open Research Software*, 2. Available at: https://doi.org/10.5334/jors.bl.

Tinevez, J.-Y. *et al.* (2009) 'Role of cortical tension in bleb growth.', *Proceedings of the National Academy of Sciences of the United States of America*, 106(44), pp. 18581–18586. Available at: https://doi.org/10.1073/pnas.0903353106.

Verbrugghe, K.J.C. and White, J.G. (2004) 'SPD-1 is required for the formation of the spindle midzone

but is not essential for the completion of cytokinesis in C. elegans embryos.', *Current biology : CB*, 14(19), pp. 1755–1760. Available at: https://doi.org/10.1016/j.cub.2004.09.055.

West-Foyle, H. *et al.* (2018) '14-3-3 proteins tune non-muscle myosin II assembly', *Journal of Biological Chemistry*, 293(18), pp. 6751–6761. Available at: https://doi.org/10.1074/jbc.M117.819391.

Zaatri, A., Perry, J.A. and Maddox, A.S. (2021) 'Septins and a formin have distinct functions in anaphase chiral cortical rotation in the Caenorhabditis elegans zygote.', *Molecular biology of the cell*, 32(14), pp. 1283–1292. Available at: https://doi.org/10.1091/mbc.E20-09-0576.

Zhou, Q. *et al.* (2010) '14-3-3 coordinates microtubules, rac, and myosin II to control cell mechanics and cytokinesis', *Current Biology*, 20(21), pp. 1881–1889. Available at: https://doi.org/10.1016/j.cub.2010.09.048.

CHAPTER IV

EQUATORIAL NON-MUSCLE MYOSIN II AND PLASTIN COOPERATE TO ALIGN AND COMPACT F-ACTIN BUNDLES IN THE CYTOKINETIC RING

This chapter was published as in:
Leite J., Chan F. Y., Osório D. S., Saramago J., Sobral A. F., Silva A. M., Gassmann R., Carvalho A. X. (2020). Equatorial non-muscle myosin II and plastin cooperate to align and compact F-actin bundles in the cytokinetic ring. *Frontiers in Cell and Developmental Biology*, 25;8:573393. doi: 10.3389/fcell.2020.573393.

Re-produced under permission of Elsevier's Journal Author Rights:
As the author of this Elsevier article, Joana Leite retains the right to include it in a thesis or dissertation.

Personal contribution: Joana Leite participated in the conceptualization, experimental design, investigation and formal data analysis (except Supplementary Figures S4.1 and S.4.2C), methodology (except acquisition of some of the microscopy movies used in Figures 4.1 and 4.2, S4.1 and S4.2) and the generation of the Plastin^{PLST-1} mutant lacking the actin binding domain), figures preparation (except Supplemental Figure S4.1 and S4.2A,C), as well as manuscript writing, reviewing and editing.

Equatorial Non-muscle Myosin II and Plastin Cooperate to Align and Compact F-actin Bundles in the Cytokinetic Ring

Abstract

Cytokinesis is the last step of cell division that physically partitions the mother cell into two daughter cells. Cytokinesis requires the assembly and constriction of a contractile ring, a circumferential array of filamentous actin (F-actin), non-muscle myosin II motors (myosin), and actin-binding proteins that forms at the cell equator. Cytokinesis is accompanied by long-range cortical flows from regions of relaxation toward regions of compression. In the *C. elegans* one-cell embryo, it has been suggested that anterior-directed cortical flows are the main driver of contractile ring assembly. Here, we use embryos co-expressing motor-dead and wild-type myosin to show that cortical flows can be severely reduced without major effects on contractile ring assembly and timely completion of cytokinesis. Fluorescence recovery after photobleaching in the ingressing furrow reveals that myosin recruitment kinetics are also unaffected by the absence of cortical flows. We find that myosin cooperates with the F-actin crosslinker plastin to align and compact F-actin bundles at the cell equator, and that this cross-talk is essential for cytokinesis. Our results thus argue against the idea that cortical flows are a major determinant of contractile ring assembly. Instead, we propose that contractile ring assembly requires localized concerted action of motor-competent myosin and plastin at the cell equator.

Introduction

Animal cytokinesis relies on the assembly and constriction of an actomyosin contractile ring at the cell equator, which pinches the plasma membrane inwards, ultimately separating the two daughter cells (reviewed in Leite et al., 2019). The contractile ring is a circumferential array of filamentous actin (F-actin), non-muscle myosin II (hereafter myosin) and actin-binding proteins, including formins and F-actin crosslinkers, such as α-actinin, fimbrin/plastin (hereafter plastin), anillin and septins (reviewed in Green et al., 2012). At cytokinesis onset, RhoA activation at the cell equator triggers the recruitment and activation of downstream effectors to assemble the contractile ring, particularly diaphanous-related formins (Prokopenko et al., 2000; Großhans et al., 2005; Watanabe et al., 2010; Melak et al., 2017) and Rho kinase, which promote the assembly of linear F-actin and the activation of myosin, respectively (Matsumura, 2005; Vicente-Manzanares, 2009). Experimental evidence from electron microscopy in marine invertebrate and newt eggs and cultured mammalian cells

suggests that the contractile ring is a thin layer of closely packed F-actin of mixed polarities (Schroeder, 1968, 1970, 1972; Arnold, 1969; Selman and Perry, 1970; Sanger and Sanger, 1980; Maupin and Pollard, 1986; Mabuchi et al., 1988; Henson et al., 2017) surrounded by a mostly branched network (Henson et al., 2017). How F-actin and myosin accumulate and organize into a circumferential array at the cell equator to form the contractile ring is a central question that remains to be fully resolved. Two main mechanisms have been implicated: equatorial compression due to cortical flows and local RhoA-dependent *de novo* assembly at the equator. According to the former, both F-actin and myosin are advected by flow from the poles towards the equator due to a tension differential between these regions. The persistent convergence at the equator creates a region where filaments are constantly compressed and aligned (White and Borisy, 1983; Salbreux et al., 2009; Turlier et al., 2014; Khaliullin et al., 2018). According to the latter, F-actin and myosin are directly recruited to the equatorial cortex from the cytoplasm, leading to local alignment of F-actin bundles (Kimura et al., 1996; Bement et al., 2005; Vavylonis et al., 2008; Uehara et al., 2010; Spira et al., 2017). The relative contribution of these two mechanisms to cytokinesis has been difficult to ascertain, because flows are myosin-dependent (Reymann et al., 2016) yet myosin perturbations may prevent cytokinesis simply because myosin-dependent force generation at the equator is essential for equatorial deformation and continued furrow ingression (Davies et al., 2014; Osorio et al., 2019). While actomyosin cortical flows towards the cell equator during cytokinesis have been described in several experimental systems, including *C. elegans* (Reymann et al., 2016; Khaliullin et al., 2018; Singh et al., 2019), they are less evident in some mammalian cells and are absent in yeast (Cao and Wang, 1990; Murthy and Wadsworth, 2005; Wu and Pollard, 2005; Vavylonis et al., 2008; Laplante et al., 2015). It remains to be determined whether cortical flows actually drive assembly of a contractile ring or whether they are simply a consequence of the tension differential that arises from equatorial stimulation and polar relaxation.

The involvement of F-actin crosslinkers (hereafter crosslinkers) in contractile ring assembly remains poorly explored. Depending on their size and structure, crosslinkers can form tight and parallel F-actin bundles or loosely crosslinked F-actin networks with distinct architectures and mechanical properties (Faix et al., 1996; Mavrakis et al., 2014; Srivastava and Robinson, 2015). A common feature is that crosslinkers provide interconnectivity, which is important for contractility of actomyosin networks (Ennomani et al., 2016; Descovich et al., 2017). To date, the only crosslinker whose perturbation is known to negatively impact cytokinesis in *C. elegans* embryos is the plastin PLST-1. A *plst-1* loss-of-function mutant decreased F-actin network connectivity and resulted in short-range and erratic F-actin cortical flows (Ding et al., 2017). Plastin is a globular protein that can assemble F-actin into tightly packed bundles with

uniform or mixed polarity (Bretscher, 1981; Matsudaira et al., 1983; Skau et al., 2011). Plastin localizes to dense F-actin bundles and is particularly abundant in the cytokinetic ring (Ding et al., 2017), but whether it contributes to the organization and/or stabilization of F-actin bundles in this region is unknown.

We previously generated *C. elegans* expressing motor-dead mutants of myosin (NMY-2) and showed that myosin motor activity is essential for cytokinesis in the one-cell embryo (Osorio et al., 2019). In this study, we use these *nmy-2* mutants, as well as a *plst-1* mutant, to explore the role of cortical flows during cytokinesis in the one-cell *C. elegans* embryo. Our data from quantitative live imaging assays for cortical F-actin and myosin flows, contractile ring assembly and furrow ingression, myosin turnover dynamics, and F-actin bundle alignment at the cell equator, collectively support the idea that contractile ring assembly and furrow ingression requires the concerted action of motor-competent myosin and plastin at the cell equator and is largely independent of compressive cortical flows.

Results

Long-Range Cortical F-actin Flows Are Dispensable for Contractile Ring Formation and Furrow Ingression

To investigate the importance of compressive cortical flows for assembly and constriction of the contractile ring (Figures 4.1A,B), we analyzed F-actin cortical flow profiles in one-cell embryos co-expressing endogenous motor-dead NMY-2(S251A) or NMY-2(R252A) and a transgenic wild-type version of NMY-2 that is mCherry-tagged and RNAi-sensitive (NMY-2::mCherry^{sen}; Figure 4.1C) (Osorio et al., 2019). NMY-2(S251A) and NMY-2(R252A) are unable to translocate F-actin but retain the ability to bind F-actin *in vitro* (Osorio et al., 2019), and embryos expressing endogenous motor-dead myosins fail cytokinesis after penetrant RNAi-mediated depletion of NMY-2::mCherry^{sen} (Osorio et al., 2019). Mild RNAi-mediated depletion of NMY-2::mCherry^{sen} slows but does not prevent cytokinesis.

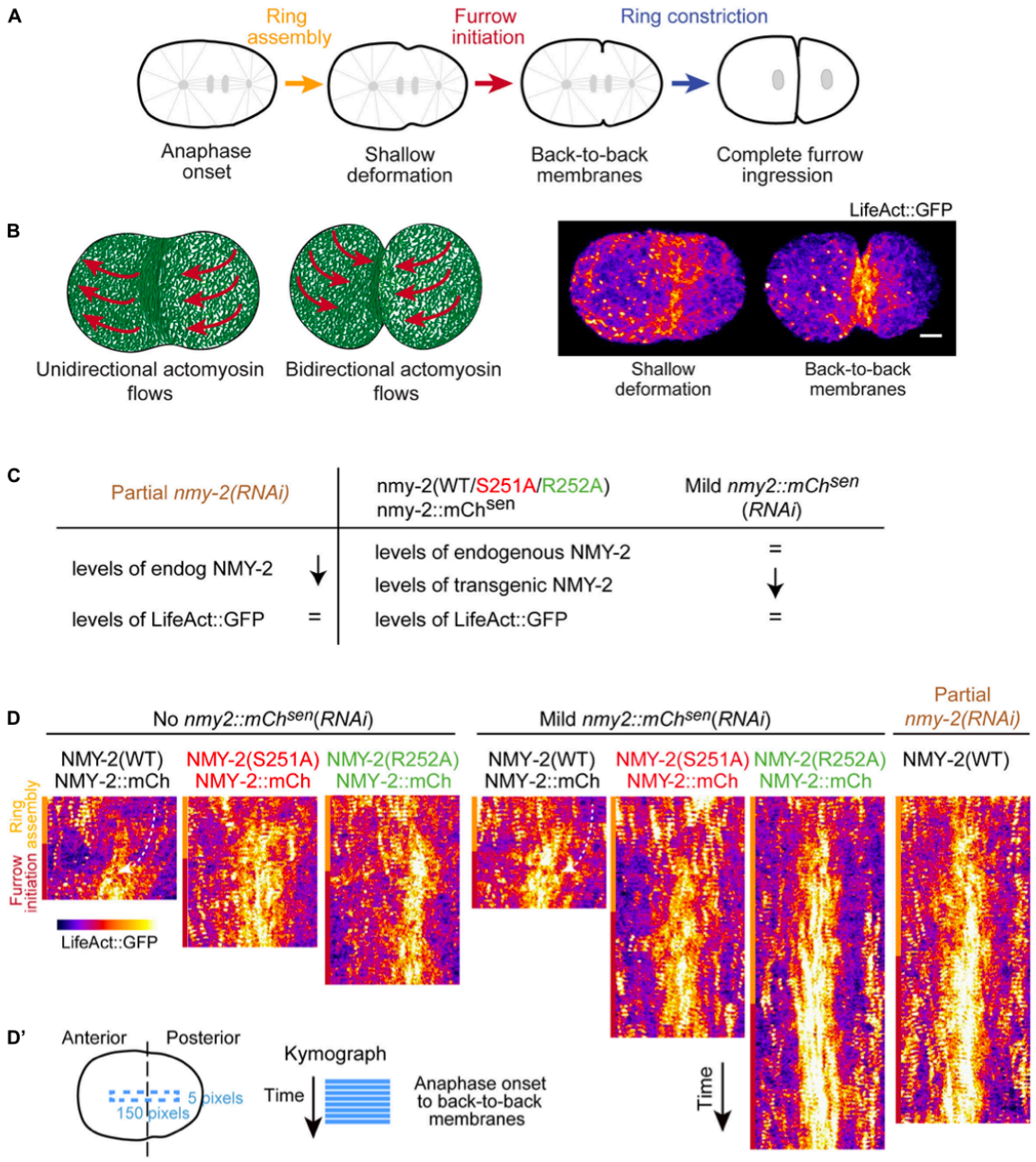

FIGURE 4.1. Perturbation of myosin motor activity or reduction of myosin levels lead to significantly reduced cortical F-actin flows. **(A)** Schematic of cytokinesis. Reference points used for measurements of ring assembly and furrow initiation intervals are indicated. Ring assembly: time interval between anaphase onset and the formation of a shallow equatorial deformation, when contractile ring components are being recruited to the cell equator. Furrow initiation: time interval between shallow deformation and the folding of the plasma membrane into a back-to-back configuration. Ring constriction: time interval between back-to-back membrane configuration and full furrow ingression. **(B)** Stills of cortical images of an embryo expressing LifeAct::GFP at shallow deformation and furrow initiation with a schematic illustrating the transition from unidirectional cortical flows during ring assembly to bidirectional flows starting at the onset of ring constriction. **(C)** Perturbations used and their effect on the levels of endogenous and transgenic NMY-2 and LifeAct::GFP relative to controls with no RNAi, as described in Osorio et al. (2019). **(D)** Kymographs of LifeAct::GFP cortical flows along the longitudinal axis in one-cell embryos for the conditions indicated in **(C)**. Yellow and red bars correspond to ring assembly and furrow initiation time intervals,

respectively. Curved arrows indicate posterior-anterior flow direction. **(D')** Schematic illustrating the region of the embryo used for the kymographs in **(D)**. Scale bar, 5 µm.

F-actin flow analysis was performed using transgenic LifeAct::GFP, whose cortical levels are unaffected by myosin inhibition (Osorio et al., 2019). We chose LifeAct::GFP (Silva et al., 2016; Chan et al., 2019; Osorio et al., 2019) rather than LifeAct::mKate2 (Reymann et al., 2016), because in our hands one-cell embryos expressing LifeAct::mKate2 exhibited delayed furrow initiation and had a significantly reduced contractile ring constriction rate when compared to embryos expressing other fluorescent contractile ring components (Supplementary Figure S1A). In contrast, cytokinesis kinetics were normal in embryos expressing LifeAct::GFP. Moreover, the cortical distribution of LifeAct::GFP, but not that of LifeAct::mKate2, was similar to the cortical distribution of endogenous PLST-1::GFP (Supplementary Figure S4.1B), which binds all F-actin pools during cytokinesis (Ding et al., 2017).

Kymographs of the cortical region between the onset of anaphase and the establishment of a back-to-back plasma membrane configuration revealed F-actin flows directed from the posterior towards the anterior pole in control embryos (Figures 4.1A–D). Even without depletion of transgenic NMY-2::mCherry, flows were barely detectable in *nmy-2(S251A)* and *nmy-2(R252A)* embryos, nor were they evident in embryos partially depleted of endogenous wild-type myosin (Figures 4.1C,D). To quantitatively analyze cortical flows, we performed particle image velocimetry (PIV) analysis (Figure 4.2A). Flow velocity was calculated by averaging the X- or Y-components (anterior-posterior and dorsal-ventral, respectively) of the velocity vectors in two regions positioned over the anterior and posterior half of the embryo, for each time point between anaphase onset and back-to-back membrane configuration (Figures 4.2B,C). Like reported in Singh et al. (2019), the Y-component was essentially absent when embryos were imaged without compression in an open chamber (Supplementary Figures S4.2A,B; Singh et al., 2019), yet these embryos completed cytokinesis with kinetics that were indistinguishable from those in embryos imaged under compression (Supplementary Figure S4.2C). We therefore focused our attention on the X-component. Negative velocity values indicate posterior-anterior oriented flows and positive velocity values indicate anterior-posterior oriented flows (Figure 4.2A). In agreement with a prior study (Reymann et al., 2016), control embryos presented anterior-directed F-actin cortical flows that started just prior to equatorial shallow deformation, peaked shortly thereafter, and remained high for approximately 50 seconds (Figure 4.2B). In contrast to controls, most vectors detected in *nmy-2(S251A)* and *nmy-2(R252A)*embryos were extremely weak, had no coherent directionality, and did not increase in magnitude after equatorial

shallow deformation (Figures 4.2B,F). This flow profile was observed regardless of whether transgenic NMY-2::mCherry^{sen} was mildly depleted by RNAi or not (Figures 4.2C,G). We further analyzed the flow velocity profiles by averaging the X-component of the vectors for each position along the length of the embryo during the first 50 seconds after equatorial shallow deformation, when flows in control embryos showed coherent direction and velocity (region highlighted in gray in Figure 4.2B). In control embryos, flow velocity was higher in the posterior half of the embryo, reaching a maximum velocity of −4.5 μm/min and decreasing toward the anterior pole (Figure 4.2D). In *nmy-2(S251A)* and *nmy-2(R252A)*embryos the flow profile was flat with or without depletion of transgenic NMY-2::mCherry^{sen}, reaching a maximum velocity of −1 μm/min (Figures 4.2D,E). We conclude that endogenous motor-dead myosin has a dominant inhibitory effect on cortical flows in embryos expressing transgenic NMY-2::mCherry^{sen}. Similarly weak flow profiles were observed in embryos after partial depletion of endogenous wild-type NMY-2 (Figure 4.2E and Supplementary Figures S4.3C, S4.6C).

Analysis of cytokinesis kinetics showed that in the presence of transgenic NMY-2::mCherry^{sen}, *nmy-2(S251A)* and *nmy-2(R252A)* embryos exhibited only minor delays in contractile ring assembly and furrow initiation despite severely impaired cortical flows (Figure 4.2F). In contrast, mild depletion of transgenic NMY-2::mCherry^{sen} in these embryos resulted in substantial delays in cytokinesis and occasional cytokinesis failure, while cortical flows were similar to those observed in the absence of RNAi treatment (Figure 2G). We conclude that there is no obvious correlation between perturbed cortical flows and delayed cytokinesis. This argues against the idea that persistent, unidirectional actin cortical flows are a major determinant of cytokinesis.

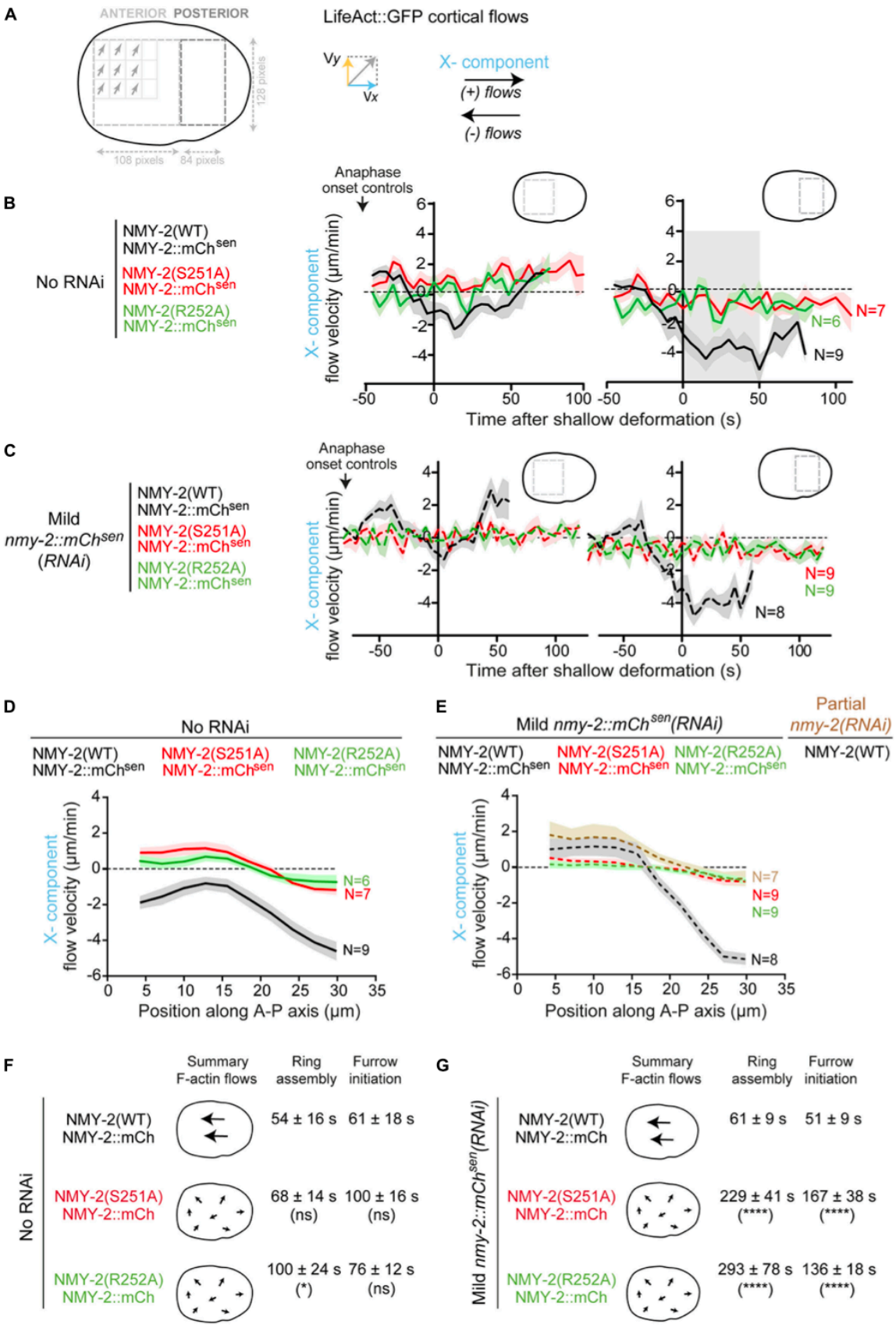

FIGURE 4.2. Contractile rings assemble and cytokinesis completes in a timely manner when long-range cortical actin flows are drastically reduced. **(A)** Schematic illustrating how cortical LifeAct::GFP flows were analyzed by

particle image velocimetry (PIV; see more details in "Materials and Methods" section). **(B,C)** Longitudinal (X-component) flow velocity (mean ± SEM) over time in the anterior or posterior half of embryos. Curves were aligned to the time of shallow deformation. N is the number of embryos analyzed. Period of consistently strong, posterior-anterior directed flows is indicated in gray. **(D,E)** Longitudinal (X-component) velocity profiles of Lifeact::GFP cortical flows along anterior-posterior (A-P) axis averaged for a period of 50 seconds starting at shallow deformation. Flow profiles show mean X-component velocity ± SEM. N is the number of embryos analyzed. **(F,G)** The schematic on the left summarizes overall flow intensity and directionality (X-component). Ring assembly and furrow initiation time intervals (mean ± SD) are indicated. Statistical significance in (D), (E) was determined using two-way ANOVA for repeated measures, and in (F), (G) using one-way ANOVA followed by Bonferroni's multiple comparison test; $*P < 0.05$, $****P < 0.0001$, ns, not significant.

Cortical Flows Are Dispensable for Accumulation of Myosin in the Ingressing Furrow

To further probe the significance of cortical flows, we sought to evaluate the possibility that flowing myosin generates tension that pushes F-actin to the equator. We first compared cortical flows of LifeAct::GFP and NMY-2::GFP using PIV analysis, which showed that F-actin and myosin flow toward the equator in a concerted manner (Supplementary Figures S4.3A,B): unidirectional cortical flows from the posterior pole toward the anterior side of the embryo initiate shortly after anaphase, and flow velocities increase linearly until a maximum velocity is reached and maintained for ~50 seconds. This is followed by a period of bidirectional flows starting at constriction onset, in which actin and myosin flow from both poles towards the ingressing furrow (positive flow velocity in the anterior and negative flow velocity in the posterior side of the embryo).

Next, we determined myosin turnover at the cell cortex outside the equator. We reasoned that if flowing myosin actively slides F-actin, myosin turnover should be relatively slow, since myosin is known to be stabilized at sites of increased tension such as the contractile ring (Reichl et al., 2008; Srivastava and Robinson, 2015). We photobleached NMY-2::GFP at the posterior polar region at shallow deformation and followed signal recovery during the period of contractile ring formation and compaction. By the time of shallow deformation, some myosin has already been cleared from the posterior pole (Supplementary Figures S4.4A,B), and therefore confounding effects of flows on the measurement of signal recovery after photobleaching should be reduced. Fluorescence recovery data could be fitted with a single exponential from which we extrapolated a half time of recovery (τ_{half}) of 4.9 ± 2.4 seconds (Figures 4.3A,A'). As a control, we photobleached a region of identical size in the posterior cytoplasm, for which signal recovery was significantly faster (τ_{half} of 2.6 ± 1.8 seconds; $P < 0.05$; Supplementary Figures S4.5C,D). Assuming a diffusion-dominated recovery profile for cortical myosin, we calculated a dissociation constant (k_{off}) of 0.07 ± 0.03 s^{-1} (equation 1 in

"Materials and Methods" section). Fast myosin turnover in the polar cortex indicates that flowing myosin is in constant exchange with the cytoplasmic pool before reaching the cell equator.

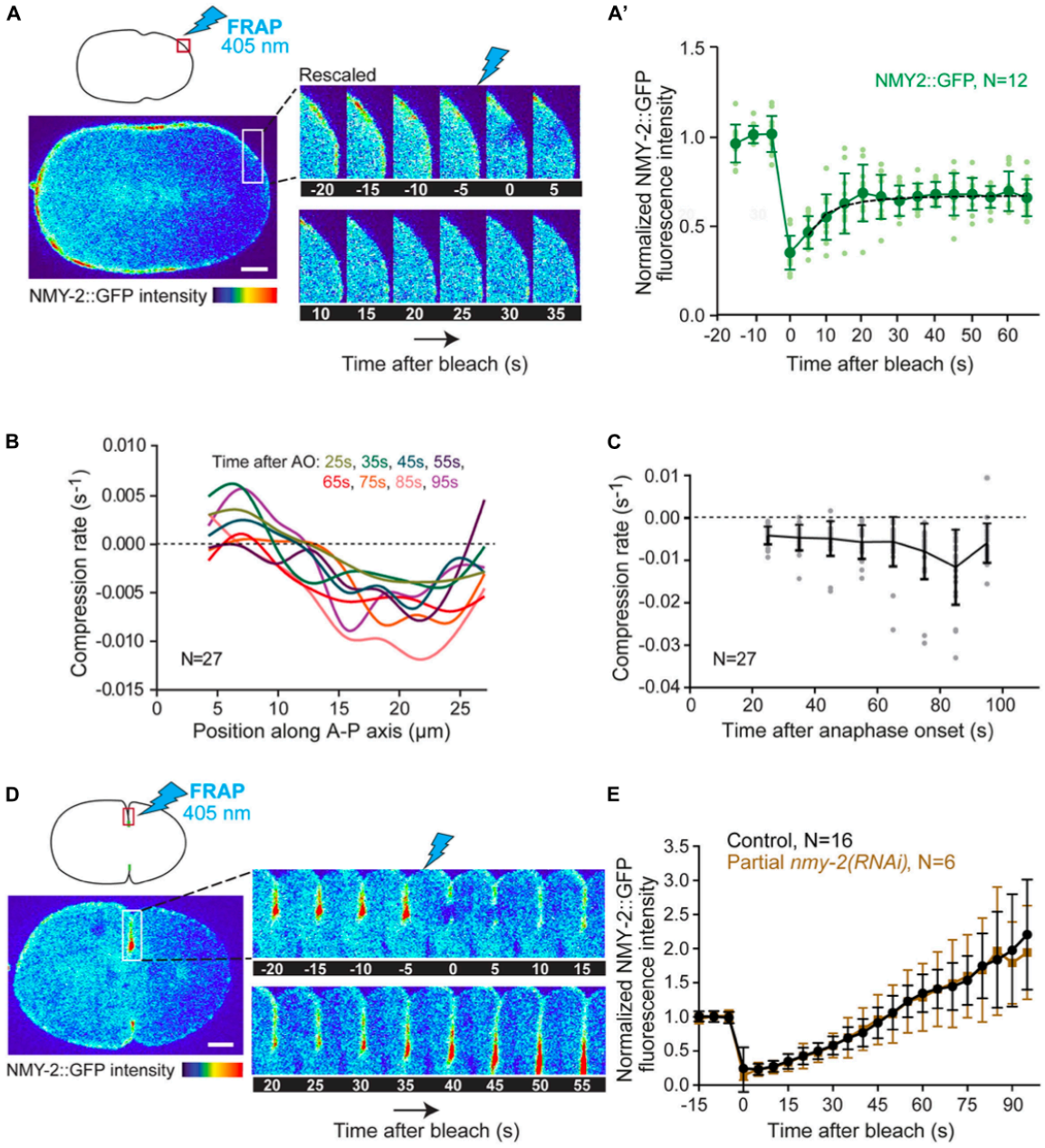

FIGURE 4.3. Cortical myosin turnover and flow-induced compression rates. **(A)** Schematic showing the photobleached region at the posterior pole of the embryo at shallow deformation (top left) and selected images from a time-lapse series showing NMY-2::GFP fluorescence over time pre- and post-bleaching. **(A')** Quantification of NMY-2::GFP fluorescence recovery after photobleaching at the posterior pole. Data from individual embryos (light green) and the mean ± SD (dark green) are plotted. The black dashed line is the single exponential fitting curve from which the half time of recovery and myosin k_{off} were extrapolated. **(B)** Average compression rate by flow calculated as the spatial derivative of the longitudinal flow profiles for each position along the anterior-posterior (A-P) axis of the embryo from 25 to 95 seconds after anaphase onset (AO). Compression is uniform in the equatorial

region (15–25 μm). Colors represent different time intervals as indicated. **(C)**Average compression rate by flow over time after anaphase onset for the region of equatorial compression (15–25 μm). Data from individual embryos (gray) and the mean ± SD (black) are plotted. **(D)** Schematic showing the photobleached region just behind the tip of the ingressing furrow after back-to-back membrane configuration is achieved (top left) and selected images from a time-lapse series showing the NMY-2::GFP fluorescence over time pre- and post-bleaching. **(E)** Quantification of NMY-2::GFP fluorescence recovery after photobleaching in the ingressing furrow in control and NMY-2 depleted embryos. The mean ± SD is plotted. N is the number of embryos analyzed. Scale bars, 5 μm.

We next determined the rate at which cortical flow compresses F-actin towards the equatorial region. We measured the flow X-component as a function of the position along the anterior-posterior axis for 10 seconds intervals, from 25 seconds until 95 seconds after anaphase onset, and estimated the compression rate by flow for each time interval by calculating the spatial derivative of the flow velocity for each position (Figure 4.3B). Compression was found to be uniform in the equatorial region (15–25 μm). The average compression rate for the equatorial region increased over time, reaching a maximum of 0.012 ± 0.009 s^{-1} 85 seconds after anaphase onset (Figure 4.3C). As the maximum compression rate is slower than the rate of myosin dissociation from the cortex, these data argue against the idea that flowing myosin is responsible for F-actin bundle compression at the cell equator.

To confirm this, we assessed myosin turnover in the ingressing furrow. We photobleached a small region just behind the tip of the ingressing furrow and followed NMY-2::GFP signal recovery in the moving region as the furrow continued to ingress. NMY-2::GFP fluorescence intensity in the bleached region increased until the end of ingression without reaching a plateau (Figure 4.3E). Similar results were obtained when the entire division plane was photobleached at shallow deformation (Supplementary Figures S4.5A,B). These demonstrate that myosin continues to accumulate in the contractile ring during furrow ingression. Myosin could accumulate by incoming flow, by localized recruitment from the cytoplasm, or both. To distinguish between these possibilities, we examined embryos partially depleted of NMY-2, in which the initial unidirectional flows are essentially absent, bidirectional flows are significantly decreased, and cytokinesis still completes (Supplementary Figure S4.3C). Under these conditions, NMY-2::GFP was still visible at the tip of the furrow, which allowed us to perform the photobleaching experiment. Normalized recovery profiles of NMY-2-depleted embryos were identical to those of non-depleted embryos (Figure 4.3E). These results support the idea that the contribution of cortical flows to myosin accumulation at the cell equator is minor and that equatorial myosin is therefore primarily recruited from the cytoplasm. Further support for this idea comes from the observation that the amount of myosin that accumulates at the cell equator after anaphase onset is much higher than the amount of myosin that leaves the polar regions (Supplementary Figure S4.4B).

The F-actin Crosslinker Plastin Cooperates With Myosin to Align F-actin Bundles at the Division Plane

We previously found that *nmy-2(S251A)* and *nmy-2(R252A)* embryos depleted of transgenic NMY-2::mCherry^{sen} accumulated equatorial F-actin bundles with a tilted orientation (Osorio et al., 2019). Based on this observation, we speculated that F-actin crosslinkers could also contribute to the organization of F-actin bundles at the cell equator. The plastin ortholog PLST-1 was a promising candidate, as it localizes in the contractile ring and the surrounding cortex and has been implicated in cytokinesis (Ding et al., 2017).

To determine whether NMY-2 and PLST-1 cooperate to compact and align F-actin bundles at the cell equator, we used genome editing to generate a *plst-1* mutant, *plst-1(prt89)*, which contains a premature stop codon in its open reading frame and is homozygous viable, like another previously described *plst-1*mutant (Ding et al., 2017). Using LifeAct::GFP, we quantified F-actin bundle alignment at the equatorial region over time, starting at anaphase onset (Figures 4.4A,B and Supplementary Movie S1). Analysis of F-actin bundle orientation in control embryos revealed fast bundle alignment perpendicular to the longitudinal axis of the embryo with bundles reaching maximum alignment shortly after shallow deformation (deviation from vertical alignment close to 0°). In embryos partially depleted of NMY-2, F-actin bundle alignment was significantly slower and continued throughout furrow initiation. In *plst-1(prt89)* embryos, F-actin bundle alignment was also slower than in control embryos, with F-actin bundles becoming mostly aligned at shallow deformation and reaching maximum alignment just before furrow initiation. In *nmy-2(RNAi)*;*plst-1(prt89)* embryos, F-actin bundles became completely unstable and failed to align, exhibiting oscillating orientations between 20° and 50° relative to vertical alignment.

In *nmy-2(RNAi)* embryos, median contractile ring assembly was delayed threefold (155 seconds *versus* 53 seconds in controls), but 92% of embryos were able to complete cytokinesis (Figures 4.4C,E). In *plst-1(prt89)*embryos, contractile ring assembly was delayed twofold (110 seconds), and cytokinesis was successful in all embryos. Strikingly, contractile ring assembly was delayed sixfold (298 seconds) in *nmy-2(RNAi)*; *plst-1(prt89)* embryos, and 89% of embryos failed to initiate furrowing (Figures 4.4C,E).

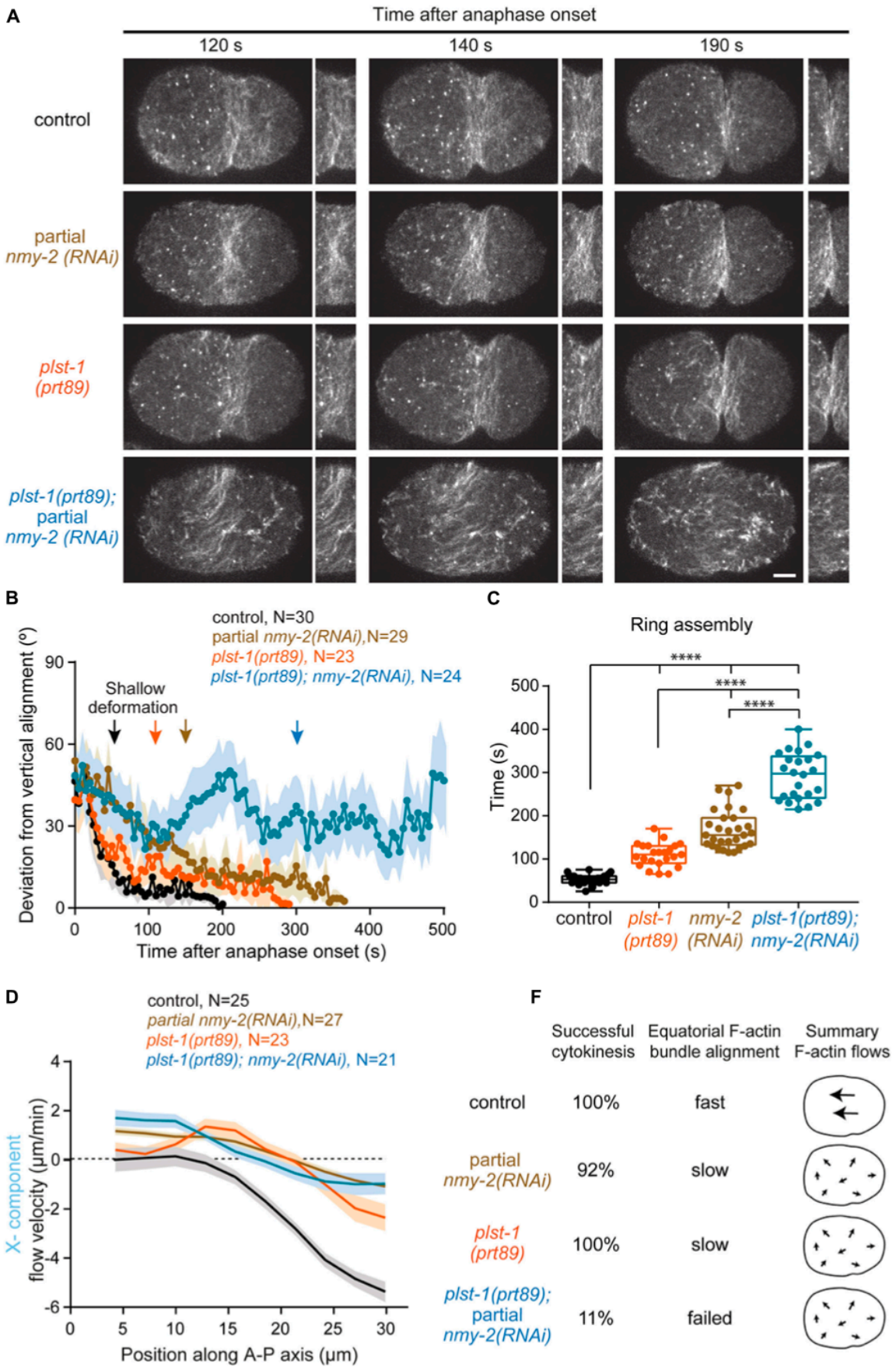

FIGURE 4.4. The F-actin crosslinker plastin cooperates with myosin to align F-actin bundles at the division plane. **(A)**Images of the cortical plane of embryos expressing LifeAct::GFP showing the evolution of the equatorial

F-actin band relative to anaphase onset. Also see Supplementary Movie S1. **(B)** Deviation from vertical alignment of F-actin bundles at the equatorial cortex relative to anaphase onset (mean ± SEM). **(C)** Boxplots showing the dispersion of contractile ring assembly times. In each box, the central line is the median, the boundaries of the box are the 25th and 75th percentiles; the whiskers extend to include the maximum and minimum values. **(D)** Longitudinal (X-component) velocity profiles of Lifeact::GFP cortical flows along anterior-posterior (A-P) axis averaged for a period of 50 seconds starting at shallow deformation. Flow profiles show mean X-component velocity ± SEM. **(E)** Values on the left indicate percentage of embryos that completed cytokinesis successfully. On the right, a summary of F-actin bundle alignment at the equator and overall flow intensity and directionality (X-component). N is the number of embryos analyzed. Statistical significance of ring assembly times in (C) was determined using one-way ANOVA followed by Bonferroni's multiple comparison test. $^{****}P < 0.0001$. Scale bar, 5 µm.

We asked whether deficient alignment of F-actin bundles at the cell equator and cytokinesis failure in *nmy-2(RNAi);plst-1(prt89)* embryos could be due to aggravated cortical flows (Figures 4.4D,E and Supplementary Figure S4.6). Using PIV analysis of LifeAct::GFP, we determined flow velocities from anaphase onset until the back-to-back membrane configuration (Supplementary Figure S4.6C). In *plst-1(prt89)* embryos, cortical flows were decreased and erratic compared to controls. There were no periods of unidirectional or bidirectional flows, as the cortex was constantly moving back and forth in opposite directions (Supplementary Figures S4.6A,C). In *nmy-2(RNAi)*; *plst-1(prt89)* embryos, there was no further aggravation of flow profiles compared to the single perturbations. Analysis of flow velocity along the anterior-posterior axis for the period of persistent unidirectional flow, as defined in control embryos (50 seconds starting at shallow deformation), revealed that *plst-1(prt89)* embryos showed an intermediate profile between that of control and *nmy-2(RNAi)* embryos, with a maximum flow velocity at the posterior pole of −2.5 µm/min (Figure 4.4D). In *nmy-2(RNAi)*; *plst-1(prt89)* embryos, flow velocities were similar to those observed in *nmy-2(RNAi)*embryos. We further investigated the correlation between vectors as a function of the distance between them for the period of persistent unidirectional flows (Supplementary Figure S4.6B; equation 2 in "Materials and Methods" section). The closer the cosine similarity is to 1, the higher the correlation between vectors and the more coherent the flow directionality. In control embryos, the cosine similarity was close to 1 for neighboring vectors and decayed gradually as the distance between vectors increased, approaching a minimum of 0.7 for vectors located on opposite poles. In *nmy-2(RNAi)* embryos, the cosine similarity decayed significantly faster, reaching a minimum of approximately 0.2 for the maximum distance between vectors. The correlation was even worse for *plst-1(prt89)* embryos, with minimum values approaching 0, meaning that vectors were pointing in opposite directions. In *nmy-2(RNAi)*; *plst-1(prt89)* embryos, cosine similarity was identical to that in *plst-1(prt89)* embryos, revealing similar problems in flow directionality. We conclude that cytokinesis failure in *nmy-2*(*RNAi);plst-1(prt89)* embryos is unlikely to be caused by an aggravation of cortical flows.

We also inspected the behavior of NMY-2::mCherry signal in the single and double perturbations (Supplementary Movie S1). Interestingly, we observed that residual myosin in *nmy-2(RNAi);plst-1(prt89)* embryos accumulates at the equator more slowly than in *nmy-2(RNAi)* embryos. These results suggest that PLST-1, in addition to its role in promoting connectivity throughout the cell cortex, has a localized role at the cell equator independently of cortical flows. We conclude that localized synergistic action of NMY-2 and PLST-1 at the division plane is critical for F-actin alignment and compaction into a circumferential array that is capable of sustaining furrow ingression.

Discussion

Unidirectional Long-Range Cortical Flows Play a Minor Role During Cytokinesis

Several models have been proposed to explain how the cell shape changes that occur during cytokinesis are triggered. The first theories date back to the 1950s and considered cleavage as an integrated process involving reorganization of the entire cell surface. While Mitchison (1952); Mitchison and Swann (1955), and Swann and Mitchison (1958) proposed that cytokinetic furrow formation was a passive event resulting from an active expansion at the poles that would spread toward the equator, Marsland proposed that the furrow region was itself contractile, independently of the poles (Marsland, 1950, 1956a,b). Wolpert's astral relaxation theory specifically proposed that a negative signal from the astral microtubules would make the poles relax, allowing the equator to contract (Wolpert, 1960). While the molecular mechanisms for polar relaxation have only recently started to be unraveled (Mangal et al., 2018; Chapa-y-lazo et al., 2020), it has become widely accepted that cytokinesis requires a positive signal from the central spindle that activates the small GTPase RhoA, which in turn promotes the accumulation of contractile ring components, F-actin and myosin, at the cell equator. F-actin alignment and accumulation via flow-driven equatorial compression and RhoA-dependent local recruitment are the two main mechanisms thought to drive the assembly of a circumferentially aligned contractile ring.

A recent study showed that F-actin cortical flows are myosin-dependent and that compression by flow, equatorial F-actin alignment, and furrow ingression show similar spatiotemporal dynamics in the one-cell *C. elegans* embryo (Reymann et al., 2016). The authors proposed that persistent, unidirectional compressive flows towards the cell equator dictate the timing of equatorial F-actin alignment and furrow formation. We find that embryos co-expressing similar amounts of endogenous motor-dead and transgenic wild-type myosin have severely decreased F-actin cortical flows, yet contractile ring assembly and furrow initiation still occur in a timely manner, and cytokinesis completes. Lowering the levels of transgenic wild-type

myosin in these embryos results in substantial cytokinesis delays with no additional effects on cortical flows. While these results show that both long-range cortical flows and cytokinesis require myosin motor activity, they suggest that cortical flows are neither essential for cytokinesis nor a major determinant of cytokinesis kinetics.

Apart from the cytokinetic furrow, *C. elegans* one-cell embryos also form a transient furrow, which partially ingresses and then regresses, during the period of polarity establishment that precedes the first mitotic division. Unlike cytokinesis, pseudocleavage lacks equatorial accumulation of active RhoA, F-actin and myosin (Mayer et al., 2010; Reymann et al., 2016). Moreover, counter-rotating flows in the two halves of the embryo occur during pseudocleavage initiation that do not occur during cytokinetic furrow initiation (Naganathan et al., 2014). While our results argue that cortical flows play a relatively minor role in furrow formation during cytokinesis, it remains possible that cortical flows are essential for furrow formation during pseudocleavage, as proposed by Reymann et al. (2016).

Myosin Accumulation at the Cell Equator Occurs Primarily by Recruitment From the Cytoplasm

There is evidence that myosin and other crosslinkers become stabilized and immobilized in regions of increased tension, such as the contractile ring (Reichl et al., 2008; Srivastava and Robinson, 2015). Our experiments of fluorescence recovery after photobleaching and measurements of flow-driven equatorial F-actin compression suggest that the rate of myosin turnover at the cortex outside the cell equator is significantly faster than the rate at which cortical flow compresses the actomyosin network toward the equator. The results agree with findings in *D. discoideum* cells, where cortical myosin did not move all the way to the equator, but rather appeared and disappeared shortly after from the cortex (Yumura et al., 2008). This indicates that flowing myosin may not be able to generate substantial amounts of compressing force. Thus, tension generated by equatorial myosin activity is likely more relevant for the alignment and compaction of F-actin bundles, which is in agreement with sustained RhoA positive signaling at this location. It also indicates that compression and alignment of the equatorial F-actin bundles may occur independently of flows. We show that unidirectional and bidirectional cortical flows can be severely reduced without affecting the recovery profile of photobleached myosin in the ingressing furrow. This suggests that cortical flows may not be the main source of myosin loading onto the contractile ring, in contrast to a previous model (Khaliullin et al., 2018). We propose that myosin accumulates at the furrow primarily by direct recruitment from the cytoplasm to the cell equator and largely independently of cortical flows.

Plastin-Mediated Bundling and Myosin Motor Activity Are Locally Required for F-actin Alignment at the Division Plane and Deformation of the Equator

The contractile ring must produce sufficient force to deform the plasma membrane against the overall cell shape. Actomyosin contractility must therefore be optimized at the cell equator, which involves the organization of F-actin in circumferentially aligned and compacted linear bundles. An F-actin network architecture composed of modules of antiparallel F-actin bundles is optimal for contraction, as filaments are already aligned and oriented such that myosin-dependent filament sliding is facilitated and tension can be readily propagated across the network (Ennomani et al., 2016). It is still unclear, however, whether F-actin bundles in the contractile ring are organized in an antiparallel manner (reviewed in Pinto et al., 2013; Murrell et al., 2015) and whether contractile modules exist (Carvalho et al., 2009; Silva et al., 2016). In fact, *in vitro* reconstituted circular actomyosin networks have been shown to contract in the absence of a modular organization, as long as F-actin crosslinkers are present (Ennomani et al., 2016; Wollrab et al., 2019). Our *in vivo* data show that myosin struggles to align and compact equatorial F-actin at the cell equator without the crosslinking activity of plastin in *plst-1(prt89)* embryos. We envision that plastin facilitates myosin-driven alignment by organizing formin-nucleated linear F-actin into tight bundles, so that tension can be efficiently amplified and propagated throughout the network to rapidly compact it into a circumferential array (Figure 5). Without plastin, myosin may initially spend energy on sorting randomly oriented F-actin instead of productive filament sliding. When myosin levels are reduced in the presence of plastin (partial depletion of NMY-2), F-actin bundles also struggle to align and compact, likely because of insufficient motor activity to produce tension in the network. When both F-actin bundling and myosin levels are reduced in *nmy-2(RNAi);plst-1(prt89)* embryos, equatorial F-actin bundles become unstable and never orient along the division plane. Consequently, contractile ring assembly fails altogether. The enhanced defects in the plastin/myosin double perturbation cannot be ascribed to aggravated cortical flows, since these are already severely affected in the single perturbations, in which a contractile ring assembles and cytokinesis completes. This strongly suggests that myosin and plastin cooperate locally at the cell equator.

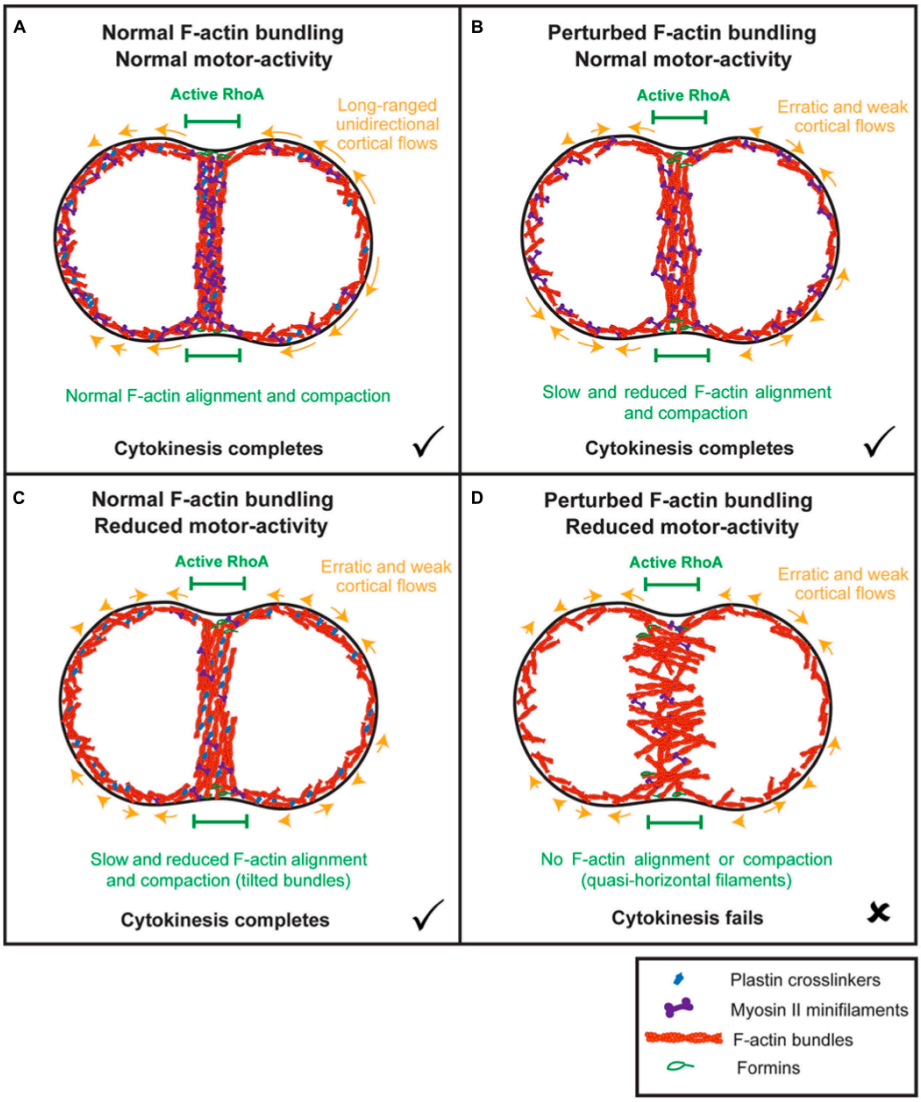

FIGURE 4.5. Model: the combined synergistic action of plastin and myosin aligns and compacts F-actin at the division plane independently of actomyosin cortical flows. **(A)** When both plastin and myosin accumulate at the equator, F-actin bundles are properly connected, and myosin is able to efficiently align and compact them into a circumferential array to maximize tension. Early actomyosin flows are unidirectional and long-ranged. **(B)** In the absence of plastin-mediated bundling, myosin struggles to align and compact F-actin bundles, initially spending energy on filament sorting instead of filament sliding. Cortical flows are reduced and erratic and cytokinesis completes with delays in F-actin alignment and contractile ring formation. **(C)** In the presence of plastin-mediated F-actin bundling and decreased myosin levels, F-actin bundles are connected to each other but tilt and struggle to orient along the division plane and to compact because of insufficient motor-activity. Cortical flows are severely reduced and erratic and cytokinesis completes with delays in F-actin alignment and contractile ring formation. **(D)** When both plastin-mediated bundling and myosin levels are decreased, equatorial actin filaments become unstable and start rotating and oscillating, adopting a quasi-horizontal orientation. Cortical flows are reduced and erratic, as in the individual plastin and myosin perturbations. F-actin bundles never align to form the contractile ring and cytokinesis fails.

Interestingly, the observation that residual myosin in *nmy-2(RNAi)*; *plst-1(prt89)* embryos accumulates at the equator more slowly than in *nmy-2(RNAi)* embryos suggests that plastin-dependent F-actin bundling may stabilize myosin at the equatorial cortex. This is not the first time cooperation between a passive and an active crosslinker has been observed. In *C. elegans*, a previous study demonstrated that plastin provides the connectivity for coalescence and maturation of myosin foci from distant nascent filaments in the cortex, amplifying the range of contractile domains during polarity establishment (Ding et al., 2017). In *D. discoideum*, myosin and the crosslinker cortexillin have been proposed to stabilize each other at sites of increased mechanical load: cortexilin I, as a long-lived crosslinker, anchors F-actin in the network so that myosin can exert more tension, and this promotes accumulation of yet more myosin and cortexillin (Ren et al., 2009). Whether a similar mechanosensing mechanism between myosin and plastin operates during cytokinesis in *C. elegans* embryos is an interesting hypothesis to test in the future.

Conclusion

In conclusion, while cortical flows may help compress and align F-actin at the equator, our results argue that this is not the main mechanism that drives contractile ring assembly. Instead, we propose that contractile ring assembly requires the localized and concerted action of myosin and the F-actin bundler plastin.

Materials and Methods

C. elegans Strains

Strains used in this study are listed in Supplementary Table S4.1 and were maintained at 20°C on nematode growth medium (NGM) plates seeded with OP50 *E. coli*.

NMY-2 motor-dead mutants and the RNAi-sensitive wild-type nmy-2 transgene fused to mCherry are described in a previous study (Osorio et al., 2019). To generate the allele *plst-1(prt89)*, the endogenous locus of *plst-1* was modified using CRISPR/Cas9-mediated genome editing. An extra nucleotide and a *Nhe*I restriction site were introduced to cause a frameshift and premature stop at the beginning of the *plst-1* coding sequence. Note that the *plst-1* sequence in WormBase (version WS276) lacks the first part of the gene corresponding to the EF hands and CH1 domain of the PLST-1 protein (Ding et al., 2017). The premature stop codon that we introduced occurs after amino acid 262 in the CH2 domain of PLST-1 (Ding et al., 2017). The repair template for this modification was the following:

5′*ctctgaaaatccacaaatttccagactgctccgcgacggtgaaactcttgaagatctc*aggcgtctgtccccagaagaaattct catgAaga**gctagc**tgggttaattatcatttagaacg tgcta*gaactcaacgtcgcctacacaatttcacatcagatattgtcgattcagagatttatac*-3′, where the extra nucleotide is in uppercase, the *Nhe*I restriction site for diagnostic PCR of the genomic edit is in bold, silent mutations introduced to avoid repair template recognition by Cas9 are underlined, and flanking 58 bp homology regions are in italics. Three single guide RNAs (sgRNAs) were chosen using the online tool http://crispr.mit.edu and cloned into the pDD162 vector (Dickinson et al., 2013): 5′-TTCTTCTGGGGACAGACGCCGG-3′, 5′-ATTATCATTTGGAACGTGCTGG-3′ and 5′-AGATGGGTTAATTATCATTTGG-3′. Underlined in the sgRNAs are the PAM sequences, which were not included in the pDD162 vector. The single-stranded repair template (IDT) and pDD162 were mixed together and injected into gonads of young adults N2 hermaphrodites. To facilitate the identification of positive animals, the injection mix also contained a sgRNA and a repair template to generate the R92C mutation in DPY-10, which causes a dominant roller phenotype (Levy et al., 1993; Arribere et al., 2014). To screen for animals carrying the desired modification in the *plst-1* locus, amplification of a plst-1 gene fragment was performed using the primers 5′ CATGGCCTAGAAACCACTTT 3′ and 5′ GCTTCTCGGCTTCATCTAAC 3′, followed by digestion with the *Nhe*I restriction enzyme that recognizes the restriction site present in modified animals only. The modification was confirmed by DNA sequencing. To remove potential off-target mutations, the mutant was subjected to six rounds of outcrossing with N2 animals, before crossing with animals expressing LifeAct::GFP or LifeAct::GFP and NMY-2::mCherry. Although expression of the PLST-1 protein was not assessed by immunoblotting, the defects in *plst-1(prt89)* embryos are similar to those observed for *plst-1(tm4255)*, which is a null mutant (Ding et al., 2017).

RNA Interference

RNAi-mediated NMY-2 depletion was performed by feeding hermaphrodites with bacteria that express double stranded RNA (dsRNA) targeting *nmy-2*. The dsRNAs nmy-2_RNA#1 and nmy-2_RNA#2 (Supplementary Table S4.2) are described in Osorio et al. (2019). Expression of dsRNAs in transformed HT115 *E. coli*was induced with 1 mM IPTG and the bacteria were fed to hermaphrodites as described below.

In experiments where specific depletion of transgenic NMY-2::mCherry^{sen} was desired [labeled as *nmy-2::mCherry^{sen}(RNAi)* in Figures 4.1D, 4.2C,E,G], nmy-2_RNA#3 was used in GCP22, GCP618 or GCP592 L4 hermaphrodites. Mild depletions (22–26 h of RNAi treatment at 20°C) were used in Figures 4.1D, 4.2C,E,F. In experiments whose purpose was to deplete endogenous NMY-2 to an extent that did not preclude cytokinesis [labeled as partial *nmy-2*(*RNAi*)], nmy-2_RNA#1 (29–31 h of RNAi treatment at 20°C) was used in GCP113 L4

hermaphrodites for Figures 4.3D,E and Supplementary Figure S4.3C, and nmy-2_RNA#2 (23–27 h of RNAi treatment at 20°C) was used in GCP21, GCP22, and GCP927 L4 hermaphrodites for Figures 4.1D, 4.2E, 4.4A–E, and Supplementary Figure S4.6.

Live Imaging

Gravid hermaphrodites were dissected and one-cell embryos were mounted in a drop of M9 (86 mM NaCl, 42 mM Na_2HPO_4, 22 mM KH_2PO_4, and 1 mM $MgSO_4$) on 2% agarose pads overlaid with a coverslip. Live imaging of cytokinesis was performed at 20°C. Images were acquired on a spinning disk confocal system (Andor Revolution XD Confocal System; Andor Technology) with a confocal scanner unit (CSU-X1; Yokogawa Electric Corporation) mounted on an inverted microscope (Ti-E, Nikon) equipped with a 60x NA 1.4 oil-immersion Plan-Apochromat objective, and solid-state lasers of 405 nm (60 mW), 488 nm (50 mW), and 561 nm (50 mW). For image acquisition, an electron multiplication back-thinned charge-coupled device camera (iXon; Andor Technology) was used. For photobleaching experiments, a FRAPPA photobleaching module (Andor Technology) placed between the spinning disk head and the microscope was used. Photobleaching was performed by 3 sweeps of a 405 nm laser with 100% power and 100 µs dwell time in the posterior cortex, ingressing furrow and division plane (Figure 4.3 and Supplementary Figures S4.5A,B) or 10 sweeps and 40 µs dwell time in the posterior cytoplasm (Supplementary Figure S4.5C). Acquisition parameters, shutters, focus and photobleaching parameters and regions to be photobleached were controlled using Andor iQ3 software. For central plane imaging in one-cell embryos (Figure 4.3 and Supplementary Figure S4.1A), 5 × 1 µm z-stacks were collected in the 488 nm channel every 5 seconds for strains GCP113, GCP21, RZB213 and OD26, and in the 561 nm channel every 5 seconds for strain SWG001. For photobleaching experiments in the posterior cytoplasm (Supplementary Figures S4.5C,D), 5 × 1 µm z stacks were collected in the 488 nm channel every 0.78 seconds. For cortical dual-color imaging in one-cell embryos, 7 × 0.5 µm z-stacks were collected every 5 seconds for strains GCP21, GCP22, GCP592, and GCP618 (Figures 4.1, 4.2 and Supplementary Figures S4.1, S4.2), strains GCP21 and GCP113 (Figure 4.3 and Supplementary Figures S4.3–S4.5), and strains GCP22 and GCP927 (Figure 4.4 and Supplementary Figure S4.6). For cortical imaging in one-cell embryos of strains RZB213 and SWG001 (Supplementary Figure S4.1B), 7 × 0.5 µm z-stacks were collected in the 488 nm or 561 nm channels every 5 seconds, respectively.

Fluorescence Intensity Measurements

Before quantification, each time-lapse movie was corrected for fluorescence intensity decay using the simple ratio method in ImageJ's bleach correction tool. Quantification of

fluorescence recovery after photobleaching in Figures 4.3A',E was performed using 3 different ROIs to quantify mean fluorescence intensity over time. ROI 1 is the bleached region (5 × 5 pixel for the posterior cortex and posterior cytoplasm; 5 × 15 pixel for the ingressing furrow and 15 × 200 pixel for the whole division plane). ROI 2 is the whole embryo and corrects for overall photobleaching of the sample resulting from acquisition and photobleaching sweeps (oval: 305 × 205 pixels). ROI 3 is the camera background, measured outside fluorescent regions (20 × 20 pixels). After background subtraction and photobleaching correction, the data was normalized using the double normalization method, and curve fitting was performed to extrapolate the half time of recovery. All operations were performed automatically using easyFRAP software (see below).

For quantification of NMY-2::GFP levels at the equator versus poles in Supplementary Figure S4.4B, images of the central plane of dividing one-cell embryos were used. A line was traced at the poles and at the equator and the mean intensity was determined after subtraction of the camera background.

Calculation of Myosin Dissociation Rate

Assuming a diffusion-dominated recovery profile, the myosin dissociation rate (k_{off}) in Figure 4.3A' was calculated from FRAP data using the following equation (Bernetti et al., 2019):

where $\tau_{1/2}$ is the half time recovery measured from FRAP fitting curves.

Cortical Flows Quantification

Cortical flow dynamics were analyzed in one-cell embryos of strains GCP21, GCP22, GCP113, GCP562, GCP618, and GCP927 between anaphase onset and back-to-back membrane configuration. In Figures 4.22B–E, 4.4D and Supplementary Figures S4.2B, S4.3B,C, S4.6C, magnitude and direction of cortical flows were quantified using an Iterative Particle Image Velocimetry (PIV) plugin for ImageJ, https://sites.google.com/site/qingzongtseng/piv (Tseng et al., 2011). A 192 × 128 pixel (34.1 × 22.8 µm) region of interest was applied to all embryos to standardize the cortex area and exclude cortical curved peripheries. To average the maximum particle displacement with better resolution, two iterations were performed, in which the application of a larger interrogation window of 64 × 64 pixels (first iteration) was followed by a smaller interrogation window of 32 × 32 pixels (second iteration). Consecutive interrogation windows overlapped by 50%. After flow field generation, the 192 × 128 pixel region was divided in two adjacent sub-regions along the anterior-posterior axis of the embryo for quantification: anterior cortex (1st-

108th pixel; 0.2–19.2 μm) and posterior cortex (109th-192nd pixel; 19.4–34.1 μm). Each velocity vector was resolved into components along the anterior-posterior axis, Vx, and the dorsal-ventral axis, Vy. The mean Vx and Vy were estimated for each time point and plotted as a function of time to trace the cortical flow profiles in Figures 2B,C and Supplementary Figures S4.2B, S4.3B,C, S4.6C.

To plot longitudinal flow profiles (Vx) along the anterior-posterior axis in Figures 4.2D,E, 4.4D, all vectors along the dorsal-ventral axis with the same x-coordinate (corresponding to the longitudinal position) were averaged and plotted as a function of the position along the anterior-posterior axis.

The cosine similarity analysis measures the correlation between every vector pair of the flow fields as a function of the distance between them for the period of persistent unidirectional flow. A cosine similarity of 1 means the vectors are totally correlated. Cosine similarities between two vectors shown in Supplementary Figure S6B was computed using a custom MATLAB script, according to the following formula:

Calculation of Cortical Compression Rates

Longitudinal cortical compression rates in Figures 4.3B,C were estimated from cortical flow profiles along the anterior-posterior axis by approximating the spatial derivative for each position using a custom MATLAB script. Cortical compression rates were plotted as a function of both position along the anterior-posterior axis and time relative to anaphase onset in 10 seconds intervals, starting at 25 seconds (when a noticeable region of compression could be identified) and stopping at 95 seconds (start of furrow ingression) after anaphase onset.

Analysis of Bundle Alignment at the Equatorial Cortex

Deviation from vertical alignment over time in Figure 4.4B was measured using the Directionality plugin for ImageJ. A region of 30 × 70 pixels corresponding to the furrow region was selected for each movie. The average directionality (angle α, in degrees), was calculated for every frame of each movie using the local gradient orientation method. Deviation from vertical alignment (in degrees) was calculated for each angle α by subtracting the value of this angle from 90°. Absolute numbers were plotted.

Image Analysis, Quantifications, and Statistics

Image processing and image analysis were performed using Fiji(ImageJ; National Institutes of Health) (Schindelin et al., 2019) and MATLAB (MathWorks). Z-stacks acquired on the cell

cortex were projected using Fiji's maximum intensity projection tool. Images within each panel were scaled equally. Flow kymographs shown in Figure 4.1D and Supplementary Figures S4.3A, **S4.6A** were created by tracing a 150 × 5 pixel rectangle positioned at the center of the embryo on the cortical plane and mounted using Fiji's Make Montage tool, as illustrated in Figure 4.1D'. Graph plotting, linear regressions and statistical analyses were performed with Prism 6.0 (GraphPad Software). Photobleaching experiments were analyzed using easyFRAP, https://easyfrap.vmnet.upatras.gr (Koulouras et al., 2018). Measurements for cytokinetic analysis in Supplementary Figure S4.1A were performed as previously reported (Chan et al., 2019). Error bars represent the standard-deviation (SD), standard-error of the mean (SEM), or 95% confidence interval (95% CI), and statistical significance tests were performed using one-way ANOVA with Bonferroni correction, as indicated in figure legends. Statistical significance of flow profiles was performed using two-way ANOVA for repeated measures.

Supplementary Material

Supplementary Figure S1, Leite et al.

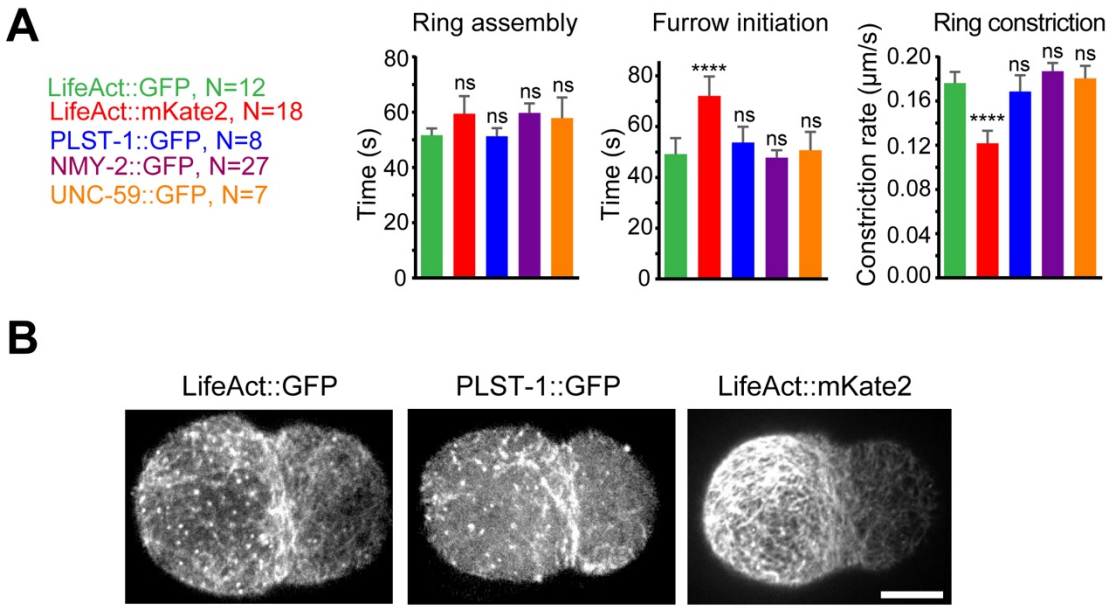

SUPPLEMENTARY FIGURE S1 | Delayed cytokinesis in embryos expressing LifeAct::mKate2. **(A)** Intervals for ring assembly/furrow initiation and ring constriction rate (mean ± 95% CI). N is the number of embryos analyzed. Statistical significance was determined using one-way ANOVA followed by Bonferroni's multiple comparison test. **** P < 0.0001, ns, not significant. **(B)** Cortical images of embryos expressing different fluorescent probes for actin. Scale bar, 10 µm.

SUPPLEMENTARY FIGURE S4.1. Delayed cytokinesis in embryos expressing LifeAct::mKate2. **(A)** Intervals for ring assembly/furrow initiation and ring constriction rate (mean ± 95% CI). N is the number of embryos analyzed.

Statistical significance was determined using one-way ANOVA followed by Bonferroni's multiple comparison test. $^{****}P < 0.0001$, ns, not significant. **(B)** Cortical images of embryos expressing different fluorescent probes for actin. Scale bar, 10 µm.

Supplementary Figure S2, Leite et al.

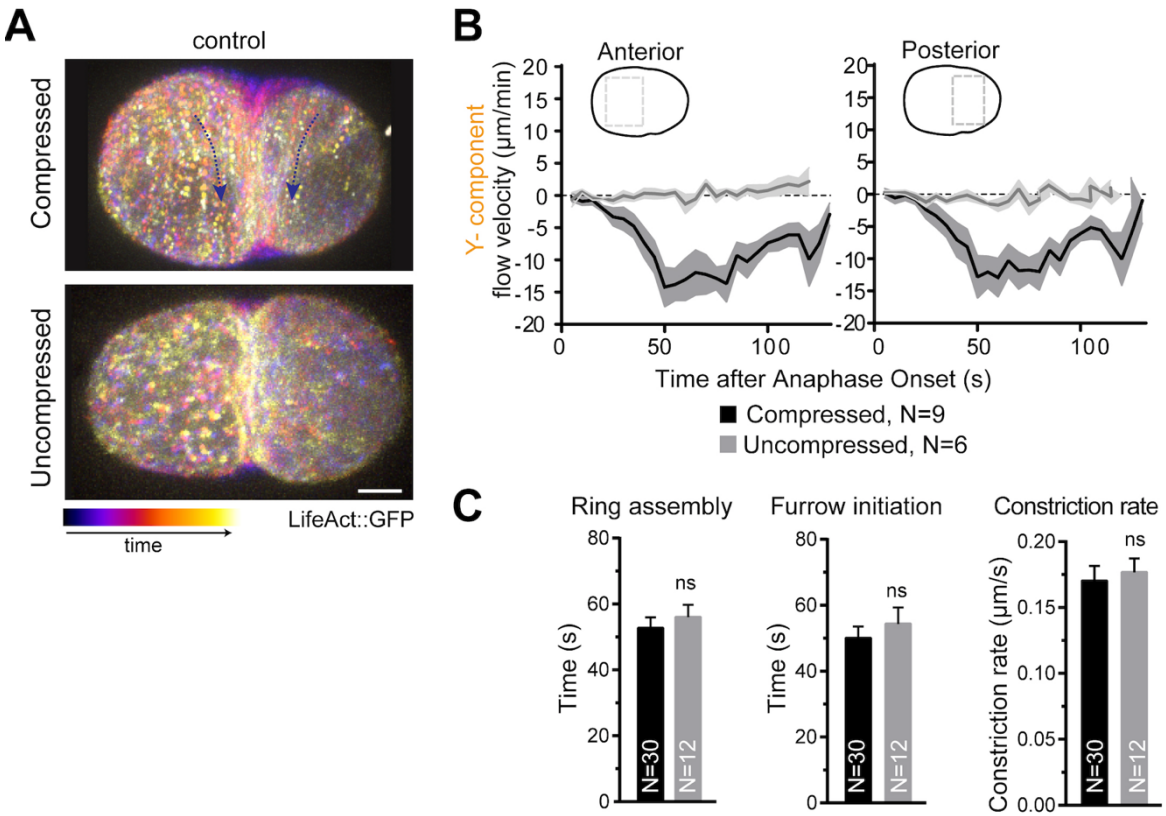

SUPPLEMENTARY FIGURE S4.2. Rotational flows are a consequence of embryo compression. **(A)** Time projections of control embryos expressing LifeAct::GFP imaged under compression (top) or without compression (bottom). Rotational (Y-component) flows are indicated by curved arrows. Scale bar, 10 µm. **(B)** Rotational (Y-component) flow velocity (mean ± SEM) in the anterior (left) or posterior (right) half of embryos imaged with (black) or without (gray) compression. **(C)** Intervals for ring assembly/furrow initiation and ring constriction rate (mean ± 95% CI) measured in embryos imaged with (black) or without (gray) compression. N is the number of embryos analyzed.

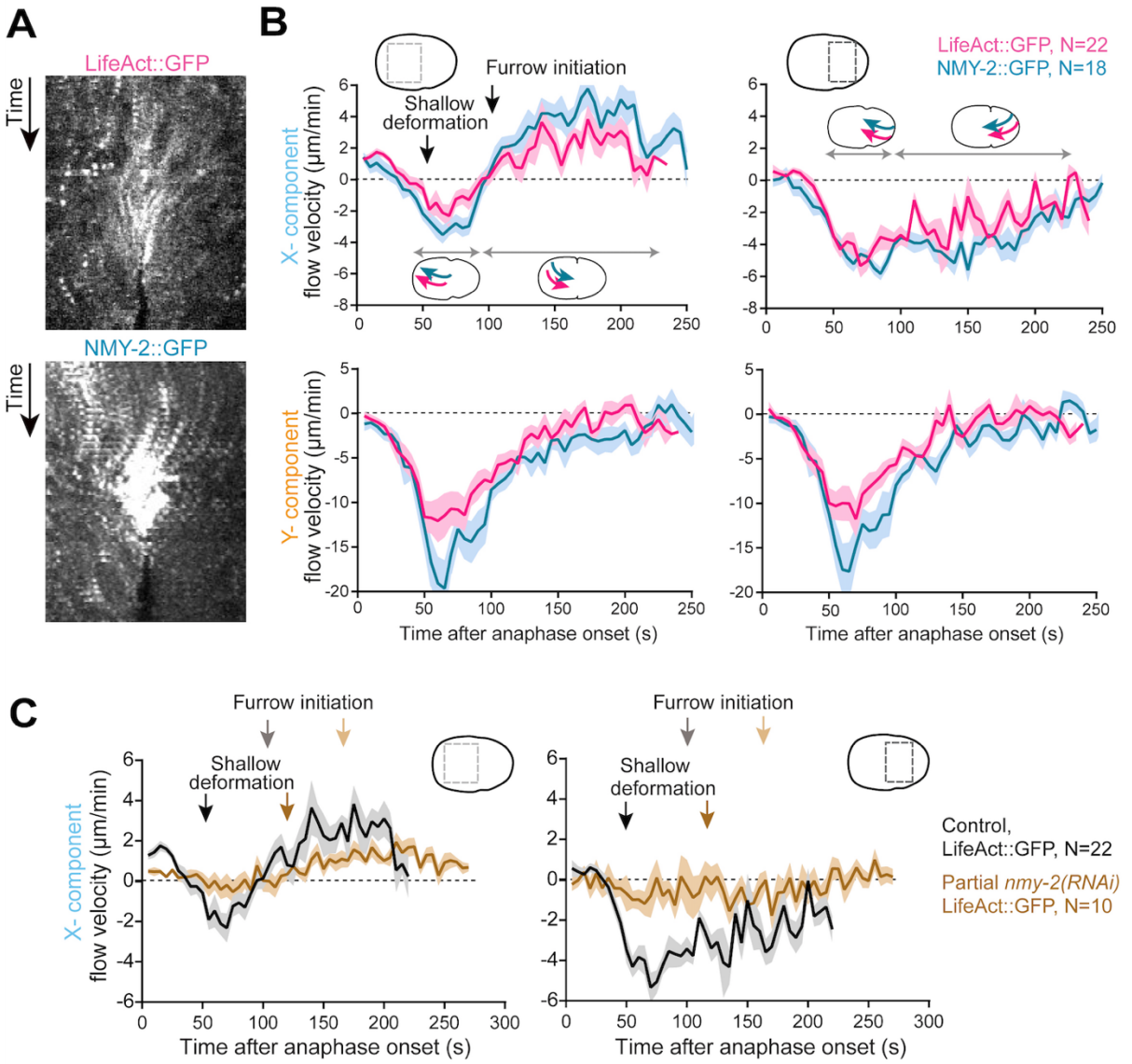

SUPPLEMENTARY FIGURE S4.3. F-actin and myosin cortical flow profiles are similar. **(A)** Kymographs depicting Lifeact::GFP (top) and NMY-2::GFP (bottom) longitudinal cortical flows from anaphase onset until complete ingression. **(B)** Longitudinal (X-component) and rotational (Y-component) flow velocities (mean ± SEM) for LifeAct::GFP and NMY-2::GFP in the anterior or posterior half of embryos, plotted over time starting at anaphase onset. The depicted interval covers both the period of unidirectional and the period of bidirectional flows. **(C)** Longitudinal (X-component) LifeAct::GFP flow velocities (mean ± SEM) over time for control and NMY-2-depleted embryos from anaphase onset until complete ingression. Arrows indicate average time of shallow deformation (darker tone) or furrow initiation (lighter tone). N is the number of embryos analyzed.

Supplementary Figure S4, Leite et al.

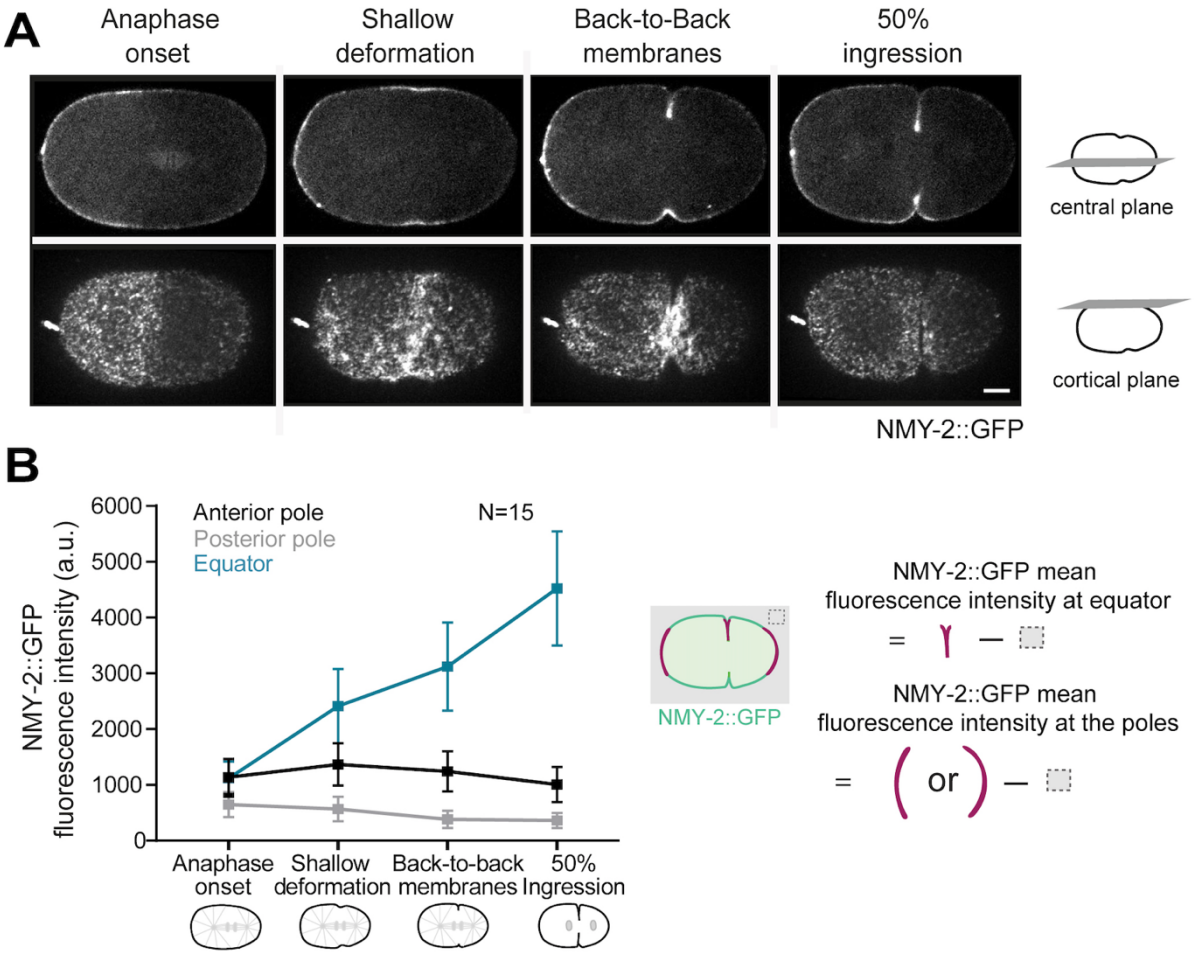

SUPPLEMENTARY FIGURE S4.4. The amount of myosin that accumulates at the cell equator is higher than the amount that leaves the cortical poles. **(A)** Images of the central and cortical planes of a dividing one-cell embryo expressing NMY-2::GFP at different time points in cytokinesis, revealing a decrease of myosin levels at the cortical poles and an increase at the cell equator. Scale bar, 5 μm. **(B)** Quantification of NMY-2::GFP levels (mean ± SD) on the anterior pole, posterior pole, and equator at the time points indicated in **(A)**, determined as indicated in the schematic on the right. N is the number of embryos analyzed.

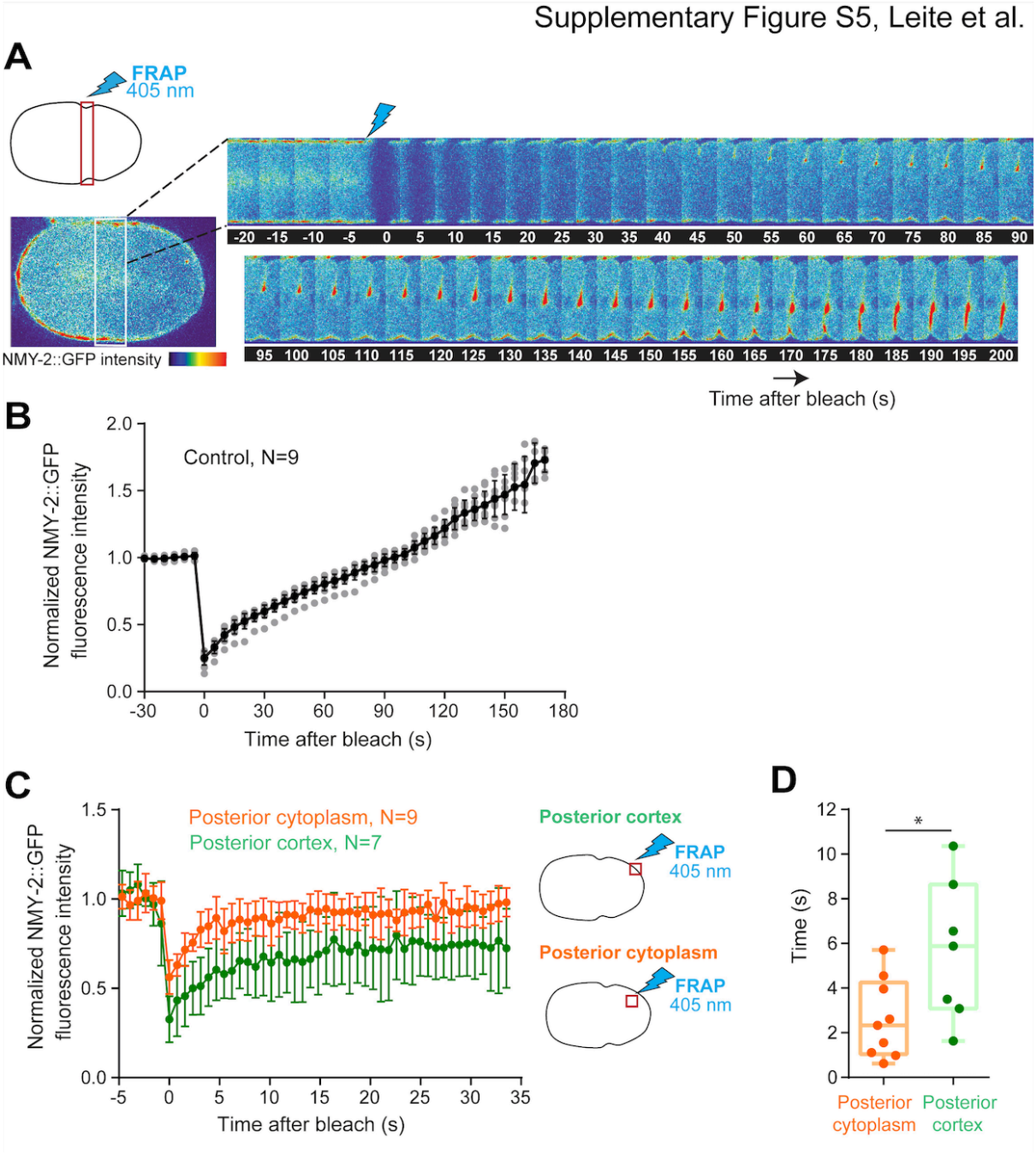

SUPPLEMENTARY FIGURE S4.5. Fluorescence recovery after photobleaching of the entire division plane indicates that myosin continues to accumulate in the contractile ring during furrow ingression. **(A)**Schematic showing the photobleached region of the entire division plane at shallow deformation (top left) and selected images from a time-lapse series showing NMY-2::GFP fluorescence over time pre- and post-bleaching. **(B)** Quantification of NMY-2::GFP fluorescence recovery after photobleaching the entire division plane at shallow deformation. Data from individual embryos (light gray) and the mean ± SD (black) are plotted. **(C)** Quantification of NMY-2::GFP fluorescence recovery after photobleaching in the posterior cytoplasm. **(D)** Boxplots showing the dispersion of half-time recovery for the posterior cytoplasm and the posterior cortex. In each box, the central line is the median, the boundaries of the box are the 25th and 75th percentiles; the whiskers extend to include the maximum and minimum values. N is the number of embryos analyzed. Statistical significance of half-time recovery in (D) was determined using unpaired Student's *t*-test: $^{*}P < 0.05$.

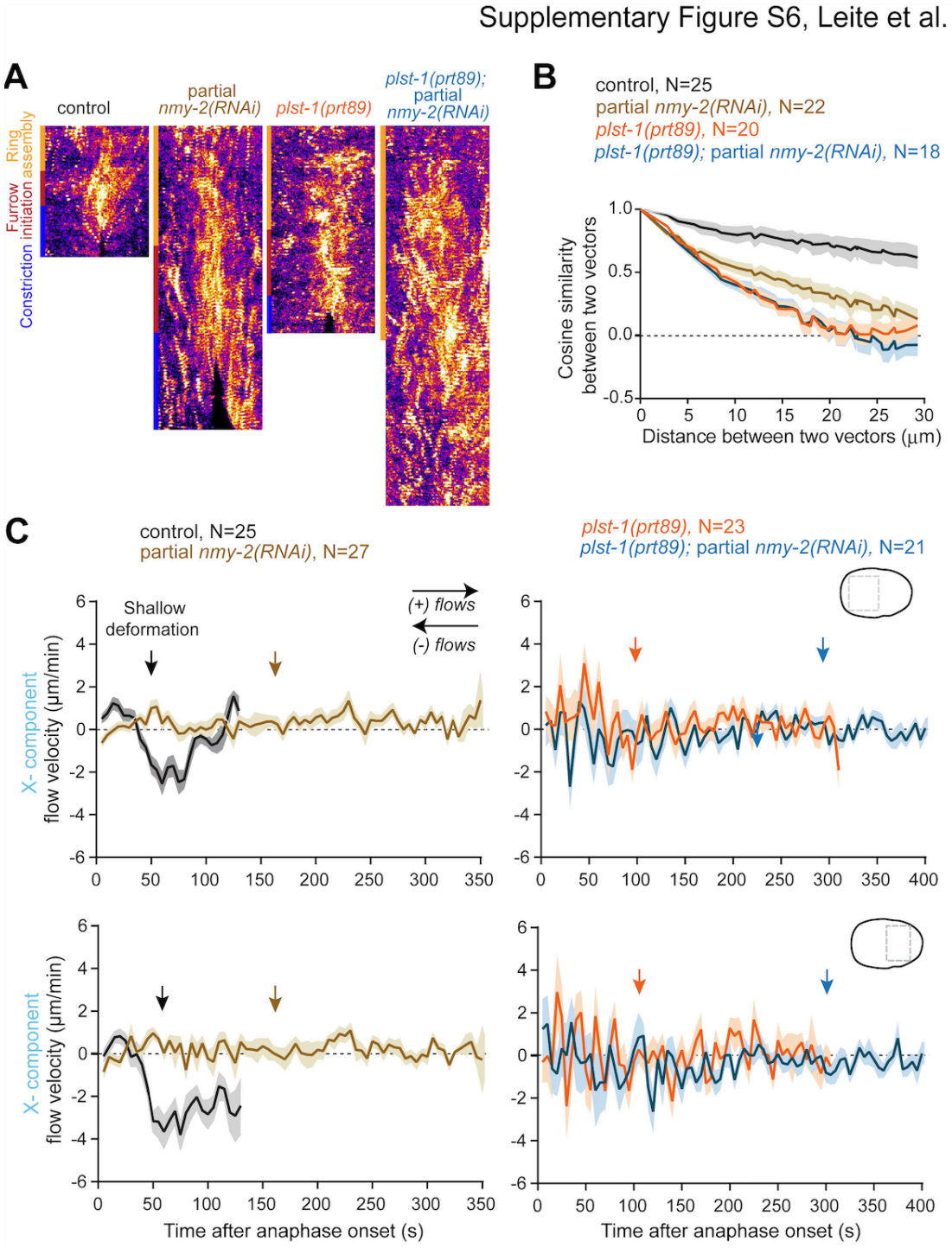

SUPPLEMENTARY FIGURE S4.6. Cortical flows are not aggravated in *nmy-2(RNAi);plst-1(prt89)* embryos. **(A)** Kymographs of LifeAct::GFP cortical flow profiles along the longitudinal axis of the embryos. Yellow, red, and blue bars correspond to contractile ring assembly, furrow initiation, and ring constriction intervals, respectively. Kymographs were built as described in Figure 1D'. **(B)** Cosine similarity between two vectors as a function of the distance between them. **(C)** Longitudinal (X-component) average flow velocity (mean ± SEM) over time after anaphase onset for LifeAct::GFP in the anterior or posterior half of the embryos. Arrows indicate the time of shallow deformation. In panels (B), (C), N is the number of embryos analyzed.

SUPPLEMENTARY TABLE S4.1. List of *C. elegans* strains used in this study.

Supplemental Table S1 - List of *C. elegans* strains used in this study

Strain	Genotype	Source/ reference
N2	Ancestral	
GCP21	ltIs157 [pAC16;Ppie-1::Life-Act::GFP; unc-119 (+)]; ltIs37 [pAA64; Ppie-1::mCherry::his-58; unc-119 (+)] IV	Our Lab (Silva et al., 2016)
GCP22	ltIs157 [pAC16;Ppie-1::Life-Act::GFP; unc-119 (+)]; unc-119(ed3)III?; prtSi2[pAC71; Pnmy-2::nmy-2reencoded::mCherry::StrepTagII::3'UTRnmy-2; cb-unc-119(+)]II	Our Lab (Osorio et al., 2019)
GCP592	nmy-2 [prt100(R252A)]I; ltIs157 [pAC16;Ppie-1::Life-Act::GFP; unc-119 (+)]; unc-119(ed3)III?; prtSi2[pAC71; Pnmy-2::nmy-2reencoded::mCherry::StrepTagII::3'UTRnmy-2; cb-unc-119(+)]II	Our Lab (Osorio et al., 2019)
GCP618	nmy-2 [prt113(S251A)]I; ltIs157 [pAC16;Ppie-1::Life-Act::GFP; unc-119 (+)]; unc-119(ed3)III?; prtSi2[pAC71; Pnmy-2::nmy-2reencoded::mCherry::StrepTagII::3'UTRnmy-2; cb-unc-119(+)]II	Our Lab (Osorio et al., 2019)
GCP812	nmy-2(cp13[nmy-2::gfp + LoxP]) I; unc-119(ed3) III?; ltIs37 [pAA64; Ppie-1::mCherry::his-58; unc-119 (+)] IV	This study
GCP927	plst-1 [(prt89)]IV; ltIs157 [pAC16;pie-1::Life-Act::GFP; unc-119 (+)]; prtSi2[pAC71; Pnmy-2:nmy-2reencoded::mCherry::StrepTagII::3'UTRnmy-2; cb-unc-119(+)]II; unc-119(ed3)III?	This study
OD26	unc-119(ed3) III; ltIs20 [pASM10; pie-1/GFP::unc-59; unc-119 (+)]	OD Lab
RZB213	[plst-1(msn190[plst-1::GFP])] IV	Zaidel-Bar Lab (Ding et al., 2017)
SWG001	[(Mex5p/lifeact/mKate); unc-119 (+)); unc-119(ed3)] III	Grill Lab (Reymann et al., 2016)

SUPPLEMENTARY TABLE S4.2. List of dsRNAs used in this study.

Name	Gene target	Foward primer	Reverse primer	RNAi
nmy-2_RNA#1	F20G4.3 (nmy-2)	GGCCCGATA TCATGAACA ACGAGCTTG AAAG	GGCACGATA TCAGCCTCC TGGATAGCC	feeding
nmy-2_RNA#2	F20G4.3 (nmy-2)	CCCAAGATA TCAATTGAAT CTCGGTTGA AGGAA	CCCCCGATA TCGACTGCA TTTCACGCAT CTTATG	feeding
nmy-2_RNA#3	nmy-2:mCherry reencoded (nmy-2::mCherry^{sen})	GGCCCGATA TCATGAATA ATGAACTCG AGTCAATC	GGCCCGATA TCACGTTCTT GAATGGCC	feeding

References

Arnold, J. M. (1969). Cleavage furrow formation in a telolecithal egg (Loligo Pealii): I. Filaments in early furrow formation. *J. Cell Biol.* 41, 894–904. doi: 10.1083/jcb.41.3.894

Arribere, J. A., Bell, R. T., Fu, B. X. H., Artiles, K. L., Hartman, P. S., and Fire, A. Z. (2014). Efficient marker-free recovery of custom genetic modifications with CRISPR/Cas9 in *Caenorhabditis elegans*. *Genetics* 198, 837–846. doi: 10. 1534/genetics.114.169730

Bement, W. M., Benink, H. A., and Von Dassow, G. (2005). A microtubule- dependent zone of active RhoA during cleavage plane specification. *J. Cell Biol.* 170, 91–101. doi: 10.1083/jcb.200501131

Bernetti, M., Masetti, M., Rocchia, W., and Cavalli, A. (2019). Kinetics of Drug Binding and Residence Time. *Annu. Rev. Phys. Chem.* 70, 143–171. doi: 10. 1146/annurev- physchem-042018- 052340

Bretscher, A. (1981). Fimbrin is a cytoskeletal protein that crosslinks F-actin in vitro. *Proc. Natl. Acad. Sci. U.S.A.* 78, 6849–6853. doi: 10.1073/pnas.78.11. 6849

Cao, L. G., and Wang, Y. L. (1990). Mechanism of the formation of contractile ring in dividing cultured animal cells. II. Cortical movement of microinjected actin filaments. *J. Cell Biol.* 111, 1905–1911. doi: 10.1083/jcb.111.5.1905

Carvalho, A., Desai, A., and Oegema, K. (2009). Structural Memory in the Contractile Ring Makes the Duration of Cytokinesis Independent of Cell Size. *Cell* 137, 926–937. doi: 10.1016/j.cell.2009.03.021

Chan, F., Silva, A. M., Saramago, J., Pereira-Sousa, J., Brighton, H. E., Pereira, M., et al. (2019). The ARP2/3 complex prevents excessive formin activity during cytokinesis. *Mol. Biol. Cell* 30, 96–107. doi: 10.1091/mbc.E18-07-0471

Chapa-y-lazo, B., Hamanaka, M., Wray, A., Balasubramanian, M. K., and Mishima, M. (2020). Polar relaxation by dynein-mediated removal of cortical myosin II. *J. Cell Biol.* 219:e201903080. doi: 10.1083/jcb.201903080

Davies, T., Jordan, S. N., Chand, V., Sees, J. A., Laband, K., Carvalho, A. X., et al. (2014). High-Resolution temporal analysis reveals a functional timeline for the molecular regulation of cytokinesis. *Dev. Cell* 30, 209–223. doi: 10.1016/j.devcel. 2014.05.009

Descovich, C. P., Cortes, D. B., Ryan, S., Nash, J., Zhang, L., Maddox, P. S., et al. (2017). Cross-linkers both drive and brake cytoskeletal remodeling and furrowing in cytokinesis. *Mol. Biol. Cell* 2, 3–4. doi: 10.1091/mbc.E17-06-0392

Dickinson, D. J., Ward, J. D., Reiner, D. J., and Goldstein, B. (2013). Engineering the Caenorhabditis elegans genome using Cas9-triggered homologous recombination. *Nat. Methods* 10, 1028–1034. doi: 10.1038/nmeth. 2641

Ding, W. Y., Ong, H. T., Hara, Y., Wongsantichon, J., Toyama, Y., Robinson, R. C., et al. (2017). Plastin increases cortical connectivity to facilitate robust polarization and timely cytokinesis. *J. Cell Biol.* 216, 1371–1386. doi: 10.1083/ jcb.201603070

Ennomani, H., Letort, G., Guérin, C., Martiel, J. L., Cao, W., Nédeléc, F., et al. (2016). Architecture and Connectivity Govern Actin Network Architecture and Connectivity. *Curr. Biol.* 26, 616–626. doi: 10.1016/j.cub.2015.12.069

Faix, J., Steinmetz, M., Boves, H., Kammerer, R. A., Lottspeich, F., Mintert, U., et al. (1996). Cortexillins, major determinants of cell shape and size, are actin- bundling proteins with a parallel coiled-coil tail. *Cell* 86, 631–642. doi: 10.1016/ S0092- 8674(00)80136- 1

Green, R. A., Paluch, E. K., and Oegema, K. (2012). Cytokinesis in Animal Cells. *Annu. Rev. Cell Dev. Biol.* 28, 29–58. doi: 10.1146/annurev- cellbio- 101011- 155718

Großhans, J., Wenzl, C., Herz, H. M., Bartoszewski, S., Schnorrer, F., Vogt, N., et al. (2005). RhoGEF2 and the formin Dia control the formation of the furrow canal by directed actin assembly during *Drosophila cellularisation*. *Development* 132, 1009–1020. doi: 10.1242/dev.01669

Henson, J. H., Ditzler, C. E., Germain, A., Irwin, P. M., Vogt, E. T., Yang, S., et al. (2017). The ultrastructural organization of actin and myosin II filaments in the contractile ring: new support for an old model of cytokinesis. *Mol. Biol. Cell* 28, 613–623. doi: 10.1091/mbc.E16-06-0466

Khaliullin, R. N., Green, R. A., Shi, L. Z., Gomez-Cavazos, J. S., Berns, M. W., Desai, A., et al. (2018). A positive-feedback-based mechanism for constriction rate acceleration during cytokinesis in *Caenorhabditis elegans*. *eLife* 7:e36073. doi: 10.7554/eLife.36073

Kimura, K., Ito, M., Amano, M., Chihara, K., Fukata, Y., Nakafuku, M., et al. (1996). Regulation of myosin phosphatase by Rho and Rho-associated kinase (Rho-kinase). *Science* 273, 245–248. doi: 10.1126/science.273.5272.245

Koulouras, G., Panagopoulos, A., Rapsomaniki, M. A., Giakoumakis, N. N., Taraviras, S., and Lygerou, Z. (2018). EasyFRAP-web: a web-based tool for the analysis of fluorescence recovery after photobleaching data. *Nucleic Acids Res.* 46, W467–W472. doi: 10.1093/nar/gky508

Laplante, C., Berro, J., Karatekin, E., Hernandez-Leyva, A., Lee, R., and Pollard, T. D. (2015). Three myosins contribute uniquely to the assembly and constriction of the fission yeast cytokinetic contractile ring. *Curr. Biol.* 25, 1955–1965. doi: 10.1016/j.cub.2015.06.018

Leite, J., Osorio, D. S., Sobral, A. F., Silva, A. M., and Carvalho, A. X. (2019). Network Contractility during Cytokinesis - From Molecular to Global Views. *Biomolecules* 9:194. doi: 10.3390/biom9050194

Levy, A. D., Yang, J., and Kramer, J. M. (1993). Molecular and genetic analyses of the *Caenorhabditis elegans* dpy-2 and dpy-10 collagen genes : a variety of molecular alterations affect organismal morphology. *Mol. Biol. Cell* 4, 803–817. doi: 10.1091/mbc.4.8.803

Mabuchi, I., Tsukita, S., Tsukita, S., and Sawai, T. (1988). Cleavage furrow isolated from newt eggs : contraction, organization of the actin filaments, and protein components of the furrow. *Proc. Natl. Acad. Sci. U.S.A.* 85, 5966–5970. doi: 10.1073/pnas.85.16.5966

Mangal, S., Sacher, J., Kim, T., Osório, D. S., Motegi, F., Carvalho, A. X., et al. (2018). TPXL-1 activates Aurora A to clear contractile ring components from the polar cortex during cytokinesis. *J. Cell Biol.* 217, 837–848. doi: 10.1083/jcb. 201706021

Marsland, D. (1950). The mechanisms of celldivision; temperature-pressure experiments on the cleaving eggs of *Arbacia punctulata*. *J. Cell Comp. Physiol.* 36, 205–227. doi: 10.1002/jcp.1030360207

Marsland, D. (1956a). Protoplasmic contractility in relation to cytokinesis. *Pubblicazioni Della Stazione Zoologica Di Napoli* 28, 182–203.

Marsland, D. (1956b). Protoplasmic contractility in relation to gel structure: temperature - pressure experiments on cytokinesis and amoeboid movement. *Int. Rev. Cytol.* 5, 199–227. doi: 10.1016/S0074-7696(08)62571-1

Matsudaira, P., Mandelkow, E., Renner, W., Hesterberg, L. K., and Weber, K. (1983). Role of fimbrin and villin in determining the interfilament distances of actin bundles. *Nature* 301, 209–214. doi: 10.1038/301209a0

Matsumura, F. (2005). Regulation of myosin II during cytokinesis in higher eukaryotes. *Trends Cell Biol.* 15, 371–377. doi: 10.1016/j.tcb.2005.05.004

Maupin, P., and Pollard, T. D. (1986). Arrangement of actin filaments and myosin- like filaments in the contractile ring and of actin-like filaments in the mitotic spindle of dividing HeLa cells. *J. Ultrastruc. Mol. Struct. Res.* 94, 92–103. doi: 10.1016/0889- 1605(86)90055- 8

Mavrakis, M., Azou-gros, Y., Tsai, F., Alvarado, J., Bertin, A., Iv, F., et al. (2014). Septins promote F-actin ring formation by crosslinking actin filaments into curved bundles. *Nat. Cell Biol.* 16, 322–334. doi: 10.1038/ncb2921

Mayer, M., Depken, M., Bois, J. S., Jülicher, F., and Grill, S. W. (2010). Anisotropies in cortical tension reveal the physical basis of polarizing cortical flows. *Nature* 467, 617–621. doi: 10.1038/nature09376

Melak, M., Plessner, M., and Grosse, R. (2017). Actin visualization at a glance. *J. Cell Sci.* 130, 525–530. doi: 10.1242/jcs.189068

Mitchison, J. (1952). Cell membranes and cell division. *Symp. Soc. Exp. Biol.* 6, 105–127.

Mitchison, J. M., and Swann, M. (1955). The mechanical properties of the cell surface: III.The sea-urchin egg from fertilization to cleavage. *J. Exp. Biol.* 32, 734–750. doi: 10.1016/0021-9290(80)90043-3

Murrell, M., Oakes, P. W., Lenz, M., and Gardel, M. L. (2015). Forcing cells into shape: the mechanics of actomyosin contractility. *Nat. Rev. Mol. Cell Biol.* 16, 486–498. doi: 10.1038/nrm4012

Murthy, K., and Wadsworth, P. (2005). Myosin-II-dependent localization and dynamics of F-actin during cytokinesis. *Curr. Biol.* 15, 724–731. doi: 10.1016/ j.cub.2005.02.055

Naganathan, S., Fürthauer, S., Rodriguez, J., Fievet, B. T., Ahringer, J., Cannistraci, C. V., et al. (2014). Morphogenetic degeneracies in the actomyosin cortex. *eLife* 7:e37677. doi: 10.7554/eLife.37677

Osorio, D. S., Chan, F., Saramago, J., Leite, J., Silva, A. M., Sobral, A. F., et al. (2019). Crosslinking activity of non-muscle myosin II is not sufficient for embryonic cytokinesis in *C. elegans*. *Development* 146:dev179150. doi: 10.1242/dev.179150

Pinto, I. M., Rubinstein, B., and Li, R. (2013). Force to divide: structural and mechanical requirements for actomyosin ring contraction. *Biophys. J.* 105, 547–554. doi: 10.1016/j.bpj.2013.06.033

Prokopenko, S. N., Saint, R., and Bellen, H. J. (2000). Untying the Gordian Knot of Cytokinesis : role of Small G Proteins and Their Regulators. *J. Cell Biol.* 148, 843–848. doi: 10.1083/jcb.148.5.843

Reichl, E. M., Ren, Y., Morphew, M. K., Delannoy, M., Effler, J. C., Girard, K. D., et al. (2008). Interactions between myosin and actin crosslinkers control cytokinesis contractility dynamics and mechanics. *Curr. Biol.* 18, 471–480. doi: 10.1016/j.cub.2008.02.056

Ren, Y., Effler, J. C., Norstrom, M., Luo, T., Firtel, R. A., Iglesias, P. A., et al. (2009). Mechanosensing through cooperative interactions between myosin II and the actin crosslinker cortexillin I. *Curr. Biol.* 19, 1421–1428. doi: 10.1016/j.cub.2009. 07.018

Reymann, A. C., Staniscia, F., Erzberger, A., Salbreux, G., and Grill, S. W. (2016). Cortical flow aligns actin filaments to form a furrow. *eLife* 5, 1–25. doi: 10.7554/ eLife.17807

Salbreux, G., Prost, J., and Joanny, J. F. (2009). Hydrodynamics of cellular cortical flows and the formation of contractile rings. *Phys. Rev. Lett.* 103:058102. doi: 10.1103/PhysRevLett.103.058102

Sanger, J. M., and Sanger, J. W. (1980). Banding and polarity of actin filaments in interphase and cleaving cells. *J. Cell Biol.* 86, 568–575. doi: 10.1083/jcb.86.2.568 Schindelin, J., Arganda-Carreras, I., Frise, E., Kaynig, V., Longair, M., Pietzsch, T.,

et al. (2019). Fiji : an open-source platform for biological-image analysis. *Nat.*

Methods 28, 676–682. doi: 10.1038/nmeth.2019
Schroeder, T. E. (1968). Cytokinesis: filaments in the cleavage furrow. *Exp. Cell Res.*

53, 272–276. doi: 10.1016/0014-4827(68)90373-x
Schroeder, T. E. (1970). The contractile ring: I. Fine structure of dividing

mammalian (HeLa) cells and the effects of cytochalasin B. *Z Zellforsch Mikrosk*

Anat. 109, 431–449. doi: 10.1007/BF00343960
Schroeder, T. E. (1972). The contractile ring: II. Determining its brief existence,

volumetric changes, and vital role in cleaving arbacia eggs. *J. Cell Biol.* 53,

419–434. doi: 10.1083/jcb.53.2.419
Selman, G. G., and Perry, M. M. (1970). Ultrastructural changes in the surface

layers of the newt's egg in relation to the mechanism of its cleavage. *J. Cell Sci.*

6, 207–227.
Silva, A. M., Osório, D., Pereira, A. J., Maiato, H., Pinto, I. M., Rubinstein,

B., et al. (2016). Robust gap repair in the contractile ring ensures timely completion of cytokinesis. *J. Cell Biol.* 215, 789–799. doi: 10.1083/jcb.20160 5080

Singh, D., Odedra, D., Dutta, P., and Pohl, C. (2019). Mechanical stress induces a scalable switch in cortical flow polarization during cytokinesis. *J. Cell Sci.* 132, jcs231357. doi: 10.1242/jcs.231357

Skau, C. T., Courson, D. S., Bestul, A. J., Winkelman, J. D., Rock, R. S., Sirotkin, V., et al. (2011). Actin filament bundling by fimbrin is important for endocytosis, cytokinesis, and polarization in fission yeast. *J. Biol. Chem.* 286, 26964–26977. doi: 10.1074/jbc.M111.239004

Spira, F., Cuylen-haering, S., Mehta, S., Samwer, M., Reversat, A., Verma, A., et al. (2017). Cytokinesis in vertebrate cells initiates by contraction of an equatorial actomyosin network composed of randomly oriented filaments. *eLife* 6:e30867. doi: 10.7554/eLife.30867

Srivastava, V., and Robinson, D. N. (2015). Mechanical stress and network structure drive protein dynamics during cytokinesis. *Curr. Biol.* 25, 663–670. doi: 10.1016/j.cub.2015.01.025

Swann, M. M., and Mitchison, J. M. (1958). The mechanism of cleavage in animal cells. *Biol. Rev. Camb. Philos. Soc.* 33, 103–135. doi: 10.1111/j.1469-185X.1958. tb01409.x

Tseng, Q., Duchemin-Pelletier, E., Deshiere, A., Balland, M., Guillou, H., Filhol, O., et al. (2011). Spatial organization of the extracellular matrix regulates cell- cell junction positioning. *Proc. Natl. Acad. Sci. U.S.A.* 109, 1506–1511. doi: 10.1073/pnas.1106377109

Turlier, H., Audoly, B., Prost, J., and Joanny, J. F. (2014). Furrow constriction in animal cell cytokinesis. *Biophys. J.* 106, 114–123. doi: 10.1016/j.bpj.2013.11.014

Uehara, R., Goshima, G., Mabuchi, I., Vale, R. D., Spudich, J. A., and Griffis, E. R. (2010). Determinants of Myosin II Cortical Localization during Cytokinesis. *Curr. Biol.* 20, 1080–1085. doi: 10.1016/j.cub.2010.04.058

Vavylonis, D., Wu, J. Q., Hao, S., O'Shaughnessy, B., and Pollard, T. D. (2008). Assembly

mechanism of the contractile ring for cytokinesis by fission yeast. *Science* 319, 97–100. doi: 10.1126/science.1151086

Vicente-Manzanares, M. (2009). Non-muscle myosin II takes centre stage in cell adhesion and migration. *Nat. Rev. Mol. Cell Biol.* 10, 778–790. doi: 10.1038/ nrm2786

Watanabe, S., Okawa, K., Miki, T., Sakamoto, S., Morinaga, T., Segawa, K., et al. (2010). Rho and Anillin-dependent Control of mDia2 Localization and Function in Cytokinesis. *Mol. Biol. Cell* 21, 3193–3204. doi: 10.1091/mbc.e10- 04- 0324

White, J. G., and Borisy, G. G. (1983). On the mechanisms of cytokinesis in animal cells. *J. Theor. Biol.* 101, 289–316. doi: 10.1016/0022-5193(83)90 342-9

Wollrab, V., Belmonte, J. M., Baldauf, L., Leptin, M., Nédeléc, F., and Koenderink, G. H. (2019). Polarity sorting drives remodeling of actin-myosin networks. *J. Cell Sci.* 132, 1–14. doi: 10.1242/jcs.219717

Wolpert, L. (1960). The mechanics and mechanism of cleavage. *Int. Rev. Cytol.* 10, 163–216.

Wu, J. Q., and Pollard, T. D. (2005). Cell biology: counting cytokinesis proteins globally and locally in fission yeast. *Science* 310, 310–314. doi: 10.1126/science. 1113230

Yumura, S., Ueda, M., Sako, Y., Kitanishi-Yumura, T., and Yanagida, T. (2008). Multiple mechanisms for accumulation of myosin II filaments at the equator during cytokinesis. *Traffic* 9, 2089–2099. doi: 10.1111/j.1600-0854.2008.00 837.x

CHAPTER V

MYOSIN TUNES BOTH CONTRACTILITY AND VISCOSITY AT THE CELL CORTEX TO ENSURE ROBUST CYTOKINESIS KINETICS

*Simulations in this chapter (Figure 5.3) were kindly provided by Dr. Hudson Rocha. The mentioned theory is also being implemented by Dr. Hudson Rocha and Dr. Hervé Turlier. Any failures in reproducing it here are however and exclusively my own.

Myosin tunes both contractility and viscosity at the cell cortex to ensure robust cytokinesis kinetics

* manuscript in preparation

Abstract

Cytokinesis is the last step of cell division that physically partitions the mother cell into two daughter cells. This process requires the assembly and constriction of a contractile ring, a tightly packed circumferential array of actin filaments, myosin motors and actin binding proteins, that forms at the cell equator. It is well-established that myosin-motor activity is essential for all phases of cytokinesis. However, to what extent the contractile ring relies on myosin-motor activity, the implications it may have for the cortex surrounding the ring or whether myosin could contribute to other mechanical properties besides contractility itself is not known.

Here, we show that the contractile ring constriction velocity in the *C. elegans* zygote does not correlate with the total amount of myosin in the ring, as contractile rings depleted of myosin up until a threshold can still constrict at normal velocities. Our preliminary 3D coarse-grained simulations show that the ring constriction velocity can only be maintained over a range of myosin levels if myosin has a contribution to both active and viscous tensions in the cortical layer: we can recapitulate our experimental observations when contractility and viscosity of the cortical layer are decreased proportionally as a function of myosin levels. In agreement with the idea that myosin does contribute to cortical viscosity, expression of increasing amounts of an inactive myosin unable to drive network contraction but in principle still able to bind actin filaments and therefore contribute to viscosity, results in a proportional decrease in ring constriction velocities *in vivo*. This is further reinforced by experiments where depleting the actin filament crosslinker plastin on myosin mutants lacking motor activity but able to bind actin rescues the decrease in ring constriction rate caused by expressing these myosins. For the first time, we model cytokinesis in an integrated manner - using both total myosin and active/inactive myosin profiles directly measured *in vivo* - and propose a novel role for myosin in regulating not only contractility, but also viscosity of the cell cortex.

Introduction

Cytokinesis, the last stage of cell division, relies on the assembly and constriction of a contractile ring - a circumferential array of actin filaments, nonmuscle myosin-II motors (hereafter, myosin) and other associated proteins (Leite *et al.*, 2019)(Green, Rebeca; Paluch and Oegema, 2012), including actin filament crosslinkers (Ding, Ong, Hara, Wongsantichon, Toyama, Robert C Robinson, *et al.*, 2017; Leite *et al.*, 2020; Sobral *et al.*, 2021) as well as the scaffolding proteins anillin (D'Avino, 2009) (Piekny and Maddox, 2010) and septin (Bridges and Gladfelter, 2015).

Contractile ring assembly is triggered by the small GTPase RhoA. At anaphase onset, RhoA is activated at the cell equator by signalling cues from the anaphase spindle (Bement, Miller and von Dassow, 2006) (Green, Rebeca; Paluch and Oegema, 2012)(Jordan and Canman, 2012)(Piekny, Werner and Glotzer, 2005), displaying an activation maximum at the equator that drops towards the poles in a gaussian-like manner (Bement, Benink and Von Dassow, 2005). Downstream of RhoA, contractile ring components are recruited locally from the cytoplasm (Yumura, 2001)(Vale, Spudich and Griffis, 2009)(Zhou and Wang, 2008): the downstream effector Rho-associated Kinase (hereafter, ROCK) promotes the activation and recruitment of myosin (Kosako *et al.*, 2000), whereas the diaphanous-related formin nucleates and elongates linear actin filaments (Otomo, Otomo, Diana R. Tomchick, *et al.*, 2005)(Watanabe *et al.*, 2008). A complementary mechanism relying on equatorial compression by actomyosin cortical flows has also been proposed (Reymann *et al.*, 2016)(Khaliullin *et al.*, 2018b). These are believed to arise from the tension differential resulting from the equatorial activation of RhoA at the equatorial cortex and its inhibition by astral microtubules at the cell poles (White and Borisy, 1983; Salbreux et al., 2009; Turlier et al., 2014; Khaliullin et al., 2018).

It is widely known that myosin, and particularly, its motor activity, are essential requirements for cytokinesis to complete in non-adherent cells (De Lozanne and Spudich, 1987)(Osório *et al.*, 2019)(Mabuchi and Okuno, 1977). Genetic perturbation, specific inhibition and injection of anti-myosin-II antibodies block furrow ingression (Straight *et al.*, 2003)(Mabuchi and Okuno, 1977)(Guo and Kemphues, 1996)(Karess *et al.*, 1991)(Shelton *et al.*, 1999). Specifically, cytokinesis fails in *C. elegans* zygotes when myosin is knocked-down by *RNAi* or when motor-dead mutants are expressed (Osório *et al.*, 2019)(Straight *et al.*, 2003).

However, it has not been fully disclosed what is the dependence of the contractile ring kinetics on the amount of myosin. Previous studies addressed this from a theoretical perspective where the constriction speed is expected to correlate linearly with the amount of myosin at the furrow or with the amount of an hypothetical Rho-like gaussian profile to simulate myosin activity (Turlier, Audoly, Prost and J.-F. Joanny, 2014)(Borja da Rocha, Bleyer and Turlier, 2022). Other agent-based models use myosin concentrations, which were not based on concentrations measured *in vivo* in the same model system, but on extrapolated numbers from yeast (Cortes, Nedelec and Maddox, 2022) or, alternatively, using concentrations measured on *C. elegans* embryos, but simulating only an isolated contractile ring (Descovich *et al.*, 2018). However, in .*C elegans* zygotes, the ring remains integrated in the surrounding cortex, which may also influence the network mechanical properties and therefore, how the contractile ring behaves (Sedzinski et al. 2011)(Yamamoto et al.2021).

To be able to translocate actin filaments and produce contractility, myosin bipolar filaments must be in an active state. This activation is believed to occur primarily through ROCK, which phosphorylates myosin regulatory light chain (Osório *et al.*, 2019) (Kosako *et al.*, 2000)(Amano *et al.*, 1996). This phosphorylation is required for cytokinesis (Kosako *et al.*, 2000; Piekny and Mains, 2002), as phosphorylation of Serine-19/Threonine-18 sites is increased in the furrow region, while decreased at polar regions (DeBiasio *et al.*, 1996;Yamashiro, Noguchi and Mabuchi, 2003; Matsumura *et al.*, 1998). Specifically, the phosphorylation of the regulatory light chain on Serine-19 has been shown to be critical for bipolar filament assembly in vertebrates (Adelstein & Anne Conti, 1975) by triggering conformational changes in myosin molecules from a folded to an open competent form (Vicente-Manzanares *et al.*, 2009; Trybus and Lowey, 1984). Myosin expressing a non-phosphorylatable regulatory light chain was shown to be unable to localize at the cleavage furrow in *D.melanogaster* S2 cells (Dean and Spudich, 2006). In human cells, light chain phosphorylation at Serine-19 is detected at the equatorial region at the same time as the heavy chain (Yamakita, Yamashiro and Matsumura, 1994). The phosphorylation state of the myosin heavy chain has been implicated in regulating the assembly of bipolar myosin filaments both in *D. discoideum* (Sabry *et al.*, 1997) and mammalian cells (Dulyaninova *et al.*, 2005;Mitsuhashi *et al.*, 2011). In *D. discoideum*, the phosphorylation of three aminoacids at the myosin heavy chain is essential for its accumulation at the cytokinetic furrow (Sabry *et al.*, 1997), but if and how the heavy chain phosphorylation regulates myosin bipolar filament assembly in other organisms is not known, including *C. elegans*. It is also not known whether myosin that is not activated can still exist in a bipolar filament form in the cell cortex and bind actin filaments. Most of the knowledge available on the regulatory light chain phosphorylation comes from *in vitro* studies, which may not exactly reproduce what happens in a living organism.

Here, for the first time, we investigate how myosin regulates cytokinesis in the *C. elegans* zygote from an integrated perspective by modelling the behaviour of the whole cortical layer as a function of myosin levels spatiotemporally measured *in vivo*. We show that cytokinesis kinetics does not linearly correlate with total myosin levels in the ring and that this is likely due to a balance of contractility *versus* viscosity, which is controlled by myosin itself between the equatorial and surrounding cortices. Contractile ring velocity is only affected when this balance is disturbed, either when there is no more myosin in the cortex surrounding the ring and a basal viscosity imposed by the crosslinked actin network is reached, or by the expression of increasing amounts of an inactive myosin that can possibly bind actin and contribute to viscosity, but progressively less capable of translocating those filaments. Our findings suggest a key role of myosin in providing cortex stability, which should be considered in future models of cytokinesis. Even though we are still far from being able to computationally model the whole cell cortex agent-wise, simulations should start including the possibility of myosin having a viscosity or stabilizing component aside from its contractile-associated function.

Results

Cytokinesis kinetics are robust to the decrease of total myosin levels at the ingressing furrow

To thoroughly investigate the dependence of contractile ring kinetics on myosin levels, we performed an RNAi time course of NMY-2, the *C. elegans* non-muscle myosin II that contributes to cytokinesis in the early embryo. The RNAi time course was performed in *C. elegans* zygotes expressing NMY-2::GFP from the endogenous locus to directly correlate the amount of NMY-2::GFP with the observed phenotypes (Figures 5.1, S5.1).

To assess myosin levels in the ring, GFP fluorescence intensity was measured within a box placed over the tip of the furrow at 50% of initial diameter and the camera background was subtracted (Figure 5.1B). Note that we did not subtract the cytoplasm intensity as background because the NMY-2::GFP intensity is decreasing progressively there as well, which could give the impression that levels in the ring were not being decreased (Figure S5.1A). The intensity for each individual example, either control or depletion, was expressed as a percentage of the average of controls. The frame when the contractile ring reached 50% of the initial diameter was chosen as reference for being the constriction mid-point. Noteworthy, the levels of NMY-2::GFP in control embryos varied from 90 to 140% (percentage of the average of controls), which already indicated that there is a range of myosin levels that allow for normal cytokinesis (Figure 5.1E). To quantify furrow formation and constriction kinetics, we used the reference points illustrated on Figure 5.1A: ring assembly time

corresponded to the time interval from anaphase onset until a first deformation of the equatorial cortex (shallow deformation), furrow initiation to the time between shallow deformation and a back-to-back membrane configuration and ring constriction to the interval between furrow initiation and full furrow ingression. All these phases of cytokinesis were significantly affected only when myosin levels at the ring were below a certain threshold, of the average control levels, around 20-30%. For myosin levels higher than this threshold, assembly and furrowing initiation occurred at similar times as controls, and the ring constriction rate was normal (Figure 5.1E). It was also confirmed that the cytoplasmic NMY-2::GFP intensity decreased linearly with the intensity at the furrow tip (Figure S5.1A). Importantly, this observation also justifies why the camera background was used for subtraction of the furrow tip and cortex contour intensities, instead of the cytoplasmic intensity: as the latter decreases linearly with the former, subtracting it to the furrow intensity would convey the idea that the NMY-2::GFP intensity is not decreasing, when it is clear it is decreasing everywhere in the embryo.

These observations revealed that the contractile ring kinetics is quite robust to the decrease in myosin levels. This raised the question on whether all myosin in the cortical network, and specifically in the ring itself, is active and, if not, what would be the contribution of this myosin to the cortex mechanics during cytokinesis. Indeed, it has been proposed that myosin outside the equatorial Rho-zone, where RhoA recruits downstream targets to increase actin polymerization and myosin activation/accumulation at the cell equator, is not active (Khaliullin et al., 2018).

To clarify this question, the NMY-2::GFP levels in the cortex contour were also quantified using central plane images of control and NMY-2 depleted embryos where NMY-2::GFP levels at the furrow tip were previously measured. This was done by tracing a line throughout the whole cortex contour, excluding the furrow region (Figure S5.1B). For the sake of consistency with previous measurements, only the frame that corresponded to 50% of the initial embryo diameter was considered. As expected when a protein is depleted by *RNAi*, a linear correlation between the NMY-2::GFP fluorescence intensity at the furrow and the surrounding cortex was obtained, as levels decrease in the whole embryo. However, as the cortical proteins flow from the poles towards the equator, having less myosin overall could also impact flow velocity and thus, myosin distribution in the embryo. Therefore, we quantified actin flow velocities in *C. elegans* embryos expressing LifeAct::GFP (a probe for F-actin) and NMY-2::mKate2 with varying levels of NMY-2 depletions, using Particle Image Velocimetry (PIV) (Figure S5.1H). Importantly, it was confirmed that *nmy-2(RNAi)* on these embryos also showed a similar threshold-dependent kinetics with the decreasing NMY-2::mKate2 levels in the ring, similarly to what was previously observed for NMY-2::GFP (data not shown). Myosin flows were also quantified in these embryos (data not shown), however, we considered actin flows may be

intrinsically more reliable as we are depleting myosin itself and the absence of enough NMY-2::mKate2 or NMY-2::GFP particles to track could lead to errors in vector tracing. The question here was whether cortical flow velocity also scaled with myosin levels as the other kinetic parameters shown on Figure 5.1E. If that was the case, cortical flow velocities should be roughly similar until a threshold of around 20-30% of myosin at the furrow tip, similarly to the constriction rate. However, cortical flow velocities started to decrease much earlier than this threshold and seemed to decrease monotonically with the myosin levels in the ring (measured at 50% of initial diameter), which is in line with the idea that these depend on myosin motor-activity (Khaliullin et al., 2018; Leite et al., 2020; A.-C. Reymann et al., 2016).

Taking these results into account, we formulated a new hypothesis. Given the 20-30% threshold where cytokinesis kinetics start becoming affected, one could wonder whether there is only a certain amount of myosin in the contractile ring that is indeed active and contributing to contractility. An excess of myosin could be recruited from the cytoplasm and delivered by flow as a safeguard to always maintain a certain tension. It would be unlikely, nonetheless, that this inactive myosin does not affect cortex mechanical properties at all, especially when 70-80% would be in that inactive state. Since myosin must bind actin filaments before executing the power stroke leading to actin translocation, we pondered that at each point in time, a percentage of total myosin was likely not active or not performing power strokes – either because the mechanochemical cycle is asynchronous between myosin heads from the same bipolar filament, or because there are permanently inactive heads that weakly bind actin. Both scenarios would pose a viscous drag on actin filament sliding. It is also possible that there is no real distinction between active/inactive myosin and the source of viscosity is the duty ratio itself - the portion of the mechanochemical cycle that myosin stays bound to actin – which may determine how fast myosin can slide actin and how long it stays bound in different phases of the cycle (e.g. the different functions of the two mammalian isoforms NMIIA in contractile tension build-up and NMIIB in stabilizing the NMIIA-generated tension, have been attributed to their low and high duty ratios, respectively (Weißenbruch *et al.*, 2021).

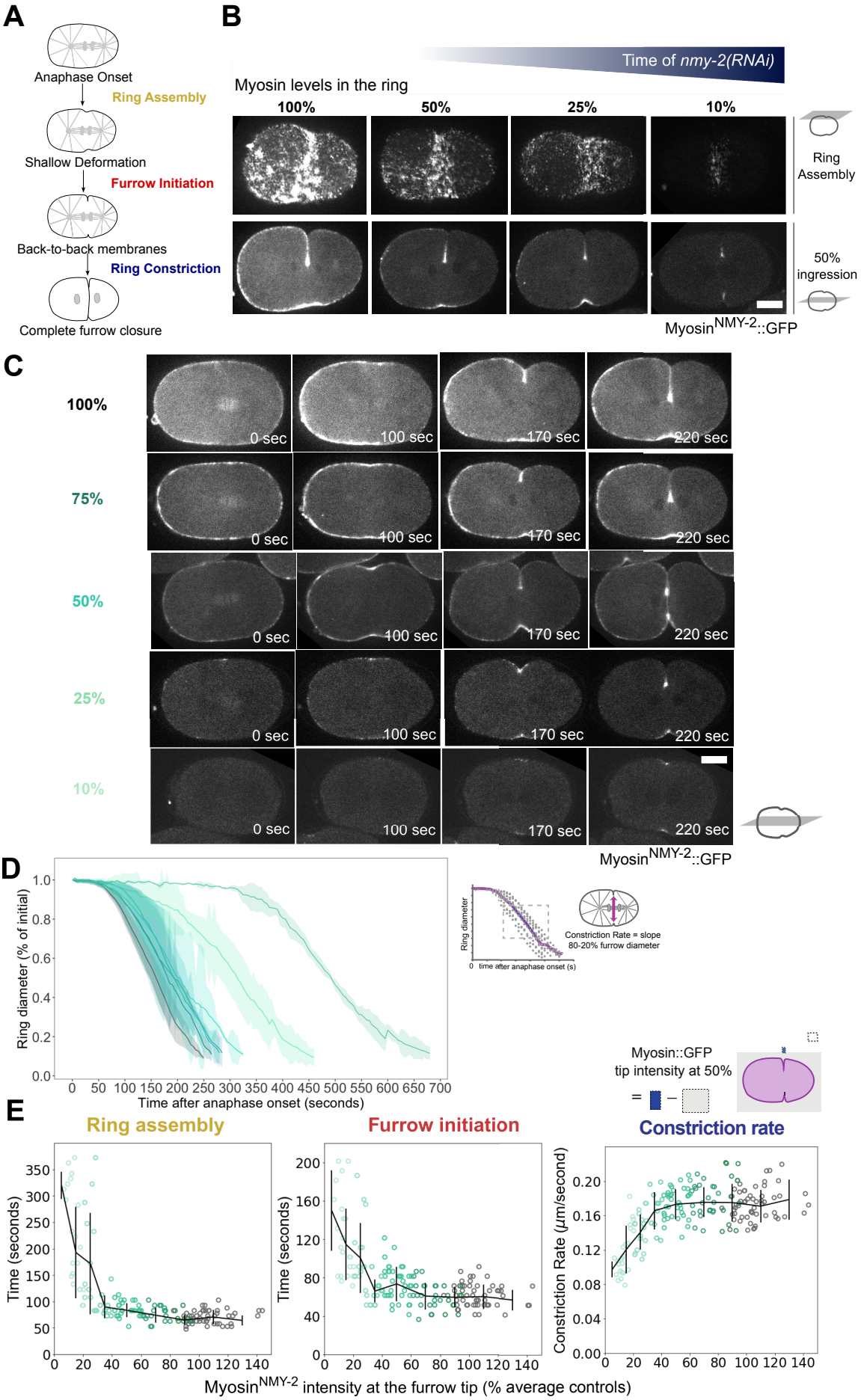
A
Anaphase Onset
Ring Assembly
Shallow Deformation
Furrow Initiation
Back-to-back membranes
Ring Constriction
Complete furrow closure
B
Time of nmy-2(RNAi)
Myosin levels in the ring
100%
50%
25%
10%
Ring Assembly
50% ingression
Myosin NMY-2::GFP
C
100%
75%
50%
25%
10%
0 sec
100 sec
170 sec
220 sec
Myosin NMY-2::GFP
D
Ring diameter (% of initial)
Time after anaphase onset (seconds)
Ring diameter
time after anaphase onset (s)
Constriction Rate = slope
80-20% furrow diameter
Myosin::GFP
tip intensity at 50%
E
Ring assembly
Furrow initiation
Constriction rate
Time (seconds)
Constriction Rate (µm/second)
Myosin NMY-2 intensity at the furrow tip (% average controls)

FIGURE 5.1. (A) Reference points used for measurements of ring assembly and furrow initiation intervals, as well as myosin NMY-2::GFP intensity. Ring assembly: time interval between anaphase onset and the formation of a shallow equatorial deformation, when contractile ring components are being recruited to the cell equator. Furrow initiation: time interval between shallow deformation and the folding of the plasma membrane into a back-to-back configuration. Ring constriction: time interval between a back-to-back configuration until full furrow ingression. **(B)** Cortical and central plane confocal images of embryos progressively depleted of NMY-2, at ring assembly and 50% furrow ingression, respectively. Image intensities are scaled equality. **(C)** Central plane images over time of embryos corresponding to the indicated percentages of myosin depletion. The chosen time points correspond to the shallow deformation, back-to-back membrane configuration and 50% ingression of controls for all depletion levels. Images intensities are scaled equally. **(D)** Ring diameter over time curves for the indicated depletion levels. The 80-20% of initial diameter interval illustrated in the schematic was used to calculate the constriction rate in (E). **(E)** Time of ring assembly and furrow initiation, and constriction rate versus myosin$^{NMY\text{-}2::GFP}$ fluorescence intensity (percentage of control average intensity)**.** The schematic on the top right shows the regions used for myosin$^{NMY\text{-}2::GFP}$ fluorescence intensity measurements in the furrow tip, cortex contour and camera background Scale bars, 10 µm.

Contractility and viscosity at the cortex must decrease proportionally to maintain the ring constriction speed constant over a wide range of myosin levels

To further investigate the biophysical principles behind these experimental data, we are conducting computational simulations that for the first time incorporate myosin profiles directly measured in embryos. We are using a 3D finite element visco-active model of the cell cortex (Borja da Rocha, Bleyer and Turlier, 2022) which is being adapted to include these myosin profiles.

To obtain the myosin profiles, a line was traced along the cortex contour in central plane images of control and NMY-2-depleted embryos expressing NMY-2::GFP (as sketched in Figure 5.2A-Left). Noteworthy, this line only covered half embryo (the side from which the furrow ingresses first and deeper) as the model considers the embryo is axisymmetric around the A-P axis and therefore, the profile from one half is extrapolated to the other. In reality, the *C. elegans* one-cell embryo does not constrict symmetrically – the furrow ingresses more from one of the sides - thus, one may ask whether this is a valid assumption for this system. Published data show that *C. elegans* embryos devoid of an eggshell – a rigid layer that confines and protects the embryo – no longer show this division plane asymmetry, which raises the possibility that it is due to physical constraints imposed by the rigid confinement itself (Koyama *et al.*, 2012; Aras *et al.*, 2018). Unlike the experimental data, where the timepoint corresponding to 50% of initial diameter has been chosen as reference for simplicity, in the simulations the spatiotemporal dynamics was considered by measuring these profiles for every timepoint from anaphase onset until the end of constriction, for some of the examples

in Figure 5.1E (we tried to only quantify examples where we could catch both the equatorial and polar regions of the embryo on the same focal plane, which greatly reduced the size of our initial sample from Figure 5.1.

The raw profiles were then fitted by a gaussian added to a linear function, as sketched in Figure 5.2A (Middle). The fittings were expected to capture the spatiotemporal evolution of the raw myosin profiles in a simplified functional form, characterized by only five parameters: amplitude A, width w, center c, slope m and intercept b (Figure 5.2A, Middle and Right). Figure 5.2B shows examples of these fittings for the respective raw profiles of some depletion levels. Note that the length L of each profile increases over time. This happens because there is new membrane being formed as cytokinesis progresses, especially in the later stages of constriction (Swann & Mitchison, 1958) (Dan, Yanagita and Sugiyama, 1937)(K Dan et al., 1938)(Dan & Ono, 1954)(Dan and Dan, 1940; Dan, 1954).

This procedure not only facilitates the integration of the measured profiles into the model framework, but it is also useful for advocating how the simplification of myosin's distribution to these parameters can carry a great amount of information that can be related to *in vivo* occurrences. The amplitude A quantifies the myosin levels in the furrow region. Since a gaussian is not found until myosin starts accumulating in the equatorial cortex, the amplitude is residual for earlier time points. This parameter is well fitted by an exponential function over time (Figure 5.2B,C), which is in agreement with previous reports (Khaliullin *et al.*, 2018c). The gaussian is also described by a width w, which may allow us to subsequently approximate the full width at half-maximum of the furrow, by multiplying $2.35w$. Note that it does not make sense to plot this parameter for the initial time points given that there is no furrow, thus the fitting reduces to an affine function. For that reason, we only plot it for time points starting at the shallow deformation (on average), for each corresponding depletion level. The center c simply defines the center of each traced line, which has been aligned to zero for all conditions (see Figure 5.2A, Left and Middle). Therefore, this parameter is expected to be roughly constant. It is interesting to observe that the slope perfectly describes the asymmetry of myosin intensities between the anterior and the posterior poles. As expected, this parameter is negative because intensities in the anterior pole are higher than in the posterior. Moreover, for non-depleted or mildly depleted embryos, it increases in magnitude from anaphase onset until shortly after the ring assembles, capturing myosin's transport from the posterior towards the anterior pole, as we have previously reported (Leite *et al.*, 2020). Subsequently, it decreases again as the furrow ingresses and bidirectional cortical flows start from both poles towards the equator. The conditions for which the slope does not change, correspond to

stronger depletions for which the myosin's distribution asymmetry between the two halves of the embryo is lost, as the myosin levels in the polar cortex reach basal levels (see Figure 5.1B,C). The intercept conveys similar, albeit less information, as it only characterizes the intensity evolution at the anterior pole (Figure 5.2C).

To investigate how myosin impacts cortex mechanical properties, we used a computational finite-element model that simulates the actomyosin cortex in 3D (Borja da Rocha et al., 2022). Despite the different numerical implementation, the general theory is based on active gels (Joanny et al., 2007; Kruse et al., 2005; Prost et al., 2015), such as in Turlier et al. (Turlier, Audoly, Prost and J. F. Joanny, 2014) The general equation of contractility $\zeta(x,t)$, which previously consisted of a gaussian curve to mimic the RhoA overactivity signal with artificial parameters written as

$$\zeta(x,t) = \zeta_0 + \delta\zeta^{\infty} I(t) e^{-\frac{x^2}{2w^2}} \ , \qquad (5.1)$$

where the basal contractility ζ_0, the amplitude A and the width w were all theoretically attributed or based on published literature.

has been changed to take *in vivo* measured myosin profiles as input. The new equation $\zeta(x,t)$ is thus given by

$$\zeta(x,t) = c_{myo}(\zeta_0 + A e^{-\frac{x^2}{2w^2}}), \qquad (5.2)$$

where $c_{myo}(x,t)$ defines the myosin intensity along the embryo profile over time, as previously depicted in Figure 5.2A-Left. The amplitude A replaces $\delta\zeta^{\infty}$ in Eq. (5.3). The fitted profiles provide us with the real values for the parameters A and w, as well as ζ_0. Note that instead of a constant basal offset in Eq. (5.4), we model the basal activity as a linear function, thus $\zeta_0(x,t) = mx + b$.

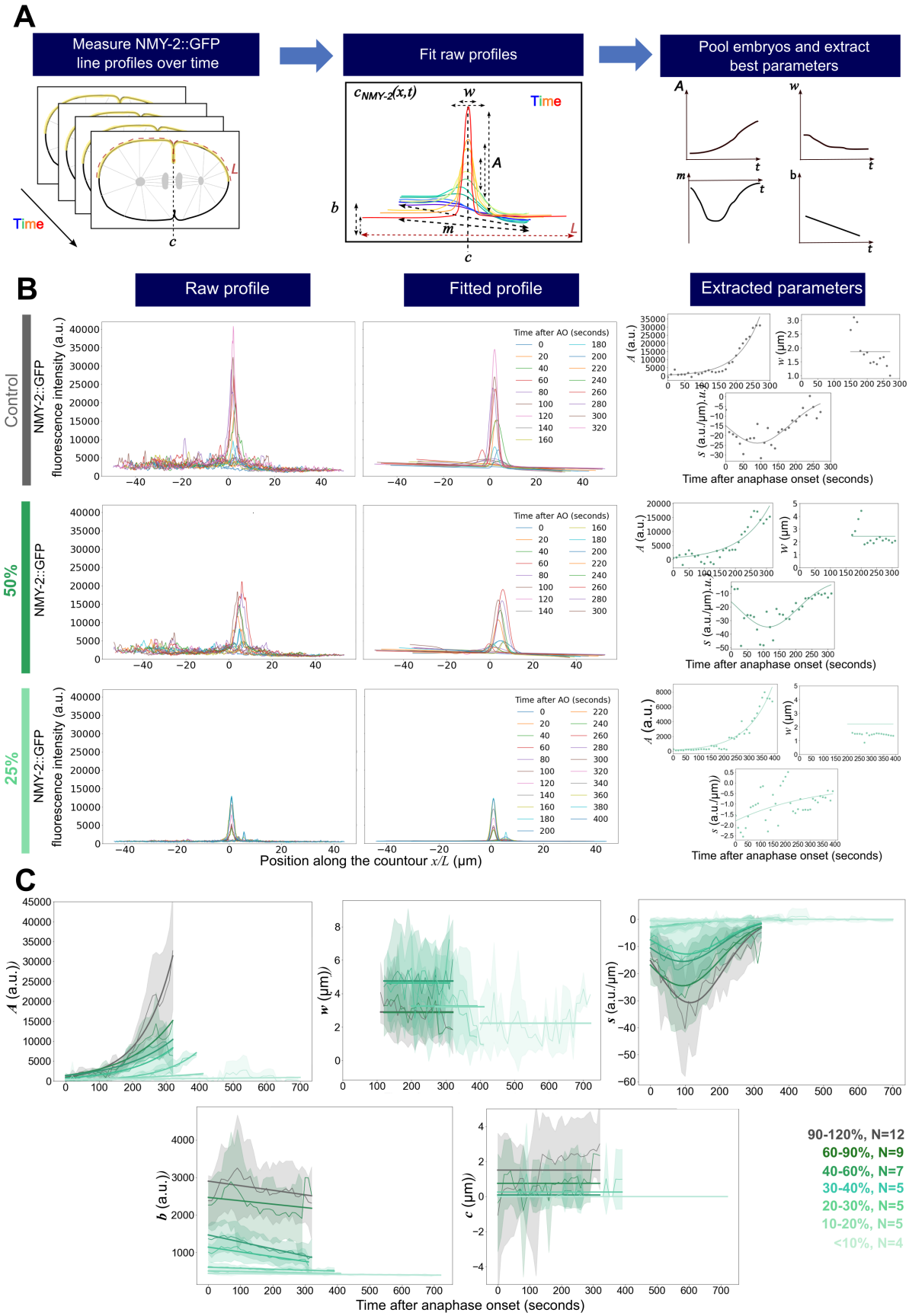

FIGURE 5.2. Spatiotemporal measurements of myosin concentration along the cortex. (A) Schematic illustrating the procedure used to measure and fit NMY-2::GFP line profiles in controls and NMY-2 depleted

embryos. Line profiles were traced for each timepoint from anaphase onset until the end of constriction, using the segmented line tool from Fiji, as illustrated by the yellow line (Left). The measurements start at the anterior pole towards the posterior and on the side where the furrow ingresses first and deeper. Each raw profile was fitted with a composite of a gaussian and a linear function (Middle). This yielded the representation of myosin concentration as a function of position and time, $c_{NMY-2}(x,t)$, by the parameters extracted from these fittings: amplitude A, width w, slope m, intercept b and center c (Right).

(B) Examples of raw (Left) and fitted (Middle) NMY-2::GFP profiles, as well as extracted parameters (Right) for the conditions indicated. For simplicity, only three depletion levels are displayed. The raw profiles were fitted with a composite of a gaussian and a linear function for each timepoint as sketched in (A). This was performed for every timepoint (timelapse = 10 seconds), however it was plotted only every 20 seconds for visibility purposes. The functional form of the profiles is described by five parameters - amplitude A, width w, slope m, intercept b and center c - but only the first three were plotted for simplicity.

(C) Best parameters (amplitude A, width w, slope m, intercept b and center c) extracted from the fittings of the average NMY-2 profiles exemplified in (B), from anaphase onset until the end of constriction for the indicated depletion levels. The thin lines and shaded regions are the averages and standard deviations of several embryos. The thicker lines are the respective fittings of the thin lines over time using the functions indicated in Table 5.3 of "Materials and Methods" for each parameter.

Computational simulations with varying contractility levels were not able to reproduce the experimental data. In these simulations, the rate of ring closure decreased linearly with the decrease in myosin levels (Figure 5.3A,C). This was expected as, according to the mathematical formulation of the model, there are two components of the cortical tension - an active and a viscous contribution – and myosin was set to only affect the active component.

As discussed in the previous subsection, a possibility could be that myosin has an additional contribution to cortex mechanics that does not necessarily involve its motor activity. It has been shown that myosin phosphorylation levels are decreased outside the equatorial region where the contractile ring forms (deBiasio et al., 1996)(Matsumura et al., 1998, Yamashiro et al.,2003). This raises the question whether the myosin outside the RhoA zone is indeed active, and, if not, whether it could still bind actin filaments and contribute to the overall viscosity of the cortex.

With this in mind, the model general equation has been changed again, this time to contain a myosin-dependent viscosity contribution. The viscosity of the network, which previously corresponded to a constant value η_0 is now given by $\eta(x,t) = \eta_0 + c_{myo}\eta_{myo}$, where $c_{myo}\eta_{myo}$ is the myosin-dependent viscosity contribution and varies with myosin levels. Thus, the functional forms of contractility $\zeta(x,t)$ and viscosity $\eta(x,t)$ can be written, respectively, as

$$\zeta(x,t) = \alpha(x,t)c_{myo}(x,t), \qquad (5.5)$$

and

$$\eta(x,t) = \eta_0 + \eta_{myo}(1-\alpha(x,t))c_{myo}(x,t), \quad (5.6)$$

where $c_{myo}(x,t)$ is parametrized as $c_{myo}(x,t) = mx + b + Ae^{-\frac{x^2}{2w^2}}$.

A new parameter α defines the fraction of myosin that contributes to activity or viscosity. Simulations with this updated framework revealed that the ring constriction rate remain similar across a wide range of contractility only if myosin-dependent viscosity was decreased proportionally with contractility when myosin levels are reduced, as shown in the radius evolution *versus* time curves, which all collapse together until a certain threshold (Figures 5.3B,D).

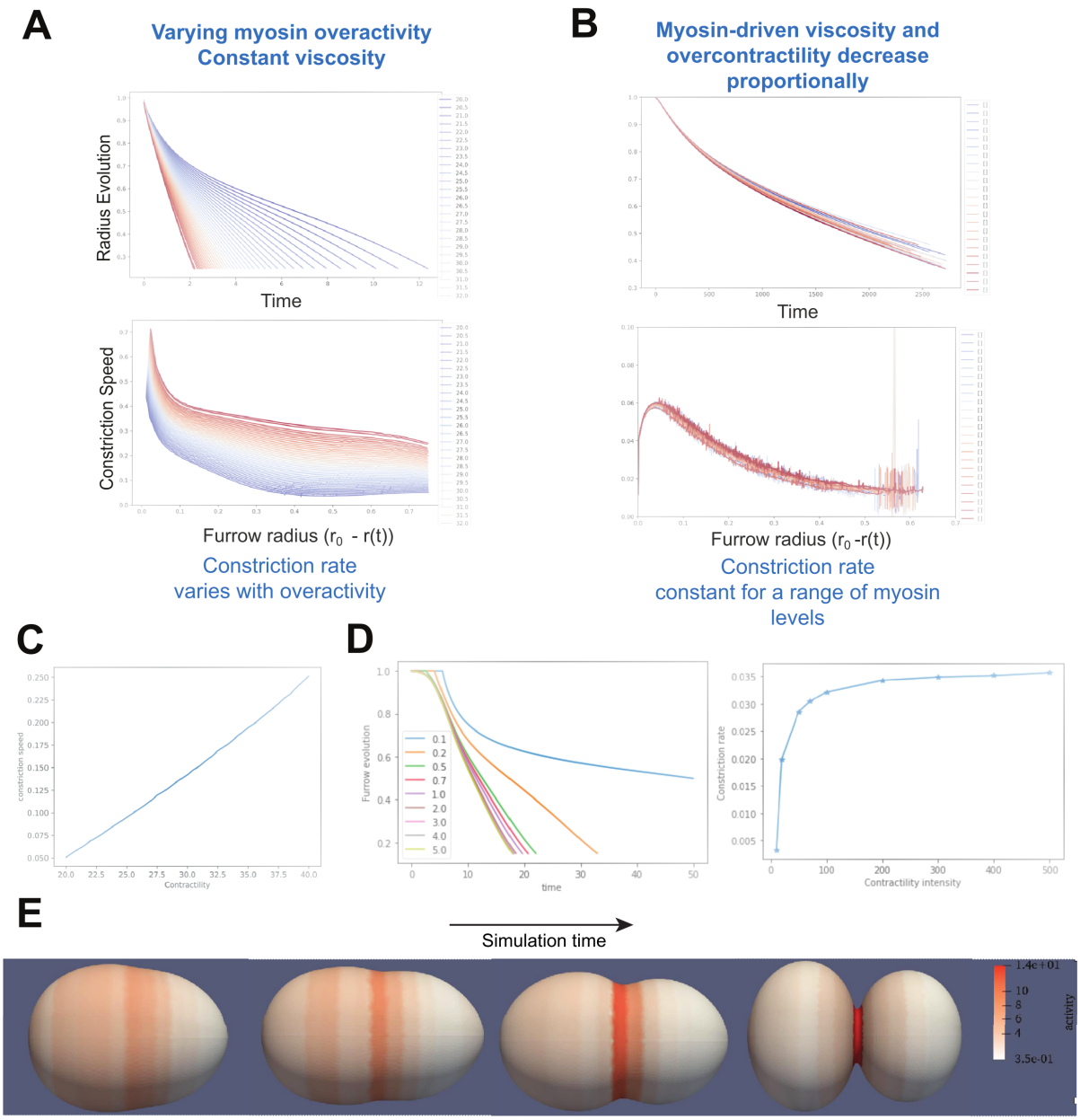

FIGURE 5.3. **Simulations using a 3D finite element model of the whole embryo suggest that myosin-driven contractility and myosin-dependent viscosity must decrease proportionally to maintain a constant ring constriction velocity over a range of myosin levels. (A)** Simulations for different levels of myosin overactivity using the model of contractility in Eq. (5. 2). Radius evolution vs. time (top) and constriction speed vs furrow radius (bottom) are plotted. **(B)** Simulations employing the modifications proposed in Eqs.(5. 7) and (5. 4). It is considered that from the total myosin, a constant fraction of myosin contributes to viscosity and the rest to contractility. The fraction of myosin that contributes to activity/viscosity can be varied. Radius evolution vs. time (top) and constriction speed *versus* furrow radius (bottom) are plotted. **(C)** Constriction rate vs contractility intensity for simulations not considering a myosin viscous contribution. **(D)** Simulations considering different fractions of myosin contributing to viscosity of the cell cortex. Left: Furrow evolution *versus* time. Right: Constriction rate *versus* contractility intensity. **(E)** Representative example of a 3D simulation using an in vivo myosin profile of a *wildtype* embryo. The scale represents activity/contractility on the cortical layer. The embryo is not confined by a rigid barrier representing the eggshell.

These simulations did not yet include the *in vivo* myosin profiles as we are struggling with having all of them constrict, even with the previous framework (Eq. (5. 2)) that does not yet consider the myosin-viscosity contribution. This is mainly due to the ratio of contractility between the equator and the poles required for full constriction in the model, which is around 14-fold (Borja da Rocha, Bleyer and Turlier, 2022). Looking at the average profiles in Figure 5.2B, the myosin ratio between the equator and the poles for controls is approximately 8-fold at the maximum and the remaining conditions are even lower than this.

To solve this issue, two approaches are being adopted.

First, nematic filament orientation is being implemented in the model as this is expected to lower the 14-fold ratio needed for constriction to about 7-fold.

Second, RhoA profiles are being quantified with the Rho biosensor GFP::AHPH, a proxy for active RhoA that contains the RhoA-binding domain of Anillin (Tse et al., 2012). This is expected to serve two purposes: 1) mimic the *in vivo* scenario, where myosin concentration alone is not sufficient for constriction, as it relies on RhoA-mediated activation, confined to the equatorial cortex (note that this conveniently favors the contractility over the viscosity fraction at the equator, while the cortex outside the ring remains mostly viscous and not contractile); 2) help defining the myosin contractility and the myosin-dependent viscosity components, controlled by the α parameter. The RhoA profile is normalized between 0 and 1 to represent the fractions of myosin-dependent contractility α and viscosity $(1 - \alpha)$.

Figure 5.4 shows preliminary quantifications of GFP::AHPH (hereafter, RhoA) line profiles in *wildtype* embryos, as well as estimations of the α parameter for different myosin levels. The profiles were measured using the same procedure of the myosin$^{NMY\text{-}2}$::GFP profiles, as indicated in Figure 5.2A. Unfortunately, the GFP::AHPH probe is extremely dim under confocal microscopy, as shown on cortical and central planes images of these embryos (Figure 5.4A), despite stronger laser power and longer exposure times have been employed. Accumulation of RhoA is only clearly visible close to when the back-to-back membrane configuration occurs. This is also visible in the line profiles shown in Figure 5.4B. We are not completely certain whether the accumulation starts earlier and we are simply unable to resolve it due to the poor probe signal. RhoA profiles in Figure 5.4B were fitted with a gaussian with constant offset (see Table 5.3 in the “Materials and Methods” section), as an asymmetry of intensities between the anterior and posterior poles was not observed. The average of the extracted best parameters across all examples and its fitting is also shown in Figure 5.4C. The difference between the amplitude A and the baseline b is slightly smaller than for the NMY-2::GFP signal (4-fold *versus* 6- to 10-fold, respectively), which can also be a consequence of

the signal to noise ration. As expected, the width w is similar to the NMY-2::GFP signal, around 4 μm.

As mentioned above, the localization and temporal evolution of RhoA dictate whether myosin is active or inactive. Figures 5.4A, B and C showed that indeed RhoA accumulates only at the equatorial region over time, thus activity levels outside the equator are likely residual. Figure 5.4D-Left illustrates this spatial distribution of active and inactive myosin. This global distribution impacts the contractility α and viscosity $(1-\alpha)$ fractions, as depicted in 5.4D-Right. Note that although these are fractions of the total myosin profile (see Eqs. (5. 3) and (5. 4)) and the general shape of the curves is maintained, this favors contractility over viscosity at the equator and the opposite in the surrounding cortex.

Finally, we averaged both the myosin profiles for each range of myosin levels and the RhoA profiles and multiplied them element-wise to obtain the activation fraction α for each position along the membrane and for every timepoint (Figure 5.4D). The average RhoA profiles were normalized to the maximum value and are expressed between 0 and 1. Figure 5.4E shows estimations of the α parameter for the indicated myosin percentages and their fittings.

Even though we do not have reasons to believe RhoA intensities will change upon myosin depletions (Basant and Glotzer, 2018b; Michaux *et al.*, 2018), these profiles should be measured for the whole range of myosin percentages from Figures 5.1, S5.1 and not just for control embryos. This will not only lend further reassurance of the results, but also allow the precise alignment of myosin and RhoA profiles in space and time (note that we could temporarily use the control GFP::AHPH profiles until 70-80% of myosin depletion because the kinetics are similar to controls, but this does no longer work for stronger depletions with slower kinetics).

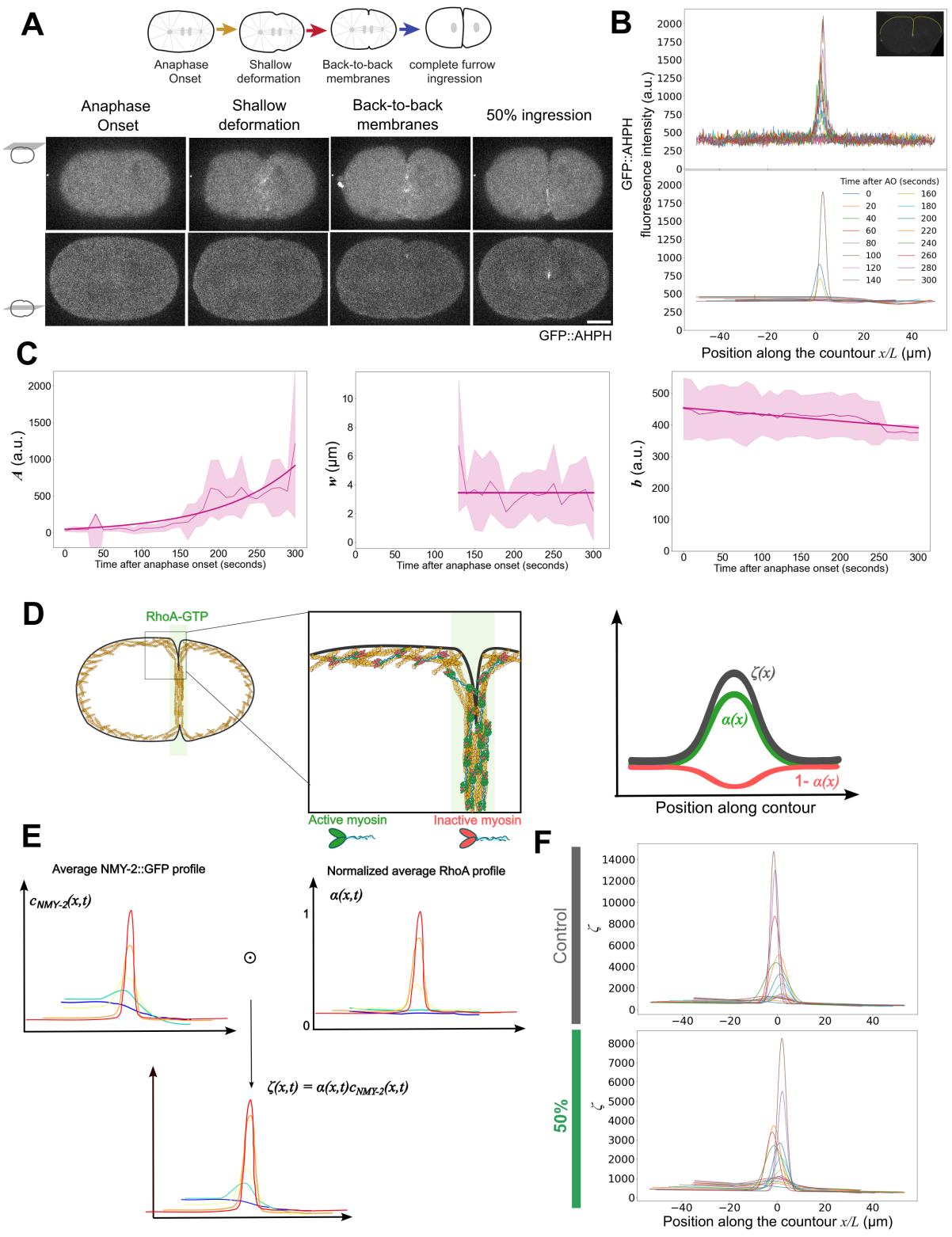

FIGURE 5.4. **Spatiotemporal measurements of RhoA levels along the cortex. (A)** Representative central plane and cortical confocal images of embryos expressing GFP:AHPH (a proxy for RhoA) for the time points indicated in the schematic. **(B)** Examples of raw (Top) and fitted (Bottom) GFP::AHPH profiles. The raw profiles were fitted with a gaussian with constant offset for each time point. was performed for every timepoint (timelapse = 10 seconds), however it was plotted only every 20 seconds for visibility purposes. The functional form of the profiles is described by four parameters - amplitude A, width w, center c and offset b. **(C)** Best parameters (amplitude A, width w, offset

b and center c) extracted from the fittings of the average GFP::AHPH profiles exemplified in (B), from anaphase onset until the end of constriction, for the indicated depletion levels. The thin lines and shaded regions are the averages and standard deviations of several embryos. The thicker lines are the respective fittings of the thin lines over time using the functions indicated in Table 5.3 of "Materials and Methods" for each parameter. **(D) Left -** Schematic illustrating the effect of the RhoA activation zone on myosin activation. Myosin may exist in two states throughout the cortex: active and inactive. RhoA triggers a signaling cascade at the equatorial cortex, increasing myosin activation levels there, whilst myosin in the surrounding cortex remains mostly inactive. **Right –** Schematic illustrating the behavior of the contractility $\alpha(x,t)$ and viscosity $\eta(x,t)$ fractions of the contractile stress $\zeta(x,t)$. **(E)** Schematic depicting how the activation fraction $\alpha(x,t)c_{myo}$ is obtained. RhoA profiles $c_{RhoA}(x,t)$ are normalized by the maximum and averaged across several examples, giving $\alpha(x,t)$. This is multiplied by the averaged myosin profiles $c_{NMY-2}(x,t)$ to yield the contractile stress $\zeta(x,t)$. **(F)** Examples of the $\alpha(x,t)c_{myo}(x,t)$ obtained the myosin levels are indicated (refer to Figure 5.1). Scale bar, 10 μm.

For illustration purposes, an example of a simulation using an *in vivo* myosin profile of an embryo whose furrow constricted is displayed in Figure 5.3E. The color scale represents contractility of the cortical layer. It is possible to observe that the embryo adopts an elongated ellipsoid shape typical of the *C. elegans* embryo, a property obtained by simply loading the intensity measurements from the myosin profiles. However, this simulated embryo is not yet confined by a rigid ellipsoid barrier to mimic the eggshell. If implemented, this is expected to yield more realistic shapes. Finally, Figure 5.3G shows simulations (purely theoretical) with varying levels of the α parameter, which allows some myosin to contribute to viscosity. For a range of values of this parameter, the simulations were able to reproduce the threshold observed in the experimental data, where the constriction rate starts to become affected around 20-30% of the average of controls. The combination of experiments and theory seem to indeed indicate a role for myosin in acting as a viscous component of the cortex. However, it would be interesting to experimentally recreate a situation where the amounts of "active" and "inactive" myosin could be more precisely controlled.

Expressing an increasing amount of inactive myosin slows down the constriction rate progressively

To further investigate the possible myosin's contribution to viscosity, we used a *C. elegans* mutant strain where the myosin regulatory light chain MLC-4 cannot be phosphorylated, rendering myosin permanently inactive.

This strain was generated by creating point mutations at residues Threonine-17 and Serine-18 (Figure 5.5A-Left), which were both replaced by Alanine (Ala). Importantly, this region is highly conserved among species (Figure 5.5A-Right). As myosin motor activity is required for a myriad of processes in the worm, worms carrying these mutations were not viable. To be able to propagate the animals, a MosSCI strategy was used (see Chapter I, subsection "Mos1-

mediated Single Copy Insertion" and "Materials and Methods" of this chapter), where a *mlc-4* transgene expressing the mutations has been introduced in the genome (Figure 5.5B). This way, it was possible to maintain the endogenous *mlc-4,* that would still allow for animal viability and propagation, and deplete it by *RNAi* to assess the effect of expressing increasing amounts of the non-phosphorylatable *MLC*-4. The *mlc-4* transgene has been reencoded so that it is resistant to the *RNAi* depletion (Figure 5.5B).

Hereafter, the following notation will be used: *mlc-4AA;mlc-4* and *mlc-4WT;mlc-4* to denote the genotypes of the respective mutated and *wildtype* strains, MLC-4AA::GFP and MLC-4WT::GFP to denote the GFP-tagged mutated and the *wildtype* transgenes and MLC-4 or *mlc-4* to denote the endogenous protein or gene, respectively. Of note, full *mlc-4(RNAi)* on the *mlc-4AA;mlc-4* led to cytokinesis failure, indeed confirming that myosin activation through di-phosphorylation on Threonine-17 and Serine-18 is an essential requirement for the process (Figures S5.2A,B). Full *mlc-4(RNAi)* of the control strain *mlc-4WT;mlc-4* always resulted in timely cytokinesis completion.

Cortical images of these strains crossed with a probe for the myosin heavy chain, NMY-2::mKate2, revealed that both the transgenic versions MLC-4WT*::GFP* or MLC-4AA::GFP co-localize at some extent with NMY-2::mKate2 (Figure 5.5C). Despite myosin hexamers having two RLCs, a heavy chain and two ELCs (Figure 5.5A-Left), these are encoded by different genes. Here, we consider that NMY-2::GFP tags the total myosin in the embryo (all the heavy chains available) whereas MLC-4WT::GFP or MLC-4AA::GFP only tag the transgenic *wild-type* and non-phosphorylatable light chains, respectively. This essentially means heavy chains could be coupled to transgenic light chains (tagged with GFP) and endogenous light chains (not tagged on these strains), forming bipolar filaments with heterotypical RLCs. As expected, both MLC-4WT::GFP (in co-expression of transgenic and endogenous *mlc-4)* and NMY-2::mKate2 concentrate in an anterior cap at anaphase onset and flow towards the equator showing the normal distribution in cortical patches throughout cytokinesis. Quite surprisingly, the non-phophorylatable MLC-4AA::GFP exhibits exactly the same localization pattern as MLC-4WT::GFP and NMY-2::mKate2. Moreover, it also accumulates in the ring with normal kinetics as its *wildtype* counterpart (Figure 5.5C). This implies that non-phosphorylatable light chains are likely incorporated into mixed bipolar filaments with the endogenous light chains, which still supports a completely normal cytokinesis.

To compare the effect of expressing increasing amounts of a myosin that cannot be activated (non-phosphorylatable) but remains attached to the cortex with total myosin depletions (*nmy-2(RNAi*) time course), a RNAi time course of a endogenous MLC-4 in one-cell embryos from the abovementioned strains was performed. Kinetical parameters of

cytokinesis were assessed in relation to the levels of MLC-4AA::GFP and MLC-4WT::GFP at the furrow tip.

Progressively stronger depletions of endogenous MLC-4 resulted in increasing levels of the transgenic proteins, as shown in Figure 5.5D-Top. We think this is because when both forms are available, the embryo may preferentially use the untagged MLC-4 form (in this case, the endogenous). However, as the endogenous starts being depleted, the embryo is forced to use progressively more of the tagged transgenic MLC-4 form. It is important to mention that this is not related with the presence of the mutation because the MLC-4AA::GFP levels increase similarly to the MLC-4WT::GFP levels for the same depletion level of the endogenous protein (Figure 5.5D-Middle). Importantly, we also have indication that total amount of NMY-2::GFP does not seem to change significantly upon progressive depletions of endogenous MLC-4 in the *mlc-4AA;mlc-4* mutant strain, which in principle indicates that the total myosin is not increasing or decreasing, but rather the ratio between the active and inactive fractions is changing (data not shown). However, this must be confirmed in the near future.

Like in the NMY-2 depletion time course (see Figure 5.1), measurements of MLC-4 fluorescence intensity were also performed at the tip of the furrow in central plane images, where the contractile ring has reached 50% of its initial diameter (Figure 5.5C). Furthermore, the same reference and kinetic measurements were employed (Figure 5.1A,5.5C).

Plotting the ring assembly time and the contractile ring closure rate as a function of MLC-4AA::GFP levels revealed that these increase or decrease, respectively, in a more or less linear fashion with increasing levels of MLC-4AA::GFP, which corresponds to the inactive myosin fraction (Figure 5.5E,F,G). Note that in the non-depleted embryos of the same strain, the kinetics are still normal, which is an important observation because they already co-express a fraction of non-phosphorylatable myosin, yet kinetics are not affected. We do not know exactly the relative expression levels of the endogenous *versus* the transgenic proteins as we only tagged the transgenic one, but it is fair to assume that the two forms express in a 1:1 ratio. As expected, the MLC-4WT::GFP levels in the control strain (*mlc-4WT::GFP;mlc-4*) also increased with increasing levels of endogenous MLC-4 depletions, but the ring assembly and furrow initiation intervals, as well as the constriction rate were not affected. For the sake of simplicity, we do not show the diameter *versus* time curves for these embryos, as the ones shown on Figure 5.5F for the *mlc-4AA;mlc-4* mutant embryos suffice to convey the message.

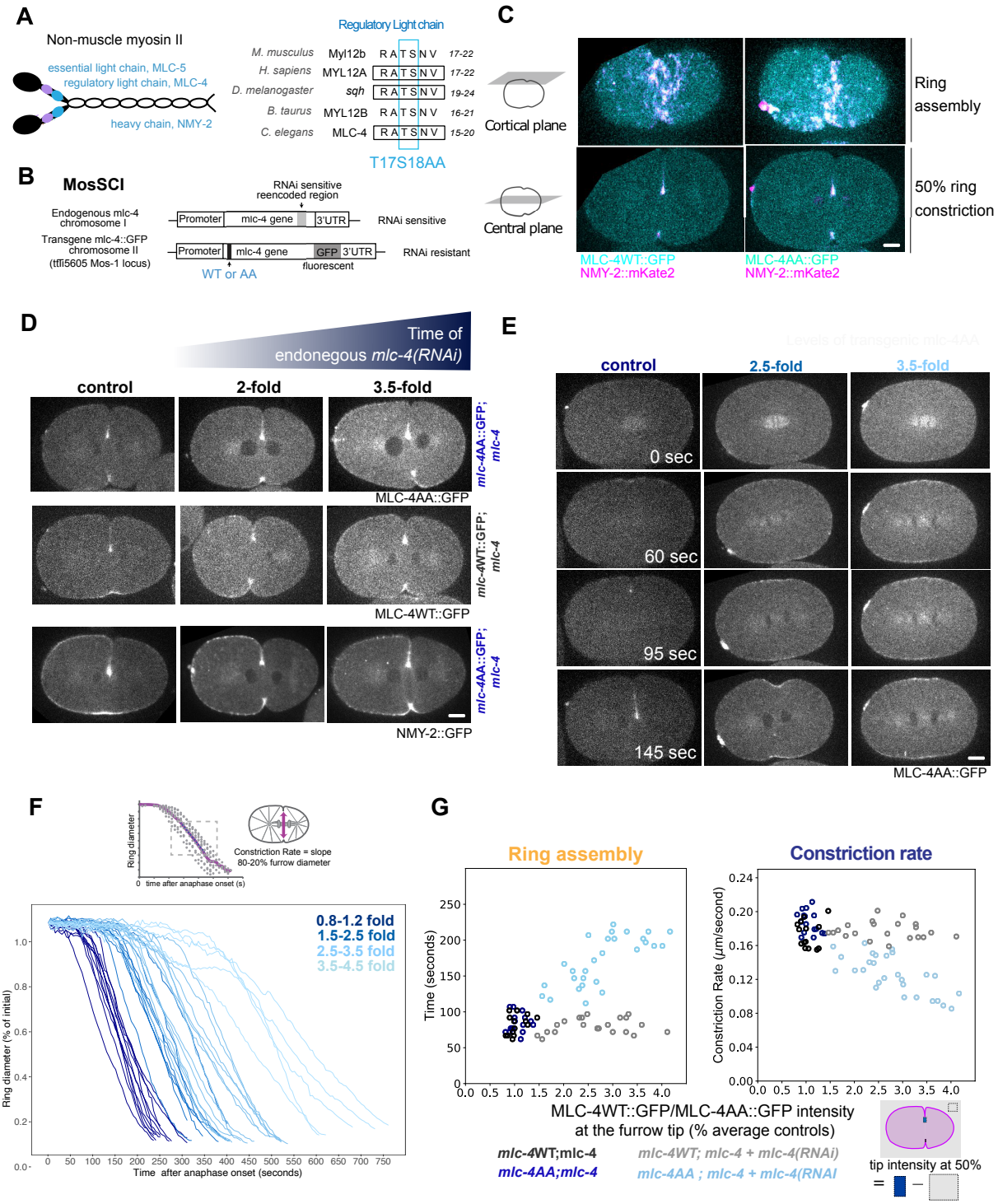

Figure 5.5. Expressing an increasing amount of inactive myosin slows down the constriction rate progressively. (A) Left - Illustration of the myosin hexamer; **Right -** Sequence alignments showing the conservation of the two amino acids known to regulate myosin RLC phosphorylation among different species. **(B)** MosSCI strategy used to generate a viable *C. elegans* strain expressing a non-phosphorylatable MLC-4. The transgene carries the mutation and is resistant to RNAi, while the endogenous *mlc-4* can be progressively depleted by *RNAi*. **(C)** Co-localization of MLC-4WT::GFP and MLC-4AA::GFP with NMY-2::mKate2 in the cortical and central plane images of one-cell embryos. **(D)** Representative images of the indicated genotypes illustrating the effect of progressively depleting the endogenous MLC-4 on the MLC-4AA::GFP and MLC-4WT::GFP fluorescence intensities in one-cell embryos. **(B)** Schematic showing the regions used for MLC-4AA::GFP or MLC-4WT::GFP

fluorescence intensity measurements in the furrow tip and camera background. **(E)** Central plane images over time corresponding to the indicated folds of MLC-4AA::GFP fluorescence intensities for depletions of the endogenous MLC-4 compared to non-depleted controls. The chosen time points correspond to the shallow deformation, back-to-back membrane configuration and 50% ingression of controls for all depletion levels. **(F)** Diameter *versus* time curves for each example of the *mlc-4AA;mlc-4* mutant with or without endogenous *mlc-4(RNAi).* The dashed box in the schematic depicts the interval of diameters used to calculate the constriction rate. **(G)** Time of ring assembly and constriction rate *versus* MLC-4AA::GFP or MLC-4WT fluorescence intensity (percentage of control average intensity, depending on the indicated genotype**.** All image intensities are scaled equally. Scale bar, 10 μm.

It should become clear at this point that expressing increasing levels of an inactive myosin artificially (Figure 5.5) does not affect cortex mechanical properties the same way as depleting myosin does (Figure 5.1) and works here as a way to recreate a scenario where we can precisely control the amount of an inactive form. In the first case, the regulatory light chain cannot be phosphorylated, therefore cannot exert motor-activity due to the inhibition of the myosin ATPase cycle. Yet, that myosin remains associated with the cortex. Though this challenges the prevalent idea that myosin tetramers with unphosphorylated regulatory light chains cannot be incorporated in bipolar thick filaments as the tails are in a closed conformation (based purely in some *in vitro* studies), we reasoned that this inactive myosin could in fact be capable of assembling into bipolar filaments and binding actin. Assuming this is true, then expressing increasing amounts of this myosin should not only decrease contractility, but also increase viscosity of the cortical layer. In the case of NMY-2 depletion, the amount of myosin bipolar filaments at the cortex is being indeed reduced, which, again assuming our hypothesis is correct, means that both cortex contractility and viscosity must decrease proportionally.

Since there is not an implemented method to measure the cortex mechanical properties in *C. elegans* embryos due to the presence of a rigid eggshell that precludes the use of techniques such as AFM or micropipette aspiration, the only way to test this hypothesis will be again through computational simulations. Of note, we tried to implement an assay which consisted in injecting very small (tens of nm) magnetic beads into the gonads of young adult worms, expecting those would be incorporated into the embryos upon fertilization. Then, a magnetic setup coupled to a confocal microscope could be used to pull the beads onto the cortex and apply appropriate magnetic fields to displace the beads long the cortical layer. The displacement of the beads was expected to provide information on the viscous properties of the cell cortex. The development of this technique encountered many difficulties that precluded its implementation during the timeframe of these doctoral studies. These included beads' size, clustering of the beads inside the microinjection needles and adherence to the glass walls

(which could not be solved by siliconizing the needles) and tuning of the beads' density that would allow enough beads to be injected while avoiding clustering.

As mentioned above, the model assumes that there are both an active and a viscous contribution for cortical tension. The idea is to use the same kind of profiles as for the *nmy-2(RNAi)* time course but now considering that a certain amount of myosin, which we can calculate precisely by calibrating the amount of MLC-4AA::GFP by the total myosin in the embryo (using a strain with untagged transgenic MLC-4AA co-expressing NMY-2::GFP or, preferentially, generate a strain expressing both MLC-4 forms (endogenous and transgenic) tagged with GFP(as illustrated in Figure S5.2D,E). This way we could have the amount of inactive/non-phosphorylatable myosin relative to the total, which would define a new fraction ρ_{AA}:

$$\rho_{AA} = \frac{[myo]^{AA}}{[myo]^{AA}+[myo]^{endo}} = \frac{inactive\ myosin}{total\ myosin} \qquad (5.5)$$

The contractility $\zeta(x,t)$ and the viscosity $\eta(x,t)$ of the cortical layer take the forms:

$$\zeta(x,t) = c^{endo}(x,t)(1-\rho_{AA}) \qquad (5.6)$$

$$\eta(x,t) = \eta_{basal} + \eta_{myo}\left[\big(1-\alpha(x,t)\big)(1-\rho_{AA})c^{endo}(x,t) + \rho_{AA}c^{AA}(x,t)\right], \qquad (5.7)$$

where

- η_{basal} corresponds to the basal (passive) viscosity and is given by actin filament network and actin crosslinking proteins.
- η_{myo} corresponds to the myosin-dependent viscosity.
- $c^{endo}(x,t)$ and $c^{AA}(x,t)$ represent the functional forms of the endogenous and transgenic *mlc-4*, respectively, which we expect to be well-fitted by a composite of a gaussian and a linear function, in similarity with the NMY-2::GFP signal (see Eqs. (5.3) and (5.4) and Figure 5.2).
- $(1-\alpha(x,t))(1-\rho_{AA})\ c^{endo}(x,t)$ represents a possible contribution to viscosity from the endogenous *mlc-4* (active myosin).
- $\rho_{AA}c^{AA}(x,t)$ represents the viscosity fraction contributed by the transgenic MLC-4AA (inactive myosin).

Note that by quantifying the amount of the transgenic MLC-4AA using the strain *mlc-4AA::GFP;mlc-4* and the total amount of *mlc-4* using the strain *mlc-4AA::GFP;mlc-4::GFP* (see

Figure S5.F,G), we can get the inactive fraction α_{AA} and the corresponding active fraction $(1 - \alpha_{AA})$.

Unfortunately, these strains and simulations were not finalized in due time for this thesis, but will be included on the manuscript we are preparing for submission.

Inhibition of the passive actin crosslinker plastin in inactive or motor-dead myosin mutant backgrounds accelerates ring constriction

To confirm whether the previous observations were indeed due to a possible increase in the cortex viscosity and not simply because there is less active myosin in the ring, which alone could also explain a decrease in the constriction rate, we considered a set of experiments that consisted in 1) deplete myosin^{NMY-2} progressively in a plastin^{PLST-1} mutant background that behaves like a *null* (see Chapter IV); and 2) deplete plastin^{PLST-1} on myosin mutants expressing a non-phosphorylatable RLC and/or myosin motor-dead mutants known to bind actin. If myosin indeed has a contribution in cortex viscosity, then it would be expected that in 1) constriction is facilitated for lower myosin levels, causing the threshold in the myosin depletion time course (Figure 5.1) where kinetics is affected to be even lower (less than the 30% observed for the *nmy-2(RNAi)* alone), and in 2) network viscosity is increased in these mutants and depleting the major crosslinker of the cortex in the *C. elegans* zygote would in turn decrease the excessive viscosity, ammeliorating the delay in the constriction rates observed in the mutants alone.

Depleting NMY-2 in a *plst-1(prt89)* background led to a faster constriction rate compared to NMY-2 depletions alone for a range of NMY-2::GFP levels between 75% and 26% of average control levels (Figure 5.6A,C). The maximum velocity for NMY-2 depletions in *wildtype* embryos was around 0.19 μm/seconds, while for depletions in a *plst-1(prt89)* background it reached more than 0.25 μm/second (Figure 5.6C). Unfortunately, a rescue or shift of the threshold towards lower NMY-2::GFP levels was not observed. This is in agreement with previous observations on Chapter IV, where NMY-2 depletions on this *plst-1* mutant fail cytokinesis much earlier than NMY-2 depletions in *wildtype* backgrounds. That explains why it was not possible to reach the threshold of the *nmy-2(RNAi)* alone, as cytokinesis fails during the assembly phase before the same levels of NMY-2::GFP are reached in *plst-1(prt89); nmy-2(RNAi)* embryos.

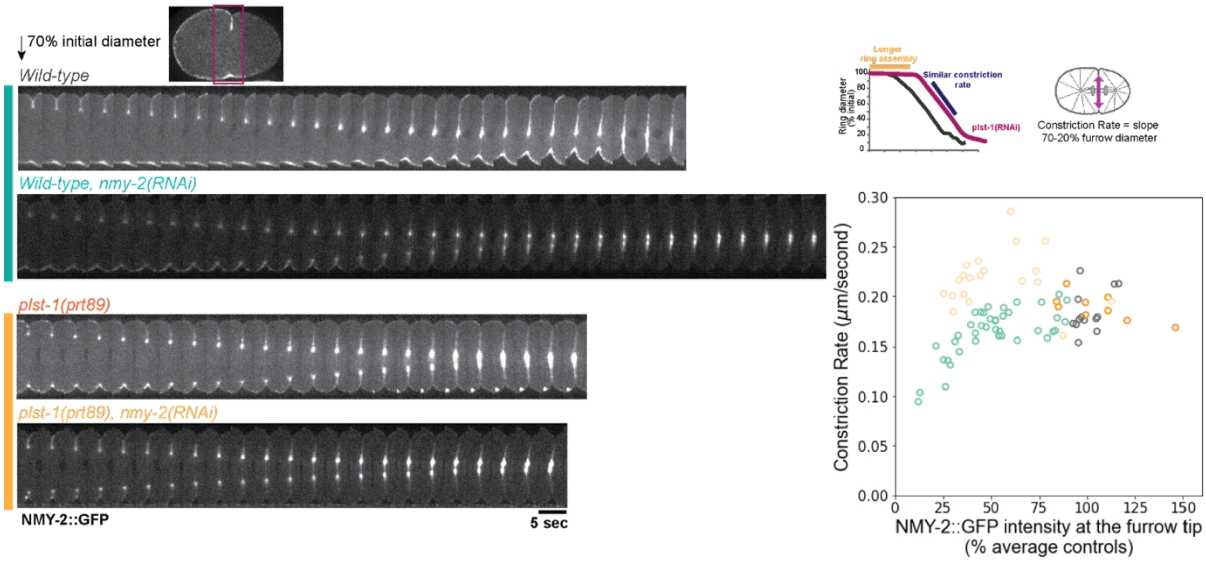

FIGURE 5.6. Plastin knockdown increases and rescues the ring closure rate in mildly and strongly NMY-2 depleted embryos. (A) Representative kymographs of the equatorial region in one-cell embryos for the conditions indicated in the legends. The first frame corresponds to 80% of the initial ring diameter. Image intensities were scaled equally. Timelapse, 5 seconds. **(B)** Schematic of the characteristic kinetics of diameter *versus* time curves between 70-20% initial ring diameter for *wildtype* and *plst-1*-mutant embryos. **(C)** Constriction rate as a function of the NMY-2::GFP levels at the furrow tip (% average of controls) for the indicated genotypes. Scale bar, 10 um.

To check whether decreasing viscosity by diminishing plastin levels on *mlc-4* mutants that we hypothesized to have a more viscous cortex (Figures 5.5, S5.2) could rescue the constriction rate, full *plst-1(RNAi)* was performed in *mlc-4AA::GFP;mlc-4* and *mlc-4WT::GFP;mlc-4* embryos, with and without depletion of the endogenous MLC-4 (Figure 5.7). For the experiments with depletion of the endogenous MLC-4 (double *mlc-4(RNAi); plst-1(RNAi)*), instead of performing *plst-1(RNAi)* over a range of MLC-4 depletions (as in Figure 5.6), we only performed one time point, before cytokinesis failed during the ring assembly phase(Leite *et al.*, 2020).

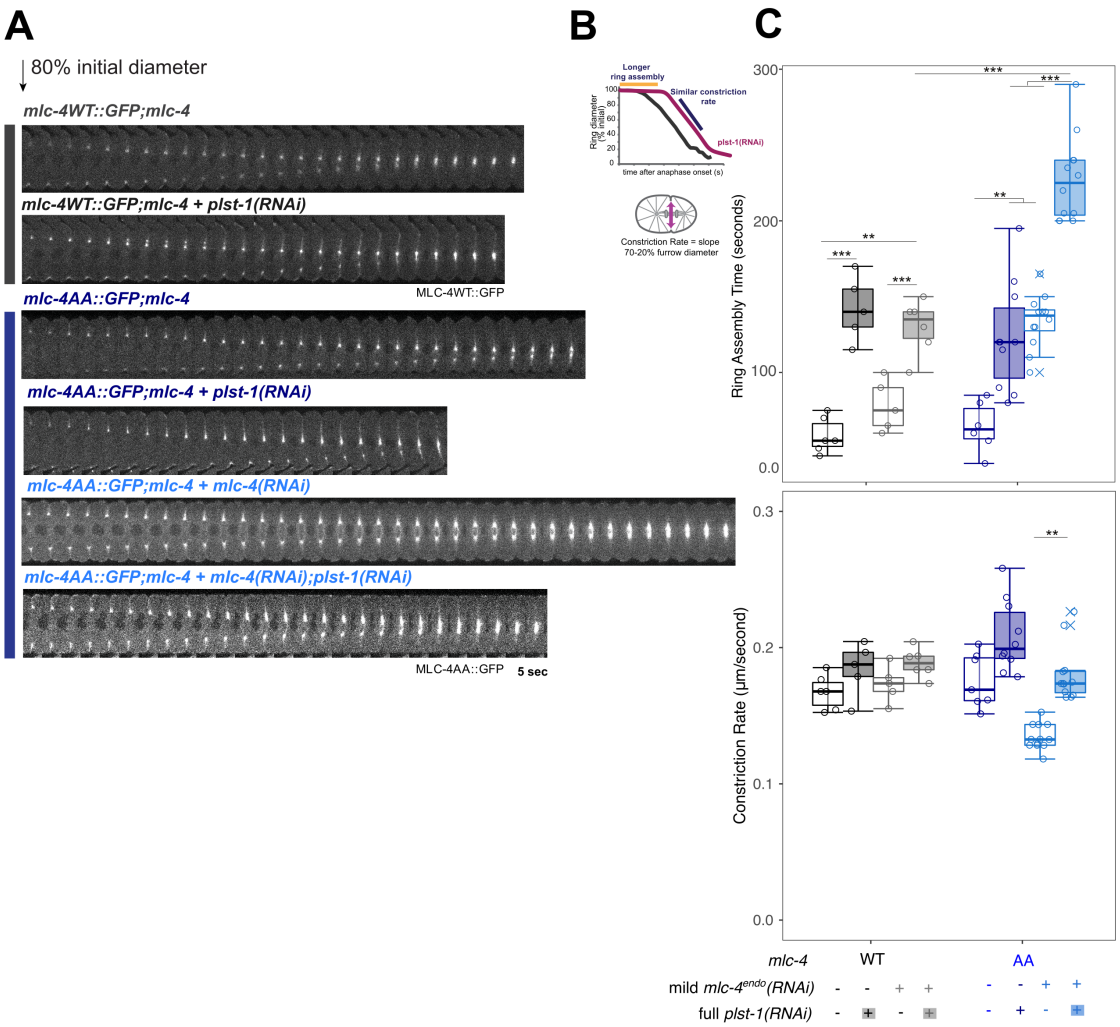

FIGURE 5.7. Depleting plastin^{PLST-1} and endogenous MLC-4 in *mlc-4AA::GFP;mlc-4 embryos* aggravates ring assembly times, but rescues the constriction rate to *wildtype* levels. (A) Kymographs of the equatorial region in central plane images of embryos with the indicated genotypes, with no depletion of the endogenous MLC-4 or PLST-1 or after mild depletion of MLC-4 alone, full PLST-1 depletion alone or MLC-4 and PLST-1 double depletion, as indicated in the legends. Shown is the fluorescent signal of transgenic MLC-4WT::GFP or MLC-4AA::GFP. Timelapse, 5 seconds. **(B)** Schematic of the characteristic kinetics of diameter *versus* time curves for control and *plst-1*-depleted embryos. **(C)** Boxplots showing ring assembly times (Top) and constriction rates (Bottom) for the indicated genotypes, as in (A). The colors of the boxes identify the perturbations. In each box, the central line is the median, the boundaries of the box are the 25th (Q1) and 75th (Q3) percentiles and define the interquartile range (IQR); the whiskers extend to include the maximum (Q3 - 1.5xIQR) and minimum (Q1 - 1.5xIQR) values; outlier data points are defined as any value reaching past 1.5 times the IQR from either the lower or upper quartile and are labeled with a "X" on the top. Statistical significance was determined with Kruskal-Wallis non-parametric test, followed by Dunn's post-hoc test for multiple comparisons; ***P≤0.001; **P≤0.01; *P≤0.05; ns, not significant (P>0.05). Non-significant differences (ns) were not included on the plots for simplicity. Some statistical relationships were also not included in cases where that can be trivially inferred from the indicated ones. Scale bars: 10 µm.

Median ring assembly times were around 2.5-fold longer for embryos expressing MLC-4AA::GFP depleted of PLST-1 or MLC-4 alone compared to non-depleted embryos. This

difference was even more drastic for double depletions, where ring assembly times were 4.6-fold longer than those in non-depleted embryos and 1.6-fold longer when compared to the single depletions (Figure 5.7A,C). The single depletions on the control *mlc-4WT::GFP;mlc-4* strain also had a similar, albeit weaker effect on the ring assembly times, but conversely, no additive effect was observed for the double depletions. This is in agreement with our previous studies that showed NMY-2 and PLST-1 cooperate to timely align F-actin bundles in the contractile ring for cytokinesis to succeed and that this synergy requires specifically the bundling activity of PLST-1 and the motor-activity of NMY-2 (Leite et al., 2020).

During the constriction phase, *plst-1(RNAi)* on the *mlc-4AA::GFP;mlc-4* mutant background already showed a tendency for a faster constriction rate than non-depleted embryos, yet this was not statistically significant. As expected, single endogenous *mlc-4(RNAi)* on these mutants led to a 1.5-fold decrease in the median constriction rate compared with non-depleted counterparts. In agreement with the hypothesis of a more viscous cortex caused by an increased expression of inactive myosin (MLC-4AA), double depletions of MLC-4 and PLST-1 led to a rescue of the slower constriction rate of single MLC-4 depletions to normal levels. For the control strain *mlc-4WT::GFP; mlc-4*, no differences were observed in the constriction rate for any of the four conditions (Figure 5.7C).

Performing a similar experiment with NMY-2 motor-dead mutants proven to bind actin (Osório *et al.*, 2019) yielded similar, albeit more drastic observations (Figure 5.8). These mutant embryos express endogenous mutated myosin (NMY-2(R252A) or NMY-2(S251A)) , and transgenic and RNAi-sensitive myosin (NMY-2^{sen}). Median ring assembly times were 4- and 3.5-fold longer in *nmy-2(R252A);nmy-2^{sen}* and *nmy-2(S251A);nmy-2^{sen}* embryos depleted of PLST-1 than in non-depleted ones. Although the difference was not significant, these myosin motor-dead mutants displayed a tendency for a slower constriction rate when co-expressed with a *wildtype nmy-2* transgene, suggesting motor-activity was already decreased (Figure 5.8A,B). Co-expression of motor-dead myosin (NMY-2(R252A) or NMY-2(S251A)) with *wildtype* myosin (NMY-2^{sen}) likely leads to the assembly of heterotypic myosin filaments with some heads being *wildtype* and others motor-dead. When PLST-1 was depleted in these backgrounds, rings constricted significantly faster. It is intriguing why there is such a great effect on the acceleration of ring closure. , which is so much more drastic than that observed for the same depletion in *mlc-4AA::GFP;mlc-4* embryos (Figure 5.7). We speculate that the difference could be related with how strongly each of these myosin forms binds actin.

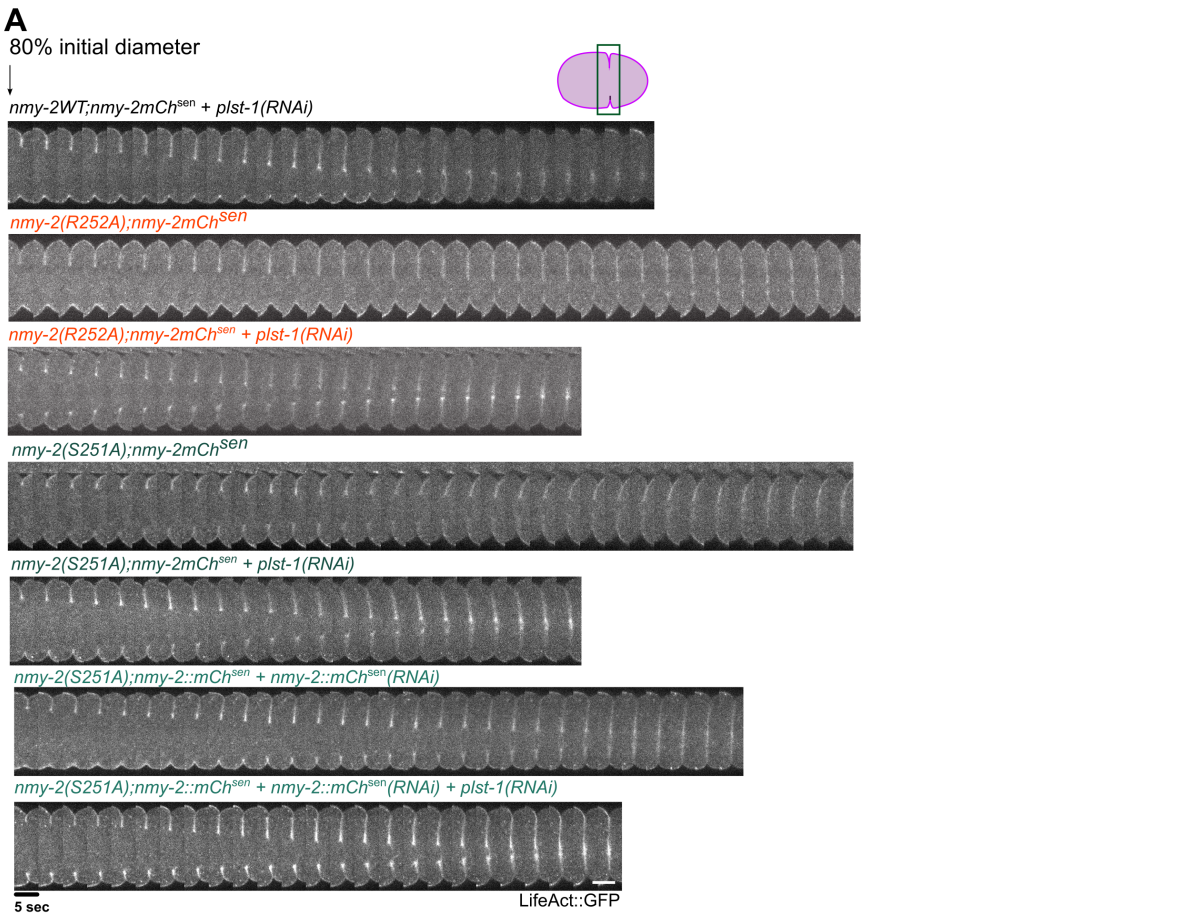
A
80% initial diameter
nmy-2WT;nmy-2mCh^sen + plst-1(RNAi)
nmy-2(R252A);nmy-2mCh^sen
nmy-2(R252A);nmy-2mCh^sen + plst-1(RNAi)
nmy-2(S251A);nmy-2mCh^sen
nmy-2(S251A);nmy-2mCh^sen + plst-1(RNAi)
nmy-2(S251A);nmy-2::mCh^sen + nmy-2::mCh^sen(RNAi)
nmy-2(S251A);nmy-2::mCh^sen + nmy-2::mCh^sen(RNAi) + plst-1(RNAi)
5 sec
LifeAct::GFP

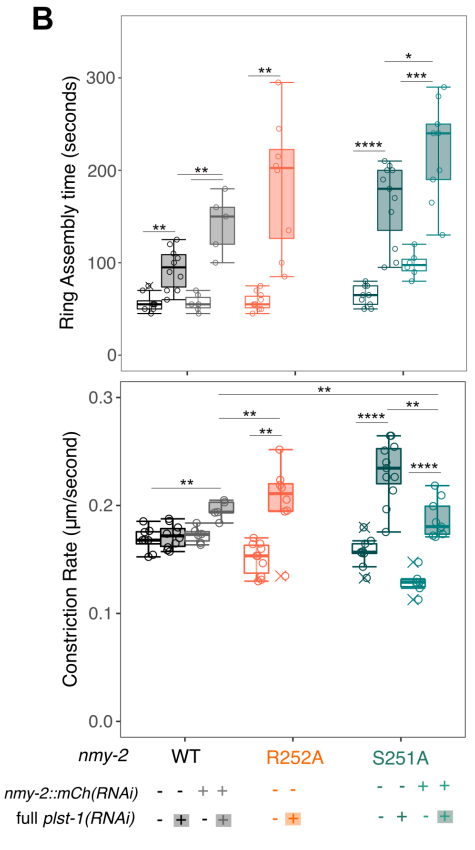
B
Ring Assembly time (seconds)
Constriction Rate (µm/second)
nmy-2
WT
R252A
S251A
nmy-2::mCh(RNAi)
full plst-1(RNAi)

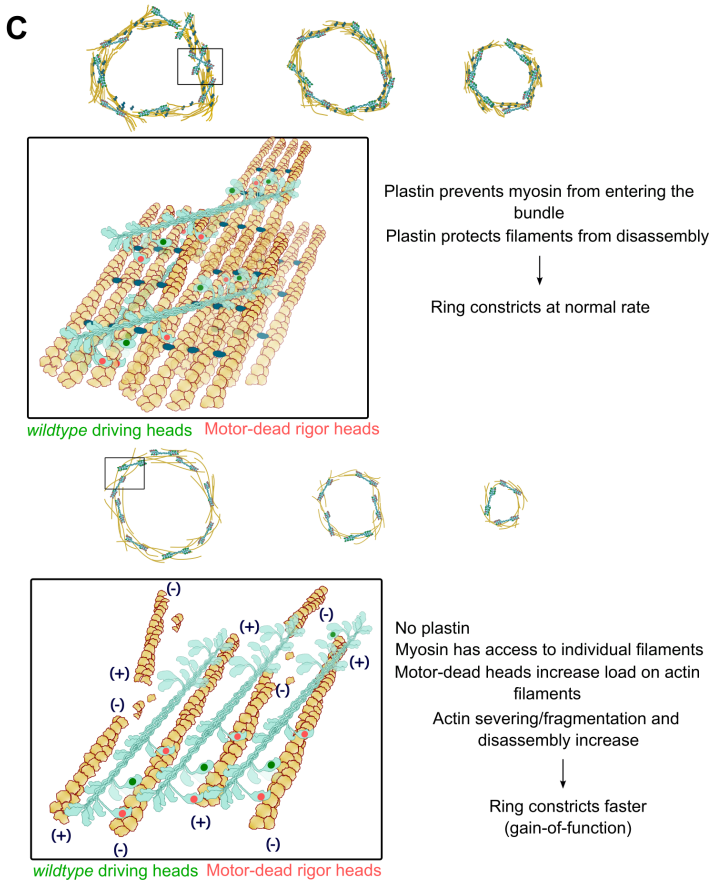
C
wildtype driving heads
Motor-dead rigor heads
Plastin prevents myosin from entering the bundle
Plastin protects filaments from disassembly
Ring constricts at normal rate
No plastin
Myosin has access to individual filaments
Motor-dead heads increase load on actin filaments
Actin severing/fragmentation and disassembly increase
Ring constricts faster (gain-of-function)

FIGURE 5.8. Depleting plastin in two motor-dead myosin mutants known to bind actin leads to longer ring assembly times and faster constriction rates than *wildtype*. (A) Kymographs of the equatorial region in central plane images of embryos with the indicated genotype. The fluorescent tag is LifeAct::GFP. Timelapse is 5 seconds. **(B)** Boxplots showing ring assembly times and constriction rates for the indicated genotypes. The colors of the boxes identify the perturbations. In each box, the central line is the median, the boundaries of the box are the 25th (Q1) and 75th (Q3) percentiles and define the interquartile range (IQR); the whiskers extend to include the maximum (Q3 - 1.5xIQR) and minimum (Q1 - 1.5xIQR) values; outlier data points are defined as any value reaching past 1.5 times the IQR from either the lower or upper quartile and are labeled with a "X". Statistical significance was determined with Kruskal-Wallis non-parametric test, followed by Dunn's post-hoc test for multiple comparisons with Holm's correction. ****$P \leq 0.0001$; ***$P \leq 0.001$; **$P \leq 0.01$; *$P \leq 0.05$; ns, not significant ($P > 0.05$). Non-significant differences (ns) were not included on the plots for simplicity. Some statistical relationships were also not included in cases where that can be trivially inferred from the indicated ones. Scale bar, 10 µm. **(C)** We speculate that in the presence of PLST-1, either in *wildtype* or in embryos co-expressing motor-dead and wildtype myosin, the bundler protects actin filaments from myosin-driven disassembly by impeding myosin from entering the bundle due to spatial constraints. This would result in a normal ring constriction rate. In the absence of plastin, myosin can access individual filaments, possibly inducing more actin fragmenting and severing events that in turn increase actin filament depolymerization rate. Since actin disassembly has been shown to be important for ring constriction, an accelerated depolymerization rate may speed-up ring constriction.

Decreasing the overall crosslinking points in the cortex leads to slower ring assembly times, but slightly faster constriction rates

Next, we wondered whether perturbing simultaneously two cortical components that could only passively contribute to set up viscous tension in the network also led to an acceleration in the constriction rate. The rationale consisted mainly in trying to understand whether two sources of passive crosslinking had a similar effect as the experiments with myosin and plastin.

We capitalized again on the *plst-1(prt89)* mutant and depleted a subunit of the ARP2/3 complex, ARX-2. Despite being mainly involved in nucleating new actin filaments on the side of existing ones, we reasoned that the ARP2/3 complex could be a player in cortex viscosity as it creates crosslinking points between the parent and the newly nucleated actin filaments. If these two proteins are indeed major contributors for cortex viscosity, then when both are abolished, the ring would be expected to constrict faster, as the viscous resistance of the surrounding cortex would be lower. Importantly, this experiment has been performed in uncompressed embryos, as *plst-1(prt89);arx-2(RNAi)*embryos were suspected to be osmotic-sensitive: filming these embryos under compression frequently led to cortical rupture of the actomyosin network and subsequent cytokinesis failure (data not shown), ARX-2-depleted embryos seemed to be smaller and already more round-shaped (Figure 5.9A).

Cortical imaging of both *plst-1(prt89)* and *plst-1(prt89);arx-2(RNAi)* embryos shows that they lose the ARP2/3-nucleated actin, as cortical LifeAct::GFP puncta are no longer observed (Chan *et al.*, 2019). Instead, filamentous actin looked more linear, brighter and elongated, particularly in the double perturbation. These actin filaments seem to alternate with regions of decreased cortex density. They also moved more “freely” around the cortex and tended to be easily reorganized into aster-like structures (this phenotype is shown and discussed in Appendix I).

As expected, the median ring assembly times were 2- and 3-fold delayed in *plst-1(prt89)* embryos and in *plst-1(prt89); arx-2(RNAi)* embryos, respectively, when compared to *wildtype* or ARX-2-depleted embryos (Figure 5.9A,B,C,E). This was expected, as *plst-1* perturbation has been previously shown to lead to longer ring assembly times in *C. elegans* zygotes due to loss of actin network interconnectivity (W. Y. Ding et al., 2017; Leite et al., 2020; Sobral et al., 2021). The fact that there is an additive effect when PLST-1 and ARX-2 are perturbed simultaneously seems to indicate that ARX-2 is involved in interconnecting actin filaments as well. Around 50% of the double perturbed embryos failed cytokinesis during the assembly phase and were not able to form a stable contractile ring, which suggests we have probably disrupted the overall connectivity within the cortex (Figure 5.9C). The embryos that were able to proceed to ingression also displayed 1.9-fold longer median furrow initiation times compared to *wildtype*, as the ring structure was presumably not fully compacted (Figure 5.9A,D). Conversely, median ring constriction velocities of these double-perturbations were slightly faster than in *wildtype* (0.18 μm/second *vs.* 0.22 μm/second) and in ARX-2-depleted embryos (0.17 μm/second *vs.* 0.22 μm/second), however statistically similar to *plst-1(prt89)* embryos (0.20 μm/second *vs.* 0.22 μm/second) (Figure 5.9A,D). These results yield the following conclusions: 1) significantly decreasing the interconnectivity of the cortex seems to indeed decrease cortex viscosity and render the cortex weaker, which is suggested by the presence of cortex invaginations at the poles; 2) the decrease in cortex viscosity causes struggles in contractile ring assembly, but slightly facilitates constriction; 3) the requirement for interconnectivity between the ring and the rest of the cortex is different during the assembly and the constriction phases: while the ring is assembling it is greatly affected by a lack of interconnectivity, ring constriction seems to be quite facilitated.

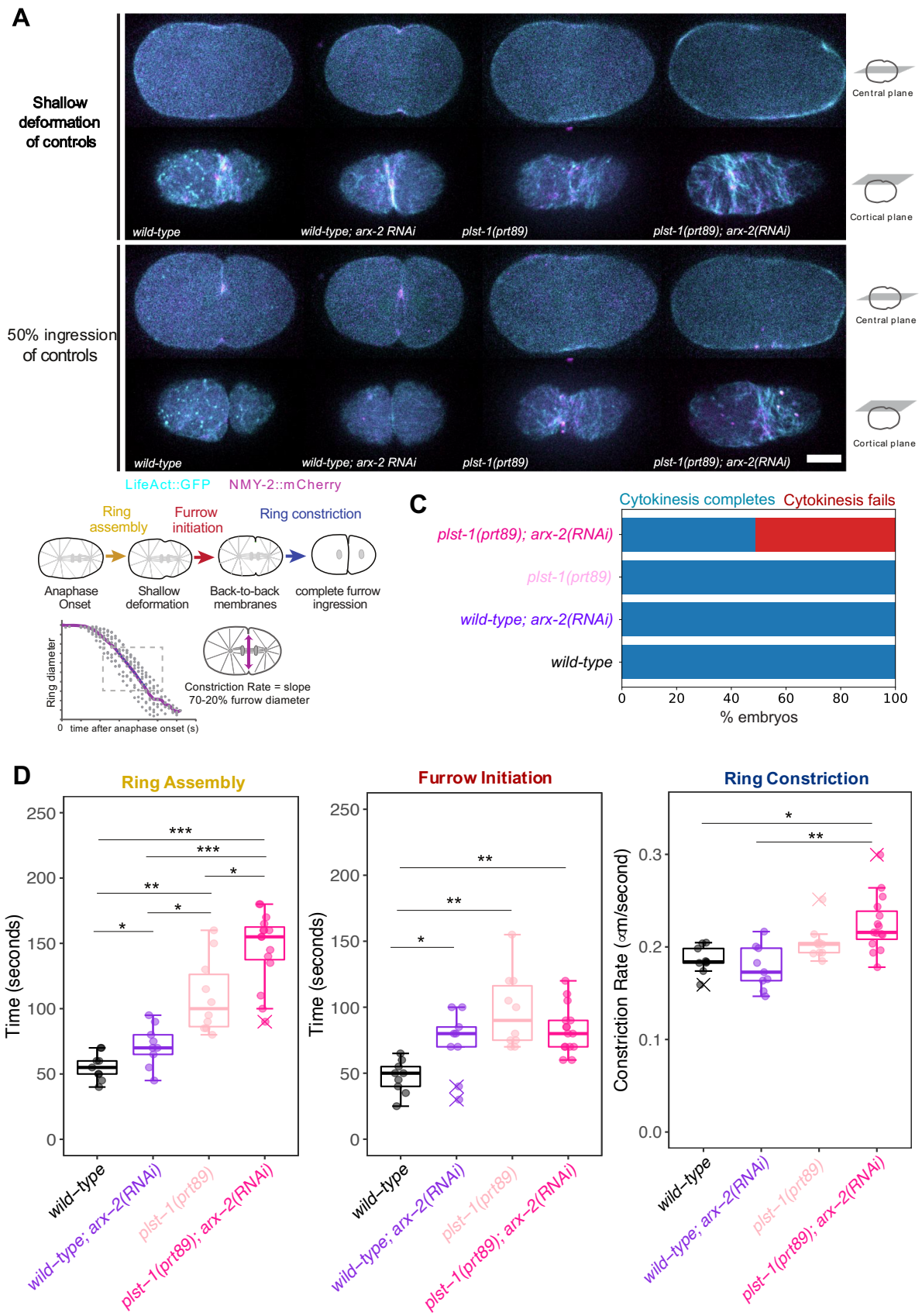

FIGURE 5.9. Depleting ARX-2 (subunit of the ARP2/3 complex) in a plastin mutant delays ring assembly and slightly accelerates constriction. (A) Representative central plane and cortical confocal images of embryos of the indicated genotypes aligned to the time point corresponding to shallow deformation and 50% ingression of

control *wild-type* embryos. Image intensities are equally scaled. **(B)** Reference points used for measurements of ring assembly and furrow initiation intervals, as well as fluorescence intensity. **(C)** Schematic showing the decrease in ring diameter over time. The dashed box depicts the interval of diameters used to calculate the constriction rate. **(D)** Percentage of cytokinesis failure of one-cell embryos for the indicated genotypes, with or without *arx-2(RNAi)*. **(E)** Boxplots showing ring assembly times and ring constriction rates for the indicated genotypes. The colors of the boxes identify the perturbations. In each box, the central line is the median, the boundaries of the box are the 25th (Q1) and 75th (Q3) percentiles and define the interquartile range (IQR); the whiskers extend to include the maximum (Q3 - 1.5xIQR) and minimum (Q1 - 1.5xIQR) values; outlier data points are defined as any value reaching past 1.5 times the IQR from either the lower or upper quartile and are labeled with a "X" on the top. Statistical significance was determined with Kruskal-Wallis non-parametric test, followed by Dunn's post-hoc test for multiple comparisons with Holm's correction; ***P≤0.001; **P≤0.01; *P≤0.05; ns, not significant (P>0.05). Non-significant differences (ns) were not included on the plots for simplicity. Scale bars: 10 μm.

Discussion

It has been established over the years that myosin, specifically, its motor-activity, is essential for cytokinesis (Mabuchi and Okuno, 1977; De Lozanne and Spudich, 1987; Osório *et al.*, 2019). Often, this conveys the idea that there is not much left to be explored. However, the extent of its requirement is not exactly known and may vary across different cells, organisms, or contexts. The studies that addressed this question are mostly theoretical and assume that the contractile ring closure speed is proportional to the amount of myosin in the ring (Khaliullin et al., 2018) or use simulated RhoA profiles as a proxy for myosin contractility (Turlier et al., 2014).

Additionally, many molecular details are still missing or are not so well-defined *in vivo*, including whether myosin bipolar filament assembly and RLC phosphorylation are dependent or independent from each other, if the number of myosin monomers and size of thick filaments are constant or vary across and/or within the same cell types and cytoskeletal structures, whether all myosin heads in a filament are activated and producing a power stroke simultaneously or if some heads are not activated and not bound or, alternatively, not activated but bound to the filaments to stabilize the power stroke generated by the active heads (Kad *et al.*, 2003). For example, it is quite a strong dogma that myosin can only bind actin and produce contractility when assembled into filaments. While studies *in vitro* and in mammalian cells suggested thick filament assembly by antiparallel association of the heavy chain tail domain is regulated by phosphorylation of the RLC (Ni et al., 2012; Taylor et al., 2014, Cross, 1988), in *D. Discoideum* this is regulated by the heavy chain phosphorylation of three-tail-domain threonine residues at positions 1823, 1833, and 2029 (Kuczmarski and Spudich, 1980; Vaillancourt, Lyons and Côté, 1988; Pasternak *et al.*, 1989; Ravid and Spudich, 1989; Lück-Vielmetter *et al.*, 1990; Thomas T. Egelhoff, Lee and Spudich, 1993) and, to the best of our knowledge, it has never been uncovered in *C. elegans*. Therefore, it is reasonable to consider

the possibility that myosin activation by phosphorylation of the RLC and bipolar filament assembly by heavy chain dephosphorylation may be independent processes.

Regarding the size of these filaments and whether this is constant or variable, recent work using quantitative time-lapse imaging suggested that myosin monomers coming from the cytoplasm can both incorporate existent myosin filaments, thereby increasing filament size, or be recruited as new filaments to the cortex, increasing filament density (Najafabadi, Leaver and Grill, 2022).

Myosin tunes contractility and viscosity at the cortex, which vary proportionally to maintain the ring constriction speed constant over a wide range of myosin levels

Here, we investigated the extent of myosin requirement during the first division of the *C. elegans* embryo by performing a time course of NMY-2 depletions and correlating NMY-2::GFP levels with kinetic parameters of ring assembly and constriction. Surprisingly, we found that contractile rings are quite robust to myosin depletion, and that rings with up to 70-80% less myosin could still constrict with velocities similar to controls. This observation could not be reproduced by computational simulations with theoretical myosin profiles that assume myosin could only contribute to active tensions in the cortical layer: decreasing contractility proportionally with the total myosin levels resulted in a linear decrease in ring constriction rate. The theoretical visco-active model considers both active and viscous contributions to cortical tension(Borja da Rocha, Bleyer and Turlier, 2022), thus it is rather trivial to reason that if it is assumed in the general equations that myosin only contributes to contractility, then the constriction rate must decrease linearly with decreasing myosin levels. This assumption has, nonetheless, failed to explain the experimental observations, suggesting other mechanical properties and mechanisms must be involved. Note that whilst these simulations were purely theoretical, we expect similar conclusions when we load myosin profiles measured *in vivo*.

Simulations fed with *in vivo* cortical myosin profiles directly measured on these embryos are still being performed. Specifically, we struggled to make even the control embryos constrict just by directly loading the NMY-2::GFP intensity profiles, as given the typical deformation timescale of the model $t_a = \frac{\eta}{\zeta}$ (ratio of the viscosity η to the contractility ζ) implies that the ratio of contractility between the equator and the poles should be equal or more than 14 for the furrow to constrict and this ratio was not observed for the NMY-2::GFP fluorescent signal. This is because the myosin on the poles observed in vivo, which is not necessarily active, contributes to a lower equator/pole ratio.

Therefore, one could reason that if myosin in the surrounding cortex could bind actin, albeit with low phosphorylation levels, it could contribute to cortex viscosity. Since myosin is also distributed throughout the surrounding cortex, one could wonder whether it could have an additional role besides its motor-activity, especially in the surrounding cortex where RhoA-dependent activation levels are known to be reduced (Basant and Glotzer, 2018b). According to this rationale, a balance of contractility and viscosity between the equatorial cortex and the polar cortex, both myosin-dependent, would explain the robustness of the process to a wide range of myosin levels. In agreement, the threshold of myosin levels where cytokinesis kinetics becomes affected seems to correspond to a level of depletion where there is no more myosin left on the surrounding cortex or where it reaches a basal level. From this point onwards, stronger depletions would only affect the contractile ring itself, whilst the viscosity of the remaining cortex would be essentially set by the actin network density and architecture, as well as crosslinking level. Motivated by this possibility, we modified the theoretical framework of our model to include a myosin's viscous contribution. Essentially, we considered that a fraction of the myosin in our profiles was contributing to contractility and the remaining fraction to viscosity, which not only recapitulates the constant constriction velocity over a range of myosin levels but also simulates the threshold behavior observed experimentally (recall Figure 5.3).

Cytokinesis kinetics depend on the relative amounts of active and inactive myosin in the cortex

To have a contribution in cortex viscosity, myosin must, in principle: 1) be in filamentous form or able to incorporate bipolar filaments; and 2) bind actin when not phosphorylated/activated.

However, the accepted idea is that myosin is only able to form thick bipolar filaments, bind actin and produce contraction when specific residues in the RLCs are phosphorylated, as described in detail on Chapter I - General Introduction, subsection "Regulation of NMII by RLC phosphorylation" (Kelly and Rice, 1969; Shoenberg, 1969; Scholey, Taylor and Kendrick-jones, 1980).

At cytokinesis onset, RhoA-GTP triggers a signaling cascade that results in increased myosin's RLCs phosphorylation via ROCK. This implies that myosin is likely in monomeric state and is only incorporated into thick filaments when and where RhoA/ROCK localizes and accumulates, i.e. the cell equator. This would in turn imply that if myosin phosphorylation via the RLC is blocked, then myosin could never assemble into thick filaments and crosslink actin. Interestingly, to our knowledge there is no experimental evidence in living organisms that ever proved this is indeed how it happens. Studies that tried to assess the conformational changes

in the myosin molecule upon RLC phosphorylation and the mechanism of bipolar thick filament assembly are purely biochemical or structural, and generally performed at the single molecule level(Wendt et al., 1999, 2001; Jung et al., 2011; Ni et al., 2012; Taylor et al., 2014), which may not replicate the behavior of myosin heads incorporated in a bipolar filament where collective effects of interactions with other myosin heads and regulators, as well as spatial constraints, must be considered. Furthermore, these works are often performed in muscle myosin, either smooth, skeletal or cardiac, thus, any extrapolations to non-muscle myosin must be cautious.

Apparently, there was some controversy on this topic in the past and some works tried to dissolve the dogma by demonstrating the existence of arrays of myosin filaments in a collection of smooth muscle types, even when those have been in relaxed state before and during fixation (Devine and Somlyo, 1971; Campbell and Chamley, 1975; Small and Sobieszek, 1980; Somlyo *et al.*, 1981). Specifically, Somlyo and colleagues have used rapid freezing techniques (to protect the *in vivo* form of myosin) to demonstrate the existence of a thick filament lattice in rabbit's vascular smooth muscle in relaxed state, where RLC phosphorylation is almost absent (Somlyo *et al.*, 1981). Despite care should be taken when extrapolating these conclusions to non-muscle cells, this is in strong agreement with our observations that unphosphorylatable RLC (MLC-4AA) is not only recruited to the cortex, but also displays a localization pattern similar to *wildtype* MLC-4 and the myosin heavy-chain NMY-2. This constitutes evidence that unphosphorylated myosin can be recruited to the cortex and incorporate bipolar filaments just like phosphorylated myosin, thus fulfilling requirement 1) that unphosphorylated myosin heads can likely incorporate bipolar filaments *in vivo*.

Also dissimilar from the classical dogma, a recent study reported that at physiological ionic strength, non-muscle myosin II monomers always exist in a folded 10S conformation, irrespective of the status of RLC phosphorylation or the presence of ATP. Instead, they found folded antiparallel dimers that either unfold to form extended bipolar dimers that assemble into filaments, or folded tetramers and hexamers that unfold and assemble into higher structures, thus speculating that intermolecular interactions within the tail region may be the driving force for opening the folded dimers and higher oligomers (Liu *et al.*, 2017).

Regarding requirement 2) bind actin when not phosphorylated/activated, recent *in vitro* motility assays and EM using *D. melanogaster*'s myosin showed that although myosin minifilaments with unphosphorylated RLC-AA do not translocate actin filaments, they still tether to the surface, suggesting that myosin bipolar filaments containing those unphosphorylated RLCs could still bind actin, albeit weakly, and crosslink actin filaments (Vasquez, Tworoger and Martin, 2014). Older studies have shown analogous behavior for unphosphorylated smooth muscle and unphosphorylated nonmuscle myosins, which could

bind to actin filaments in the presence of ATP, in a weakly bound state, despite not supporting movement (Sellers, 1985; Warshaw *et al.*, 1990). A similar conclusion has also been previously reported for mammalian unphosphorylated myosins where the velocity of actin translocation by the faster myosin varied in a highly nonlinear fashion with respect to the concentration of the slower myosin in motility assays comprising mixtures of faster and slower myosins. In other words, a slower-cycling or unphosphorylated myosin acts as a load to slow down the rate at which actin is moved by the faster cycling phosphorylated cross-bridges (Sellers, 1985; Warshaw *et al.*, 1990; Cuda *et al.*, 1997). Specifically, Warshaw and coworkers reported that in a copolymer mixture of phosphorylated and unphosphorylated myosins, actin filament velocity remained constant when the percentage of phosphorylated myosin was in the range 100 to 50% of the total. Nevertheless, when only 40% or less of the mixture was phosphorylated myosin, the velocity fell abruptly (Warshaw *et al.*, 1990). In strong resemblance, Cuda et al. showed that significant velocity reduction in actin filament translocation did not occur until more than 60% of the total myosin was unphosphorylated/slow-cycling (Cuda *et al.*, 1997). Not without some level of speculation, it is interesting to note the strong similarity between our *in vivo* data in *C. elegans* zygotes co-expressing non-phosphorylatable myosin with *wildtype* and the abovementioned reports, despite the latter being performed *in vitro* and using mainly muscle myosins. With effect, we also observe that co-expressing a non-phosphorylatable myosin with the phosphorylatable *wildtype* in the embryo, presumably at equal amounts (50-50%), does not significantly affect cytokinesis' kinetics, but even a slight depletion of the phosphorylated form already does.

We envision some possibilities of how myosin can modulate viscous resistance in the actomyosin cortex, which are sketched in Figure 5.10.

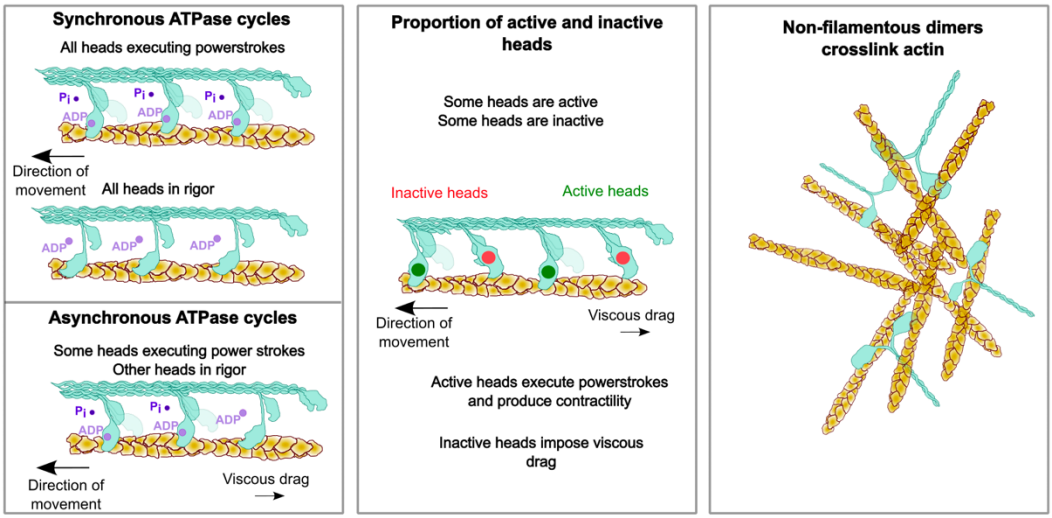

FIGURE 5.10. Different mechanisms that could explain the emergence of myosin-dependent viscous behavior in a wildtype scenario. Left – Asynchrony between ATPase cycles of myosin heads in bipolar filaments. Middle – Co-existence of active heads that can execute powerstrokes and produce contractility with inactive heads that remain in weak actin binding state, imposing a slight viscous drag. Right – Myosin dimers not integrated in bipolar filaments can still crosslink actin with the two heads.

The first possibility is related with the myosin's ATPase cycle itself (Figure 5.10-Left). Some specific steps of the myosin's ATPase cycle are indeed known for being rate limiting to the overall cycle rate, at least in muscle myosin. These include the drag stroke detachment rate after the power-stroke, potentially because of the ADP release (Siemankowski, Wiseman and White, 1985), and the weak-to-strong transition (Pate and Cooke, 1989; Millar and Homsher, 1992). Also, ATP concentration and ATPase activity affect the rate of transition between states of a myosin head (Taylor and Condeelis, 1979; Warshaw *et al.*, 1990; Homsher, Wang and Sellers, 1992). These may be further tuned depending on the myosin's category in its superfamily. For example, slower motors such as NMIIB, which is a high duty ratio motor, can have an intrinsically high binding affinity for ADP, which is generally used in saturation in biochemical assays to promote actin crosslinking by myosin used in saturation to favor crosslinking of actin filaments by myosin. Additionally, the duration of each of these steps can be further modulated by the mechanical properties of the surrounding environment, as myosin has been identified as a mechanosensory protein (Greenberg *et al.*, 2016). Macromolecular crowing effects should also be considered as myosin interacts with two ligands of different sizes - actin and ATP - which can modulate the kinetics of individual steps of the ATPase cycle (Ge *et al.*, 2016).

A second possibility lies on the existence of active and inactive myosin fractions, as we have mostly addressed in this thesis (Figure 5.10-Middle). We do not assume permanently inactive heads, but rather that any myosin head can become active/phosporylated or inactive/unphosporylated at each point in time. Therefore, we would always have an amount of active and inactive co-existing. This hypothesis assumes that unphosphorylated myosin heads can still bind actin albeit in a weakly bound state, which has been thoroughly analyzed above in this discussion. These inactive myosin heads can impair myosin's movement even at small concentrations (Umemoto and Sellers, 1990) and the effect of resistive forms of myosin on filament velocity and step size have been reported (Uyeda, Kron and Spudich, 1990; Higuchi and Goldman, 1991).

It may seem surprising that unphosphorylated cross-bridges can cause such a large resistance to actin movement given they predominantly exist in a weakly bound state, rapidly attaching and detaching from actin (Eisenberg, Hill and Chen, 1980). However, it has been

shown experimentally that unphosphorylated filaments in smooth muscle bind strongly enough to actin in the presence of MgATP. One possible explanation is that the rates of attachment and detachment can be strain dependent implying that any weakly bound cross-bridges that are attached to actin could be strained as the filament moves, which would in turn result in altered kinetics such that the weakly bound cross-bridges become more tightly bound(Somlyo *et al.*, 1988). Note that these are only hypotheses, mostly based in *in vitro* studies with muscle myosin, and none of them has experimental evidence backed by our data. We currently do not know whether this can apply to non-muscle myosins.

A third hypothesis addresses the possibility of myosin dimers (not incorporated into bipolar filaments) being a source of viscosity in the network (Figure 5.10-Right). Again, despite the prevalent dogma that myosin monomers are in a closed auto-inhibitory conformation and can only unfold, form motor-competent bipolar filaments and bind actin upon RLC's phosphorylation, a recent study has documented the existence of activated (phosphorylated at the RLC and unfolded) extended NMIIA and NMIIB monomers that co-exist with bipolar filaments in the cortex of mammalian cells (Shutova *et al.*, 2014). Even though this does not prove that inactive myosin monomers or dimers can also exist, it shows these myosin monomers can bind actin, as they are in an extended conformation, thus exposing the actin binding site. It is thus possible that these myosin heads also have an ATPase cycle with the abovementioned limiting steps or switch between active and inactive states. Another study has also observed that folded antiparallel dimers can unfold to form extended bipolar dimers that only after my assemble into filaments (Liu *et al.*, 2017). *In vitro* studies showed that NMIIB dimers crosslink actin in the presence of saturated amounts of ADP and these networks undergo viscous deformation and shear thickening, as effective viscosity increases as a function of stress (Norstrom and Gardel, 2011). Note that whilst it may seem rather unlikely that saturated conditions of ADP happen *in vivo*, high duty ratio motors such as NMIIB have been shown to exhibit high binding affinity for ADP (Greenberg *et al.*, 2016).

A role for myosin in acting as a viscous component of the cortex is also supported by experiments involving the depletion of the actin crosslinker plastin both on non-phosphorylatable and motor-dead myosin mutants. Passive crosslinkers such as plastin are known to contribute for cortex stability and viscosity (Ding, Ong, Hara, Wongsantichon, Toyama, Robert C Robinson, *et al.*, 2017; Leite *et al.*, 2020; Sobral *et al.*, 2021). When plastin is depleted in a non-phosporylatable mlc-4 co-expressed with its endogenous namesake, the ring constriction speed was slightly increased compared with the non-depleted embryos (not statistically significant), as well as *wildtype* embryos with the same level of depletion. A similar experiment with two myosin motor-dead mutant backgrounds shown to bind actin *in vitro*

(Osório et al., 2019) yielded a similar result, although the increase in the constriction rate compared to the *wildtype* was even more dramatic. Given the latter cannot exert motor-activity and are known to bind actin stronger than the *wildtype*, the rescue in the constriction rate when plastin is depleted in these embryos can be attributed to the reestablishment of viscosity back to normal or close to normal levels. One can perhaps speculate that the stronger the passive myosin binds actin, the stronger would be the effect of depleting another passive crosslinker on the cortex viscosity and the ring constriction rate. This seems to be supported by the fact that the motor-dead mutant that binds actin stronger than the *wildtype* shows the highest increase the constriction speed. However, there is not enough data yet to completely support this hypothesis. For that to be concluded, one would have to test if the myosin mutant with non-phosphorylatable RLCs indeed binds actin *in vitro* and if so, how strongly compared to the motor-dead mutants and a *wildtype* RLC. Altogether, this seems to agree with published works that reported that an intermediate level of crosslinking optimizes contractility of actomyosin networks (Ennomani *et al.*, 2016; Descovich, 2017; Ding, Ong, Hara, Wongsantichon, Toyama, Robert C Robinson, *et al.*, 2017).

It is quite intriguing though that PLST-1-depleted motor-dead mutant embryos (with no depletion of the endogenous *nmy-2*) have significantly faster rate than the same non-depleted mutant embryos, or than PLST-1-depleted *wildtype* embryos. Indeed, if plastin depletions decrease cortical viscosity, then the speed up in the constriction rate should be observed regardless of myosin being motor-dead or *wildtype*.

It is likely that this drastic increase in ring constriction plastin depletion and the expression of a motor-dead myosin stems from a decrease in the overall viscous tension of the cortical layer. Yet, a similar phenotype is not observed for PLST-1 depleted *wildtype* embryos, which should also have a less viscous cortex compared to their non-depleted namesake embryos. This suggests the molecular details underlying the change in this mechanical property are more complex to uncover. It is however very likely that this is related specifically with the co-existence of motor-dead and *wildtype* in heterotypical bipolar filaments in these embryos.

We speculate this could be explained by changes in actin filament disassembly rate. Indeed, actin filament crosslinkers have been shown to protect actin filaments from disassembly (Zigmond, Furukawa and Fechheimer, 1992; Schmoller, Semmrich and Bausch, 2011; Chikireddy *et al.*, 2024), thereby increasing viscosity not only by supporting percolation in the network *per se*, but also by increasing actin density. It is also known that myosin can disassemble actin filaments (Guha et al., 2005; Haviv et al., 2008; Murthy & Wadsworth, 2005; Wilson et al., 2010). More recently, myosin has also been shown to participate in actin filament fragmentation (Li *et al.*, 2017; Matsuda *et al.*, 2024), which can further amplify their

disassembly by creating new pointed ends to depolymerizing agents. In addition, considering the different phases of myosin's mechanochemical cycle (see Chapter I, subsection "Mechanism of filament sliding and force generation", Figure 1.7), motor-dead myosin heads are likely to stay in a strongly-bound rigor-like state, as they are unable to bind ATP and further execute the cycle. In the case where motor-dead myosin is co-expressed with the *wildtype*, heterotypical bipolar filaments may be formed. The presence of some motor-dead heads, which are non-cycling could in principle attenuate the velocity of the bipolar filaments. Nevertheless, as we have seen above in this discussion, *in vitro* studies showed that the overall velocity of bipolar filaments should not be significantly affected by the presence of a small amount of a non-cycling/slower cycling myosin (Warshaw *et al.*, 1990; Cuda *et al.*, 1997). It is possible that the presence of non-cycling and strongly-bound myosin heads in a bipolar filament amplifies the tension exerted on actin filaments by the active heads on the same motor ensemble, e.g. by increasing their residence time, thus resulting in increased fragmentation and subsequent disassembly. This would be further potentiated when plastin is depleted, since this renders actin filaments even more prone to disassembly. Given that actin disassembly is instrumental for ring constriction (Carvalho et al., 2009; Guha et al., 2005; Khaliullin et al., 2018; Mendes Pinto et al., 2012; Murthy & Wadsworth, 2005), the drastic increase in ring constriction could be explained by an increase rate of disassembly of actin filaments due to filaments becoming unbundled and more prone to fragmentation and disassembly by myosin-II and other severing or depolymerizing proteins. Note that, macroscopically, this should result in a reduction in passive viscous resistance to constriction. Consistent with the idea that increased actin disassembly can speed up contractile ring constriction, as long as it is mild, treatment with Cytochalasin D (an inhibitor of actin polymerization) at the equatorial cortex of dividing NRK cells facilitated constriction (O'Connell, Warner and Wang, 2001). Yet, addition of Latrunculin A, another inhibitor of actin polymerization, has been reported to slow down ring constriction (A M Silva *et al.*, 2016) This difference is likely explained by drug potency, as Latrunculin A is stronger than Cytochalasin D, requiring less concentration to produce very drastic effects (nanomolar range *versus* micromolar range, respectively) (Wakatsuki *et al.*, 2001). It is possible that the concentration used in latrunculin treatments was already too high, whereas the effects produced by Cytochalasin treatment were milder and allowed for a moderate actin disassembly that favoured constriction.

Despite this being a plausible explanation, other causes cannot be ruled out, including:

1) protein's relative abundances. First, we do not know which protein is more abundant in the *C. elegans* zygote cortex: myosin or plastin. This could be assessed by quantifying GFP

fluorescence intensity of both proteins fused to a GFP, but still, there might be unwanted variation in the GFP signal intensity due to them being different proteins. Another alternative would be to perform a western blot of embryo lysates. Presuming motor-dead and *wildtype* myosins are expressed at a 1:1 proportion, 50% of the myosin would be motor-dead (Kasza, Supriyatno and Zallen, 2019; Osório *et al.*, 2019). Moreover, provided that the two myosin populations can form mixed filaments, it is not known how much they may increase network's viscosity. The global contribution of myosin to the cortex mechanical properties will depend on the combined spatiotemporal densities of active driving heads, rigor heads, weakly attached heads and unbound heads. Rigor heads may be either ATP-deficient or permanently inactive, whilst weakly attached heads occur after a cycle before the release of the actin filament (Warshaw *et al.*, 1990; Homsher, Wang and Sellers, 1992). This should ultimately define the interplay between myosin-dependent contractility and myosin-dependent viscosity.

2) Protein's structural and mechanical properties, affinity for actin, duration of interaction with actin and possible competition for binding sites.

There are intrinsic differences between plastin and myosin-II, including stiffness of the protein itself, number of possible actin-binding sites and spatial conformation.
Direct competition between myosin heads and passive crosslinkers for binding sites is however unlikely because they bind to different actin regions. Spatial constraints are more likely, because depending on the spacing between actin filaments in a bundle, it may allow or impede myosin from accessing filaments inside that bundle (Alberts *et al.*, 2002). Given the spacing between actin filaments bundled by plastin is around 12 nm (N Volkmann *et al.*, 2001) and the diameter of myosin bipolar filaments has been estimated in around 30 nm for skeletal muscle myosin (reviewed in Gokhin and Fowler, 2013) with possible slight variations to non-muscle myosin II, it is likely they cannot enter these bundles. The scenario would change for α-actinin bundles, which have an approximate interfilament distance of 35-40 nm (Winkelman *et al.*, 2016).
Other possibility is that even if the absence of plastin decreases viscosity in the network, that is not enough to produce a significant acceleration in ring closure because myosin is still present to maintain the balance of equatorial contractility *versus* surrounding cortex resistance. Indeed, it is known that once myosin hexamers are assembled into bipolar filaments, the many heads may work as several binding domains and therefore, increase the binding force between F-actin bundles. Plastin is a small protein that only has two ABDs. As such, it is possible that much more plastin is needed to achieve a similar crosslinking degree than that provided by myosin. Conversely, it is not known whether all myosin heads bind the F-actin bundle simultaneously, whether they are concomitantly or alternatively activated or if

their ATPase cycles are synchronized or not, which may all affect how much of a viscous effect it may have.

4) Myosin and plastin turnover rates.

Contrarily to actin, not much is known or has been theoretically modelled about the effect of myosin turnover on cortical dynamics. A recent study has suggested that in the absence of turnover, myosin tends to hierarchically form ever-growing aggregates, which eventually result in contractile ring fracture (Thiyagarajan *et al.*, 2022). According to the known literature, the turnover dynamics of actin crosslinkers (Mukhina, Wang and Murata-Hori, 2007; Reichl *et al.*, 2008) and myosin motors (Yumura, 2001; Uehara *et al.*, 2010) seems to be around 5–10 times faster than that of actin (Guha, Zhou and Wang, 2005; Murthy and Wadsworth, 2005b), which would imply that the timescale of viscoelastic relaxation of the cortical layer is dominated by the turnover of crosslinks rather than that of actin filaments (Salbreux, Charras and Paluch, 2012). Also, computational simulations have shown that effective viscosity increases with actin filament lifetime up to a characteristic time and afterwards, it becomes more dependent on crosslinking dynamics (McFadden *et al.*, 2017). In addition, myosin-II motor-dead *Drosophila* variants have been shown to turnover slower than a *wildtype* myosin in embryos. Indeed, whereas *wildtype* myosin in control embryos displayed a uniform distribution throughout the cortex, the motor-dead variants accumulated in punctate aggregates that appeared much less dynamic than the typical pulsatile actomyosin structures, despite the overall organization of F-actin not being noticeably altered (Kasza, Supriyatno and Zallen, 2019). Myosin aggregation has also been reported for *Drosophila* myosin II tail domain mutants (T. Li *et al.*, 2016) and mutations that affect the RLC phosphorylation (Kasza, Farrell and Zallen, 2014; Vasquez, Tworoger and Martin, 2014). Interestingly, it has been found that purified and reconstituted actomyosin networks tend to spontaneously collapse into these stable aggregated structures *in vitro* when actin filaments are densely crosslinked or when ATP concentrations are decreased, thereby increasing the time myosin is strongly bound to actin (Janson, Kolega and Taylor, 1991; Mizuno *et al.*, 2007; Bendix *et al.*, 2008; Soares e Silva *et al.*, 2011; Murrell and Gardel, 2012). Similar findings on a slower ATPase cycling for motor-dead myosins still capable of biding actin have been described for mammalian cells (Kim *et al.*, 2005; X. Ma *et al.*, 2012).

Nevertheless, to answer these specific questions, the binding strength, the binding/unbinding kinetics, and the turnover of the proteins themselves would have to be investigated.

Collectively, the effects of progressively decreasing the total myosin levels in the embryo, progressively increasing the levels of inactive myosin and combining the expression of this inactive myosin with a reduction in passive crosslinking are summarized in Figure 5.11.

In a control scenario, RhoA-GTP stimulates myosin-driven contractility at the cell equator over the poles.

When total myosin levels are reduced everywhere in the embryo, the myosin-driven activity decreases proportionally with the myosin-driven viscosity allowing cytokinesis kinetics to be preserved. However, if this balance contractility-viscosity is destabilized by increasing the amount of inactive myosin, the robustness of the process is lost as the equator becomes less contractile and the whole cortex becomes more viscous. As a consequence, the constriction rate decreases progressively. Finally, decreasing the level of passive crosslinking in the actomyosin network can rescue the reduction in constriction rate when an inactive myosin is present, suggesting inactive myosin can act as a crosslinker and contribute to cortex viscosity and stability.

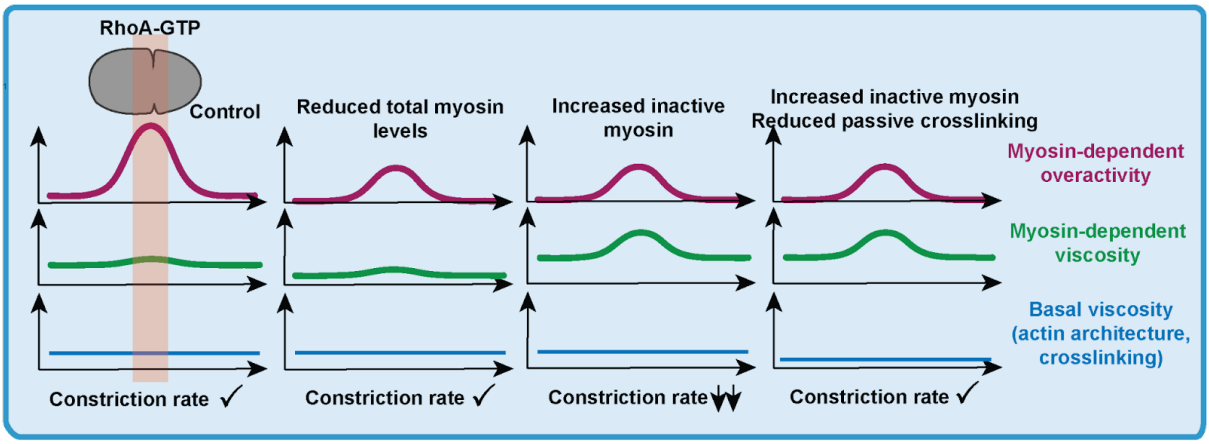

FIGURE 5.11. Mechanism of myosin-driven regulation of cortex mechanical properties during cytokinesis. In a control situation, RhoA-GTP stimulates myosin-driven contractility at the cell equator, which becomes sharply reduced towards the polar cortex in a gaussian-like manner. Viscosity of the cortex is controlled by myosin, actin architecture and crosslinking degree. Myosin-dependent viscosity is considered to be constant along the whole cortical layer, with the possibility of a slight increase at the equator due to myosin accumulation, which becomes negligible as it is dominated by the overcontractility. When total myosin levels are reduced everywhere in the embryo, the myosin-driven activity decreases proportionally with the myosin-driven viscosity, allowing the constriction rate to be maintained even with reduced myosin availability. If this balance contractility-viscosity between the equatorial and surrounding cortex is destabilized by increasing the amount of inactive myosin, the robustness of the process is lost as the equator becomes less contractile and both the equator and surrounding cortex become more viscous, which together offer more resistance to constriction. As a consequence, the constriction rate decreases progressively with the increase in the inactive myosin. Reducing the level of passive crosslinking in the actomyosin network can rescue the reduction in constriction rate when an inactive myosin is present, suggesting inactive myosin can act as a crosslinker and contribute to cortex viscosity and stability, apart from its motor function.

A modest increase in ring constriction rate was also observed when two sources of passive crosslinking in the network, the actin filament nucleator ARP2/3 and the bundler plastin, are abrogated. The ARP2/3 complex's ability to crosslink actin filaments is hardly recollected. However, it has been demonstrated in the late 90s that the Arp2/3 complex can crosslink actin, inclusively forming bundles which are mechanically stiffer than actin filaments alone, as determined by rheometric measurements and EM (Mullins *et al.*, 1998).

Note how the combined perturbation of different proteins with very different functions, e.g. myosin and plastin (a motor and active crosslinker plus a passive crosslinker) and ARP2/3 and plastin (an actin nucleator and passive crosslinker plus a passive crosslinker), can elicit similar biological responses. Both perturbations cause a delay in ring assembly times, but an acceleration of the constriction rate, despite the effects being stronger for the combination of myosin and plastin perturbations.

Altogether, this yields an important observation that the mechanical requirements of the actomyosin cortex strikingly change when the contractile ring switches from the assembly to the constriction phase.

Biological relevance of the cytokinesis kinetics' robustness to decreasing total myosin levels in the early embryo

Finally, regarding the maintenance of cytokinesis kinetics over a wide range of myosin levels, a question that may arise is what could be the biological relevance of this robustness. On the one hand, this is not completely surprising. Indeed, redundancies exist everywhere in biological systems, which have evolved to ultimately survive against the odds. On the other hand, it is quite intriguing. Two hypotheses may come to mind. The first stems from the fact that experiments in this work have been performed in the first cell of the organism. It is possible that this cell, from which every other cell of the animal will essentially arise from, has unique mechanisms to protect itself from errors. The second would be that the robustness is specifically related with myosin's function and regulation in the cell. Several future experiments could help us distinguish between these hypotheses. For example, performing a similar RNAi timecourse of other cytoskeletal proteins known to have an effect on cytokinesis success and/or dynamics when fully depleted (e.g. the formin CYK-1) could help us find out whether the robustness is cell-type specific or really myosin-specific: if the same threshold behaviour is observed, then the robustness should be associated with the cell stage itself; otherwise, it is very likely that this robustness is exclusive of myosin and its respective function. In favour of this mechanism being myosin-specific, depleting other passive crosslinkers alone in the

actomyosin network does not seem to impact the constriction rate, even when those are fully depleted (e.g. plastin).

In agreement with the latter, a recent work on HeLa cells proposed that the relative concentration of each of the two myosin paralogs, NMIIA and NMIIB, controls cortical tension differently during cytokinesis, which is suggested to be intrinsically related with the nature of the motor domain: while NMIIA has lower duty ratios and higher ATPases activity which is associated with a higher cortical tension, NMIIB does not seem to have a role in generating cortical tension because of its higher duty ratio due to a high binding affinity for ADP (Rosenfeld *et al.*, 2003), meaning it binds actin in the force-generating state for a larger proportion of its mechano-chemical cycle (Taneja *et al.*, 2020). Essentially, NMIIB seems to be mostly involved in maintaining tension rather than effectively generating it and it could indeed act more as a crosslinker due to being a slow motor (Rosenfeld *et al.*, 2003). Another previous work has reported NMII paralog specific roles in *in vivo* exocytosis, where NMIIB is also believed to behave as a membrane stabilizer while NMIIA acts to effectively generate tension (Milberg et al 2017). These two NMII isoforms have been shown to co-assemble, building heterotypical bipolar filaments in cells using total internal reflection fluorescence structured-illumination microscopy (Beach *et al.*, 2014), which could suggest a necessary tuning between force generation and stabilization.

Nevertheless, *C. elegans* contains only one myosin paralog. It is rather interesting to think that if cells from higher eukaryotes have different paralogs with distinct functions while simpler organisms only have one, this may have been a necessary diversification. The fact that human cells have different myosin paralogs may thus be a sign of a necessary evolution in more complex organisms, which in this case, would consist in myosin having a paramount role in viscously stabilizing the actomyosin cortex, apart from its motor activity. In organisms with just one paralog, this may be achieved either by spatial tuning of myosin's activity or by the mechanochemical properties of the myosin molecule itself (e.g., the duty ratio or rate limiting steps of the mechanochemical cycle). One possibility is that when there is only one myosin paralog, the duty ratio, or more generally, the ATPase cycle of that myosin is tuned by the nature of the RLC (Nayak *et al.*, 2020) or by surrounding mechanical conditions (Ge *et al.*, 2016; Greenberg *et al.*, 2016). For example, skeletal muscle myosin was one of the first recognized mechanosensors, as early as the 1920s (Fenn, 1923). A few years later, Hill noticed a few that the velocity of muscle contraction decreased nonlinearly with increasing force, thus proposing that force slows the enzymatic and motile activities of muscle myosin, which acts both as a force generator and a mechanosensor that changes its own rate of motility in response to force (Archibald Vivian Hill, 1938). Other single-molecule experiments

since then demonstrated that slowing of myosin movement by force can be explained by changes in the attachment and detachment kinetics of actin-bound myosin. This is likely related with the bond type – including catch- or slip-bonds – whose lifetimes increase or decrease, respectively, with load (Greenberg *et al.*, 2016).

Another possibility is that not all myosin heads are activated or executing power strokes simultaneously, meaning some of the heads in a bipolar thick filament would act as stabilizers while the other heads generate tension. Interestingly, *in vitro* analysis of the movement of myosin filaments on actin filaments as a function of phosphorylation level suggested that phosphorylation of both myosin heads was required for movement and that unphosphorylated myosin could decrease the rate of movement of phosphorylated myosin (Sellers, Spudich and Sheetz, 1985). Also, more generally, upstream regulators of myosin can regulate its activation level (Bement et al., 2015, Machacek et al., 2009, Martin et al., 2009).

We propose that most likely, not all myosin in the embryo is active during cytokinesis and that myosin that is not phosphorylated by upstream regulators, especially in the surrounding cortex outside the RhoA activation zone, can still bind actin and contribute to set the viscoelastic properties of the cell cortex. One may still argue that the polar viscosity or stability could be regulated by other proteins controlling the properties of the actin network density, architecture and crosslinking degree. In part, this seems reasonable as well. So, why would myosin play such an important role at stabilizing the surrounding cortex, if it is built to be a motor? Besides the hypotheses described in Figure 5.10, an additional explanation is that the embryo would regulate the amount of myosin recruited to the furrow depending on the amount that is in the polar cortex. The explanation is quite logical: embryos with less myosin on the cortex overall, that is with less viscous resistance, would also need less myosin at the equator to produce the amount of contractility needed to constrict. This would imply that there is no specific amount of myosin in the contractile ring needed for normal constriction kinetics, but rather that this quantity varies from embryo to embryo according to the viscous resistance of the overall cell cortex, as has been previously proposed in *D. discoideum* (Robinson et al., 2002). This crosstalk would ensure cytokinesis fidelity over a wide range of myosin levels. Another possibility is that the more contractile the equator becomes, the higher the intracellular pressure. As previously reported, the embryo must have a strategy to counteract this increase in internal pressure, otherwise, cortex instabilities – membrane blebs - may arise at the polar cortex, compromising cytokinesis fidelity, as previously reported (Sedzinski et al., 2011; Tinevez et al., 2009). Indeed, very differently from organisms such as *D. Discoideum*, a segregation of specific crosslinkers or proteins/effectors to the equatorial *versus* the polar cortex has not been found in *C. elegans*. Most of the cortical proteins localize both on the

equatorial and the polar cortices during cytokinesis and differences in their contribution for the mechanical properties in each region may depend on ratios between spatial distributions, activation levels, or tuning of mechanochemical properties of the motor ensembles.

Conclusion

In this chapter, it has been found that cytokinesis kinetics in *C. elegans* zygotes is robust to a decrease in total myosin levels. By combining experimental and theoretical approaches, we suggest that this robustness is attributed to a specific role of myosin in tuning both activity and viscosity at the cell cortex to ensure a balance of contractile and viscous forces between the equatorial and polar cortices during cytokinesis. We identify a possible role for myosin in setting cortex viscosity, which is reinforced by experiments that show an affectation of cytokinesis kinetics through expression of an inactive myosin form that can still bind actin, which can be rescued by the depletion of a passive crosslinker. We thoroughly discuss hypotheses that may explain how myosin can impose a viscous drag on its own movement in a *wildtype* scenario, which can include differences in ATPase cycle rates or asynchronous cycles, the co-existence of active and inactive fractions or the presence of non-filamentous myosin forms. Finally, we also find that the mechanical requirements of the cell cortex change from the ring assembly to the constriction phase as cortex connectivity is paramount for ring assembly, but seems to be dispensable or even slightly impeditive for constriction.

Materials and Methods

C. elegans strains

Strains used in this study and their genotypes are listed in Table 5.1 and were maintained on nematode growth medium (NGM) plates seeded with OP50 *E. coli* at 20°C using standard techniques (Stiernagle, 2006).

Table 5.1. List of *C. elegans* strains used in this study.

Name	**Genotype**	**Source/ Reference**
N2	Ancestral	*Caenorhabditis* Genetics Center

GCP22	ltIs157 [pAC16;pie-1/LifeAct::GFP; unc-119 (+)]; unc-119(ed3) III (?); prtSi2[pAC71;Pnmy-2:nmy-2reencoded::mCherrry::StrepTagII::3'UTR-nmy-2; cb-unc-119(+)]II	Our lab (Osório *et al.*, 2019)
GCP113/ GCP812	nmy-2(cp13[nmy-2::GFP+LoxP]) I; unc-119(ed3) III (?); ltIs37 [pAA64; pie-1/mCherry::his-58; unc-119 (+)]	Our lab (Silva et al., 2016)
GCP179	nmy-2(cp13[nmy-2::gfp + LoxP]) I; ltIs44 [pAA173; pie-1/mCherry::PH(PLC1delta1); unc-119 (+)]	Our lab (Silva et al., 2016)
GCP570	plst-1(prt89) IV; nmy-2(cp13[nmy-2::GFP+LoxP]) I; unc-119(ed3) III (?); ltIs37 [pAA64; pie-1/mCherry::his-58; unc-119 (+)]	Our lab (Sobral et al, 2021)
GCP592	nmy-2 [prt100(R252A)]I; ltIs157 [pAC16;pie-1/Life-Act::GFP; unc-119 (+)]; unc-119(ed3)III; prtSi2[pAC71; Pnmy-2:nmy-2reencoded::mCherry::StrepTagII::3'UTRnmy-2; cb-unc-119(+)]II	Our lab (Osório et al., 2019)
GCP618	nmy-2 [prt113(S251A)]I; ltIs157 [pAC16;Ppie-1::Life-Act::GFP; unc-119 (+)]; unc-119(ed3)III; prtSi2[pAC71; Pnmy-2::nmy-2reencoded::mCherry::StrepTagII::3'UTRnmy-2; cb-unc-119(+)]II	Our lab (Osório et al., 2019)
GCP723	nmy-2(cp52[nmy-2::mkate2+ LoxP unc-119(+) LoxP]I; unc-119(ed3) III histone mCherry; unc-119(ed3)III; prtSi4[pAC72; Pmlc-4:mlc-4 reencoded::GFP::StrepTagII::3'UTRmlc-4; cb-unc-119(+)]II; ltIs37 [pAA64; pie-1/mCHERRY::his-58; unc-119 (+)] IV	Our lab

GCP748	nmy-2(cp52[nmy-2::mkate2+ LoxP unc-119(+) LoxP]I ; unc-119(ed3)III; prtSi46[pAC127; Pmlc-4:mlc-4_T17S18AA_reencoded::GFP::StrepTagII::3'UTRmlc-4; cb-unc-119(+)]II	Our lab
GCP752	nmy-2(cp52[nmy-2::mKate2 + LoxP unc-119(+) LoxP]) I; ltIs157 [pAC16;pie-1/LifeAct::GFP; unc-119 (+)]; ltIs37 [pAA64; pie-1/mCherry::his-58; unc-119 (+)] IV; unc-119(ed3) III	This thesis
GCP1299	zbIs2(pie-1::lifeACT::RFP); unc-119(ed3) III histone mCherry; unc-119(ed3)III; prtSi4[pAC72; Pmlc-4:mlc-4 reencoded::GFP::StrepTagII::3'UTRmlc-4; cb-unc-119(+)]II; ltIs37 [pAA64; pie-1/mCHERRY::his-58; unc-119 (+)] IV	This thesis
GCP1300	zbIs2(pie-1::lifeACT::RFP); unc-119(ed3)III; prtSi46[pAC127; Pmlc-4:mlc-4_T17S18AA_reencoded::GFP::StrepTagII::3'UTRmlc-4; cb-unc-119(+)]II	This thesis
MG617	mgSi5[cb-UNC-119 (+) GFP::ANI-1(AH+PH)]II	Michael Glotzer lab (Tse et al., 2012)
EG6699	ttTi5605 II; unc-119(ed3) III; oxEx1578	*Caenorhabditis* Genetics Center

RNA interference

RNAi was performed either by feeding animals with E. coli HT115 bacteria expressing double stranded RNA (dsRNA) or by injecting animals with dsRNA. To produce dsRNA for injection, primers with tails containing T3 and T7 RNA polymerase promoters were used to amplify the

desired regions from N2 cDNA.The PCR products were transcribed with T3 or T7 RNA polymerases (MEGAscript Transcription Kit; ThermoFischer Scientific). Transcription reactions were cleaned up (NucleoSpin RNA Clean-up, Macherey-Nagel) and diluted with 3 3 soaking buffer (32.7 mM Na2HPO4, 16.5 mM KH2PO4, 6.3 mM NaCl, and 14.1 mM NH4Cl). Injection of dsRNA at 1 mg/ml was performed in L4-stage animals of the strains used on each experiment. The dsRNAs used in this study are listed on Table 5.2.

For RNAi by feeding, the RNAi feeding vector L4440 transformed into E. coli HT115 was used. L4440 vectors for RNAi. The bacteria were grown overnight at 37ºC in 50 mL Luria broth (LB) medium containing 12.5 mg/ml tetracycline and 100 mg/ml ampicillin. The culture was centrifuged for 10 minutes at 2,500 g. The cell pellet was resuspended in 2.5 mL Luria broth medium containing 12.5 mg/ml tetracycline, 100 mg/ml ampicillin, and 1 mM IPTG. 75 ml were used to inoculate NGM plates to which 100 ml of a 1:1:1 mix of 100 mg/ml ampicillin, 1 M IPTG, and 5 mg/ml tetracycline had been added 2 hours prior. The expression of double-stranded RNA was induced overnight at room temperature and in the dark. 25-30 L4-stage animals of strains GCP22, GCP179, GCP812, GC380, GCP570, GCP592, GCP618, GCP752, GCP1299 ,GCP1300 ,GCP927, GCP1444 and GCP1445 were added to the plates and incubated at 20ºC for the adequate time of depletion prior to dissection for imaging.

For the *nmy-2(RNAi)* timecourse in Figures 5.1, S5.1 and 5.6, different levels of *nmy-2* depletion were achieved by varying the time of *RNAi* or age of worms subject to *RNAi*. L4 worms from strains GCP179, GCP380, GCP570, GCP752 or GCP812 expressing NMY-2::GFP from the endogenous locus, were subject to depletion of endogenous *nmy-2* by feeding RNAi (nmy-2_RNA#1) or injection between 20 and 40 hours at 20 °C. Alternatively, adult worms were fed or injected between 9 and 14 hours. For the endogenous *mlc-4(RNAi)* timecourse in Figures 5.5 and S5.2, L4 worms of strains GCP1299, GCP1300, GCP1444 and GCP1445 were depleted of endogenous *mlc-4* by feeding *RNAi* (mlc-4_RNA#2), in a range between 18 and 32 hours, at 20 °C. Full depletions of the endogenous *mlc-4* on Figure S5.2 required feeding times of 33-36 hours at 20ºC. For the experiments in Figure 5.7, GCP1299 and GP1300 were depleted of *plst-1* by injection of dsRNA for 48 hours at 20ºC and by *mlc-4* feeding *RNAi* (mlc-4_RNA#2) for 18-21 hours at 20ºC. Double depletions were achieved by injecting worms of these strains with *plst-1* dsRNA, keeping them in normal NGM plates and then transferring some of them to *mlc-4* feeding *RNAi* plates. In Figure 5.8, GCP22, GCP592 and GCP618 were depleted of the *nmy-2*^{sen} transgene by feeding RNAi (nmy-2_RNA #2) in a range between 16 and 28h. Double depletions of *nmy-2*^{se}and plst-1 were achieved by injecting worms of these strains with *plst-1* dsRNA (plst-1_RNA#1), keeping them in normal NGM plates and then transferring some of them to *nmy-2*^{sen} feeding *RNAi* plates (nmy-2_RNA #2). In Figures 5.9 and A5.1 (in Appendix I), worms from strains GCP22 and GCP927 were depleted of arx-2 by feeding (arx-2_RNA#2) or injection (arx-2_RNA#1) for 48-52h at 20ºC.

Table 5.2. List of dsRNAs used in this study.

Name	Gene target	Forward Primer	Reverse Primer	RNAi type
nmy-2_RNA #1	*nmy-2* (does not target re-encoded nmy-2:mCherrysen)	GGCCCGATAT CATGAACAAC GAGCTTGAAA G	GGCACGATAT CAGCCTCCTG GATAGCC	Feeding
nmy-2_RNA #2	re-encoded nmy-2::mCherrysen (does not target endogenous *nmy-2*)	GGCCCGATAT CATGAATAAT GAACTCGAGT CAATC	GGCCCGATAT CACGTTCTTG AATGGCC	Feeding
mlc-4_RNA#1	*mlc-4*	aattaaccctcactaa ag gctcccgcaaaaccgt aaac	taatacgactcactata gg cttaatcggagcatctc taaag	Injection
mlc-4_RNA#2	mlc-4	CAACAGATATC GCCTCCCGCAA AACCG	CCCCCGATATC CTTAATCGGAG CATCTC	Feeding
arx-2_RNA#1	arx-2 (K07C5.1)	AATTAACCCTC ACTAAAGGAGG AACCAATTTCC CAGCTC	TAATACGACTC ACTATAGGTCC GAAAAGAAGTT CCGAGA	Injection
arx-2_RNA#2	arx-2	—----------	—----------	Feeding (Ahringer library)
plst-1_RNA#1	plst-1 (Y104H12BR.1)	AATTAACCCTC ACTAAAGGACT CGGAGTCCATG GAAATG	TAATACGACTC ACTATAGGCAC CATTTTTGGCTT CACCT	Injection
plst-1_RNA#2	plst-1	—----------	—----------	Feeding (Ahringer library)

Live imaging

Gravid hermaphrodites were dissected and one-cell embryos were mounted in a drop of M9 (86 mM NaCl, 42 mM Na2HPO4, 22 mM KH2PO4, and 1 mM MgSO4) on 2% agarose pads overlaid with a coverslip. Live imaging of cytokinesis was performed at 20°C. Images were acquired on a spinning disk confocal system (Andor Revolution XD Confocal System; Andor Technology) with a confocal scanner unit (CSU-X1; Yokogawa Electric Corporation) mounted on an inverted microscope (Ti-E, Nikon) equipped with a 60x NA 1.4 oil-immersion Plan-Apochromat objective, and solid-state lasers of 405 nm (60 mW), 488 nm (50 mW), and 561 nm (50 mW). For image acquisition, an electron multiplication back-thinned charge-coupled device camera (iXon; Andor Technology) was used. Acquisition parameters, shutters and

focus were controlled using Andor iQ3 software. For central plane imaging in one-cell embryos, 6 × 1 µm z-stacks were collected in the 488 nm and 561 nm channels every 5 seconds. For cortical dual-color imaging in one-cell embryos, 7 × 0.5 µm z-stacks were collected every 5 seconds for strains GCP812, GCP179, GCP1299, GCP1300.

Measurement of cytokinesis, ring assembly and furrow initiation time intervals, and ring constriction rate

Measurement of cytokinesis, ring assembly and furrow initiation time intervals, as well as ring constriction rate were performed in one-cell embryos of the following strains: GCP812, GCP179, GCP752, GCP723, GCP748, GCP1299 and GCP1300. This analysis only included embryos that completed ring constriction. Cytokinesis time was the interval between anaphase onset and the time when the contractile ring reached a diameter of ~5 µm. Ring assembly consisted in the time interval between anaphase onset and the establishment of a shallow deformation in the equatorial region (time point when the equator shows first sign of deformation). Furrow initiation time corresponded to the time interval between the establishment of the shallow deformation and the time when the plasma membranes of the nascent daughter cells became juxtaposed to one another (back-to-back membrane configuration). During ring constriction, the distance between the two sides of the ring was measured in the z-plane where this distance was widest at each time point and plotted against time. Ring constriction rate was the slope of the linear region between ~70% and 30% ingression, or 80-20%, as indicated in the respective figures. All intervals and ring constriction rate were determined on central plane images of the embryos.

Fluorescence intensity measurements

To quantify the levels of NMY-2::GFP at the tip of the cytokinetic furrow in one-cell embryos, the mean fluorescence intensity in a 15-pixel wide, 20-pixel long box drawn over the tip of the furrow at 50% ingression was determined, and the mean camera background was subtracted. To quantify the levels of NMY-2::GFP in the surrounding cortex contour, a line was traced along the cortex contour and the mean camera background was subtracted.

Cortical flow quantification

Cortical flow dynamics were analyzed in one-cell embryos of strains GCP752 between anaphase onset until the end of constriction. Magnitude and direction of cortical flows were quantified using an Iterative Particle Image Velocimetry (PIV) plugin for ImageJ, Myosin cortical flows were determined in maximum projections of cortical planes in embryos expressing NMY–2::GFP. Flows were analyzed between anaphase onset and the end of

cytokinetic furrow ingression. Magnitude and direction of cortical flows were quantified using a Particle Image Velocimetry (PIV) MATLAB script (Thielicke & Stamhuis, 2014). A 216 x 128 pixel (38.5 x 22.8 mm) region was applied to all embryos to exclude cortical curved peripheries. Two iterations were performed to calculate maximum particle displacement: a larger interrogation window of 64 x 64 pixels was used in the first iteration and a smaller interrogation window of 32 x 32 pixels was used in the second iteration. Consecutive interrogation windows overlapped by 50%. After flow field generation, the 216 x 128 pixel region was divided in two adjacent anterior and posterior regions: anterior cortex (1st-148th pixel; 0.0–26.3 mm) and posterior cortex (149th-216th pixel; 26.3–38.4 mm). Each velocity vector was resolved into a Vx component along the anterior-posterior axis and a Vy component along the dorsal-ventral axis. The mean Vx and Vy in the anterior and posterior cortex were estimated for each time point and plotted as a function of time to trace the cortical flow profiles.

Measurement of NMY-2::GFP, GFP::AHPH (RhoA biosensor) profiles along the cortex contour

Fluorescence intensity quantifications along the cortex contour of NMY-2::GFP (Figure 5.1,S5.1) and GFP::AHPH (Figure 5.3) in one-cell embryos were performed using the Plot Profile tool in Fiji (ImageJ; National Institutes of Health) (Schindelin et al., 2019). Image stacks were all oriented such that the anterior pole was always on the left side and the side where the furrow has ingressed more along the dorsal-ventral (D-V) axis. Using the segmented line tool with a line width of 3 pixels, a line was traced throughout the cortex contour, starting on the left and ending on the right side. The profile was only traced for half embryo as the theoretical model considers a symmetry around the A-P axis, which means the intensity at one half can be extrapolated to the other taking advantage of this axisymmetry.

Fittings of NMY-2::GFP and GFP::AHPH profiles

Profiles in Figures 5.2A,B, 5.3B were fitted with a gaussian added to a linear function for each timepoint. The parameters for the best fitting – amplitude A, width w, center c, slope s and intercept b – were extracted and averaged across all embryos for each condition to construct the plots in Figure 5.2C and 5.3C. The averages of each parameter over time (Figures 5.2C and 5.3C) were then fitted themselves with other appropriate functions. The functions used to fit each profile or the parameters of a profile fitting are indicated in Table 5.3. The Python script used for batch analysis and profile fitting is freely available in https://github.com/joanaleite92/embryo_profile_fitter.

Table 5.3. Functions used to fit line profiles and parameters of those profile fittings.

Profile/parameter	Function
NMY-2::GFP MLC-4WT::GFP/MLC-4AA::GFP	Gaussian + Linear $f(x, A, \mu, \sigma, m, b) = \frac{A}{\sigma\sqrt{2\pi}} e^{[-(x-\mu)^2/2\sigma^2]} + mx + b$
GFP::AHPH (RhoA biosensor)	Gaussian + constant offset $f(x, A, \mu, \sigma, c) = \frac{A}{\sigma\sqrt{2\pi}} e^{[-(x-\mu)^2/2\sigma^2]} + c$
Amplitude, A	Exponential $f(x, A, \tau) = Ae^{-x/\tau}$
Width, σ	Constant $f(x) = c, \ x \geq \bar{t}_{shallow\ deformation}$
Mean, μ	Constant $f(x) = c$
Slope, m	Gaussian $f(x, A, \mu, \sigma) = \frac{A}{\sigma\sqrt{2\pi}} e^{[-(x-\mu)^2/2\sigma^2]}$

Image processing, quantifications and statistical analysis

Image processing and image analysis were performed using Fiji(ImageJ; National Institutes of Health) (Schindelin et al., 2019) and MATLAB (MathWorks). Z-stacks acquired on the cell cortex were projected using Fiji's maximum intensity projection tool. Images within each panel were scaled equally. Error bars represent the standard-deviation (SD) or the standard-error of the mean (SEM), as indicated in figure legends. Z-stacks acquired on the cell cortex were projected using Fiji's maximum intensity projection tool. Images within each panel were scaled equally. Error bars represent the standard-deviation (SD), standard-error of the mean (SEM) as indicated in figure legends. All plots were generated using custom Python or R code. Statistical significance was performed as indicated in figure legends using the R statistics library rstatix. Illustrations and graphics were performed on the open-source vector graphics editor Inkscape.

Supplementary Material

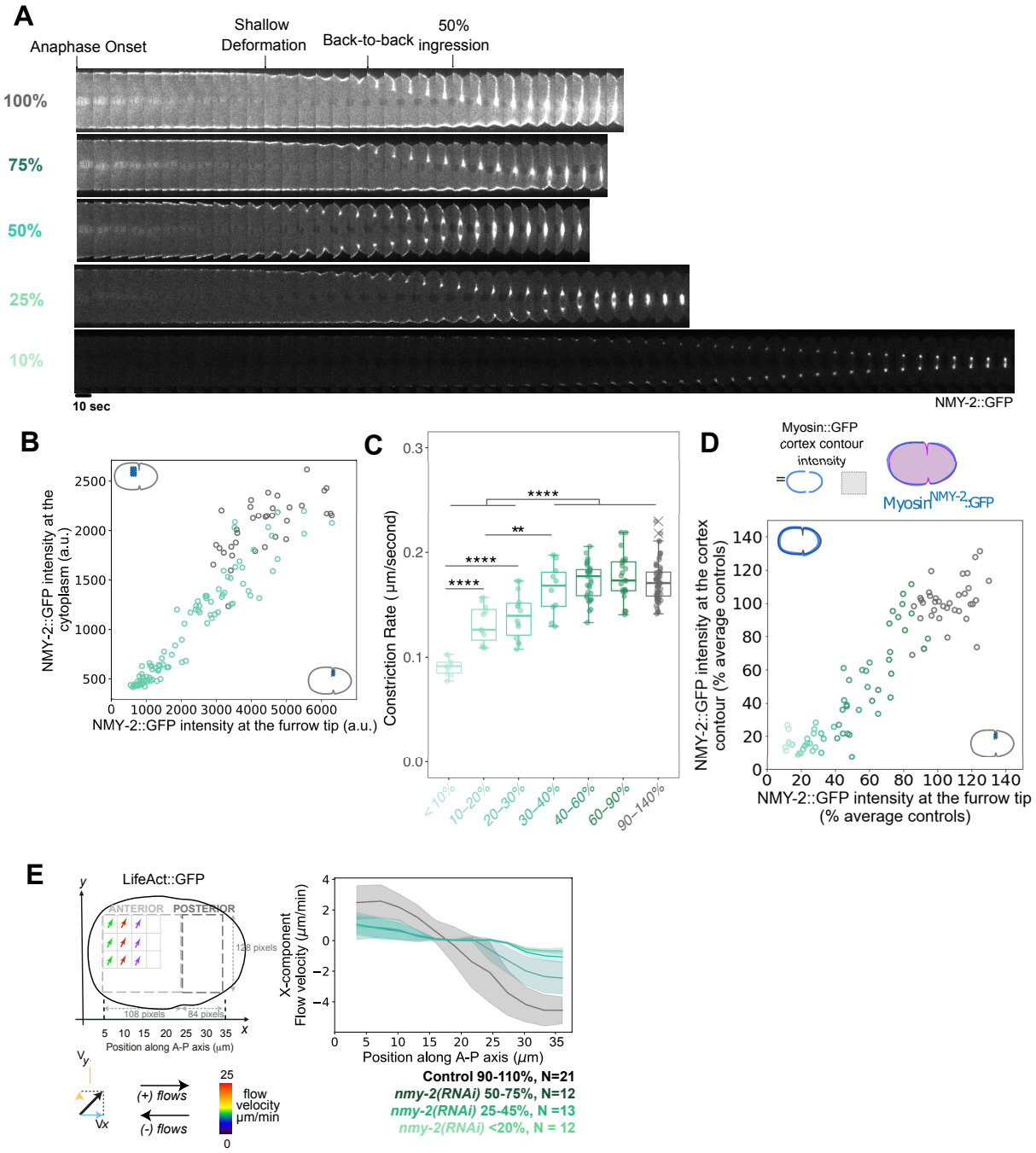

FIGURE S5.1 - (A) Kymographs of the equatorial region of central plane images for the myosin percentages indicated. The fluorescent tag is NMY-2::GFP. **(B)** Measurements of NMY-2 intensity at the furrow tip versus cytoplasm. **(C)** Boxplots showing the distribution of constriction rates for the indicated myosin percentages.. In each box, the central line is the median, the boundaries of the box are the 25th (Q1) and 75th (Q3) percentiles and define the interquartile range (IQR); the whiskers extend to include the maximum (Q3 - 1.5xIQR) and minimum (Q1 - 1.5xIQR) values; outlier data points are defined as any value reaching past 1.5 times the IQR from either the lower or upper quartile and are labeled with a "X" on the top. Statistical significance was determined with Kruskal-Wallis non-parametric test, followed by Dunn's post-hoc test for multiple comparisons with Holm's correction; ****$P \leq 0.0001$; **P≤0.01; ns, not significant ($P > 0.05$). Non-significant differences (ns) were not included on the plots for simplicity. **(D)** Measurements of NMY-2 intensity at the furrow tip versus surrounding cortex contour (excluding

equator) as a percentage of the average intensity of controls. **(E)** Schematic illustrating flow analysis with PIV and quantification of longitudinal (X-component) cortical flows for control and several levels of NMY-2 depletion along the A-P axis for an average of 50 seconds after a back-to-back membrane configuration. The curves show mean flow velocity ± SEM. N is the number of embryos analyzed. Scale bar, 10 μm.

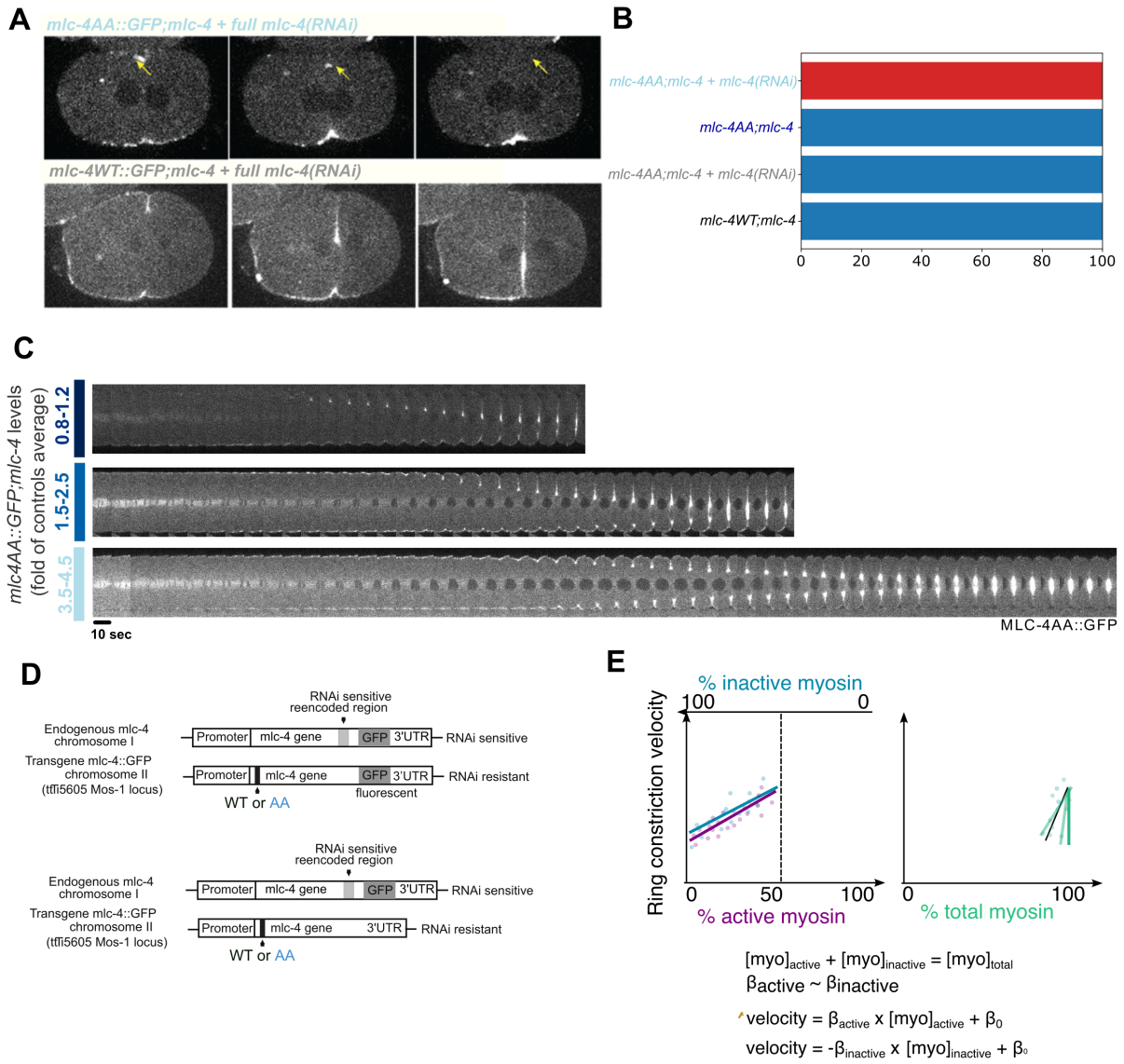

FIGURE S5.2 – (A) Representative images of the indicated genotypes with and without full *RNAi* of the endogenous *mlc-4*, showing cytokinesis failure for full the *mlc-4AA;mlc-4 + mlc-4(RNAi)* condition. The yellow arrows indicate furrow regression. **(B)** Percentage of cytokinesis failure of one-cell embryos for the indicated genotypes, with or without full *RNAi* of the endogenous *mlc-4*. **(C)** Kymographs of the equatorial region of confocal central plane images for the indicated genotype with varying levels of endogenous mlc-4 depletion. The fluorescent tag is MLC-4AA::GFP. **(D)** Schematics illustrating four new strains to be generated: mlc-4AA::GFP;mlc-4::GFP, mlc-4AA;mlc-4::GFP and their respective controls mlc-4WT::GFP;mlc-4::GFP and mlc-4WT;mlc-4::GFP; **(E)** Hypothetical constriction rate *versus* the percentage of unphosphorylated (mlc-4AA::GFP;mlc-4), phosphorylated (mlc-4AA;mlc-4::GFP) or the total (mlc-4AA::GFP;mlc-4::GFP) mlc-4 curve, as indicated in different colors. The total amount is expected to remain roughly constant, whereas the amounts of phosphorylated/unphosporylated are

expected to be inverses of one another. The equations represent line fittings to align embryos from different strains by the constriction rate.

APPENDIX I: Additional findings and observations

Depletion of arx-2 in a *plst-1(prt89)* background seems to favour the formation of large and transient actomyosin asters in the cortex and ultimately, lead to cortex fluidization

While investigating the effect of abrogating two major sources of crosslinking in the cortex, plst-1 and arx-2, we observed a quite unexpected phenotype, which was not related with the main objective of this experiment. As this has never been observed *in vivo*, at least to the best of our knowledge, it is worth reporting and discussing this finding.

In *plst-1(prt89);arx-2(RNAi)* embryos, the cortex displayed a completely different organization than in the other three scenarios. Figure A5.1 shows several cortical plane images of embryos expressing LifeAct::GFP and NMY-2::mCherry. *Wildtype* embryos show the usual distribution of F-actin and myosin, enriched in an anterior cap and showing an ARP2/3-dependent punctate structure at anaphase onset, which is progressively lost as cytokinesis proceeds and those cortical proteins start flowing, first unidirectionally and then bidirectionally, and accumate in the ingressing furrow. Conversely, *arx-2*-depleted embryos lose this punctate actin distribution in the anterior cortex and display F-actin structures that look more linear. This is consistent with the two major F-actin nucleators in the cortical layer competing for monomers, meaning that when one of them is perturbed, the other is favoured. In this case, there seems to be an increase in formin-nucleated linear filaments, as previously indicated(Chan *et al.*, 2019). As previously reported, *plst-1(prt89)* embryos still display the ARP2/3-dependent actin puncta, but the cortical layer looks much more unstable with erratic cortical flows that do not show a clear directionality. Finally, when *arx-2* is depleted on the *plst-1(prt89)* background, the cortex structure and dynamics seem to change drastically. First, one can observe the total disappearance of ARP2/3 dependent puncta and the emergence of long linear structures throughout the whole cortex. These linear actin bundles seem brighter and longer than the ones observed in the *arx-2* depletion alone. Furthermore, they seem to float around in the cortex quite 'freely', frequently forming structures that look like actin asters or stars - structures formed by myosin-driven polarity sorting of F-actin, in which myosin motors move towards the plus-ends of filaments packing them together on a myosin core formed at the center, with minus ends radiating outwards. If asters come close enough, they can even merge together and form bigger asters. These structures have been recently observed *in vitro* (Wollrab *et al.*, 2018), but to my current knowledge, they have never been observed *in vivo* and the perfect

conditions for their formation or how they affect the macroscopic mechanical properties of the cell cortex is not known.

In the most severe cases, myosin localizes in dotty structures in the cortex, instead of the usual patchy distribution observed in *wildtype* embryos, as also observed in other double perturbations that affect interconnectivity of the actomyosin network (Sobral *et al.*, 2021). All these observations seem to constitute hallmarks of complete loss of connectivity. In the cases where a large number of these myosin dots are observed, the formation of asters seems to cease almost completely, being replaced by dense regions of long F-actin bundles that simply float very fast all over the cortical layer intercalled with regions that seem almost devoid of any actin. Myosin dots were also observed, but those seemed to struggle to catch and translocate any of those F-actin bundles floating around, which is then again, a sign that connectivity is completely compromised. It is also possible that these structures assumed to be actin asters, correspond, alternatively, to pulsed contractions mediated by the continuous cycling between RhoA-GDP and RhoA-GTP. Indeed, pulsed contractions have been documented in the polarization of *C. elegans* zygotes (Munro, Nance and James R. Priess, 2004). These pulsed contractions have been suggested as a mechanism to allow for rapid cell and tissue deformations while maintaining overall integrity (Vasquez, Tworoger and Martin, 2014).

The formation of asters would somewhat imply that myosin is able to walk on actin filaments to pull them together, therefore suggesting that this myosin must be in an activated state. It is known, as previously mentioned, that the levels of myosin activation outside the furrowing region during cytokinesis are very low. It is possible that the inhibition of ARX-2, which has been previously proposed to antagonize RhoA, leads to the extension of RhoA activity to the surrounding cortex and therefore, the increased activation of myosin together with the lack of connectivity set up the conditions for the formation of asters.

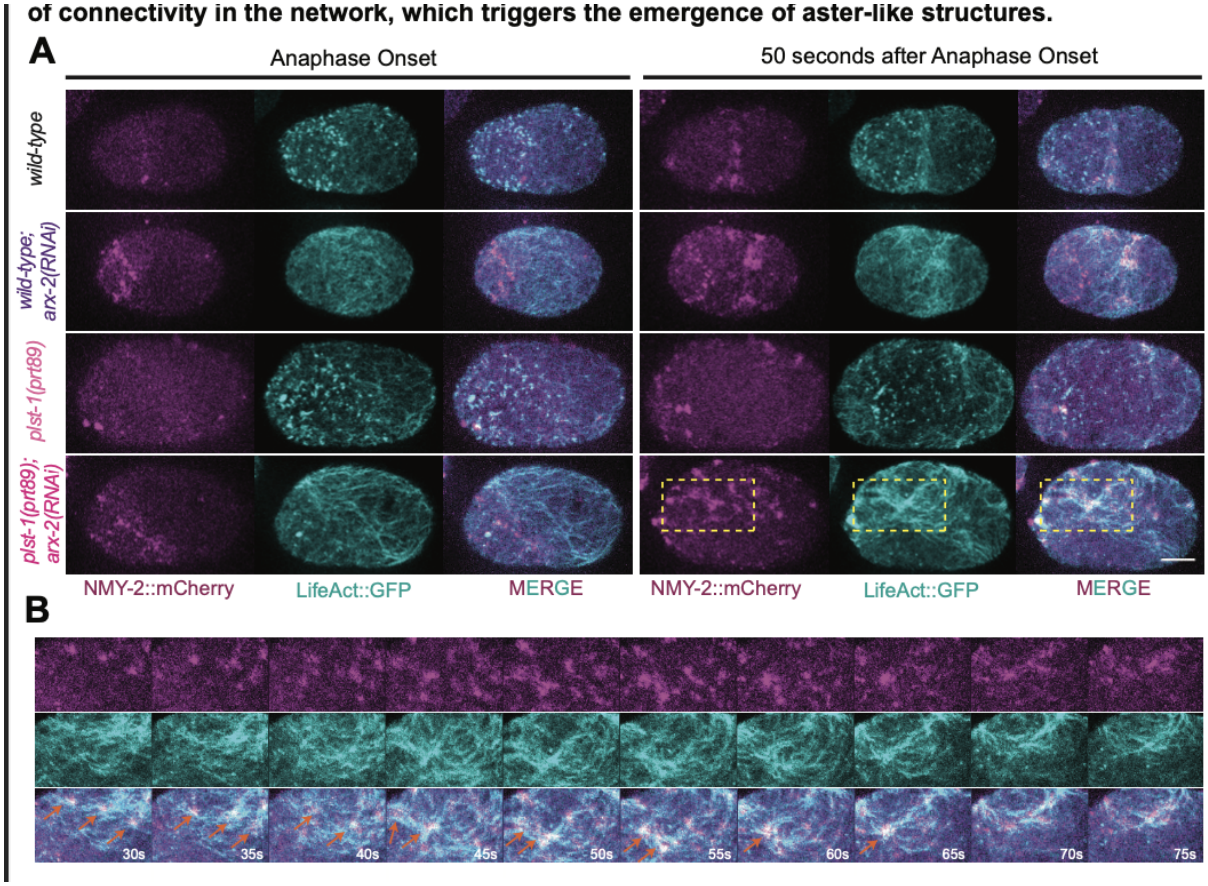

FIGURE A5.1. Abolishing crosslinking points in the cortex by ARX-2 (subunit of the ARP2/3 complex) depletion in a plst-1 mutant lacking the actin-binding domain leads to cortex fluidization and loss of connectivity in the network, which triggers the emergence of aster-like structures. (A) Stills of a time lapse video showing the cortex of *wild-type* and *plst-1(prt89)* embryos expressing LifeAct::GFP and NMY-2::m- Cherry, with and without *arx-2(RNAi)*, at anaphase onset and 50 seconds after anaphase onset. When ARX-2 is depleted in *plst-1(prt89)* embryos, long linear actin filaments are observed, which move 'freely' and frequently assemble into large transient aster-like structures. These asters have been observed *in vitro* and form by polarity sorting, a mechanism through which myosin motors move towards the plus-ends of actin filaments and dwell there, packing them together in a myosin core with their minus ends radiating outwards. These have never been observed *in vivo* and the conditions for their appearance or their impact on the mechanical properties of the cortex are not known. **(B)** Inset showing the evolution of a group of asters in the cortex of an ARX-2-depleted *plst-1(prt89)* embryo shown in A (yellow dashed rectangle). Smaller asters appear 30 seconds after anaphase onset, converging into one bigger aster 35 seconds later, which disassembles in 5 seconds. Orange arrows indicate the referred asters. Time-lapse: 5 seconds.

References

ADELSTEIN, R.S. and ANNE CONTI, M. (1975) 'Phosphorylation of platelet myosin increases actin-activated myosin ATPase activity', *Nature*, 256(5518), pp. 597–598. Available at: https://doi.org/10.1038/256597a0.

Alberts, B. *et al.* (2002) *Molecular biology of the cell*. 4th Editio. New York: Garland Science; 2002.

Available at: https://search.library.wisc.edu/catalog/999598982402121.

Amano, M. *et al.* (1996) 'Phosphorylation and activation of myosin by Rho-associated kinase (Rho-kinase).', *The Journal of biological chemistry*, 271(34), pp. 20246–20249. Available at: https://doi.org/10.1074/jbc.271.34.20246.

Aras, B.S. *et al.* (2018) 'The importance of mechanical constraints for proper polarization and psuedo-cleavage furrow generation in the early Caenorhabditis elegans embryo', *PLoS Computational Biology*, 14(7), pp. 1–19. Available at: https://doi.org/10.1371/journal.pcbi.1006294.

Archibald Vivian Hill (1938) 'The heat of shortening and the dynamic constants of muscle', *Proceedings of the Royal Society of London. Series B - Biological Sciences*, 126(843), pp. 136–195. Available at: https://doi.org/10.1098/rspb.1938.0050.

Basant, A. and Glotzer, M. (2018) 'Spatiotemporal Regulation of RhoA during Cytokinesis', *Current Biology*, 28(9), pp. R570–R580. Available at: https://doi.org/10.1016/j.cub.2018.03.045.

Beach, J.R. *et al.* (2014) 'Nonmuscle myosin II isoforms coassemble in living cells', *Current Biology*, 24(10), pp. 1160–1166. Available at: https://doi.org/10.1016/j.cub.2014.03.071.

Bement, W.M., Benink, H.A. and Von Dassow, G. (2005) 'A microtubule-dependent zone of active RhoA during cleavage plane specification', *Journal of Cell Biology*, 170(1), pp. 91–101. Available at: https://doi.org/10.1083/jcb.200501131.

Bement, W.M., Miller, A.L. and von Dassow, G. (2006) 'Rho GTPase activity zones and transient contractile arrays.', *BioEssays : news and reviews in molecular, cellular and developmental biology*, 28(10), pp. 983–993. Available at: https://doi.org/10.1002/bies.20477.

Bendix, P.M. *et al.* (2008) 'A quantitative analysis of contractility in active cytoskeletal protein networks.', *Biophysical journal*, 94(8), pp. 3126–3136. Available at: https://doi.org/10.1529/biophysj.107.117960.

Borja da Rocha, H., Bleyer, J. and Turlier, H. (2022) 'A viscous active shell theory of the cell cortex', *Journal of the Mechanics and Physics of Solids*, 164, p. 104876. Available at: https://doi.org/https://doi.org/10.1016/j.jmps.2022.104876.

Bridges, A.A. and Gladfelter, A.S. (2015) 'Septin form and function at the cell cortex', *Journal of Biological Chemistry*, 290(28), pp. 17173–17180. Available at: https://doi.org/10.1074/jbc.R114.634444.

Campbell, G.R. and Chamley, J.H. (1975) 'Thick filaments in vertebrate smooth muscle', *Cell and Tissue Research*, 156(2), pp. 201–216. Available at: https://doi.org/10.1007/BF00221803.

Carvalho, A., Desai, A. and Oegema, K. (2009) 'Structural Memory in the Contractile Ring Makes the Duration of Cytokinesis Independent of Cell Size', *Cell*, 137(5), pp. 926–937. Available at:

https://doi.org/10.1016/j.cell.2009.03.021.

Chan, F.-Y. *et al.* (2019) 'The ARP2/3 complex prevents excessive formin activity during cytokinesis.', *Molecular biology of the cell*, 30(1), pp. 96–107. Available at: https://doi.org/10.1091/mbc.E18-07-0471.

Chikireddy, J. *et al.* (2024) 'Fascin-induced bundling protects actin filaments from disassembly by cofilin', *The Journal of cell biology*, 223(6). Available at: https://doi.org/10.1083/jcb.202312106.

Cuda, G. *et al.* (1997) 'In vitro actin filament sliding velocities produced by mixtures of different types of myosin', *Biophysical Journal*, 72(4), pp. 1767–1779. Available at: https://doi.org/10.1016/S0006-3495(97)78823-4.

D'Avino, P.P. (2009) 'How to scaffold the contractile ring for a safe cytokinesis - lessons from Anillin-related proteins.', *Journal of cell science*, 122(Pt 8), pp. 1071–1079. Available at: https://doi.org/10.1242/jcs.034785.

Dan, K., Dan, J.C. and Yanagita, T. (no date) *Behaviour of the Cell Surface During Cleavage. II*. Available at: https://www.jstage.jst.go.jp/article/cytologia1929/8/3-4/8_3-4_521/_pdf (Accessed: 25 November 2018).

DAN, K. and ONO, T. (1954) 'A METHOD OF COMPUTATION OF THE SURFACE AREA OF THE CELL*', *Embryologia*, 2(10), pp. 87–99. Available at: https://doi.org/https://doi.org/10.1111/j.1440-169X.1954.tb00043.x.

Dan, K., Yanagita, T. and Sugiyama, M. (1937) 'Behavior of the cell surface during cleavage. I', *Protoplasma*, 28(1), pp. 66–81. Available at: https://doi.org/10.1007/BF01624958.

Dean, S.O. and Spudich, J.A. (2006) 'Rho kinase's role in myosin recruitment to the equatorial cortex of mitotic Drosophila S2 cells is for myosin regulatory light chain phosphorylation.', *PloS one*, 1(1), p. e131. Available at: https://doi.org/10.1371/journal.pone.0000131.

DeBiasio, R.L. *et al.* (1996) 'Myosin II transport, organization, and phosphorylation: evidence for cortical flow/solation-contraction coupling during cytokinesis and cell locomotion.', *Molecular biology of the cell*, 7(8), pp. 1259–1282. Available at: https://doi.org/10.1091/mbc.7.8.1259.

Descovich, C.P. *et al.* (2018) 'Cross-linkers both drive and brake cytoskeletal remodeling and furrowing in cytokinesis.', *Molecular biology of the cell*, 29(5), pp. 622–631. Available at: https://doi.org/10.1091/mbc.E17-06-0392.

Descovich, C.P. et al. (2017) 'Crosslinkers both drive and brake cytoskeletal remodeling and furrowing in cytokinesis', *Molecular Biology of the Cell*, 2, pp. 3–4.

Devine, C.E. and Somlyo, A.P. (1971) 'Thick filaments in vascular smooth muscle.', *The Journal of cell biology*, 49(3), pp. 636–649. Available at: https://doi.org/10.1083/jcb.49.3.636.

Ding, W.Y., Ong, H.T., Hara, Y., Wongsantichon, J., Toyama, Y., Robinson, Robert C, *et al.* (2017) 'Plastin increases cortical connectivity to facilitate robust polarization and timely cytokinesis.', *The Journal of cell biology*, 216(5), pp. 1371–1386. Available at: https://doi.org/10.1083/jcb.201603070.

Ding, W.Y., Ong, H.T., Hara, Y., Wongsantichon, J., Toyama, Y., Robinson, Robert C., *et al.* (2017) 'Plastin increases cortical connectivity to facilitate robust polarization and timely cytokinesis', *Journal of Cell Biology*, 216(5), pp. 1371–1386. Available at: https://doi.org/10.1083/jcb.201603070.

Dulyaninova, N.G. *et al.* (2005) 'Regulation of myosin-IIA assembly and Mts1 binding by heavy chain phosphorylation.', *Biochemistry*, 44(18), pp. 6867–6876. Available at: https://doi.org/10.1021/bi0500776.

Egelhoff, T.T., Lee, R.J. and Spudich, J.A. (1993) 'Dictyostelium myosin heavy chain phosphorylation sites regulate myosin filament assembly and localization in vivo', *Cell*, 75(2), pp. 363–371. Available at: https://doi.org/10.1016/0092-8674(93)80077-R.

Eisenberg, E., Hill, T.L. and Chen, Y. (1980) 'Cross-bridge model of muscle contraction. Quantitative analysis.', *Biophysical journal*, 29(2), pp. 195–227. Available at: https://doi.org/10.1016/S0006-3495(80)85126-5.

Ennomani, H. *et al.* (2016) 'Architecture and Connectivity Govern Actin Network Contractility.', *Current biology : CB*, 26(5), pp. 616–626. Available at: https://doi.org/10.1016/j.cub.2015.12.069.

Fenn, W.O. (1923) 'A quantitative comparison between the energy liberated and the work performed by the isolated sartorius muscle of the frog.', *The Journal of physiology*, 58(2–3), pp. 175–203. Available at: https://doi.org/10.1113/jphysiol.1923.sp002115.

Ge, J. *et al.* (2016) 'Macromolecular Crowding Modulates Actomyosin Kinetics', *Biophysical Journal*, 111(1), pp. 178–184. Available at: https://doi.org/10.1016/j.bpj.2016.05.035.

Gokhin, D.S. and Fowler, V.M. (2013) 'A two-segment model for thin filament architecture in skeletal muscle', *Nature Reviews Molecular Cell Biology*, 14(2), pp. 113–119. Available at: https://doi.org/10.1038/nrm3510.

Green, Rebeca; Paluch, E. and Oegema, K. (2012) 'Cytokinesis in Animal Cells', *Annual Review of Cell and Developmental Biology*, 28, pp. 29–58. Available at: https://doi.org/10.1146/annurev-cellbio-101011-155718.

Greenberg, M.J. *et al.* (2016) 'A Perspective on the Role of Myosins as Mechanosensors', *Biophysical Journal*, 110(12), pp. 2568–2576. Available at: https://doi.org/10.1016/j.bpj.2016.05.021.

Guha, M., Zhou, M. and Wang, Y.-L. (2005) 'Cortical actin turnover during cytokinesis requires myosin II.', *Current biology : CB*, 15(8), pp. 732–736. Available at: https://doi.org/10.1016/j.cub.2005.03.042.

Guo, S. and Kemphues, K.J. (1996) ‘Molecular genetics of asymmetric cleavage in the early Caenorhabditis elegans embryo.’, *Current opinion in genetics & development*, 6(4), pp. 408–415. Available at: https://doi.org/10.1016/s0959-437x(96)80061-x.

Haviv, L. *et al.* (2008) ‘A cytoskeletal demolition worker: myosin II acts as an actin depolymerization agent.’, *Journal of molecular biology*, 375(2), pp. 325–330. Available at: https://doi.org/10.1016/j.jmb.2007.09.066.

Higuchi, H. and Goldman, Y.E. (1991) ‘Sliding distance between actin and myosin filaments per ATP molecule hydrolysed in skinned muscle fibres’, *Nature*, 352(6333), pp. 352–354. Available at: https://doi.org/10.1038/352352a0.

Homsher, E., Wang, F. and Sellers, J.R. (1992) ‘Factors affecting movement of F-actin filaments propelled by skeletal muscle heavy meromyosin.’, *The American journal of physiology*, 262(3 Pt 1), pp. C714-23. Available at: https://doi.org/10.1152/ajpcell.1992.262.3.C714.

Janson, L.W., Kolega, J. and Taylor, D.L. (1991) ‘Modulation of contraction by gelation/solation in a reconstituted motile model.’, *The Journal of cell biology*, 114(5), pp. 1005–1015. Available at: https://doi.org/10.1083/jcb.114.5.1005.

Joanny, J.F. *et al.* (2007) ‘Hydrodynamic theory for multi-component active polar gels’, *New Journal of Physics*, 9(11), p. 422. Available at: https://doi.org/10.1088/1367-2630/9/11/422.

Jordan, S.N. and Canman, J.C. (2012) ‘Rho GTPases in animal cell cytokinesis: an occupation by the one percent.’, *Cytoskeleton (Hoboken, N.J.)*, 69(11), pp. 919–930. Available at: https://doi.org/10.1002/cm.21071.

Kad, N.M. *et al.* (2003) ‘A mutant heterodimeric myosin with one inactive head generates maximal displacement.’, *The Journal of cell biology*, 162(3), pp. 481–488. Available at: https://doi.org/10.1083/jcb.200304023.

Karess, R.E. *et al.* (1991) ‘The regulatory light chain of nonmuscle myosin is encoded by spaghetti-squash, a gene required for cytokinesis in Drosophila’, *Cell*, 65(7), pp. 1177–1189. Available at: https://doi.org/https://doi.org/10.1016/0092-8674(91)90013-O.

Kasza, K.E., Farrell, D.L. and Zallen, J.A. (2014) ‘Spatiotemporal control of epithelial remodeling by regulated myosin phosphorylation.’, *Proceedings of the National Academy of Sciences of the United States of America*, 111(32), pp. 11732–11737. Available at: https://doi.org/10.1073/pnas.1400520111.

Kasza, K.E., Supriyatno, S. and Zallen, J.A. (2019) ‘Cellular defects resulting from disease-related myosin II mutations in Drosophila’, *Proceedings of the National Academy of Sciences*, 116(44), pp. 22205–22211. Available at: https://doi.org/10.1073/pnas.1909227116.

Kelly, R.E. and Rice, R. V (1969) ‘Ultrastructural studies on the contractile mechanism of smooth

muscle.', *The Journal of cell biology*, 42(3), pp. 683–694. Available at: https://doi.org/10.1083/jcb.42.3.683.

Khaliullin, R.N. *et al.* (2018a) 'A positive-feedback-based mechanism for constriction rate acceleration during cytokinesis in Caenorhabditis elegans', *eLife*, 7. Available at: https://doi.org/10.7554/eLife.36073.

Khaliullin, R.N. *et al.* (2018b) 'A positive feedback-based mechanism for constriction rate acceleration during cytokinesis in C. elegans', *eLife*, 7, p. e36073. Available at: https://doi.org/10.7554/eLife.36073.

Kim, K.-Y. *et al.* (2005) 'Disease-associated mutations and alternative splicing alter the enzymatic and motile activity of nonmuscle myosins II-B and II-C.', *The Journal of biological chemistry*, 280(24), pp. 22769–22775. Available at: https://doi.org/10.1074/jbc.M503488200.

Kosako, H. *et al.* (2000) 'Rho-kinase/ROCK is involved in cytokinesis through the phosphorylation of myosin light chain and not ezrin/radixin/moesin proteins at the cleavage furrow.', *Oncogene*, 19(52), pp. 6059–6064. Available at: https://doi.org/10.1038/sj.onc.1203987.

Koyama, H. *et al.* (2012) 'A High-Resolution Shape Fitting and Simulation Demonstrated Equatorial Cell Surface Softening during Cytokinesis and Its Promotive Role in Cytokinesis'. Available at: https://doi.org/10.1371/journal.pone.0031607.

Kruse, K. *et al.* (2005) 'Generic theory of active polar gels: A paradigm for cytoskeletal dynamics', *European Physical Journal E*, 16(1), pp. 5–16. Available at: https://doi.org/10.1140/epje/e2005-00002-5.

Kuczmarski, E.R. and Spudich, J.A. (1980) 'Regulation of myosin self-assembly: phosphorylation of Dictyostelium heavy chain inhibits formation of thick filaments.', *Proceedings of the National Academy of Sciences of the United States of America*, 77(12), pp. 7292–7296. Available at: https://doi.org/10.1073/pnas.77.12.7292.

Leite, J. *et al.* (2019) 'Network Contractility During Cytokinesis-from Molecular to Global Views.', *Biomolecules*, 9(5). Available at: https://doi.org/10.3390/biom9050194.

Leite, J. *et al.* (2020) 'Equatorial Non-muscle Myosin II and Plastin Cooperate to Align and Compact F-actin Bundles in the Cytokinetic Ring.', *Frontiers in cell and developmental biology*, 8, p. 573393. Available at: https://doi.org/10.3389/fcell.2020.573393.

Li, J. *et al.* (2017) 'Buckling-induced F-actin fragmentation modulates the contraction of active cytoskeletal networks', *Soft Matter*, 13(17), pp. 3213–3220. Available at: https://doi.org/10.1039/c6sm02703b.

Li, T. *et al.* (2016) 'The E3 ligase Ubr3 regulates Usher syndrome and MYH9 disorder proteins in the auditory organs of Drosophila and mammals.', *eLife*, 5. Available at:

https://doi.org/10.7554/eLife.15258.

Liu, X. *et al.* (2017) 'Effect of ATP and regulatory light-chain phosphorylation on the polymerization of mammalian nonmuscle myosin II', *Proceedings of the National Academy of Sciences of the United States of America*, 114(32), pp. E6516–E6525. Available at: https://doi.org/10.1073/pnas.1702375114.

De Lozanne, A. and Spudich, J.A. (1987) 'Disruption of the Dictyostelium myosin heavy chain gene by homologous recombination.', *Science (New York, N.Y.)*, 236(4805), pp. 1086–91. Available at: http://www.ncbi.nlm.nih.gov/pubmed/3576222 (Accessed: 30 September 2018).

Lück-Vielmetter, D. *et al.* (1990) 'Replacement of threonine residues by serine and alanine in a phosphorylatable heavy chain fragment of Dictyostelium myosin II.', *FEBS letters*, 269(1), pp. 239–243. Available at: https://doi.org/10.1016/0014-5793(90)81163-i.

Ma, X. *et al.* (2012) 'Nonmuscle myosin II exerts tension but does not translocate actin in vertebrate cytokinesis.', *Proceedings of the National Academy of Sciences of the United States of America*, 109(12), pp. 4509–4514. Available at: https://doi.org/10.1073/pnas.1116268109.

Mabuchi, I. and Okuno, M. (1977) 'The effect of myosin antibody on the division of starfish blastomeres.', *The Journal of cell biology*, 74(1), pp. 251–63. Available at: https://doi.org/10.1083/JCB.74.1.251.

Matsuda, K. *et al.* (2024) 'Myosin-induced F-actin fragmentation facilitates contraction of actin networks', *Cytoskeleton*, (January), pp. 1–17. Available at: https://doi.org/10.1002/cm.21848.

Matsumura, F. *et al.* (1998) 'Specific localization of serine 19 phosphorylated myosin II during cell locomotion and mitosis of cultured cells', *Journal of Cell Biology*, 140(1), pp. 119–129. Available at: https://doi.org/10.1083/jcb.140.1.119.

McFadden, W.M. *et al.* (2017) 'Filament turnover tunes both force generation and dissipation to control long-range flows in a model actomyosin cortex', *PLOS Computational Biology*, 13(12), p. e1005811. Available at: https://doi.org/10.1371/journal.pcbi.1005811.

Mendes Pinto, I. *et al.* (2012) 'Article Actin Depolymerization Drives Actomyosin Ring Contraction during Budding Yeast Cytokinesis'. Available at: https://doi.org/10.1016/j.devcel.2012.04.015.

Michaux, J.B. *et al.* (2018) 'Excitable RhoA dynamics drive pulsed contractions in the early C. elegans embryo', *Journal of Cell Biology*, 217(12), pp. 4230–4252. Available at: https://doi.org/10.1083/jcb.201806161.

Millar, N.C. and Homsher, E. (1992) 'Kinetics of force generation and phosphate release in skinned rabbit soleus muscle fibers.', *The American journal of physiology*, 262(5 Pt 1), pp. C1239-45. Available at: https://doi.org/10.1152/ajpcell.1992.262.5.C1239.

Mitsuhashi, M. *et al.* (2011) 'Dynamic assembly properties of nonmuscle myosin II isoforms revealed by combination of fluorescence correlation spectroscopy and fluorescence cross-correlation spectroscopy.', *Journal of biochemistry*, 149(3), pp. 253–263. Available at: https://doi.org/10.1093/jb/mvq134.

Mizuno, D. *et al.* (2007) 'Nonequilibrium mechanics of active cytoskeletal networks.', *Science (New York, N.Y.)*, 315(5810), pp. 370–373. Available at: https://doi.org/10.1126/science.1134404.

Mukhina, S., Wang, Y.-L. and Murata-Hori, M. (2007) 'Alpha-actinin is required for tightly regulated remodeling of the actin cortical network during cytokinesis.', *Developmental cell*, 13(4), pp. 554–565. Available at: https://doi.org/10.1016/j.devcel.2007.08.003.

Mullins, R.D. *et al.* (1998) 'Arp2/3 complex from Acanthamoeba binds profilin and cross-links actin filaments', *Molecular Biology of the Cell*, 9(4), pp. 841–852. Available at: https://doi.org/10.1091/mbc.9.4.841.

Munro, E., Nance, J. and Priess, J.R. (2004) 'Cortical flows powered by asymmetrical contraction transport PAR proteins to establish and maintain anterior-posterior polarity in the early C. elegans embryo', *Developmental Cell*, 7(3), pp. 413–424. Available at: https://doi.org/10.1016/j.devcel.2004.08.001.

Murrell, M.P. and Gardel, M.L. (2012) 'F-actin buckling coordinates contractility and severing in a biomimetic actomyosin cortex.', *Proceedings of the National Academy of Sciences of the United States of America*, 109(51), pp. 20820–20825. Available at: https://doi.org/10.1073/pnas.1214753109.

Murthy, K. and Wadsworth, P. (2005) 'Myosin-II-Dependent Localization and Dynamics of F-Actin during Cytokinesis', *Current Biology*, 15, pp. 724–731. Available at: https://doi.org/10.1016/j.cub.2005.02.055.

Najafabadi, F.R., Leaver, M. and Grill, S.W. (2022) 'Orchestrating nonmuscle myosin II filament assembly at the onset of cytokinesis.', *Molecular biology of the cell*, 33(8), p. ar74. Available at: https://doi.org/10.1091/mbc.E21-12-0599.

Nayak, A. *et al.* (2020) 'Single-molecule analysis reveals that regulatory light chains fine-tune skeletal myosin II function', *Journal of Biological Chemistry*, 295(20), pp. 7046–7059. Available at: https://doi.org/10.1074/jbc.RA120.012774.

Norstrom, M. and Gardel, M.L. (2011) 'Shear thickening of F-actin networks crosslinked with non-muscle myosin IIB.', *Soft matter*, 2011(7), pp. 3228–3233. Available at: https://doi.org/10.1039/C0SM01157F.

O'Connell, C.B., Warner, A.K. and Wang, Y. (2001) 'Distinct roles of the equatorial and polar cortices in the cleavage of adherent cells.', *Current biology : CB*, 11(9), pp. 702–707. Available at:

https://doi.org/10.1016/s0960-9822(01)00181-6.

Osório, D.S. *et al.* (2019) 'Crosslinking activity of non-muscle myosin II is not sufficient for embryonic cytokinesis in C. elegans.', *Development (Cambridge, England)*, 146(21). Available at: https://doi.org/10.1242/dev.179150.

Otomo, T. *et al.* (2005) 'Structural basis of Rho GTPase-mediated activation of the formin mDia1', *Molecular Cell*, 18(3), pp. 273–281. Available at: https://doi.org/10.1016/j.molcel.2005.04.002.

Pasternak, C. *et al.* (1989) 'Intermolecular versus intramolecular interactions of Dictyostelium myosin: possible regulation by heavy chain phosphorylation.', *The Journal of cell biology*, 109(1), pp. 203–210. Available at: https://doi.org/10.1083/jcb.109.1.203.

Pate, E. and Cooke, R. (1989) 'A model of crossbridge action: the effects of ATP, ADP and Pi.', *Journal of muscle research and cell motility*, 10(3), pp. 181–196. Available at: https://doi.org/10.1007/BF01739809.

Piekny, A., Werner, M. and Glotzer, M. (2005) 'Cytokinesis: welcome to the Rho zone', *Trends in Cell Biology*, 15(12), pp. 651–658. Available at: https://doi.org/https://doi.org/10.1016/j.tcb.2005.10.006.

Piekny, A.J. and Maddox, A.S. (2010) 'The myriad roles of Anillin during cytokinesis.', *Seminars in cell & developmental biology*, 21(9), pp. 881–891. Available at: https://doi.org/10.1016/j.semcdb.2010.08.002.

Piekny, A.J. and Mains, P.E. (2002) 'Rho-binding kinase (LET-502) and myosin phosphatase (MEL-11) regulate cytokinesis in the early Caenorhabditis elegans embryo.', *Journal of cell science*, 115(Pt 11), pp. 2271–2282. Available at: https://doi.org/10.1242/jcs.115.11.2271.

Prost, J., Jülicher, F. and Joanny, J.-F. (2015) 'Active gel physics', *Nature Physics*, 11(2), pp. 111–117. Available at: https://doi.org/10.1038/nphys3224.

Ravid, S. and Spudich, J.A. (1989) 'Myosin heavy chain kinase from developed Dictyostelium cells. Purification and characterization.', *The Journal of biological chemistry*, 264(25), pp. 15144–15150.

Reichl, E.M. *et al.* (2008) 'Interactions between Myosin and Actin Crosslinkers Control Cytokinesis Contractility Dynamics and Mechanics', *Current Biology*, 18(7), pp. 471–480. Available at: https://doi.org/10.1016/j.cub.2008.02.056.

Reymann, A.-C. *et al.* (2016) 'Cortical flow aligns actin filaments to form a furrow', *eLife*, 5. Available at: https://doi.org/10.7554/eLife.17807.

Robinson, D.N. *et al.* (2002) 'Quantitation of the distribution and flux of myosin-II during cytokinesis', *BMC Cell Biology*, 3, pp. 1–13. Available at: https://doi.org/10.1186/1471-2121-3-4.

Rosenfeld, S.S. *et al.* (2003) 'Myosin IIB is unconventionally conventional', *Journal of Biological Chemistry*, 278(30), pp. 27449–27455. Available at: https://doi.org/10.1074/jbc.M302555200.

Sabry, J.H. *et al.* (1997) 'Myosin heavy chain phosphorylation sites regulate myosin localization during cytokinesis in live cells', *Molecular Biology of the Cell*, 8(12), pp. 2605–2615. Available at: https://doi.org/10.1091/mbc.8.12.2605.

Salbreux, G., Charras, G. and Paluch, E. (2012) 'Actin cortex mechanics and cellular morphogenesis', *Trends in Cell Biology*, 22(10), pp. 536–545. Available at: https://doi.org/10.1016/j.tcb.2012.07.001.

Schmoller, K.M., Semmrich, C. and Bausch, A.R. (2011) 'Slow down of actin depolymerization by cross-linking molecules', *Journal of Structural Biology*, 173(2), pp. 350–357. Available at: https://doi.org/10.1016/j.jsb.2010.09.003.

Scholey, J.M., Taylor, K.A. and Kendrick-jones, J. (1980) 'Regulation of non-muscle myosin assembly by calmodulin-dependent light chain kinase', *Nature*, pp. 233–235. Available at: https://doi.org/10.1038/287233a0.

Sedzinski, J. *et al.* (2011) 'Polar actomyosin contractility destabilizes the position of the cytokinetic furrow', *Nature*, 476(7361), pp. 462–466. Available at: https://doi.org/10.1038/nature10286.

Sellers, J.R. (1985) 'Mechanism of the phosphorylation-dependent regulation of smooth muscle heavy meromyosin.', *Journal of Biological Chemistry*, 260(29), pp. 15815–15819. Available at: https://doi.org/https://doi.org/10.1016/S0021-9258(17)36331-7.

Sellers, J.R., Spudich, J.A. and Sheetz, M.P. (1985) 'Light chain phosphorylation regulates the movement of smooth muscle myosin on actin filaments.', *The Journal of cell biology*, 101(5 Pt 1), pp. 1897–1902. Available at: https://doi.org/10.1083/jcb.101.5.1897.

Shelton, C.A. *et al.* (1999) 'The nonmuscle myosin regulatory light chain gene mlc-4 is required for cytokinesis, anterior-posterior polarity, and body morphology during Caenorhabditis elegans embryogenesis', *The Journal of cell biology*, 146(2), pp. 439–451.

Shoenberg, C.F. (1969) 'An electron microscope study of the influence of divalent ions on myosin filament formation in chicken gizzard extracts and homogenates.', *Tissue & cell*, 1(1), pp. 83–96. Available at: https://doi.org/10.1016/s0040-8166(69)80007-8.

Shutova, M.S. *et al.* (2014) 'Endogenous species of mammalian nonmuscle myosin IIA and IIB include activated monomers and heteropolymers.', *Current biology : CB*, 24(17), pp. 1958–1968. Available at: https://doi.org/10.1016/j.cub.2014.07.070.

Siemankowski, R.F., Wiseman, M.O. and White, H.D. (1985) 'ADP dissociation from actomyosin subfragment 1 is sufficiently slow to limit the unloaded shortening velocity in vertebrate muscle.', *Proceedings of the National Academy of Sciences of the United States of America*, 82(3), pp. 658–662.

Available at: https://doi.org/10.1073/pnas.82.3.658.

Silva, A.M. *et al.* (2016) 'Robust Gap Repair in the Contractile Ring Ensures Timely Completion of Cytokinesis', 215(6), pp. 789–799. Available at: https://doi.org/10.1083/jcb.201605080.

Small, J.V. and Sobieszek, A. (1980) 'The Contractile Apparatus of Smooth Muscle', in G.H. Bourne, J.F. Danielli, and K.W.B.T.-I.R. of C. Jeon (eds). Academic Press, pp. 241–306. Available at: https://doi.org/https://doi.org/10.1016/S0074-7696(08)60239-9.

Soares e Silva, M. *et al.* (2011) 'Active multistage coarsening of actin networks driven by myosin motors', *Proceedings of the National Academy of Sciences*, 108(23), pp. 9408–9413. Available at: https://doi.org/10.1073/pnas.1016616108.

Sobral, A.F. *et al.* (2021) 'Plastin and spectrin cooperate to stabilize the actomyosin cortex during cytokinesis.', *Current biology : CB*, 31(24), pp. 5415-5428.e10. Available at: https://doi.org/10.1016/j.cub.2021.09.055.

Somlyo, A. V. *et al.* (1981) 'Myosin filaments have non-phosphorylated light chains in relaxed smooth muscle', *Nature*, 294(5841), pp. 567–569. Available at: https://doi.org/10.1038/294567a0.

Somlyo, A. V *et al.* (1988) 'Cross-bridge kinetics, cooperativity, and negatively strained cross-bridges in vertebrate smooth muscle. A laser-flash photolysis study.', *Journal of General Physiology*, 91(2), pp. 165–192. Available at: https://doi.org/10.1085/jgp.91.2.165.

Straight, A.F. *et al.* (2003) 'Dissecting temporal and spatial control of cytokinesis with a myosin II Inhibitor.', *Science (New York, N.Y.)*, 299(5613), pp. 1743–1747. Available at: https://doi.org/10.1126/science.1081412.

SWANN, M.M. and MITCHISON, J.M. (1958) 'the Mechanism of Cleavage in Animal Cells', *Biological Reviews*, 33(1), pp. 103–135. Available at: https://doi.org/10.1111/j.1469-185X.1958.tb01409.x.

Taneja, N. *et al.* (2020) 'Precise Tuning of Cortical Contractility Regulates Cell Shape during Cytokinesis.', *Cell reports*, 31(1), p. 107477. Available at: https://doi.org/10.1016/j.celrep.2020.03.041.

Taylor, D.L. and Condeelis, J.S. (1979) 'Cytoplasmic structure and contractility in amoeboid cells.', *International review of cytology*, 56, pp. 57–144. Available at: https://doi.org/10.1016/s0074-7696(08)61821-5.

Thiyagarajan, S. *et al.* (2022) 'Myosin turnover controls actomyosin contractile instability.', *Proceedings of the National Academy of Sciences of the United States of America*, 119(43), p. e2211431119. Available at: https://doi.org/10.1073/pnas.2211431119.

Tinevez, J.-Y. *et al.* (2009) 'Role of cortical tension in bleb growth', *Proceedings of the National Academy of Sciences*, 106(44), pp. 18581–18586. Available at:

https://doi.org/10.1073/pnas.0903353106.

Trybus, K.M. and Lowey, S. (1984) 'Conformational states of smooth muscle myosin. Effects of light chain phosphorylation and ionic strength.', *The Journal of biological chemistry*, 259(13), pp. 8564–8571.

Tse, Y.C. *et al.* (2012) 'RhoA activation during polarization and cytokinesis of the early Caenorhabditis elegans embryo is differentially dependent on NOP-1 and CYK-4', *Molecular Biology of the Cell*, 23(20), pp. 4020–4031. Available at: https://doi.org/10.1091/mbc.E12-04-0268.

Turlier, H., Audoly, B., Prost, J. and Joanny, J.-F. (2014) 'Furrow constriction in animal cell cytokinesis.', *Biophysical journal*, 106(1), pp. 114–23. Available at: https://doi.org/10.1016/j.bpj.2013.11.014.

Turlier, H., Audoly, B., Prost, J. and Joanny, J.F. (2014) 'Furrow constriction in animal cell cytokinesis', *Biophysical Journal*, 106(1), pp. 114–123. Available at: https://doi.org/10.1016/j.bpj.2013.11.014.

Uehara, R. *et al.* (2010) 'Determinants of myosin II cortical localization during cytokinesis.', *Current biology : CB*, 20(12), pp. 1080–1085. Available at: https://doi.org/10.1016/j.cub.2010.04.058.

Umemoto, S. and Sellers, J.R. (1990) 'Characterization of in vitro motility assays using smooth muscle and cytoplasmic myosins.', *The Journal of biological chemistry*, 265(25), pp. 14864–14869.

Uyeda, T.Q., Kron, S.J. and Spudich, J.A. (1990) 'Myosin step size. Estimation from slow sliding movement of actin over low densities of heavy meromyosin.', *Journal of molecular biology*, 214(3), pp. 699–710. Available at: https://doi.org/10.1016/0022-2836(90)90287-V.

Vaillancourt, J.P., Lyons, C. and Côté, G.P. (1988) 'Identification of two phosphorylated threonines in the tail region of Dictyostelium myosin II.', *The Journal of biological chemistry*, 263(21), pp. 10082–10087.

Vale, R.D., Spudich, J.A. and Griffis, E.R. (2009) 'Dynamics of myosin, microtubules, and Kinesin-6 at the cortex during cytokinesis in Drosophila S2 cells.', *The Journal of cell biology*, 186(5), pp. 727–738. Available at: https://doi.org/10.1083/jcb.200902083.

Vasquez, C.G., Tworoger, M. and Martin, A.C. (2014) 'Dynamic myosin phosphorylation regulates contractile pulses and tissue integrity during epithelial morphogenesis.', *The Journal of cell biology*, 206(3), pp. 435–450. Available at: https://doi.org/10.1083/jcb.201402004.

Vicente-Manzanares, M. *et al.* (2009) 'Non-muscle myosin II takes centre stage in cell adhesion and migration.', *Nature reviews. Molecular cell biology*, 10(11), pp. 778–790. Available at: https://doi.org/10.1038/nrm2786.

Volkmann, N. *et al.* (2001) 'An atomic model of actin filaments cross-linked by fimbrin and its implications for bundle assembly and function.', *The Journal of cell biology*, 153(5), pp. 947–956.

Available at: https://doi.org/10.1083/jcb.153.5.947.

Wakatsuki, T. *et al.* (2001) 'Effects of cytochalasin D and latrunculin B on mechanical properties of cells', *Journal of Cell Science*, 114(5), pp. 1025–1036. Available at: https://doi.org/10.1242/jcs.114.5.1025.

Warshaw, D.M. *et al.* (1990) 'Smooth muscle myosin cross-bridge interactions modulate actin filament sliding velocity in vitro', *Journal of Cell Biology*, 111(2), pp. 453–463. Available at: https://doi.org/10.1083/jcb.111.2.453.

Watanabe, S. *et al.* (2008) 'mDia2 induces the actin scaffold for the contractile ring and stabilizes its position during cytokinesis in NIH 3T3 cells.', *Molecular biology of the cell*, 19(5), pp. 2328–2338. Available at: https://doi.org/10.1091/mbc.e07-10-1086.

Weißenbruch, K. *et al.* (2021) 'Distinct roles of nonmuscle myosin ii isoforms for establishing tension and elasticity during cell morphodynamics', *eLife*, 10, pp. 1–35. Available at: https://doi.org/10.7554/ELIFE.71888.

Wendt, T. *et al.* (1999) 'Visualization of head-head interactions in the inhibited state of smooth muscle myosin.', *The Journal of cell biology*, 147(7), pp. 1385–1390. Available at: https://doi.org/10.1083/jcb.147.7.1385.

Wendt, T. *et al.* (2001) 'Three-dimensional image reconstruction of dephosphorylated smooth muscle heavy meromyosin reveals asymmetry in the interaction between myosin heads and placement of subfragment 2', *Proceedings of the National Academy of Sciences of the United States of America*, 98(8), pp. 4361–4366. Available at: https://doi.org/10.1073/pnas.071051098.

Wilson, C.A. *et al.* (2010) 'Myosin II contributes to cell-scale actin network treadmilling through network disassembly.', *Nature*, 465(7296), pp. 373–377. Available at: https://doi.org/10.1038/nature08994.

Winkelman, J.D. *et al.* (2016) 'Fascin- and α-Actinin-Bundled Networks Contain Intrinsic Structural Features that Drive Protein Sorting', *Current Biology*, 26(20), pp. 2697–2706. Available at: https://doi.org/10.1016/j.cub.2016.07.080.

Wollrab, V. *et al.* (2018) 'Polarity sorting drives remodeling of actin-myosin networks.', *Journal of cell science*, 132(4). Available at: https://doi.org/10.1242/jcs.219717.

Yamakita, Y., Yamashiro, S. and Matsumura, F. (1994) 'In vivo phosphorylation of regulatory light chain of myosin II during mitosis of cultured cells.', *The Journal of cell biology*, 124(1–2), pp. 129–137. Available at: https://doi.org/10.1083/jcb.124.1.129.

Yamashiro, S., Noguchi, T. and Mabuchi, I. (2003) 'Localization of two IQGAPs in cultured cells and early embryos of Xenopus laevis', *Cell Motility*, 55(1), pp. 36–50. Available at: https://doi.org/https://doi.org/10.1002/cm.10109.

Yumura, S. (2001) ‘Myosin II dynamics and cortical flow during contractile ring formation in Dictyostelium cells.’, *The Journal of cell biology*, 154(1), pp. 137–146. Available at: https://doi.org/10.1083/jcb.200011013.

Zhou, M. and Wang, Y.-L. (2008) ‘Distinct pathways for the early recruitment of myosin II and actin to the cytokinetic furrow.’, *Molecular biology of the cell*, 19(1), pp. 318–326. Available at: https://doi.org/10.1091/mbc.e07-08-0783.

Zigmond, S.H., Furukawa, R. and Fechheimer, M. (1992) ‘Inhibition of actin filament depolymerization by the Dictyostelium 30,000-D actin-bundling protein.’, *The Journal of cell biology*, 119(3), pp. 559–567. Available at: https://doi.org/10.1083/jcb.119.3.559.

CHAPTER VI

CONCLUDING REMARKS AND FUTURE PERSPECTIVES

Concluding Remarks and Future Perspectives

In this thesis, we investigated the mechanics of cytokinesis, specifically the interplays between the contractile ring and the surrounding cortex during ring assembly and constriction. In Chapter III, the influence of the polar cortex in contractile ring assembly and constriction dynamics is addressed, specifically the extent and timing of myosin polar clearance. We identify two proteins likely to be direct or indirectly involved in this process, 14-3-3^{PAR-5} and PRC1^{SPD-1}. This was nonetheless not explored further, as the main interest at the time was to assess whether we could manipulate myosin localization and see an affect in cytokinesis kinetics.

In Chapter IV, we investigate possible mechanisms for contractile ring assembly. It has been debated whether the ring assembles due to compression of the cortex by cortical flows (Reymann *et al.*, 2016) or, alternatively, by localized recruitment from the cytoplasm at the cell equator. By measuring cortical flows with PIV and analyzing myosin dynamics via FRAP, we find that actomyosin accumulates at the equatorial cortex preferentially by localized recruitment from the cytoplasm, likely via RhoA signaling. Myosin cooperates locally with the main actin filament bundler, plastin, to efficiently assemble the ring, as depletion of both proteins results in cytokinesis failure during this phase.

Finally, in Chapter V, the idea that the regulation of myosin's activity has a contribution for both contractility and viscosity in the cell cortex, which confers robustness to cytokinesis kinetics, is introduced. We find that cytokinesis kinetics are resistant to myosin's knockdown until a certain threshold, which is due to a proportional reduction of contractility and viscosity, both myosin-dependent. Simulations implementing this proportionality using theoretical profiles strongly favor this hypothesis as simulated embryos with decreasing levels of myosin show similar constriction velocities until a similar threshold. Of note, this result is not expected to change in future simulations fed with myosin profiles measured *in vivo*, as the theory implemented remains the same. The viscosity component is likely to arise from the intrinsic regulation of myosin bipolar filaments, where cycling/active and non-cycling/inactive heads co-exist at each point in time, meaning not all heads in a bipolar filament are active simultaneously, or due to asynchronous mechanochemical cycles. The inactive heads, which should be able to bind actin in a weak state, act as a viscous drag to the movement produced by the active heads.

As to the biological relevance of this robustness, it is possible that this is myosin specific. In higher eukaryotes such as mammals, there is more than one non-muscle myosin II and these have been shown to play different and somewhat complementary roles. It is possible that this was a necessary evolution to provide some stability to the cell cortex while the cell

divides. These hypotheses are however quite farfetched, as there is currently no experimental data nor a theory that supports them.

In addition, we also conclude that the mechanical requirements for the ring assembly phase are very different from those necessary for ring constriction. Specifically, whilst the cortex must remain overall connected as the position of the division plane is determined and the contractile ring assembles, connectivity throughout the cortical layer seems rather dispensable during ring constriction. This is supported by the following observations: 1) the depletion of plastin – the only actin crosslinker that alone has an effect in cytokinesis – results in slower ring assembly times, but has no significant effect in ring constriction; 2) the depletion of plastin on unphosphorylatable or motor-dead myosin mutant backgrounds or the double depletion of myosin and plastin lead to additively slower ring assembly times or cytokinesis failure during that phase, yet rings constrict as in *wildtype* embryos or faster, depending on the amount of active myosin available to generate contractile forces.

Still, many questions remain unanswered, both in this work and in general. Fortunate, or unfortunately, many more than when the work for this thesis has kicked-off. Also, ideas that got lost or ended up not being sufficiently explored. It is easy to fall for the trap that the biggest questions have been asked and the big discoveries have been made. There has been an incredible amount of research on cytokinesis ever since actin and myosin have been discovered as the main contractile ring components and it undeniably seems that every question raised is just an extension of past investigations. Looking profoundly at certain topics reveals nevertheless that we still have not fully worked out core questions such as the structure of the contractile ring or even how myosin exactly operates in non-muscle cells and how it contributes to cortex mechanical properties aside from producing contractility.

As such, inspired by Thomas Pollard's thoughts on the Cell Division in 2017 (Pollard, 2017), just a few months before these doctoral studies kicked off, this manuscript will be concluded with what I believe to be, from my own perspective, nine unanswered questions about cytokinesis and actomyosin networks.

1. *Is myosin activation independent of bipolar filament assembly? Can myosin exist in bipolar filaments and be inactive?*

It is undeniable that myosin motor activity is essential for processes that involve contractility in the cell cortex. However, many molecular details are still missing or are not so well-identified, including how exactly myosin assembles into thick filaments in many organisms, whether its activation and filament assembly are dependent or independent events, if the number of myosin monomers and size of thick filaments is constant or variable, and whether all myosin heads in a filament are activated and producing a power stroke

simultaneously, or if some heads are not activated and not bound or, alternatively, not activated but bound to the filaments to stabilize the power stroke generated by the active heads (Kad *et al.*, 2003). As we have seen in Chapter V, although the general accepted idea based on *in vitro* studies is that myosin monomers exist in a "closed" conformation that prevents both bipolar filament assembly and actin binding, in Chapter V we showed that in the *C.elegans* early embryo, a non-phosphorylatable myosin localizes in the cortex with the myosin heavy chain in a similar pattern as *wildtype* embryos, suggesting this myosin can be recruited to the cortex and incorporate bipolar filaments, thus in principle it cannot be in a "closed" conformation. Therefore, further studies will be needed to understand how these processes occur *in vivo*.

2. What is the relevance of chirality for cell division and organism development?

In *C. elegans* embryos active torque generation in the actomyosin layer promotes left–right symmetry breaking by driving chiral counterrotating cortical flows (Naganathan *et al.*, 2016).

However, even though it is likely chirality perturbations will have dramatic consequences in organism development later on, it does seem to be paramount for division success in the early embryo. In Chapter IV, we observed that rotational flows are dispensable for cytokinesis kinetics and asymmetric division. However, those do not display chiral properties, as they rotate in the same direction in both halves of the embryo. Also, recent works that analyzed chiral perturbations in the *C. elegans* embryo do not seem to indicate that disrupting chirality results in division failure (Middelkoop *et al.*, 2021; Zaatri, Perry and Maddox, 2021) It would be interesting to investigate whether there are several proteins playing redundant functions in left-right asymmetry and chirality, allowing divisions to proceed normally when one of them is perturbed. Simultaneous perturbations may ultimately result in division failure in early embryos.

3. *What are the relevant mechanical properties of the cell cortex during cytokinesis? Are they different during contractile ring assembly and constriction?*

In Chapters III and IV of this thesis, it has been found that the motor protein myosin and the actin filament crosslinker plastin display some kind of cooperation. However, while they seem to synergize for an efficient ring assembly, the story changes when the ring is actively constricting: upon perturbation of both proteins, rings struggle to assemble and end up failing cytokinesis; the rings that eventually manage to assemble tend to go faster during the constriction phase. This raises questions on possible different requirements of cortical connectivity during the assembly *versus* constriction of the ring. Chapter V further clarifies this

4. *How do the main cortex components (actin, myosin and actin crosslinkers) turnover and what is the impact on cortex mechanics?*

This is perhaps one of the least understood topics. Turnover of actin has been investigated, but only in some organisms or cells. The lack of a reliable fluorescent probe to track monomeric actin has largely limited the estimation of assembly and disassembly constants in other organisms. Despite this, the effect of actin turnover in the cortex is more or less well-understood.

Myosin turnover and its effects on cortex mechanics are much less understood. Measurements are scarce, but . In Chapter IV of this thesis, we used FRAP to assess myosin's dynamics, only to find myosin accumulates progressively over time as the contractile ring constricts, which can mask the rate at which it is disassembling from the cortex (Leite *et al.*, 2020). A recent publication addressed the role of myosin turnover in contractile rings of fission yeast cell ghosts where component turnover is absent, finding that if myosin does not turnover, it tends to merge into progressively larger aggregates that grow apart from each other, ultimately resulting in loss of tension (Thiyagarajan *et al.*, 2022).

An important message that has hardly been conveyed is what the concept of turnover means. Take actin as an example. Treadmilling, disassembly and turnover are sometimes used interchangeably, however, whist actin treadmilling describes the microscopic dynamics of an individual filament, turnover is generally described as an experimentally measurable property (via FRAP) that captures global remodeling of actin networks and thus may encompass several processes. FRAP may tell us about the rate at which actin monomers are turning over, but it is harder to envision the real implications this microscopic change has on macroscopic cortex mechanics. Biophysical models demonstrate that actin turnover leads to stress relaxation in the network (Halavatyi *et al.*, 2010), but the molecular details that explain this have not been uncovered.

In addition, the turnover of each of these cortical proteins may have implications on the turnover of others, which further complicates the uncoupling of these processes *in vivo*.

5. *What are the molecular cues involved in actomyosin polar clearance and what is quantitatively the relevance for contractile ring assembly and constriction?*

In Chapter III, we identified two proteins that participate in myosin clearance from the polar cortex, 14-3-3^{PAR-5} and PRC1^{SPD-1}. Whether their role in the process is direct or indirect and the respective mechanism remains elusive. This question has recently been addressed in recent studies where some proteins have been identified (Mangal *et al.*, 2018; Chapa-Y-Lazo *et al.*, 2020; Chen *et al.*, 2021), however, the findings are not necessarily similar among them and the full pathways have not been disclosed. It is still unclear whether different

proteins, such as actin, myosin and anillin are cleared independently or whether the clearance of some is the consequence of the clearance of others.

6. *What is the structural organization of the equatorial and polar cortices during cytokinesis? How does this spatial/structural organization affect the mechanical properties and force generation?*

The structural organization of actomyosin networks can better be observed by EM. However, in biological processes such as cell division, which requires dramatic shape changes and reorganization of the cell cortex, visualizing the cortical meshwork with sufficient detail becomes a difficult task that requires specialized techniques and equipment. This may include EM or Super-resolution microscopy. For example, just as when we thought we had it all figured out about myosin, its regulation and how it produces contraction of actomyosin networks, it has been revealed that myosin does not always overlap with actin at the cortex, but rather resides closest to the cytoplasm when cortical tension is low. This is attributed to myosin bipolar filaments' size, which is larger than the actin cortex meshsize (Truong Quang *et al.*, 2021).

7. *Can proteins with different functions contribute for setting the same mechanical properties?*

As suggested in Chapter V of this thesis, myosin has a role in controlling cortex viscosity, aside from its evident contribution to contractility. There are currently no other models of cell cortex mechanics, or specifically cell division, that consider this contribution. Most models assume that the only sources of cortex viscosity are crosslinking proteins, as well as actin filament length and density. In this work, we show that expressing an unphosporylatable or a motor-dead myosin slows down the ring constriction rate, which can be rescued by depleting plastin, the main actin filament bundler in the *C. elegans* early embryo. This highly suggests that the cortex becomes too viscous when expressing these myosins because they crosslink actin filament bundles, despite having decreased motor-activity. Depleting plastin decreases the excessive viscosity and rings can thus constrict at almost normal velocities. Another case is the ARP2/3 complex, which creates crosslinking points in the actomyosin network due to its branched mechanism of actin polymerization, yet it is rarely brought about as a player in cortex viscosity. In this thesis, we also show that depleting an ARP2/3 complex subunit on a plastin mutant unable to bind actin, leads to a slight increase in the constriction rate compared to the *wildtype* embryos. Overall, proteins that are mostly known for other functions can perform the same function of actin filament crosslinkers, thus raising the question whether cytokinesis does not fail in the absence of a single actin crosslinker, as there are likely many proteins, including other conventional (e.g. βH-spectrin (Sobral *et al.*, 2021)) or unconventional (e.g.,

non-muscle myosin II (Leite *et al.*, 2020) or the ARP2/3) crosslinking proteins that maintain the cortex connected.

8. *Is cytokinesis robustness to myosin levels reduction a specific characteristic of unicellular contexts? Does it persist in multicellular contexts?*

We have shown in Chapter V that cytokinesis kinetics are robust to a reduction in myosin levels and that this is due to a proportionality between contractility and viscosity in the cortex, both myosin dependent. The biological relevance of this robustness is however not known. It may be a mechanism to keep the cortex stable as it undergoes dramatic structural changes during cell division. In support of this, more complex organisms have three non-muscle myosin II orthologs, two of which have been shown to play complementary roles in driving contraction *versus* setting viscous tension, a possible hallmark of necessary evolution. On the other hand, this can be exclusive of the one-cell embryo, as it is the first and likely the most sensitive cell of the future organism. It would be interesting to investigate whether this robustness extends to the next *C. elegans* early divisions and if it exists in embryos of other organisms.

9. How exactly does cortex mechanics arising from specific molecular entities impact cell fate and organism development and survival?

The concept of cell fate is intrinsically related with that of asymmetric division. Asymmetric cell division is an essential process in developmental biology that allows a single cell to give rise to a multi-cellular organism with diverse cell types, as the two daughter cells adopt distinct fates. This encompasses physical size asymmetry through polarity establishment, spindle positioning (see Cai *et al.*, 2003; McCarthy and Goldstein, 2006; Kiyomitsu, 2015) and division site specification, as well as differential fate specification involving the localization and function of intrinsic fate determinants or stimuli from the surrounding environment. Cell cortex mechanics has been implicated as a possible player in cell fate. For example, in mice, asymmetric segregation of the apical domain generates blastomeres with different contractilities which triggers their sorting into inner and outer positions, therefore revealing that contractility couples the positioning and fate specification of blastomeres (Maître *et al.*, 2016). Another recent study reported that polarized branched actin tunes cortex mechanics to produced cells of different sizes in asymmetric division in *Drosophila* (Daeden *et al.*, 2023). RhoA GTPases have also been recently associated with mechanosensitive cell fate (Sampayo *et al.*, 2023). Interesting, even though we did not discuss this in much detail, here we observed that in the *C.elegans* early embryo, myosin itself controls cell size asymmetry, which is lost for myosin depletions stronger than the threshold we observed in Chapter V for he kinetic parameters, suggesting a role in asymmetric division and possibly cell fate. Similar results have been described for the two-cell embryo (Ozugergin *et*

al., 2022). Many references are certainly missing here, as this topic could be much extended. However, for simplicity, we only mean to convey the message that apart from the well-known cues coming from the spindle, polarity and specific signaling pathways, cortex mechanical properties such as contractility or viscosity, may also have a role in coordinating cell fate, either directly or indirectly, by controlling the former cues.

In conclusion, whilst efforts are being made to answer some of these questions, others have not been the focus of recent research, probably due to the belief that these have already been answered, but mostly because of experimental limitations. *In vitro* and *in silico* studies have been instrumental to understand how isolated molecular interplays affect cortex mechanics over the past few years, but one may not disregard that they lack the *in vivo* complex environment and regulatory pathways, which may result. Some questions will unavoidably be answered only when these processes can be visualized *in vivo* and in real time. There is an urge for new experimental methods to be developed and for a continuous effort between experimental biology and theoretical physics to collectively understand biological phenomena.

References

Cai, Y. *et al.* (2003) 'Apical complex genes control mitotic spindle geometry and relative size of daughter cells in Drosophila neuroblast and pI asymmetric divisions', *Cell*, 112(1), pp. 51–62. Available at: https://doi.org/10.1016/S0092-8674(02)01170-4.

Chapa-Y-Lazo, B. *et al.* (2020) 'Polar relaxation by dynein-mediated removal of cortical myosin II.', *The Journal of cell biology*, 219(8). Available at: https://doi.org/10.1083/jcb.201903080.

Chen, A. *et al.* (2021) 'Inhibition of polar actin assembly by astral microtubules is required for cytokinesis.', *Nature communications*, 12(1), p. 2409. Available at: https://doi.org/10.1038/s41467-021-22677-0.

Daeden, A. *et al.* (2023) 'Polarized branched Actin modulates cortical mechanics to produce unequal-size daughters during asymmetric division', *Nature Cell Biology*, 25(2), pp. 235–245. Available at: https://doi.org/10.1038/s41556-022-01058-9.

Halavatyi, A.A. *et al.* (2010) 'A mathematical model of actin filament turnover for fitting FRAP data', *European Biophysics Journal*, 39(4), pp. 669–677. Available at: https://doi.org/10.1007/s00249-009-0558-2.

Kad, N.M. *et al.* (2003) 'A mutant heterodimeric myosin with one inactive head generates maximal

displacement.', *The Journal of cell biology*, 162(3), pp. 481–488. Available at: https://doi.org/10.1083/jcb.200304023.

Kiyomitsu, T. (2015) 'Mechanisms of daughter cell-size control during cell division.', *Trends in cell biology*, 25(5), pp. 286–295. Available at: https://doi.org/10.1016/j.tcb.2014.12.003.

Leite, J. *et al.* (2020) 'Equatorial Non-muscle Myosin II and Plastin Cooperate to Align and Compact F-actin Bundles in the Cytokinetic Ring.', *Frontiers in cell and developmental biology*, 8, p. 573393. Available at: https://doi.org/10.3389/fcell.2020.573393.

Maître, J.L. *et al.* (2016) 'Asymmetric division of contractile domains couples cell positioning and fate specification', *Nature*, 536(7616), pp. 344–348. Available at: https://doi.org/10.1038/nature18958.

Mangal, S. *et al.* (2018) 'TPXL-1 activates Aurora A to clear contractile ring components from the polar cortex during cytokinesis', *Journal of Cell Biology*, 217(3), pp. 837–848. Available at: https://doi.org/10.1083/jcb.201706021.

McCarthy, E.K. and Goldstein, B. (2006) 'Asymmetric spindle positioning.', *Current opinion in cell biology*, 18(1), pp. 79–85. Available at: https://doi.org/10.1016/j.ceb.2005.12.006.

Middelkoop, T.C. *et al.* (2021) 'CYK-1/Formin activation in cortical RhoA signaling centers promotes organismal left-right symmetry breaking.', *Proceedings of the National Academy of Sciences of the United States of America*, 118(20). Available at: https://doi.org/10.1073/pnas.2021814118.

Naganathan, S.R. *et al.* (2016) 'Actomyosin-driven left-right asymmetry: from molecular torques to chiral self organization.', *Current opinion in cell biology*, 38, pp. 24–30. Available at: https://doi.org/10.1016/j.ceb.2016.01.004.

Ozugergin, I. *et al.* (2022) 'Diverse mechanisms regulate contractile ring assembly for cytokinesis in the two-cell Caenorhabditis elegans embryo', *Journal of Cell Science*, 135(3), p. jcs258921. Available at: https://doi.org/10.1242/jcs.258921.

Pollard, T.D. (2017) 'Nine unanswered questions about cytokinesis', *Journal of Cell Biology*, 216(10), pp. 3007–3016. Available at: https://doi.org/10.1083/jcb.201612068.

Reymann, A.-C. *et al.* (2016) 'Cortical flow aligns actin filaments to form a furrow', *eLife*, 5. Available at: https://doi.org/10.7554/eLife.17807.

Sampayo, R.G. *et al.* (2023) 'Mechanosensitive stem cell fate choice is instructed by dynamic fluctuations in activation of Rho GTPases', *Proceedings of the National Academy of Sciences*, 120(22), p. e2219854120. Available at: https://doi.org/10.1073/pnas.2219854120.

Sobral, A.F. *et al.* (2021) 'Plastin and spectrin cooperate to stabilize the actomyosin cortex during cytokinesis.', *Current biology : CB*, 31(24), pp. 5415-5428.e10. Available at:

https://doi.org/10.1016/j.cub.2021.09.055.

Thiyagarajan, S. *et al.* (2022) 'Myosin turnover controls actomyosin contractile instability.', *Proceedings of the National Academy of Sciences of the United States of America*, 119(43), p. e2211431119. Available at: https://doi.org/10.1073/pnas.2211431119.

Truong Quang, B.A. *et al.* (2021) 'Extent of myosin penetration within the actin cortex regulates cell surface mechanics', *Nature Communications*, 12(1), pp. 1–12. Available at: https://doi.org/10.1038/s41467-021-26611-2.

Zaatri, A., Perry, J.A. and Maddox, A.S. (2021) 'Septins and a formin have distinct functions in anaphase chiral cortical rotation in the Caenorhabditis elegans zygote.', *Molecular biology of the cell*, 32(14), pp. 1283–1292. Available at: https://doi.org/10.1091/mbc.E20-09-0576.